Reaction Kinetics for Mechanistic Elucidations of Non-Heme Mononuclear Enzymomimetic Model Systems

A Thesis Submitted in Partial Fulfillment of the
Requirements for the degree of

DOCTOR OF PHILOSOPHY

GOURAB MUKHERJEE

Department of Chemistry
Indian Institute of Technology Guwahati
Guwahati, India

Prof. Chivukula V. Sastri; Adviser

August 2019

Dedicated to

My brother,

Sourav Mukherjee,

for always being there.

CONTENTS

STATEMENT

In presenting this thesis in partial fulfilment of the requirements for the doctoral degree at Indian Institute of Technology Guwahati, I hereby declare that the matter embodied in this thesis is a result of investigations carried out by myself in the Department of Chemistry, Indian Institute of Technology Guwahati, India, under the supervision of Prof. Chivukula Vasudeva Sastri within the time frame 2014 to 2019. In keeping with the general practice of reporting scientific observations, due acknowledgements have been made and references have been cited to the original source wherever the work is based on the findings of other investigators.

Gourab Mukherjee

Date: _____/_____/_______

Place: Guwahati, 781039, India

CERTIFICATE

This is to certify that Gourab Mukherjee (146122021), a regular full-time PhD research scholar registered to the Department of Chemistry, Indian Institute of Technology Guwahati, has been working under my supervision since July 2014. I am forwarding his thesis entitled “**Reaction Kinetics for Mechanistic Elucidations of Non-Heme Mononuclear Enzymomimetic Model Systems**” for being submitted for the PhD (Science) degree of this institute. I certify that he has fulfilled all the requirements according to the rules of this institute regarding the investigations embodied in his thesis and this work has not been submitted elsewhere for a degree.

Prof. Chivukula V. Sastri

Thesis Supervisor

Department of Chemistry

Indian Institute of Technology Guwahati

ACKNOWLEDGEMENTS

The research work that I carried out throughout the past five years has been categorically put into order in the form of this thesis. But there were many characters behind the scenes, whose direct or indirect contribution has impacted this thesis in one way or the other. The list is long and I should start with the mentor. I am immensely grateful to my PhD adviser, Prof. Chivukula V. Sastri, for providing me with the opportunity to work and cultivate ideas with utmost freedom and ease. His friendly approach and ever-presence for any kind of discussions is highly appreciated. During difficult times, he was highly motivating, patient and inspirational and always tried to inculcate a unique approach to any kind of problem. He taught more than just Chemistry, and hence is an exemplar of what we say, 'a friend, philosopher and guide.'

I would also like to thank my Doctoral Committee Chairman and Members, Prof. Mohd. Qureshi, Prof. Gopal Das and Prof. Ashish Gupta respectively for timely evaluation of my progress and useful tips for the betterment of my research work. I express my thankfulness to the former and existing HODs of the department of Chemistry and its other faculty members. The Department of Chemistry and the staff members are also highly regarded for their useful contribution in sorting out the administrative matters. I thank the Central Instruments Facility (CIF) for providing expensive instruments and infrastructure; the Param Ishan for providing Computational facilities. I also feel highly obliged to IIT Guwahati and MHRD (Govt. of India) for financially supporting me during the whole tenure and providing useful resources. I am also grateful to my collaborators, Dr. Sam P. de Visser (University of Manchester, UK), Prof. Dr.

Peter Comba (University of Heidelberg, Germany) and Prof. Devesh Kumar (Babasaheb Bhimrao Ambedkar University, India) for their vital contributions to my work.

I am very happy to have friends in Sayanta and Umesh who apart from being my lab mates, are also great persons to hang out with. I also thank my senior, Dr. Prasenjit Barman, for his help and lessons. They made the lab a beautiful working environment to thrive productive ideas. Daily discussions on anything and everything over a cup of tea were tonics of motivation to carry on. I feel very fortunate to be surrounded by friends who were crucial during my stay in Guwahati. As a fresher and newcomer, I was a bit tensed when I arrived at IITG. But I was greeted with wide open arms by some wonderful people, viz. Shubhadip Das, Uday Pan, Soumen Saha, Shilaj Roy and Satyapriya Bhandari. After that with passing days, the list lengthened. Kallol Mondal, Ramiz Akhtar, Koushik Paul, Arindam Ghosh, Palashuddin Sk, Sudin Ganguly, Anabil Gayen, Debashis Koner, Sourav Chattopadhyay, Anindya Sunder Patra, Kobirul Islam, Srikrishna Ghosh, Anirban Mazumdar, Subhankar Panda, Sayan Roy Chowdhury, Sourav Ghosh, Sumit Goswami, Sandip Mondal, Gobinda Dolai, Karuna Sindhu, Shantiram Mahata are wonderful people with whom I share great memories of fun, touring and playing football. I cannot thank them enough. The football ground at IITG was the sink for me where I could forget the monotony and dump out the frustrations of research. I, therefore, thank the sports board too for the resources. I have been a life-long fan of Chelsea FC and thank the same for many precious memories. Other friends from the department, especially, Pinaki Bhusan De and Nilotpal Singha, are also highly regarded who were always there for any help I needed.

I should thank all of my teachers for being the steps in the ladder and helping me climb. Special mention goes to my childhood Chemistry teacher, Raja Da, for instilling in me the love for this subject. I wish to carry bits and pieces of *some of my teachers from my graduation and masters' days, viz. HGM Sir, DB Sir, PB Sir, BKG Sir, AKG Sir and RG Sir.*

Last but never the least, my family and loved ones. I feel profoundly fortunate to have the love and support of my parents, Shri Amar Sankar Mukherjee and Smt. Smita Mukherjee, the blessings and affection from my grand-mother, Smt. Sova Mukherjee and grand-father, Late Shri Sudhanshu Sekhar Mukherjee, and solidarity and support from my brother, Shri Sourav Mukherjee and sister-in-law, Smt. Madhumita Mukherjee. They have always been by my side through thick and thin. I can never imagine reaching this stage without their endless support and sacrifices. Another special person who deserves a mention and had been a constant driving force in my life is Poly. Keeping faith in my potential she kept on pushing me beyond my limits. Without her moral support and encouragement, it would have been difficult to reach this far. I would also take this opportunity to thank my extended family; specially Jethu, Jamma, Dimma, Amma, Rangamoni, Masimoni and Chomi for their fondness and for always believing in me. Special accreditation should be given to my sister, Purna, who is perhaps even more excited about this thesis than me. She has always been by my side and I can't thank her enough for that. During these years, home-comings were always special and were made so by my siblings, Tua, Ani, Dada, Tina, Purna, Buiya and Gungun. I acknowledgement them for all the fun and also for keeping me grounded.

I feel fortunate to have so many well-wishers around that it is difficult for me to name them all. I cordially thank them all for making me the person I am.

ABSTRACT

Metalloenzymes are known to play pivotal role in catalyzing a plethora of biological and biochemical reactions. These transformations are directed by a variety of high valent reactive intermediates that undergo crucial redox reactions by atom transfer or electron transfer or radical reaction pathways. These high valent reactive intermediates of non-heme model systems are being studied for quite some time and are known to be influenced by factors like coordination motifs and topology, ligand architecture, pH, spin states of metal ions, solvation and temperature. However, designing efficient synthetic biomimetic catalysts remains a major challenge due to the unattainability of physiological conditions. The stability and reactivity of these metastable intermediates are hugely affected by simple modifications in the ligand backbone. The factors that govern the reactivity profiles are often associated with the mechanistic pathways followed. Hence in order to have a clear idea, it is important to dig deep into the mechanistic details of the reactions performed by these model systems.

Non-heme iron-oxo intermediates have been identified as potential reactive intermediates in a variety of electrophilic reactions. It can catalyze C-H activation reactions of active and inactive C-H bonds. Other than C-H activation reactions, it can also undergo heteroatom oxidation reactions. Herein, subtle modifications in a ligand skeleton can be seen to hugely accelerate reaction rates catalyzed by non-heme iron-oxo complexes. Also with the help of a series of structurally tweaked ligand frameworks, the governing factors that orchestrate the eccentric reactivity trends of iron-oxo moieties have been brought to the forefront. With the help of a couple of isomeric bispidine Mn(III)-peroxo complexes, a new mechanism for aldehyde deformylation reaction has been established. A very basic keto-enol

tautomerism in the reaction mechanism can be seen to trigger an electrophilic pathway instead of the commonly portrayed nucleophilic mechanism in aldehyde deformylation reactions. Another intended engineering in the bispidine framework resulted in stabilizing a metastable non-heme iron(III)-alkylperoxo complex. These complexes are generally non-reactive. Surprisingly, however, versatile reactivity towards both electrophiles and nucleophiles have been observed for the same.

LIST OF TABLES

LIST OF SCHEMES & FIGURES

ABBREVIATIONS

ESI-MS	Electrospray Ionization Mass Spectrometry
UV/Vis	Ultraviolet Visible
NMR	Nuclear Magnetic Resonance
VT-NMR	Variable Temperature Nuclear Magnetic Resonance
XRD	X-Ray Diffraction
GC	Gas Chromatography
LCMS	Liquid Chromatography Mass Spectrometry
UPLC	Ultra Performance Liquid Chromatography
EPR	Electron Paramagnetic Resonance
ROS	Reactive Oxygen Species
HRP	Horseradish Peroxidase
CYP	Cytochrome P450
NADPH	Dihydronicotinamide Adenine Dinucleotide Phosphate
SOR	Superoxide Reductase
SOD	Superoxide Dismutase
His	Histidine
α-KG	α-ketoglutarate
TauD	taurine/α-KG dioxygenase
pdb	Protein Data Bank
BLM	Bleomycin
A-BLM	Activated Bleomycin
MCD	Magnetic Circular Dichroism

EXAFS	Extended X-ray Absorption Fine Structure
RNR	Ribonucleotide Reductase
Cat	Catalase
PhIO	Iodosylbenzene
TPA	tris(2-pyridylmethyl)amine
*t*BuOOH	*tert*-butyl hydroperoxide
CmOOH	cumene hydroperoxide
TMC	Tetramethylcyclam
TBC	Tetrabenzylcyclam
TMG$_3$tren	1,1,1-tris{2-[N2-(1,1,3,3-tetramethylguanidino)]ethyl}amine
TQA	tris(2-quinolinylmethyl)amine
TAML	Tetraamidomacrocyclic ligand
BnTPEN	N^1-benzyl-N^1,N^2,N^2-tris(pyridine-2-ylmethyl)ethane-1,2-diamine
OOH	Hydroperoxo
OOR	Alkylperoxo
HAA	Hydrogen Atom Abstraction
OAT	Oxygen Atom Transfer
DFT	Density Functional Theory
TEA	Triethylamine
KO$_2$	Potassium superoxide
THF	Tetrahydrofuran
DCM	Dichloromethane
CAN	Cerium (IV) ammonium nitrate
DMS	dimethylsulfide

m.p.	Melting point
RT	Room temperature
THA	Thioanisole
DBT	Dibenzothiophene
CHD	1,4-Cyclohexadiene
2-PPA	2-phenylpropionaldehyde
CCA	cyclohexanecarboxaldehye
DHA	9,10-Dihydroanthracene
PhEt	Ethylbenzene
DMAP	4-Dimethylaminopyridine
PTFE	Polytetrafluoroethylene
OTf	triflate
ppm	Parts per million
Q-TOF	Quadrupole Time of Flight
KIE	Kinetic Isotope Effect
k_{obs}	pseudo first-order rate constant
k_2	second-order rate constant
BDE	bond dissociation energy
EA	Electron affinity
MLCT	Metal to ligand charge transfer
LMCT	Ligand to Metal charge transfer
NIR	Near-Infrared

COMPOUND ABBREVIATIONS

Chapter	**Index**	**Description**
Chapter III, IV	L1	N4Py ligand
	1a	$[Fe^{II}(N4Py)]^{2+}$
	1b	$[Fe^{IV}(O)(N4Py)]^{2+}$
Chapter III	L2	2PyN2Q ligand
	2a	$[Fe^{II}(2PyN2Q)]^{2+}$
	2b	$[Fe^{IV}(O)(2PyN2Q)]^{2+}$
Chapter IV	L3	$N4Py^{Me}$ ligand
	3a	$[Fe^{II}(N4Py^{Me})]^{2+}$
	3b	$[Fe^{IV}(O)(N4Py^{Me})]^{2+}$
	L4	$^{Me}N4Py$ ligand
	4a	$[Fe^{II}(^{Me}N4Py)]^{2+}$
	4b	$[Fe^{IV}(O)(^{Me}N4Py)]^{2+}$
Chapter V	L8	Bispidine ligand
	8a	$[Mn^{II}(L8)]^{2+}$
	8b	$[Mn^{III}(O_2)(L8)]^{+}$
	L9	Bispidine ligand
	9a	$[Mn^{II}(L9)]^{2+}$
	9b	$[Mn^{III}(O_2)(L9)]^{+}$
Chapter VI	L10	Bispidine ligand
	10a	$[Fe^{II}(L10)(OTf)]^{+}$
	10b	$[Fe^{III}(L10)(t\text{BuOO})]^{2+}$

GRAPHICAL ABSTRACT

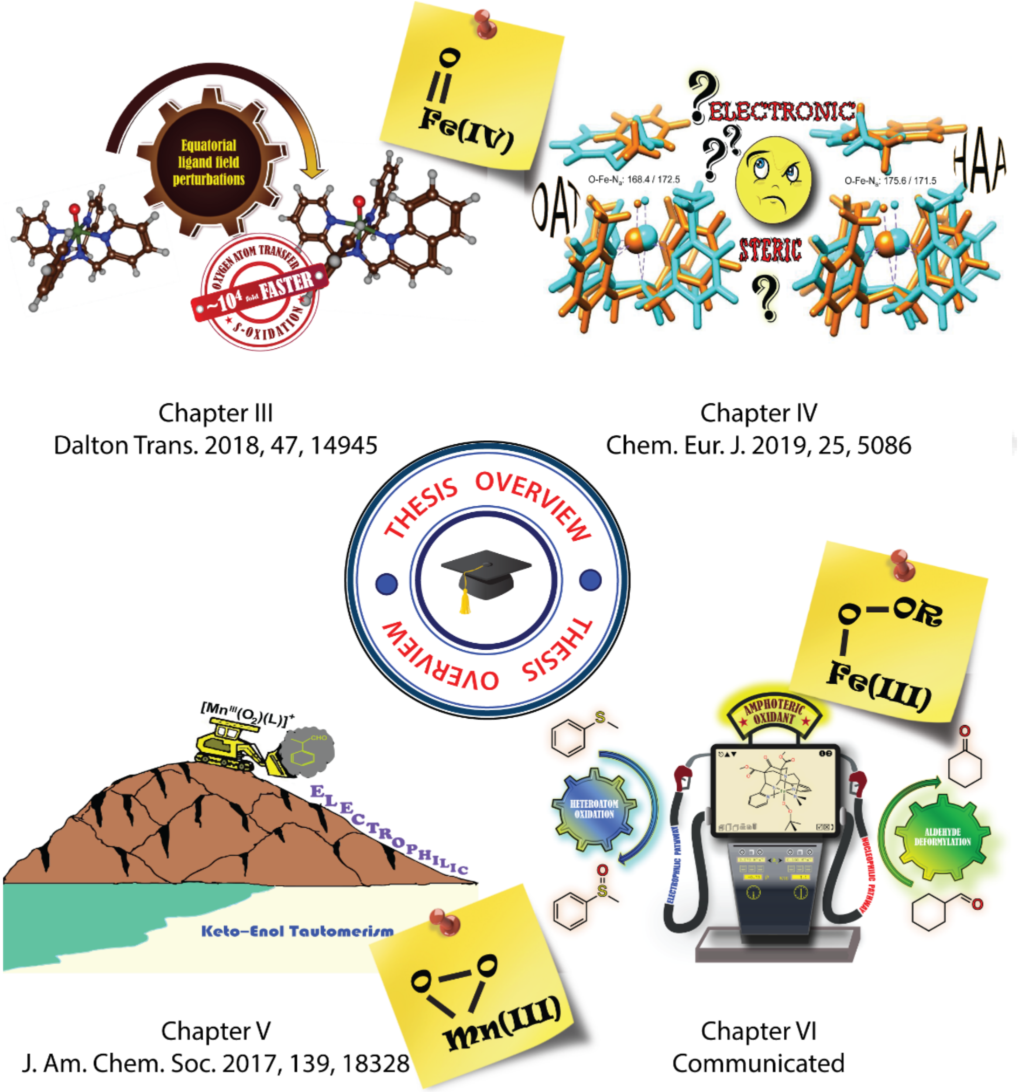

Chapter III
Dalton Trans. 2018, 47, 14945

Chapter IV
Chem. Eur. J. 2019, 25, 5086

Chapter V
J. Am. Chem. Soc. 2017, 139, 18328

Chapter VI
Communicated

CHAPTER – 1

A General Overview of Dioxygen Activation by Heme and Non-Heme Metalloenzymes and their Synthetic Molecular Models

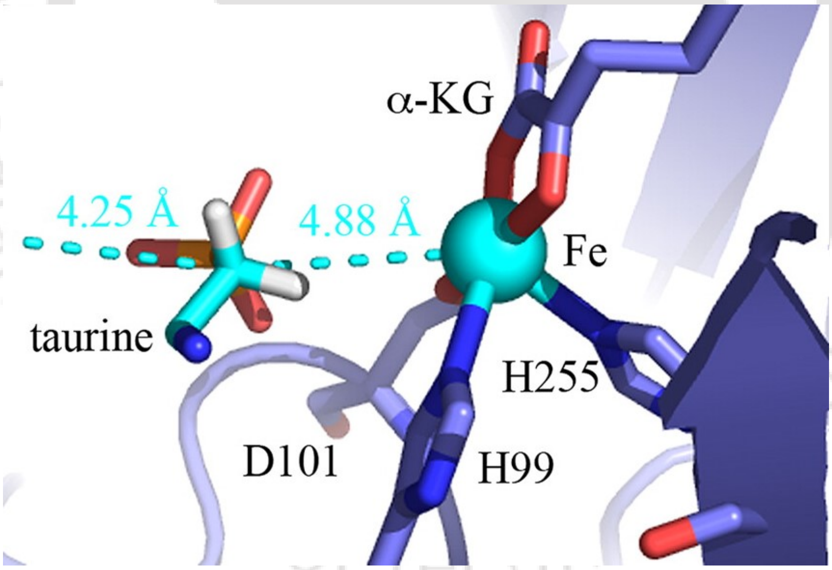

1.1. Introduction

Thousands of years of evolution and adaptation has led to clinical updates and intricate modifications of the wonderful molecular machines that we live in. Nature has employed specific tools and methods for each and every function associated with life processes. One such vital role is played by the metalloproteins that are responsible for a huge diversity of specified catalytic transformations. Metalloenzymes are the subclass of metalloproteins that have been meticulously used by Nature to mitigate the problems of various oxidation reactions under mild and physiological conditions. Various biochemical reactions are catalysed by these metalloenzymes that use metal ions as cofactors. These metal ions can exist in multiple oxidation states thereby affording the possibility of redox biological reactions. Enzymomimetics can be considered as a sub-set of Biomimetics and can be coined as the efforts to mimic the potential active sites of the metalloenzymes by the generation of synthetic model systems and reactive intermediates. This thesis mainly focuses on the mechanistic details of the synthetic enzymomimetic model systems and their reactivity studies with competent organic substrates.

1.2. Dioxygen Activation

The atmosphere chosen by Nature for living organisms to thrive is an oxidizing one.[1] The presence of oxygen in the atmosphere has been vital in the evolutionary process of living beings on earth. The utility of dioxygen as an efficient oxidant is mainly due to its peculiar electronic feature, *i.e.* having two unpaired electrons, thereby making it a radical species. Thus, it requires a thermodynamically favoured reaction of the addition of four more electrons to form water which is a universal solvent in living creatures.[1,2] This molecular oxygen is usually activated by different metalloenzymes in order to perform diverse oxidative reactions. Upon binding to the metal centre, dioxygen gets reduced to different forms like superoxide (O_2^-), peroxide (O_2^{2-}), oxide (O^{2-}) or hydroxyl radical ($OH^\bullet$)[3]. Such species are coined as reactive oxygen species[4] (ROS). These ROS are also associated with oxidative injuries to an organism; mainly Parkinson's disease, mutagenesis, etc.[5,6] Indeed, the superoxide is very much selective towards attacking substrates and thus is well known to be a toxic substance towards the health of an organism.[5-7] These vulnerabilities are well dealt with by Nature with the use of various metalloenzymes and hence the study of the ROS is imperative. These enzymes, particularly the non-heme iron enzymes, can act as a defence unit to detoxify these ROS.[8]

Although the metal ions in metalloenzymes contribute less than a percent of the total protein weight, yet they are vital for the catalytic activity and to promote various biochemical and biological reactions like oxygen activation with special selectivity.[9] These metal ions are mainly coordinated by N, O or S of the amino acid residues in the polypeptide linkages of the protein. They can effectively stabilize various reactive intermediates, that are crucial in the catalytic cycle of the metalloenzyme. In fact, the nature of the metal ion and coordination motifs plays a huge role in determining the activity of the enzyme. The coordination geometry of the metal centre along with its relative spatial orientation in a three-dimensional configuration is responsible for the shape and structure of the active site of the metalloenzyme and controls the accessibility and trajectory of the substrates approaching nearby. The numerous reactions taking place inside a living body is extremely synchronous to the surrounding and utility, but modelling the same keeping the physical and chemical characteristics of the enzymes intact is equally difficult. Most of these reactions are multistep reactions within millisecond time scale and the characterization of the reactive intermediates of such reactions is a fundamental obstacle faced by researchers. Another approach is to freeze the reactions at lower temperatures in order to mimic their reaction pathway and to ascertain each step. That would imply the usage of a non-aqueous solvent system, as water is not a proper solvent at lower temperatures. Again under organic solvents, there is a high chance of rupture of the hydrogen bonding among the protein chains thereby resulting in denaturation of the protein. Thus, the kinetic limitation is a major challenge faced by researchers while dealing with enzymomimetics. These limitations were partly addressed by employment of synthetic small molecular models that mimic the active site and primary coordination sphere of the metalloenzymes.[10] With the use of these molecular model systems, researchers were able to mimic the reactions of the relevant metalloenzymes by use of organic solvents and could exercise the ease of working over a wide range of temperature scale.[11]

1.3. Heme and Non-Heme Metalloenzymes containing Iron and Manganese

1.3.1. Heme Systems

Iron is the fourth most abundant element in the earth crust and its ability to exist in a wide range of oxidation states like Fe(I), Fe(II), Fe(III), Fe(IV) and Fe(V) makes it a suitable element for metalloenzymes.[11] Hence, it is found in different types of enzymes like oxidases, hydrogenases, reductases, oxygenases and dehydrogenases.[12] Systems like heme, iron-sulfur proteins and non-heme systems with mononuclear and dinuclear centres contain and utilise the redox efficiency of iron. These enzymes can be classified in a number of ways. If both the oxygen atoms of dioxygen are incorporated to the substrate, they are termed as dioxygenases, while incorporation of one oxygen atom makes it a monooxygenase. Again they can be structurally categorized as heme systems and non-heme systems. Heme iron oxygenase mainly consist of a proto-heme IX prosthetic group as shown in Fig. 1.1.

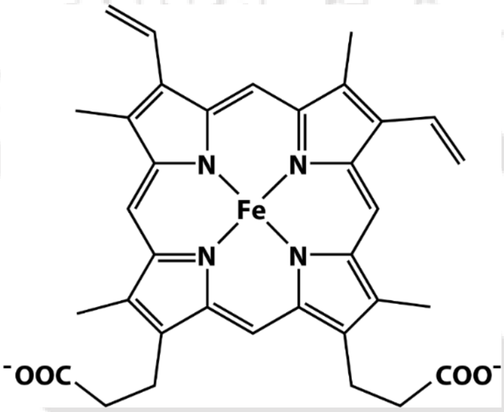

Fig. 1.1. Basic structure of Proto-heme IX.

Tryptophan dioxygenase, secondary amine monooxygenase[13] and cytochrome P450 super family[14] are heme containing iron enzymes that oxidize substrates by activating molecular oxygen. Other enzymes like heme peroxidase,[15] chloroperoxidase[16] and horseradish peroxidase[17] (HRP) have structural resemblance but uses hydrogen peroxide as the oxidant instead of dioxygen, thereby, are not O_2 activating enzymes. The iron(IV)-oxo or iron(V)-oxo or (Por$^{+\bullet}$)-iron(IV)-oxo are proposed to be the key activated species in the heme iron oxygenases and in heme peroxidases. Hemoglobin is an iron-containing metalloenzyme that constitutes four myoglobin units linked by protein chains. The former is used for oxygen transport while the latter is an oxygen storage functional. Synthetic active site modelling studies have been performed but the role of the globin protein cannot be discarded as its absence leads to the formation of a binuclear dimeric Fe(III) species, hematin, that is further incapable of oxygen transport and storage.

One of the most remarkably diverse group of oxygen activating metalloenzyme is the cytochrome P450 (CYP).[14] This is a versatile metalloenzyme that exhibits a variety of oxidation reactions like alkane hydroxylation, olefin epoxidation, heteroatom oxidation, N-dealkylation, etc. The mechanism of O_2 activation shown below (Fig. 1.2) has been accepted as the general mechanism for the P450 super family.[18,19] The iron(III) in its resting state is bound by four nitrogen donors in the equatorial plane and is coordinated to the protein *via* a cysteine thiolate linkage to the iron and a water molecule axially *trans* to the sulfur. Upon approach of the substrate the labile water coordination is broken to form the iron(III) species [A]. The ferric species is reduced by an electron from NADPH to the ferrous form [B] that can activate dioxygen to form [C]. [C] is a ferric-superoxo intermediate bonded in an end-on fashion. A second electron and a proton transfer forms the ferric-hydroperoxo species [D] which is also known to be an active oxidant for many epoxidation reactions.[20,21] Heterolysis of the O-O bond as a combination of the *push effect* of cysteine and *pull effect* of the distal protein results in the formation of an iron(IV)-oxo cation radical species [E].[22-24] Species [E] is known as the compound I that abstracts a hydrogen atom from the substrate to form a substrate based radical and the hydroxoiron(IV) species [F], which is similar to compound II in the catalytic cycle of chloroperoxidase.[25] [F] further liberates the hydroxylated compound R-OH by rebound of the hydroxyl group to the substrate radical.[13,26-30] Thus, compound I is the active oxidizing species in the catalytic cycle. This species has not been directly isolated hitherto,[31] but similar iron(IV)-oxo species of cytochrome C peroxidase have been successfully crystallised.[32,33] The cytochrome P450 is one of the most vividly studied enzyme. More than 50,000 distinct CYPs have been identified across all kingdoms of life. They are involved in the biosynthetic processes of numerous compounds in nature including hormones, cholesterol and vitamin D and are also crucial in detoxification of many toxic compounds. For example, some human CYPs can breakdown quinine to its less toxic hydroxylated form, 3-hydroxyquinine.

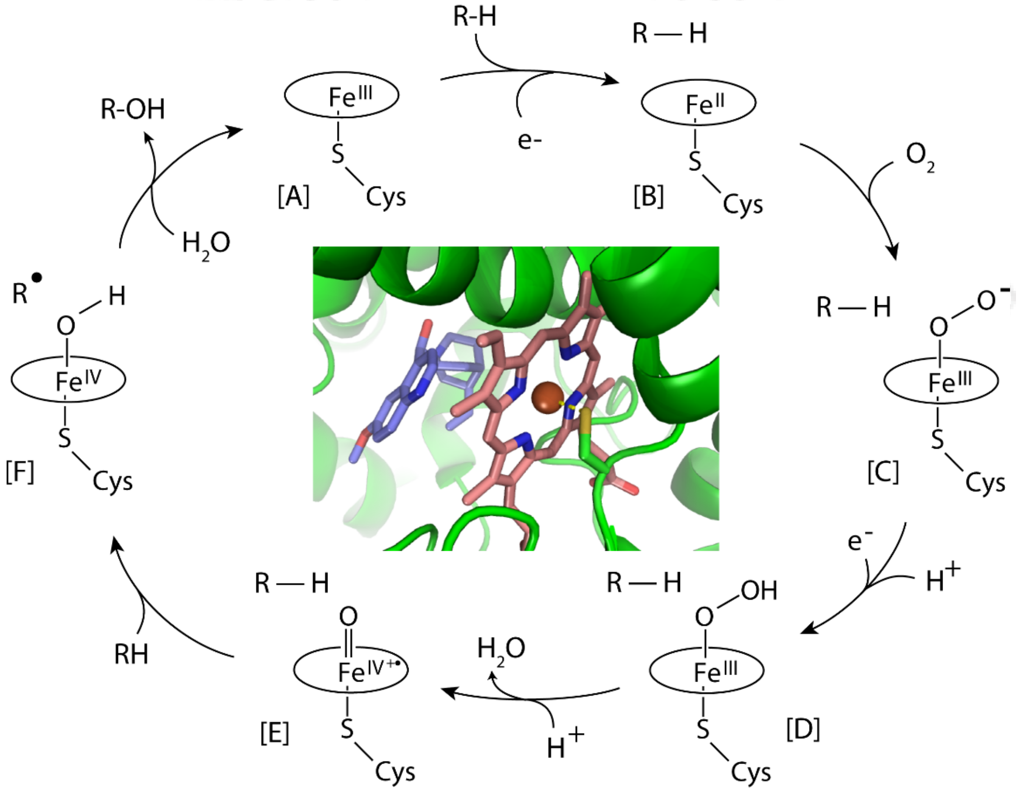

Fig. 1.2. General mechanism of dioxygen activation by cytochrome P450. Inset shows the heme-binding in cytochrome P450 along with its cysteine linkage with the protein and the quinine substrate in the background.

1.3.2. Non-Heme Systems

A non-heme metalloenzyme that has a similar coordination motif as cytochrome P450 is the superoxide reductase (SOR). It has a similar N4S donor system in the primary coordination sphere, where histidine residues take place instead of the heme prosthetic group. However, the structure-function relationship slightly changes in SOR, where, the Fe-O bond in the ferric-hydroperoxide cleaves to release hydrogen peroxide instead of O-O bond rupture in CYPs. Another striking dissimilarity is in the spin state of the iron centre. Unlike in P450, where the peroxo species contains a low-spin iron ($S = 1/2$), the spin state of iron in SOR is high-spin ($S = 5/2$). As can be envisaged from the occupancy of the bonding and antibonding orbitals of iron, it can be predicted that the low-spin moiety in P450 would have a weak O-O bond and a strong Fe-O bond, while that in SOR indicates strong O-O bond and a weaker Fe-O bond – thereby favouring Fe-O bond cleavage. Another non-heme metalloenzyme is the superoxide dismutase (SOD). Superoxide (O_2^-) can be formed *in vivo* by a simple one-electron procurement by dioxygen. Although superoxide is not that strong oxidant, it is an active precursor to the other ROS. SOD enzymes undergo a disproportionation reaction of superoxide into hydrogen peroxide and dioxygen *via* stepwise reduction and oxidation of the metal cofactor as shown below:

$$M^{n+} + O_2^- \longrightarrow M^{(n-1)+} + O_2$$

$$M^{(n-1)+} + O_2^- + 2H^+ \longrightarrow M^{n+} + H_2O_2$$

A particular coordination motif observed in many non-heme iron oxygenases is the 2-His-1-carboxylate facial triad where a couple of histidines and a carboxylate residue are coordinated in a facial manner to the metal (see Fig. 1.3).

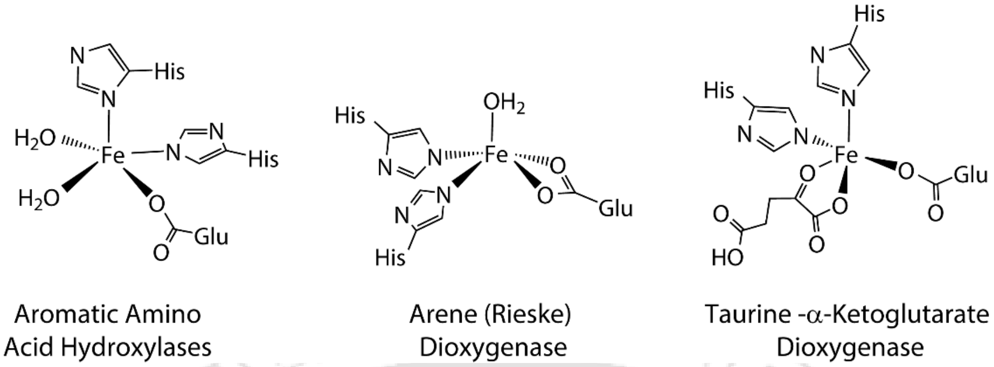

Aromatic Amino Acid Hydroxylases

Arene (Rieske) Dioxygenase

Taurine -α-Ketoglutarate Dioxygenase

Fig. 1.3. Coordination motifs of few non-heme mononuclear iron enzymes.

Examples include enzymes like Aromatic amino acid hydroxylases, Arene (rieske) dioxygenase, TauD, Isopenicillin N-synthase, etc.[34-40] This leaves three coordination sites vacant for exogeneous ligands to bind. These non-heme iron oxygenases activate dioxygen and reduce it by four electrons. The source of these electrons vary and sometimes the coordinated substrate acts as the supplier as in the cases of biopterin dependent amino acid hydroxylases and α-ketoglutarate dependent enzymes.[41,42] Rieske dioxygenase functions by *cis*-hydroxylating arenes like naphthalene by and contains two [Fe_2S_2] iron sulfur clusters nearby that act as the electron source.[43,44] Isopenicillin N-synthase extracts all four electrons from the substrate.[45,46]

Direct characterization of an iron(IV)-oxo intermediate has been provided by studies of several α-ketoglutarate (α-KG) dependent oxygenases (TauD) that catalyze hydroxylation or halogenation of the substrates.[47] The catalytic cycle as shown in Fig. 1.4 is a consensus mechanism of oxygen activation by α-KG dependent enzymes using TauD as the active site.[48]

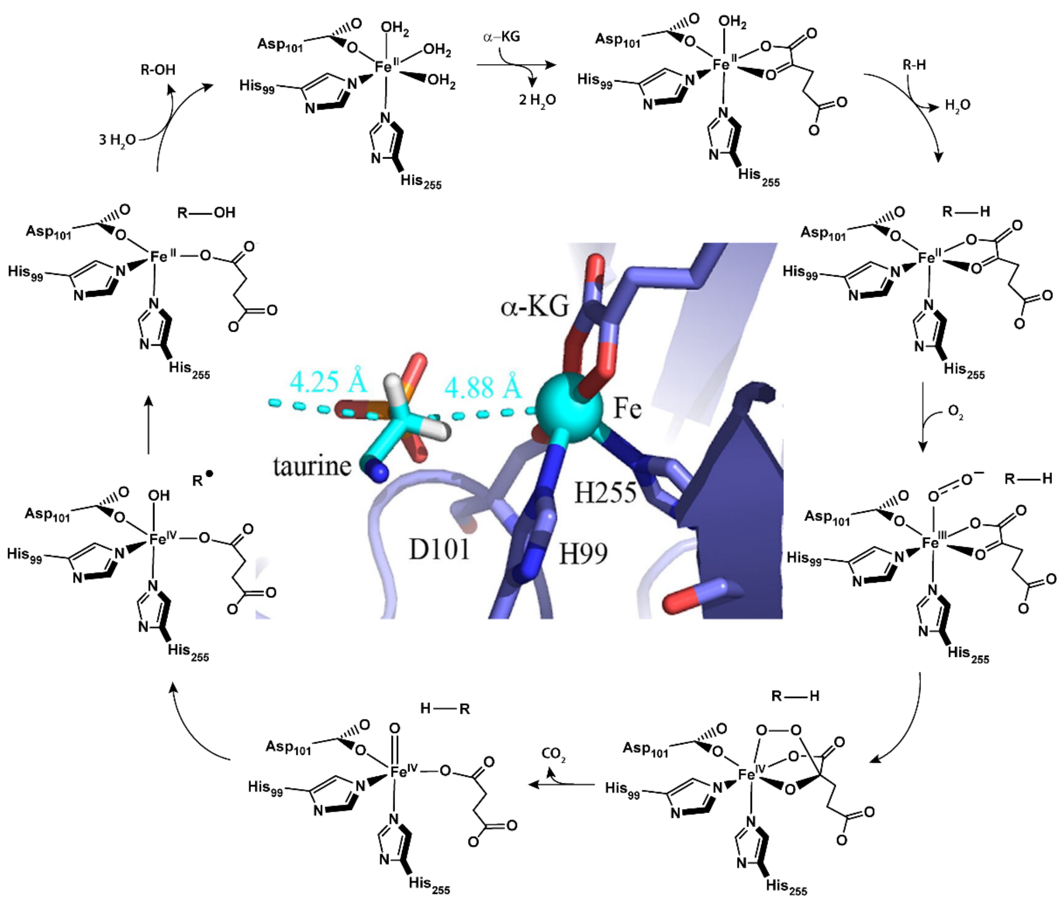

Fig. 1.4. General mechanism of oxygen activation by TauD enzyme. Inset shows the active-site architecture of wild-type TauD, from pdb 1OS7 (23).[54]

The introduction of α-KG displaces two water molecules from the primary coordination sphere and binds to the iron centre in a bidentate fashion. Upon approach of the substrate, the remaining water molecule is also displaced making space for the dioxygen which then binds in an end-on fashion to form the iron(III)-superoxide species. The distal oxygen atom attacks the α-KG and decarboxylates.

Subsequent O-O bond cleavage leads to the formation of the putative high valent iron(IV)-oxo species,[49-52] that is mainly responsible for C-H bond hydroxylation. In comparison to heme systems, the reactive intermediates in non-heme metalloenzymes can be trapped with the help of rapid freeze-quench techniques.[53] The first crystal structure of iron(II) coordinated to a α-keto acid using benzoylformate as the model α-keto acid was identified by Prof. Que and co-workers.[49]

In both heme system (cytochrome P450) and non-heme system (TauD), the substrate hydroxylation process takes place by a '*rebound mechanism*'. The iron(IV)-oxo moiety abstracts an active hydrogen atom from the substrate thus forming a one electron reduced iron(IV)-hydroxo species and the corresponding substrate radical. This is followed by rebound of the –OH group from iron to the substrate radical thereby forming a new C-O bond and reducing the iron centre (see Scheme 1.1).[55,56]

Scheme 1.1. Oxygen rebound mechanism of substrate hydroxylation by iron(IV)-oxo systems.

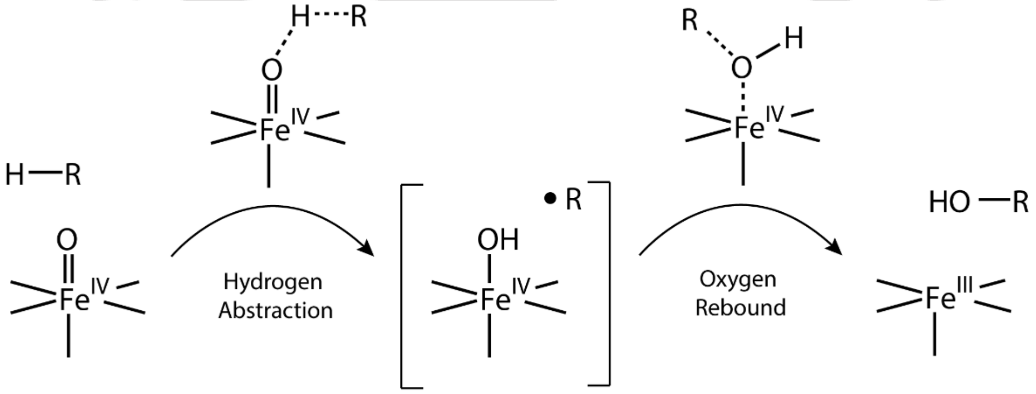

Another non-heme histidine-containing glycopeptide antibiotic is Bleomycin (BLM) that is a clinically useful antitumor agent (Blenoxane).[57] This catalyses dioxygen and Fe(II) dependent oxidative DNA cleavage.[58-63] Unlike P450 and non-heme SOR, that offers a square pyramidal geometry with N4S donor atoms, similar geometry I adopted by Bleomycin with the help of an N5 donor set of atoms. As can be seen from Fig. 1.5, the iron in the centre is coordinated by five nitrogen atoms from a histidine, a pyrimidine, a deprotonated peptide function, a primary amine and a secondary amine in the primary coordination sphere.[64-67] Thus one dioxygen unit can occupy the axial coordination site of the distorted square pyramid to form an octahedral activated complex known as activated bleomycin (A-BLM). This activated species has been characterised by EPR spectroscopy to be a low-spin iron(III) complex (*s* = ½) with g values at 2.26, 2.17, 1.80.[68] A-BLM was also generated by treatment of BLM with hydrogen peroxide and was latter characterised successfully by ESI-MS,[69] MCD,[70] EXAFS[71] and Mössbauer spectroscopy.[72] These spectroscopic tools inferred A-BLM to be a low-spin ferric-hydroperoxide species.

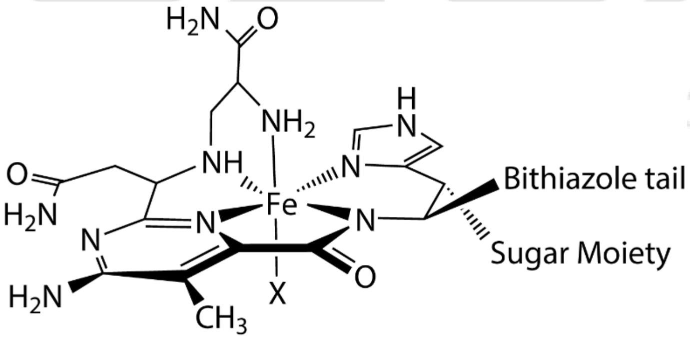

Fig. 1.5. Distorted **s**quare pyramidal geometry of Fe-BLM (X being the vacant site).

In order to know the influence of different donor groups that affect the process of O_2 activation in BLM and the various reactions at its active site, several types of ligand scaffolds were studied over the years.

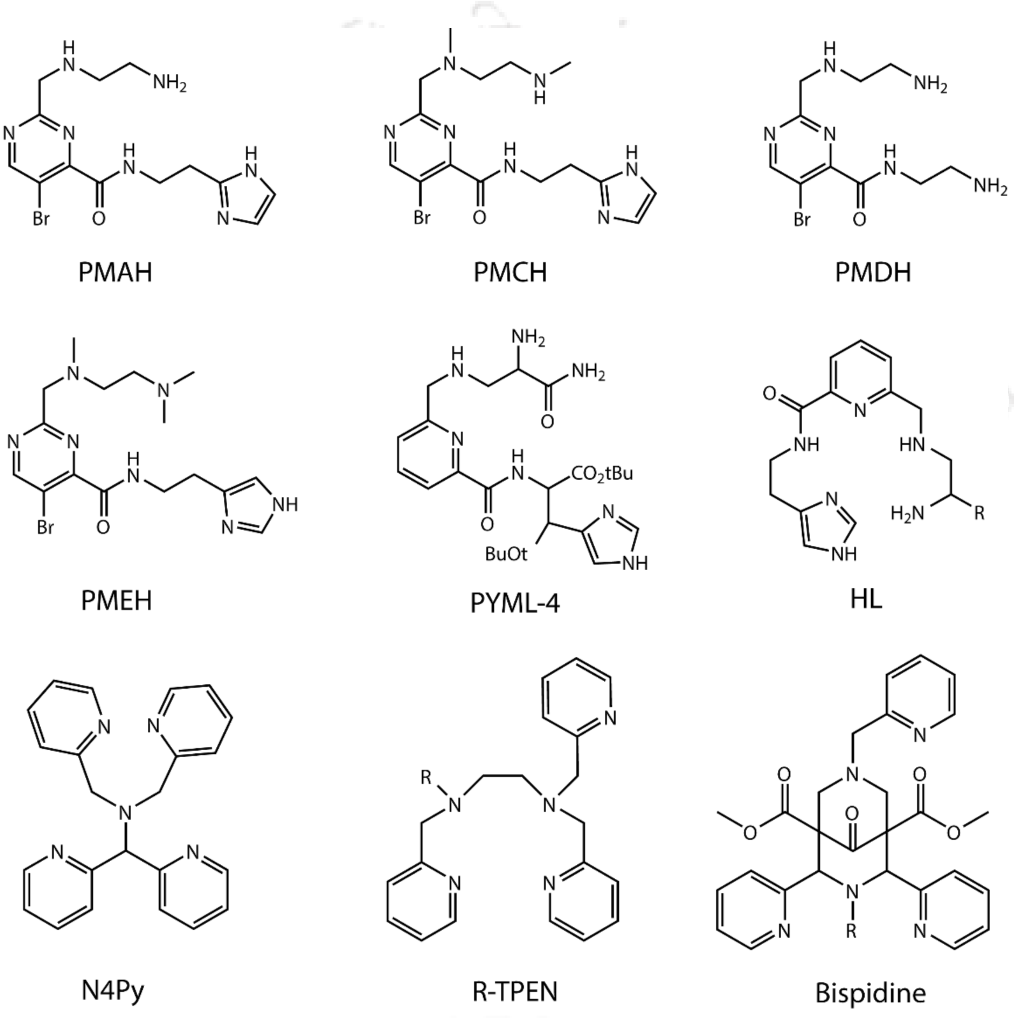

Fig. 1.6. Ligand scaffolds with pentadentate N5 donor set to mimic BLM activities.

Model systems to mimic the active site of BLM include ligand frameworks with N5 donor set and can be either amidate based ligands or neutral N-donors. For example, frameworks like PMAH,[73] PMCH,[74] PMDH,[75] PMEH,[75] PYLM-4,[76] and HL[77] were classified under the former category (see Fig. 1.6) that contain primary, secondary and also tertiary amine groups other than heterocyclic N donors. The other category consists of pentadentate N5 donor set of either heterocyclic pyridine rings or tertiary amine groups (Fig. 1.6). The ligands N4Py[78-81] and R-TPEN[82-86] are popular ligand scaffolds to generate and stabilize a number of high valent metal intermediates. Bispidine frameworks are another class of ligands that can also provide a pentadentate N5 donor linkage to a metal ion.[87-90] Apart from that, its adamantane type skeleton is an optimum balance of rigidity and flexibility, thereby, offering the metal ions a suitable cavity size to sit upon.

Apart from iron, manganese-oxygen adducts are also highly significant among the biological and synthetic systems. Those include dioxygen adducts like superoxo-Mn(III) and peroxo-Mn(III) species.[91] These adducts are quite relevant to synthetic model systems as well as to several Mn containing enzymes like Mn-superoxide dismutase (Mn-SOD), Mn-catalase (Mn-Cat), Mn-ribonucleotide reductase (Mn-RNR) and Mn-dependent catechol oxygenases (MndD). These activated species are crucial in various functions like detoxification of ROS,[92,93] aromatic hydroxylation,[94] conversions of ribo- to deoxyribonucleotides,[95,96] and formation of O_2 from water.[97]

For example, in eukaryotes, Mn-SOD is located in mitochondria. The one-electron reduction of O_2 is a thermodynamically favoured process. This is due to a reduction potential of -0.16 V for the conversion of O_2 to O_2^{-}.[98] Structurally the Mn- and Fe-SOD are homologous. The Mn-SOD is either a homodimer or a homotetramer while Fe-SOD is always a homodimer. The primary coordination sphere around the metal ion (Fe or Mn) is occupied by three histidines, one aspartate and one water in a distorted trigonal bipyramial geometry. Mn-SOD is the major antioxidant in the mitochondria and disproportionates O_2^- *via* sequential oxidation (Mn^{3+}) and reduction (Mn^{2+}). At higher concentration of superoxide, the catalytic activity of Mn-SOD is accelerated, whereas at lower superoxide concentrations, the reaction is slowed down. The mechanism by which the Mn-SOD performs can be of two types. Either it can be a 'prompt protonation' pathway, where instantaneous protonation and dissociation of the peroxo moiety takes place, or it can be an 'inner-sphere' pathway where a potent side-on Mn(III)-peroxo species has been detected.[99] This side-on Mn(III)-peroxo species has also been referred to as a 'product-inhibited' complex. This species finally abstracts a proton to complete the inner-sphere mechanism. Thus, the mechanism of reaction adopted by these reactive Mn-intermediates has been subject of debate over the years. Rapid reaction kinetics makes the characterization of the intermediates very difficult.[94,100]

1.4. Enzymomimetic Model Systems and Reactive Intermediates

There are several other non-heme metalloenzymes of Fe and Mn existent and functioning in the biological system. From the survey of the library of numerous such systems that constitutes the rich literature of non-heme metalloenzymes, what has been perceived is the need of synthetic model systems that could mimic their active site and biological functions. These synthetic model systems are coordination complexes of metal ions which react with several oxidants to generate the high valent reactive intermediates. Inspired by the expertise of Nature, many researchers have devoted themselves to understand the reaction profiles of the metalloenzymes by use of synthetic model systems.[101,102] The primary challenges involve the stabilization and characterization of the transient species and taming the fast reaction kinetics for some of those. The focus of this thesis is the synthesis of relevant and appropriate model systems, that could contain the metal ions like iron and manganese and generation of their oxidized reactive state by interaction with suitable oxidants, followed by testing their reaction kinetics with various types of organic substrates. Thus, different types of model reactions were exercised and mechanistic investigations were done.

While dealing with the aforementioned processes, several types of reaction intermediates were successfully generated and characterised, *viz.* iron(IV)-oxo, iron(III)-alkylperoxo and Mn(III)-peroxo. The reactivity profiles of those metastable species were studied at either normal or lower temperatures depending upon their stability and reaction kinetics.

1.4.1. Iron(IV)-Oxo Mimics

The catalytic cycle of many non-heme iron enzymes are speculated to contain iron(IV)-oxo species. The only mononuclear non-heme enzyme known to have such species is the α-keto acid dependent TauD enzyme.[47,103] This led to the characterization of a number of iron(IV)-oxo species belonging to model systems.[104-108] These oxo complexes were obtained by reaction of the precursor complexes with oxidants like iodosylbenzene, peracetic acid or hydrogen peroxide.[109] These complexes are quite efficient in affecting a number of oxidation reactions.[110] The first example of catalytic hydroxylation of non-activated alkanes by a mononuclear Fe(III) complex of 5,10,15,20-tetrakis(phenyl)porphyrin with iodosylbenzene (PhIO) was reported by Groves and co-workers in 1979.[111] Upon introduction of bulky, substituted arene units in the *meso* positions and electron-withdrawing substituents to the pyrrole β-position, the stability of the catalyst was increased under oxidizing conditions.[112] Thus, the nature of the ligand and the oxidant significantly influence catalytic performance. In the early 1990s, Que and co-workers reported catalytic activity of iron complexes, $[Fe^{III}(TPA)Cl_2](ClO_4)$ and $[Fe^{III}(TPA)Br_2](ClO_4)$ towards cyclohexane.[113,114] Soon after that, a series of TPA derivatives were studied and the μ-oxo bridged diiron complexes showed considerable turnovers in their reaction with cyclohexane in presence of *tert*-butyl hydroperoxide (*t*BuOOH).[115,116] The catalytic activity was also tested by manifestations in the ligand skeleton as Hitomi et al introduced three nitro groups in the TPA ligand framework but this led to lower yield and selectivity in cyclohexane oxidation.[117,118] The effect of solvent was also significant as was observed in the case of both TPA and N3Py based complexes, the selectivity in oxidation reactions of cyclohexane and *cis*-1,2-dimethylcyclohexane was lowered in acetone than in acetonitrile.[119,120] The first non-heme iron(IV)-oxo species was stabilised by a cyclam acetate ligand reported by the Weighardt group in 2000.[121] Mössbauer data ($\delta = 0.01$ mm/s and $\Delta E_Q = 1.37$ mm/s) obtained for the same were consistent with heme iron(IV)-oxo model systems. The research groups of Prof. Larry Que, Jr. and Prof. Wonwoo Nam reported non-heme iron(IV)-oxo complex $[Fe^{IV}(O)(TMC)(CH_3CN)]^{2+}$ using the macrocyclic N4 ligand (TMC) by treatment of the iron(II) precursor with either PhIO or H_2O_2 at -40 °C in CH_3CN, thereby, producing a green solution with λ_{max} at 820 nm ($\varepsilon = 400$ M^{-1} cm^{-1}). The formation of iron(IV)-oxo was confirmed by Mössbauer analysis ($\delta = 0.17$ mm/s and $\Delta E_Q = 1.24$ mm/s).[105] Using the same TMC framework, later the effect of axial ligand tuning was categorically studied by Sastri et al and with the use of CH_3CN, CF_3COO^-, and N_3^- as the axial ligands interesting outcome were observed for hydrogen atom abstraction (HAA) of phenols and hydrocarbons and oxygen atom transfer (OAT) reactions of PPh_3.[122] In fact, the effect of ring strain was also established by the Nam group. A comparison of TBC and TMC framework shows the introduction of four benzyl groups instead of methyl groups and in spite of added strain in the molecule, the $[Fe^{IV}(O)(TBC)(CH_3CN)]^{2+}$ shows $>10^2$ times enhanced rates than $[Fe^{IV}(O)(TMC)(CH_3CN)]^{2+}$ towards HAA and OAT reactions.[123] A tetradentate ligand TPA was employed by Que and co-workers to synthesize the $[Fe^{IV}(O)(TPA)(CH_3CN)]^{2+}$ complex at low temperature. It showed a low intensity near-IR absorption band at 724 nm ($\varepsilon = 300\ M^{-1}\ cm^{-1}$) which is also supported by Mössbauer and ESI-MS analysis.[124] A number of other non-heme mononuclear iron(IV)-oxo complexes have been synthesised and characterised, but most of them are in organic solvents and contain low-spin $S = 1$ iron.[107,108,125-128] An exceptional high-spin iron(IV)-oxo complex $[Fe^{IV}(O)(OH_2)_5]^{2+}$ was reported by Bakac and co-workers that was formed in aqueous phase.[129-131] Que et al reported another high- spin iron(IV)-oxo complex in TMG_3tren. $[Fe^{IV}(O)(TMG_3tren)](CF_3SO_3)_2$ has a half-life period of 4.3 h at -30 °C and around 30 sec at 25 °C.[132] Later Nam and co-workers also reported another iron(IV)-oxo complex that is even more reactive than the cytochrome P450 model compound I. By the introduction of three N-methylbenzimidazole groups instead of pyridine rings the reactivity profiles of the new iron(IV)-oxo complex was enhanced manifold.[133] But the high-spin character in an iron(IV)-oxo complex not necessarily guarantee faster reactivity.[134] By the introduction of steric crowding in the pyridine α-position of TPA, Que and co-workers substituted the pyridine groups of TPA by quinoline and synthesised a new iron(IV)-oxo complex, $[Fe^{IV}(O)(TQA)]^{2+}$. This restricted the formation of shorter Fe-N bonds required for a low-spin species and thereby formed a high-spin S= 2 iron-oxo complex.[135] Later a handful of high-spin iron(IV)-oxo complexes has been reported in which the metal centre is positioned in a sterically encumbered cavity with the forceful occupation of a trigonal bipyramidal geometry.[136-138] The research group of Collins have successfully been able to contain an iron(V)-oxo moiety with the help of ligation from the TAML framework.[139,140] The electron-rich almost square planer cavity provided by the TAML ligand stabilises $S = ½$ oxo complex. Various factors that influence the structure-function relationships of iron(IV)-oxo complexes like ligand topology,[107,133,141] axial ligation,[122,142] spin states of iron[134] and binding of different metal ions and protons[143-146] to the iron-oxo moiety have been studied over the years.

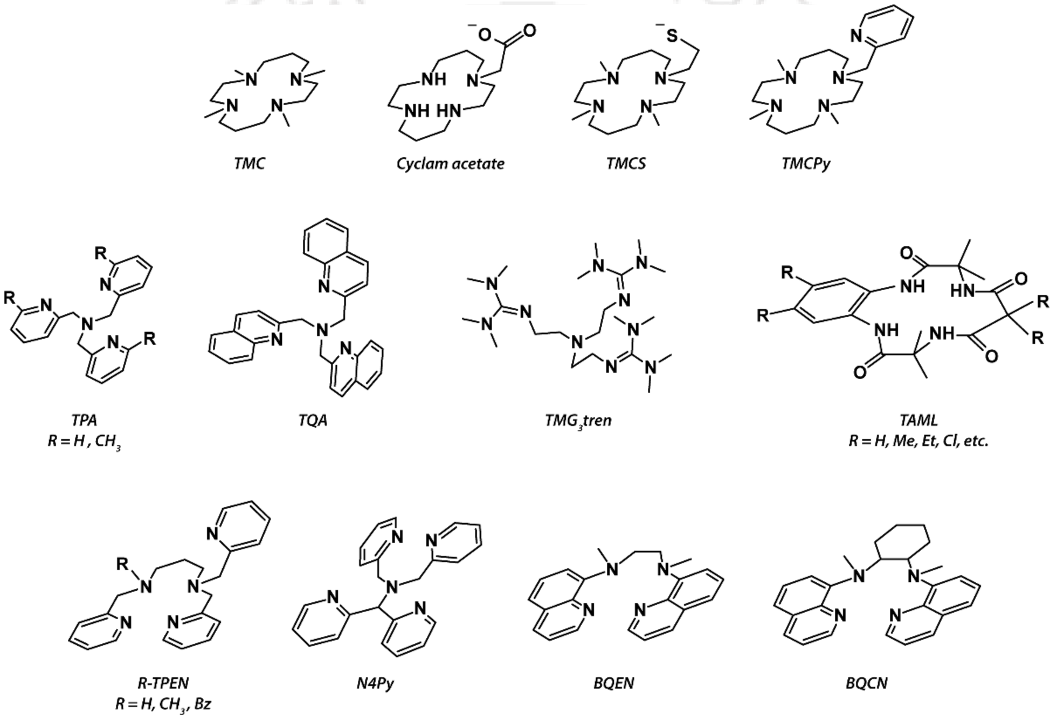

Fig. 1.7. Ligand frameworks discussed above that can stabilize high valent iron-oxo complexes.

1.4.2. Iron(III)-hydroperoxo and Iron(III)-alkylperoxo Mimics

Hydrogen peroxide is formed by two-electron/two-proton reduction of dioxygen or of water can exhibit amphoteric properties, *i.e.* it can exhibit electron donor properties (reduction) and also electron acceptor properties (oxidation) to produce O_2 and H_2O respectively.[147,148] This hydrogen peroxide when reacts with Fe-complex in a methanolic solution, forms an end-on Fe(III)-hydroperoxide complex. These species are also termed as the 'second electrophilic oxidant' in many oxygenation reactions.[149-157] Abstraction of the terminal proton of the -OOH adduct in the presence of base, generates a side-on peroxo moiety.[158] However, in biomimetic chemistry, the iron(III)-hydroperoxides were known to be sluggish oxidants towards various oxidation reactions.[159] Later however halide oxidation abilities of ferric hydroperoxides were tested to be positive.[160,161] In enzymatic reactions, the formation of metal-hydroperoxo intermediates is proposed to be formed in HAT reactions of metal-superoxo species, followed by the subsequent O–O bond cleavage to form metal-oxo species.[162-168] The iron(III)-hydroperoxo complex $[Fe^{III}(14\text{-}TMC)(OOH)]^{2+}$ complex was formed by protonation of the iron(III)-peroxo complex $[Fe^{III}(14\text{-}TMC)(O_2)]^{+}$ *via* a metastable side-on protonated intermediate. The $[Fe^{III}(14\text{-}TMC)(OOH)]^{2+}$ is then converted to the corresponding iron(IV)-oxo complex $[Fe^{IV}(O)(14\text{-}TMC)]^{2+}$ by the homolysis of the O–O bond.[169]

The iron(III)-alkylperoxo species has been reported to be involved in the biological reactions of homoprotocatechuate-2,3-dioxygenase and purple lipoxygenase.[170,171] Model systems of synthetic iron(III)-alkylperoxo complexes have been prepared and studied. These systems provided significant mechanistic insights into the catalytic reactions of iron-containing enzymes.[172-180] However, unlike other metal-alkylperoxido complexes, synthetic model systems of Fe(III)-alkylperoxide moieties have been reported to be sluggish oxidants towards a variety of organic substrates.[181] The reluctance towards reactivity with organic substrates originates from the competitive cleavage of the O-O bond, resulting in the in situ formation of iron(IV)-oxo complexes that are reactive towards electrophilic reactions. In fact, the presence of an exogenous Lewis base like pyridine N-oxide or thiocyanate is known to accelerate the conversion of Fe(III)-OOR to Fe(IV)-oxo by a ‘push effect’ on the homolytic O-O cleavage for heme and non-heme enzymatic models.[182,183] These additives act as the sixth proximal ligand in the Fe(III)-OOR adducts with tetradentate ligands that typically promote the scission of the O-O bond.[184,185] Although a number of ferric alkylperoxo systems have been reported among the synthetic models, most of their studies have been limited to successful characterization.[128,172-178,185-200] The spin state of the metal centre is known to play a pivotal role in determining the reaction pathway by modulating the bond strength of Fe-O and O-O bonds.[197] Quantum-chemical calculations (generally density functional theory, DFT) have led to the conclusion that the high-spin Fe(III)-alkylperoxido complexes preferentially cleave the Fe-O bond, while low-spin Fe(III)-OOR contains an activated O-O bond and eventually undergoes homolytic O-O bond scission.[90,178]

1.4.3. Manganese(III)-Peroxo Mimics

Manganese centres react with oxygen and its reduced derivatives play important roles in biological systems, including the detoxification of superoxide and hydrogen peroxide and the bioremediation of aromatics.[92,100,201-203] Many synthetic Mn(III)-peroxo intermediates have been generated by oxidizing Mn(II) complexes with hydrogen peroxide or potassium superoxide.[204-210] However, the interaction of dioxygen to form a high-spin ($S = 2$) peroxomanganese(III) complex has also been reported. It was reported to react with aldehydes.[211] Generally an O-O bond length of around 1.40 Å is found for the peroxo moieties.[205,207,209] Using TMC ligand framework, Nam and co-workers have shown the formation of peroxomanganese(III) species, $[Mn^{III}(O_2)(TMC)]^+$ using 5 equivalents of H_2O_2 in the presence of base triethylamine (TEA) at 25 °C.[207] This complex was unusually stable probably due to steric crowding around the peroxo group from the N-methyl substituents of the TMC macrocycle. A series of peroxomanganese(III) complexes supported by aminopyridyl ligands were synthesized using H_2O_2/TEA or KO_2 in acetonitrile at -40 °C.[210] Such Mn(III)-peroxo complexes could also be generated electrochemically.[212] The reactivity profiles of these intermediates were studied previously and aldehyde deformylation is a standard reaction exercised by these peroxomanganese complexes. However, most of these complexes were reported to perform the same reaction in a nucleophilic fashion.[213-218] By tuning the axial ligation using a series of axial ligands (X) like CN^-, NCS^-, $CF_3CO_2^-$, and N_3^- in $[Mn^{III}(O_2)(13\text{-TMC})(X)]^+$, the rates of aldehyde deformylation could be controlled and varied with X by three orders of magnitude.[219]

1.5. Scope and Aim of the Thesis

As evident from the comprehensive literature survey delineated above, exploring the lucrative field of non-heme enzymomimetic chemistry seems very promising. Nature provides us with a plethora of diversely functional metalloenzymes that operates through successfully tuned and manifested reaction cycles. Researchers feel obligated to study and mimic these flawless molecular machines and reproduce their performance, although, over the decades of extensive research, artificially built molecular models of these metalloenzymes could achieve very little of what the natural ones are enriched with. The stability factor, phase issues, selectivity problems, turnover numbers and characterization of the intermediate species inflict tough challenges to the research community. Subtle modifications in the primary and secondary coordination spheres can lead to drastic changes in stability, spin states, reactivity and other structural aspects of these synthetic models. This thesis is a small contribution to the huge literature of non-heme mononuclear enzymomimetic model systems and their structure-function relationships. Models of pentadentate N5 donor ligand sets have been synthesized and complexes of iron and manganese followed. These Fe/Mn complexes were precursors to a number of different high valent reaction intermediates. These intermediates play crucial roles in the catalytic cycles of many metalloenzymes. In order to stabilize these metal intermediates, special attention was given in designing the ligand scaffolds, that were, in fact, primary reasons behind the unorthodox reactivity trends. Reaction conditions were moderated using suitable organic substrates to manoeuvre reaction kinetics. Mechanistic probes were employed and procedures were customized to ascertain intriguing reaction mechanisms in this study. Chapter-II describes the usage of reagents, solvents, oxidants and the synthetic procedures of different ligand frameworks, metal complexes. Also, their spectroscopic characterizations have been discussed. Chapter-III depicts the effect of equatorial ligand field perturbations on the reactivity of a new iron(IV)-oxo complex. Subtle modifications in the ligand framework resulted in dramatic changes in the reaction rates towards OAT and HAA reactions. Chapter-IV analyses the influence of steric and electronic factors on the reactivity of the iron(IV)-oxo complexes. Using a benchmark of new and existing complexes, this study focussed on the substrate approach trajectory and factors that influence the same. Chapter-V reveals a novel mechanism of aldehyde deformylation reactions by Mn(III)-peroxo complexes. Unlike the traditional nucleophilic attack at the carbonyl centre, an electrophilic C-H abstraction initiates the deformylation reaction. Finally, Chapter-VI provides the first example of amphoteric reactivity of iron(III)-alkylperoxo complex towards both electrophilic and nucleophilic reactions.

1.6. References

1. J. M. McCord, *Am. J. Med.* **2000**, *108*, 652-659.
2. J. M. McCord, *J. Nutr.* **2004**, *134*, 3171S-3172S.
3. R. Y. N. Ho, J. F. Liebman, J. S. Valentine, In *Active Oxygen in Biochemistry*, J. S. Valentine, C. S. Foote, A. Greenberg, J. F. Liebman, Ed.; Chapman & Hall, New York, **1995**, Vol. 3, pp. 1-36.
4. J. M. McCord, *Semin Hematol*, **1998**, *35*, 5-12.
5. H. Otani, M. Umemoto, K. Kagawa, Y. Nakamura, K. Omoto, K. Tanaka, T. Sato, A. Nonoyama, T. Kagawa, *J. Surg. Res.* **1986**, *41*, 126-133.
6. I. Fridovich, *Annu. Rev. Pharmacol. Toxicol.* **1983**, *23*, 239-257.
7. I. Fridovich, *J. Exp. Biol.* **1998**, *201*, 1203-1209.
8. F. Auchère, F. Rusnak, *J. Biol. Inorg. Chem.* **2002**, 7, 664-667.
9. I. Bertini, H. B. Gray, E. I. Stiefel, S. J. Valentine, *Biological Inorganic Chemistry: Structure and Reactivity*. University Science Books, Sausalito, California, **2007**.
10. L. Que, Jr., *Acc. Chem. Res.* **2007**, *40*, 493-500.
11. H. B. Kraatz, N. Metzler-Nolte, *Concepts and Models in Bioinorganic Chemistry*. Wiley-VCH, Weinheim, **2006**.
12. F. A. Cotton, G. Wilkinson, C. A. Murillo, M. Bochmann, Copper: Group 11. In *Advanced Inorganic Chemistry*, 6th Ed. John Wiley and Sons, New York, **1999**.
13. M. Sono, M. P. Roach, E. D. Coulter, J. H. Dawson, *Chem. Rev.* **1996**, *96*, 2841-2887.
14. *Cytochrome P-450: Structure, Mechanism and Biochemistry*, P. R. Oritz de Montellano, Ed. Plenum Press, New York, **1995**.
15. W. D. Hewson, L. P. Hager, *Porphyrins*, **1979**, *7*, 295-298.

16. C. E. Shultz, P. W. Devaney, H. Winkler, P. G. Derunner, N. Doan, R. Chiang, R. Rutter, L. P. Hager, *FEBS Lett.* **1979**, *103*, 102-105.
17. I. Yamakai, In *Molecular Mechanisms of Oxygen Activation*, O. Hayashi, Ed.; Academic Press, New York, **1974**.
18. J. T. Groves, *J. Chem. Ed.* **1985**, *62*, 928-931.
19. J. T. Groves, Y.-Z. Han, In *Cytochrome P-450: Structure, Mechanism and Biochemistry*, P. R. Oritz de Montellano, Ed. Plenum Press, New York, **1995**, pp. 3-48.
20. S. Jin, T. M. Makris, T. A. Bryson, S. G. Sligar, J. H. Dawson, *J. Am. Chem. Soc.* **2003**, *125*, 3406-3407.
21. I. G. Denisov, T. M. Makris, S. G. Sligar, I. Schlichting, *Chem. Rev.* **2005**, *105*, 2253-2277.
22. F. Ogliaro, S. P. de Visser, S. Shaik, *J. Inorg. Biochem.* **2002**, *91*, 554-567.
23. D. L. Harris, G. H. Loew, *J. Am. Chem. Soc.* **1998**, *120*, 8941-8948.
24. D. L. Harris, G. H. Loew, *J. Am. Chem. Soc.* **1996**, *118*, 6377-6387.
25. M. T. Green, J. H. Dawson, H. B. Gray, *Science*, **2004**, *304*, 1653-1656.
26. J. T. Groves, In *Cytochrome P450: Structure, Mechanism, and Biochemistry*; 3rd ed.; P. R. Ortiz de Montellano, Ed.; Plenum Publishers: New York, **2005**, pp. 1-43.
27. M. Newcomb, M.-H. Le Tadic, D. A. Putt, P. F. Hollenberg, *J. Am. Chem. Soc.* **1995**, *777*, 3312-3313.
28. V. W. Dowry, K. U. Ingold, *J. Am. Chem. Soc.* **1991**, *113*, 5699-5707.
29. M. Filatov, N. Harris, S. Shaik, *Angew. Chem. Int. Ed. Engl.* **1999**, *38*, 3510-3512.
30. F. Ogliaro, N. Harris, S. Cohen, M. Filatov, S. P. deVisser, S. Shaik, *J. Am. Chem. Soc.* **2000**, *122*, 8977-8989.

31. T. M. Makris, K. von Koenig, I. Schlichting, S. G. Sligar, *Journal of Inorganic Biochemistry*, **2006**, *700*, 507-518.
32. C. A. Bonagura, B. Bhaskar, H. Shimizu, H. Li, M. Sundaramoorthy, D. E. McRee, D. B. Goodin, T. L. Poulos, *Biochemistry*, **2003**, *42*, 5600-5608.
33. S. L. Edwards, X. Nguyen-Huu, R. C. Hamlin, J. Kraut, *Biochemistry*, **1987**, *26*, 1503-1511.
34. H. Erlandsen, E. Bjorgo, T. Flatmark, R. C. Stevens, *Biochemistry*, **2000**, *39*, 2208-2217.
35. E. I. Solomon, E. G. Pavel, K. E. Loeb, C. Campochiaro, *Coordination Chemistry Reviews*, **1995**, *144*, 369-460.
36. J. M. Elkins, M. J. Ryle, I. J. Clifton, J. C. Dunning Hotopp, J. S. Lloyd, N. I. Burzlaff, J. E. Baldwin, R. P. Hausinger, P. L. Roach, *Biochemistry*, **2002**, *41*, 5185-5192.
37. A. Karlsson, J. V. Parales, R. E. Parales, D. T. Gibson, H. Eklund, S. Ramaswamy, *Science*, **2003**, *299*, 1039-1042.
38. P. L. Roach, I. J. Clifton, V. Fulop, K. Harlos, G. J. Barton, J. Hajdu, I. Andersson, C. J. Schofield, J. E. Baldwin, *Nature*, **1995**, *375*, 700-704.
39. J. Choi, J. K. Chon, S. Kim, W. Shin, *Proteins: Structure, Function, and Bioinformatics*, **2008**, *70*, 1023-1032.
40. S. A. Gillmor, A. Villasenor, R. Fletterick, E. Sigal, M. F. Browner, *Nature Structural & Molecular Biology*, **1991**, *4*, 1003-1009.
41. T. J. Kappock, J. P. Caradonna, *Chemical Reviews*, **1996**, *96*, 2659-2756.
42. R. P. Hausinger, *Critical Reviews in Biochemistry and Molecular Biology*, **2004**, *39*, 21-68.
43. L. P. Wackett, *Enzyme and Microbial Technology*, **2002**, *37*, 577-587.
44. T. D. H. Bugg, *Tetrahedron*, **2003**, *59*, 7075-7101.
45. J. E. Baldwin, M. Bradley, *Chem. Rev.* **1990**, *90*, 1079-1088.

46. W. Ge, I. J. Clifton, J. E. Stok, R. M. Adlington, J. E. Baldwin, P. J. Rutledge, *J. Am. Chem. Soc.* **2008**, *130*, 10096-10102.
47. J. C. Price, E. W. Barr, B. Tirupati, J. M. Bollinger Jr., C. Krebs, *Biochemistry*, **2003**, *42*, 7497-7508.
48. J. M. Bollinger, Jr., J. C. Price, L. M. Hoffart, E. W. Barr, C. Krebs, *Eur. J. Inorg. Chem.* **2005**, 4245-4254.
49. Y.-M. Chiou, L. Que, Jr., *J. Am. Chem. Soc.* **1995**, *117*, 3999-4013.
50. E. H. Ha, R. Y. N. Ho, J. F. Kisiel, J. S. Valentine, *Inorg. Chem.* **1995**, *34*, 2265-2266.
51. E. L. Hegg, R. Y. N. Ho, L. Que, Jr., *J. Am. Chem. Soc.* **1999**, *121*, 1972-1973.
52. H. M. Hanauske-Abel, V. Günzler, *Theor. Biol.* **1982**, *94*, 421-455.
53. C. Krebs, J. C. Price, J. Baldwin, L. Saleh, M. T. Green, J. M. Bollinger, Jr., *Inorg. Chem.* **2005**, *44*, 742-757.
54. K. P. McCusker, J. P. Klinman, *Proc. Natl. Acad. Sci.* **2009**, *106*, 19791-19795.
55. R. J. Balahura, A. Sorokin, J. Bernadou, B. Meunier, *Inorg. Chem.* **1997**, *36*, 3488-3492.
56. M. Costas, *Coord. Chem. Rev.* **2011**, *255*, 2912-2932.
57. J. S. Lazo, B. A. Chabner, *Cancer Chemotherapy and Biotherapy: Principles and Practice*, 2nd ed., Lippincott Raven, Philadelphia, PA, **1996**.
58. J. Stubbe, J. W. Kozarich, *Chem. Rev.* **1987**, *87*, 1107-1136.
59. J. Stubbe, J. W. Kozarich, W. Wu, D. E. Vanderwall, *Acc. Chem. Res.* **1996**, *29*, 322-330.
60. F. Hutchinson, L. F. Povirk, *Bleomycin: Chemical, Biochemical, and Biological Aspects*, Springer-Verlag, New York, **1979**.

61. E. A. Sausville, 1. Peisach, S. B. Horwitz, *Biochemistry*, **1978**, *17*, 2740-2746.
62. M. Chikira, T. Iiyama, K. Sakamoto, W. E. Antholine, D. H. Petering, *Inorg. Chem.* **2000**, *39*, 1779-1786.
63. R. M. Burger, *Struct. Bonding*, **2000**, *97*, 287-303.
64. K. E. Loeb, J. M. Zaleski, C. D. Hess, S. M. Hecht, E. I. Solomon, *J. Am. Chem. Soc.* **1998**, *120*, 1249-1259.
65. J. W. Sam, X.-J. Tang, J. Peisach, *J. Am. Chem. Soc.* **1994**, *116*, 5250-5256.
66. Y. Sugiura, *J. Am. Chem. Soc.* **1980**, *102*, 5208-5215.
67. K. E. Loeb, J. M. Zaleski, T. E. Westre, R. J. Guajardo, P. K. Mascharak, B. Hedman, K. O. Hodgson, E. I. Solomon, *J. Am. Chem. Soc.* **1995**, *117*, 4545-4561.
68. R. M. Burger, J. Peisach, S. B. Horwitz, *J. Biol Chem.* **1981**, *256*, 11636-11644.
69. I. W. Sam, X.-J. Tang, J. Peisach, *J. Am. Chem. Soc.* **1994**, *116*, 5250-5256.
70. F. Neese, J. M. Zaleski, K. L. Zaleski, E. I. Solomon, *J. Am. Chem. Soc.* **2000**, *122*, 11703-11724.
71. T. E. Westre, K. E. Loeb, J. M. Zaleski, B. Hedman, K. O. Hodgson, E. I. Solomon, *J. Am. Chem. Soc.* **1995**, *117*, 1309-1313.
72. R. M. Burger, T. A. Kent, S. B. Horwitz, E. Münck, J. Peisach, *J. Biol. Chem.* **1983**, *258*, 1559-1564.
73. R. J. Guajardo, S. E. Hudson, S. J. Brown, P. K. Mascharak, *J. Am. Chem. Soc.* **1993**, *115*, 7971-7977.
74. R. J. Guajardo, J. D. Tan, P. K. Mascharak, *Inorg. Chem.* **1994**, *33*, 2838-2840.
75. R. J. Guajardo, F. Chavez, E. T. Farinas, P. K. Mascfaarak, *J. Am. Chem. Soc.* **1995**, *117*, 3883-3884.

76. A. Kittaka, Y. Sugano, M. Otsuka, Y. Sugiura, H. Umezawa, *Tetrahedron Lett.* **1986**, *27*, 3631-3634.
77. H. Kurosaki, K. Hayashi, Y. Ishikawa, M. Goto, K. kiada, I. Taniguchi, M. Shionoya, E. Kimura, *Inorg. Chem.* **1999**, *38*, 2824-2832.
78. G. Roelfes, M. Lubben, K. Chen, R. Y. N. Ho, A. Meetsma, S. Genseberger, R. M. Hermant, R. Hage, S. K. Mandal, V. G. Young, Jr., Y. Zang, H. Kooijman, A. L. Spek, L. Que, Jr., B. L. Feringa, *Inorg. Chem.* **1999**, *38*, 1929-1936.
79. R. Y. N. Ho, G. Roelfes, B. L. Feringa, L. Que, Jr., *J. Am. Chem. Soc.* **1999**, *121*, 264-265.
80. G. Roelfes, Y. Vrajmisu, K. Chen, R. Y. N. Ho, J.-U. Rohde, C. Zondervan, R. M. la Crois, E. P. Schudde, M. Lutz, A. L. Spek, R. Hage, B. L. Feringa, E. Münck, L. Que, Jr., *Inorg. Chem.* **2003**, *42*, 2639-2653.
81. M. Lubben, A. Meetsma, E. C. Wilkinson, B. Feringa, L. Que, Jr., *Angew. Chem. Int. Ed. Engl.* **1995**, *34*, 1512-1514.
82. I. Bernal, I. M. Jensen, K. B. Jensen, C. J. McKenzie, H. Toftlund, J. P. Tuchagues, *J. Chem. Soc., Dalton Trans.* **1995**, 3667-3675.
83. A. J. Simaan, S. Dopner, F. Banse, S. Bourcier, G. Bouchoux, A. Boussac, P. Hildebrandt, J.-J. Girerd, *Eur. J. Inorg. Chem.* **2000**, 1627-1633.
84. P. Mialane, A. Nivorojkine, G. Pratviel, L. Azema, M. Slany, F. Godde, A. Simaan, F. Banse, T. Kargar-Grisel, G. Bouchoux, J. Sainton, O. Homer, J. Guilhem, L. Tchertanova, B. Meunier, J.-J. Girerd, *Inorg. Chem.* **1999**, *38*, 1085-1092.
85. A. J. Simaan, F. Banse, J.-J. Girerd, K. Wieghardt, E. Bill, *Inorg. Chem.* **2001**, *40*, 6538-6540.
86. A. Hazell, C. J. McKenzie, L. P. Nielsen, S. Schindler, M. Weitzer, *J. Chem. Soc. Dalton Trans.* **2002**, 310-317.

87. P. Comba, M. Kerscher, *Cryst. Eng*. **2003**, *6*, 197-211.
88. P. Comba, W. Schiek, *Coord. Chem. Rev.* **2003**, *238-239*, 21-29.
89. P. Comba, M. Kerscher, M. Merz, V. Müller, H. Pritzkow, R. Remenyi, W. Schiek, Y. Xiong, *Chem. Eur. J.* **2002**, *8*, 5750-5760.
90. P. Comba, M. Kerscher, K. Rück, M. Starke, *Dalton. Trans*. **2018**, *47*, 9202-9220.
91. L. Vaska, *Acc. Chem. Res*. **1975**, *9*, 175-183.
92. A. J. Wu, J. E. Penner-Hahn, V. L. Pecoraro, *Chem. Rev*. **2004**, *104*, 903-938.
93. A. F. Miller, *Superoxide processing, In Comprehensive Coordination Chemistry II*; Elsevier Ltd: Oxford, UK., **2004**.
94. J. P. Emerson, E. G. Kovaleva, E. R. Farquhar, J. D. Lipscomb, L. Que, Jr., *Proc. Natl. Acad. Sci*. **2008**, *105*, 7347-7352.
95. J. A. Cotruvo, J. Stubbe, *Biochemistry*, **2010**, *49*, 1297-1309.
96. A. Willing, H. Follmann, G. Auling, *Eur. J. Biochem*. **1988**, *170*, 603-611.
97. V. L. Pecoraro, W. Y. Hsieh, *Inorg. Chem*. **2008**, *47*, 1765-1778.
98. P. M. Wood, *Trends in Biochemical Sciences*, **1987**, *12*, 250-251.
99. T. A. Jackson, T. C. Brunold, *Acc. Chem. Res*. **2004**, *37*, 461-470.
100. W. A. Gunderson, A. I. Zatsman, J. P. Emerson, E. R. Farquhar, L. Que, Jr., J. D. Lipscomb, M. P. Hendrich, *J. Am. Chem. Soc*. **2008**, *130*, 14465-14467.
101. J.-J. Girerd, F. Banse, A. J. Simaan, *Struct. Bonding*, **2000**, *97*, 145-177.
102. J.-U. Rohde, M. R. Bukowski, L. Que, Jr., *Curr. Op. Chem. Biol.* 2003.
103. D. A. Proshlyakov, T. F. Henshaw, G. R. Monterosso, M. J. Ryle, R. P. Hausinger, *J. Am. Chem. Soc*. **2004**, *126*, 1022-1023.
104. C. A. Grapperhaus, B. Mienert, E. Bill, T. Weyhermtiller, K. Wieghardt, *Inorg. Chem*. **2000**, *39*, 5306-5317.

105. J.-U. Rohde, J.-H. In, M. H. Lim, W. W. Brennessel, M. R. Bukowski, A. Stubna, E. Münck, W. Nam, L. Que, Jr., *Science*, **2003**, *299*, 1037-1039.
106. M. H. Lim, J.-U. Rohde, A. Stubna, M. R. Bukowski, M. Costas, R. Y. N. Ho, E. Münck, W. Nam, L. Que, Jr., *Proc. Natl. Acad. Sci. USA*, **2003**, *100*, 3665-3670.
107. J. Kaizer, E. J. Klinker, N. Y. Oh, J.-U. Rohde, W. J. Song, A. Stubna, J. Kim, W. Nam, E. Münck, L. Que, Jr., *J. Am. Chem. Soc.* **2004**, *126*, 472-473.
108. V. Balland, M.-F. Chariot, F. Banse, J.-J. Girerd, T. A. Mattioli, E. Bill, J.-F. Bartoli, P. Battioni, D. Mansuy, *Eur. J. Inorg. Chem.* **2004**, 301-308.
109. J.-U. Rohde, L. Que, Jr., *Angew. Chem. Int. Ed.* **2005**, *44*, 2255-2258.
110. J. T. Groves, J. T. In *Cytochrome P450: Structure, Mechanism, and Biochemistry*; 3rd ed.; Ortiz de Montellano, P. R., Ed.; Plenum Publishers: New York, **2005**, p 1-43.
111. J. T. Groves, T. E. Nemo, R. S. Myers, *J. Am. Chem. Soc.* **1979**, *101*, 1032–1033.
112. B. Meunier, *Chem. Rev.* **1992**, *92*, 1411–1456.
113. R. A. Leising, R. E. Norman, L. Que, Jr., *Inorg. Chem.* **1990**, *29*, 2553–2555.
114. R. A. Leising, B. A. Brennan, L. Que, Jr., B. G. Fox, E. Münck, *J. Am. Chem. Soc.* **1991**, *113*, 3988–3990.
115. T. Kojima, R. A. Leising, S. Yan, L. Que, Jr., *J. Am. Chem. Soc.* **1993**, *115*, 11328–11335.
116. R. A. Leising, J. Kim, M. A. Pérez, L. Que, Jr., *J. Am. Chem. Soc.* **1993**, 115, 9524–9530.
117. Y. Hitomi, S. Furukawa, M. Higuchi, T. Shishido, T. Tanaka, *J. Mol. Catal. A: Chem.* **2008**, *288*, 83–86.

118. H. Jaafar, B. Vileno, A. Thibon, D. Mandon, *Dalton Trans.* **2011**, *40*, 92–106

119. A. Mairata i Payeras, R. Y. N. Ho, M. Fujita, L. Que, Jr., *Chem. –Eur. J.* **2004**, *10*, 4944–4953.

120. M. Klopstra, G. Roelfes, R. Hage, R. M. Kellogg, B. L. Feringa, *Eur. J. Inorg. Chem.* **2004**, 846–856.

121. C. A. Grapperhaus, B. Mienert, E. Bill, T. Weyhermüller, K. Wieghardt, *Inorg. Chem.* **2000**, *39*, 5306-5317.

122. C. V. Sastri, J. Lee, K. Oh, Y. J. Lee, J. Lee, T. A. Jackson, K. Ray, H. Hirao, W. Shin, J. A. Halfen, J. Kim, L. Que, Jr., S. Shaik, W. Nam, *Proc. Natl. Acad. Sci.* **2007**, *104*, 19181-19186.

123. S. A. Wilson, J. Chen, S. Hong, Y.-M. Lee, M. Clémancey, R. Garcia-Serres, T. Nomura, T. Ogura, J.-M. Latour, B. Hedman, K. O. Hodgson, W. Nam, E. I. Solomon, *J. Am. Chem. Soc.* **2012**, *134*, 11791−11806.

124. M. H. Lim, J.–U. Rohde, A. Stubna, M. R. Bukowski, M. Costas, R. Y. N. Ho, E. Münck, W. Nam, L. Que, Jr., *Proc. Natl. Acad. Sci. USA.* **2003**, *100*, 3665–3670.

125. M. R. Bukowski, K. D. Koehntop, A. Stubna, E. L. Bominaar, J. A. Halfen, E. Münck, W. Nam, L. Que, Jr., *Science*, **2005**, *310*, 1000–1002.

126. J. Kaizer, M. Costas and L. Que, Jr., *Angew. Chem. Int. Ed.* **2003**, *42*, 3671–3673.

127. M. Martinho, F. Banse, J.–F. Bartoli, T. A. Mattioli, P. Battioni, O. Horner, S. Bourcier, J.–J. Girerd, *Inorg. Chem.* **2005**, *44*, 9592–9596.

128. T. K. Paine, M. Costas, J. Kaizer, L. Que, Jr., *J. Biol. Inorg. Chem.* **2006**, *11*, 272–276.

129. O. Pestovsky, S. Stoian, E. Bominaar, X. Shan, E. Münck, L. Que, Jr., A. Bakac, *Angew. Chem. Int. Ed.* **2005**, *44*, 6871–6874.

130. C. V. Sastri, M. S. Seo, M. J. Park, K. M. Kim, W. Nam, *Chem. Commun.* **2005**, 1405–1407.

131. J. Bautz, M. R. Bukowski, M. Kerscher, A. Stubna, P. Comba, A. Lienke, E. Münck, L. Que, Jr., *Angew. Chem. Int. Ed*. **2006**, *45*, 5681–5684.

132. J. England, Y. Guo, E. R. Farquhar, V. G. Young Jr., E. Münck, L. Que, Jr., *J. Am. Chem. Soc.* **2010**, *132*, 8635–8644.

133. M. S. Seo, N. H. Kim, K.-B. Cho, J. E. So, S. K. Park, M. Clémancey, R. G. Serres, J.-M. Latour, S. Shaik, W. Nam, *Chem. Sci.* **2011**, *2*, 1039–1045.

134. D. Janardanan, Y. Wang, P. Schyman, L. Que, Jr., S. Shaik, *Angew. Chem. Int. Ed.* **2010**, *49*, 3342 –3345.

135. A. N. Biswas, M. Puri, K. K. Meier, W. N. Oloo, G. T. Rohde, E. L. Bominaar, E. Münck, L. Que, Jr., *J. Am. Chem. Soc.* **2015**, *137*, 2428–2431.

136. C. E. Macbeth, A. P. Golombek, V. G. Young Jr, C. Yang, K. Kuczera, M. P. Hendrich, A. S. Borovik, *Science*, **2000**, *289*, 938–941.

137. J. England, M. Martinho, E. R. Farquhar, J. R. Frisch, E. L. Bominaar, E. Münck, L. Que, Jr., *Angew. Chem. Int. Ed.* **2009**, *48*, 3622–3626.

138. J. P. Bigi, W. H. Harman, B. Lassalle-Kaiser, D. M. Robles, T. A. Stich, J. Yano, R. D. Britt, C. J. Chang, *J. Am. Chem. Soc.* **2012**, *134*, 1536–1542.

139. F. Tiago de Oliveira, A. Chanda, D. Banerjee, X. Shan, S. Mondal, L. Que, Jr., E. Bominaar, E. Münck, T. J. Collins, *Science*, **2007**, *315*, 835–838.

140. T. J. Collins, A. D. Ryabov, *Chem. Rev.* **2017**, *117*, 9140-9162.

141. S. Hong, Y.-M. Lee, K.-B. Cho, K. Sundaravel, J. Cho, M. J. Kim, W. Shin, W. Nam, *J. Am. Chem. Soc.* **2011**, *133*, 11876−11879.

142. H. Hirao, L. Que, Jr., W. Nam, S. Shaik, *Chem. - Eur. J.* **2008**, *14*, 1740−1756.

143. S. Fukuzumi, Y. Morimoto, Y. Kotani, P. Naumov, Y.-M. Lee, W. Nam, *Nat. Chem.* **2010**, *2*, 756−759.

144. J. Park, Y. Morimoto, Y.-M. Lee, W. Nam, S. Fukuzumi, *J. Am. Chem. Soc.* **2011**, *133*, 5236−5239.

145. J. Park, Y. Morimoto, Y.-M. Lee, Y. You, W. Nam, S. Fukuzumi, *Inorg. Chem.* **2011**, *50*, 11612−11622.

146. J. Park, Y. Morimoto, Y.-M. Lee, W. Nam, S. Fukuzumi, *J. Am. Chem. Soc.* **2012**, *134*, 3903−3911.

147. M.R.A. Blomberg, *Biochemistry*, **2016**, *55*, 489-500.

148. S. Fukuzumi, Y.-M. Lee, W. Nam, *Chem. Eur. J.* **2018**, *24*, 5016-5031.

149. P. Hlavica, *Eur. J. Biochem.* **2004**, *271*, 4335–4360.

150. S. Jin, T. A. Bryson, J. H. Dawson, J. Biol. *Inorg. Chem.* **2004**, *9*, 644–653.

151. W. Nam, Y. O. Ryu, W. J. Song, *J. Biol. Inorg. Chem.* **2004**, *9*, 654–660.

152. S. Shaik, S. P. de Visser, D. Kumar, *J. Biol. Inorg. Chem.* **2004**, *9*, 661–668.

153. M. Newcomb, P. F. Hollenberg, M. J. Coon, *Biochem. Biophys.* **2003**, *409*, 72–79.

154. W. J. Song, Y. O. Ryu, R. Song, W. Nam, *J. Biol. Inorg. Chem.* **2005**, *10*, 294–304.

155. M. Newcomb, R. Shen, S.–Y. Choi, P. H. Toy, P. F. Hollenberg, A. D. N. Vaz, M. J. Coon, *J. Am. Chem. Soc.* **2000**, *122*, 2677–2686.

156. P. H. Toy, M. Newcomb, M. J. Coon, A. D. N. Vaz, *J. Am. Chem. Soc.* **1998**, *120*, 9718–9719.

157. A. D. N. Vaz, D. F. Mc Ginnity, M. J. Coon, *Proc. Natl. Acad. Sci. U.S.A.* **1998**, *95*, 3555–3560.

158. M. R. Bukowski, P. Comba, C. Limberg, M. Merz, L. Que, Jr., T. Wistuba, *Angew. Chem. Int. Ed.* **2004**, *43*, 1283 –1283.

159. M. J. Park, J. Lee, Y. Suh, J. Kim, W. Nam, *J. Am. Chem. Soc.* **2006**, *128*, 2630-2634.

160. A. K. Vardhaman, C. V. Sastri, D. Kumar, S. P. de Visser, *Chem. Commun.* **2011**, *47*, 11044–11046.

161. A. K. Vardhaman, P. Barman, S. Kumar, C. V. Sastri, D. Kumar, S. P. de Visser, *Chem. Commun.* **2013**, *49*, 10926–10928.

162. P. L. Roach, I. J. Clifton, C. M. H. Hensgens, N. Shibata, C. J. Schofield, J. Hajdu, J. E. Baldwin, *Nature*, **1997**, *387*, 827-830.

163. K. Valegard, A. C. T. van Scheltinga, M. D. Lloyd, T. Hara, S. Ramaswamy, A. Perrakis, A. Thompson, H.-J. Lee, J. E. Baldwin, C. J. Schofield, J. Hajdu, I. Andersson, *Nature*, **1998**, *394*, 805-809.

164. N. I. Burzlaff, P. J. Rutledge, I. J. Clifton, C. M. H. Hensgens, M. Pickford, R. M. Adlington, P. L. Roach, J. E. Baldwin, *Nature*, **1999**, *401*, 721-724.

165. S. C. Peck, H. A. Cooke, R. M. Cicchillo, P. Malova, F. Hammerschmidt, S. K. Nair, W. A. van der Donk, *Biochemistry*, **2011**, *50*, 6598-6605.

166. L. M. Mirica, J. P. Klinman, *Proc. Natl. Acad. Sci. U.S.A.* **2008**, *105*, 1814-1819.

167. W. A. van der Donk, C. Krebs, J. M. Bollinger Jr., *Curr. Opin. Struct. Biol.* **2010**, *20*, 673-683.

168. J. M. Bollinger Jr., C. Krebs, *Curr. Opin. Chem. Biol.* **2007**, *11*, 151-158.

169. J. Cho, S. Jeon, S. A. Wilson, L. V. Liu, E. A. Kang, J. J. Braymer, M. H. Lim, B. Hedman, K. O. Hodgson, J. S. Valentine, E. I. Solomon, W. Nam, *Nature*, **2011**, *478*, 502-505.

170. E. G. Kovaleva, J. D. Lipscomb, *Science*, **2007**, *316*, 453-457.

171. E. Skrzypczak-Jankun, R. A. Bross, R. T. Carroll, W. R. Dunham, M. O. Funk Jr., *J. Am. Chem. Soc.* **2001**, *123*, 10814-10820.

172. N. Lehnert, R. Y. N. Ho, L. Que, Jr., E. I. Solomon, *J. Am. Chem. Soc.* **2001**, 123, 12802-12816.

173. N. Lehnert, R. Y. N. Ho, L. Que, Jr., E. I. Solomon, *J. Am. Chem. Soc.* **2001**, *123*, 8271-8290.

174. X. Shan, J.-U. Rohde, K. D. Koehntop, Y. Zhou, M. R. Bukowski, M. Costas, K. Fujisawa, L. Que, Jr., *Inorg. Chem.* **2007**, *46*, 8410-8417.

175. M. P. Jensen, A. Mariata i Payeras, A. T. Fiedler, M. Costas, J. Kaizer, A. Stubna, E. Münck, L. Que, Jr., *Inorg. Chem.* **2007**, *46*, 2398-2408.

176. S. Hong, Y.-M. Lee, K.-B. Cho, M. S. Seo, D. Song, J. Yoon, R. Garcia-Serres, M. Clémancey, T. Ogura, W. Shin, J.-M. Latour, W. Nam, *Chem. Sci*. **2014**, *5*, 156-162.

177. D. Krishnamurthy, G. D. Kasper, F. Namuswe, W. D. Kerber, A. A. N. Sarjeant, P. Moënne-Loccoz, D. P. Goldberg, *J. Am. Chem. Soc.* **2006**, *128*, 14222-14223.

178. F. Namuswe, G. D. Kasper, A. A. N. Sarjeant, T. Hayashi, C. M. Krest, M. T. Green, P. Moënne-Loccoz, D. P. Goldberg, *J. Am. Chem. Soc.* **2008**, *130*, 14189-14200.

179. J. Stasser, F. Namuswe, G. D. Kasper, Y. Jiang, C. M. Krest, M. T. Green, J. PennerHahn, D. P. Goldberg, *Inorg. Chem.* **2010**, *49*, 9178-9190.

180. F. Namuswe, T. Hayashi, Y. Jiang, G. D. Kasper, A. A. N. Sarjeant, P. MoënneLoccoz, D. P. Goldberg, *J. Am. Chem. Soc.* **2010**, *132*, 157-167.

181. M. S. Seo, T. Kamachi, T. Kouno, K. Murata, M. J. Park, K. Yoshizawa, W. Nam, *Angew. Chem. Int. Ed.* **2007**, *46*, 2291-2294.

182. K. Yamaguchi, Y. Watanabe, I. Morishima, *J. Am. Chem. Soc.* **1993**, *115*, 4058-4065.

183. S. Hong, L. Yong-Min, C. Kyung-Bin, M. S. Seo, D. Song, J. Yoon, R. Garcia-Serres, M. Clémancey, T. Ogura, W. Shin, J.-M. Latour, W. Nam, *Chem. Sci*. **2014**, *5*, 156-162.

184. M. Sono, M. P. Roach, E. D. Coulter, J. H. Dawson, *Chem. Rev*. **1996**, *96*, 2841-2887.

185. J. Kaizer, M. Costas, L. Que, Jr., *Angew. Chem. Int. Ed.* **2003**, *42*, 3671-3673.

186. M. Costas, M. P. Mehn, M. P. Jensen, L. Que, Jr., *Chem. Rev*. **2004**, *104*, 939-986.

187. T. Ogihara, S. Hikichi, M. Akita, T. Uchida, T. Kitigawa, Y. Moro-oka, *Inorg. Chem. Acta*, **2000**, *297*, 162-170.

188. A. P. Sobolev, D. E. Babushkin, E. P. Talsi, *J. Mol. Catal. A* **2000**, *159*, 233-245;

189. J. Kim, Y. Zang, M. Costas, R. G. Harrison, E. C. Wilkinson, L. Que, Jr., *J. Biol. Inorg. Chem*. **2001**, *6*, 275-284.

190. M. P. Jensen, S. J. Lange, M. P. Mehn, E. L. Que, L. Que, Jr., *J. Am. Chem. Soc*. **2003**, *125*, 2113-2128.

191. N. Lehnert, K. Fujisawa, E. I. Solomon, *Inorg. Chem*. **2003**, *42*, 469-481.

192. J.-U. Rohde, S. Torelli, X. Shan, M. H. Lim, E. J. Klinker, J. Kaizer, K. Chen, W. Nam, L. Que, Jr., *J. Am. Chem. Soc*. **2004**, *126*, 16750-16761.

193. M. P. Jensen, M. Costas, R. Y. N. Ho, J. Kaizer, A. Mariata i Payeras, E. Münck, L. Que, Jr., J.-U. Rohde, A. Stubna, *J. Am. Chem. Soc*. **2005**, *127*, 10512-10525.

194. J. Bautz, P. Comba, L. Que, Jr., *Inorg. Chem*. **2006**, *45*, 7077-7082.

195. S. Ménage, E. C. Wilkinson, L. Que, Jr., M. Fontecave, *Angew. Chem. Int. Ed*. **1995**, *34*, 203-205.

196. S. Bang, S. Park, Y.-M. Lee, S. Hong, K.-B. Cho, W. Nam, *Angew. Chem. Int. Ed.* **2014**, *53*, 7843-7847.

197. J. J. Girerd, F. Banse, A. J. Simaan, *Struct. Bonding (Berlin)*, **2000**, *97*, 145-177.

198. L. R. Widger, Y. Jiang, A. C. McQuilken, T. Yang, M. A. Siegler, H. Matsumura, P. Moënne-Loccoz, D. Kumar, S. P. de Visser, D. P. Goldberg, *Dalton Trans*. **2014**, *43*, 7522-7532.

199. Y. Zang, J. Kim, Y. Dong, E. C. Wilkinson, E. H. Appelman, L. Que, Jr., *J. Am. Chem. Soc*. **1997**, *119*, 4197-4205.

200. M. R. Bukowski, H. L. Halfen, T. A. van den Berg, J. A. Halfen, L. Que, Jr., *Angew. Chem. Int. Ed*. **2005**, *44*, 584-587.

201. J. P. Emerson, E. G. Kovaleva, E. R. Farquhar, J. D. Lipscomb, L. Que, Jr., *Proc. Natl. Acad. Sci. U.S.A.* **2008**, *105*, 7347-7352.

202. L. E. Grove, T. C. Brunold, *Comments Inorg. Chem.* **2008**, *29*, 134-168.

203. A.-F. Miller, *Curr. Opin. Chem. Biol.* **2004**, *8*, 162-168.

204. S. Groni, G. Blain, R. Guillot, C. Policar, E. Anxolabéhére-Mallart, *Inorg. Chem*. **2007**, *46*, 1951−1953.

205. N. Kitajima, H. Komatsuzaki, S. Hikichi, M. Osawa, Y. Moro-oka, *J. Am. Chem. Soc*. **1994**, *116*, 11596−11597.

206. R. L. Shook, W. A. Gunderson, J. Greaves, J. W. Ziller, M. P. Hendrich, A. S. Borovik, *J. Am. Chem. Soc*. **2008**, *130*, 8888–8889.

207. M. S. Seo, J. Y. Kim, J. Annaraj, Y. Kim, Y.–M. Lee, S.–J. Kim, J. Kim, W. Nam, *Angew. Chem. Int. Ed.* **2007**, *46*, 377–380.

208. R. A. Geiger, S. Chattopadhyay, V. W. Day, T. A. Jackson, *Dalton Trans.* **2011**, *40*, 1707–1715.

209. R. B. VanAtta, C. E. Strouse, L. K. Hanson, J. S. Valentine, *J. Am. Chem. Soc*. **1987**, *109*, 1425–1434.

210. R. A. Geiger, S. Chattopadhyay, V. W. Day, T. A. Jackson, *J. Am. Chem. Soc.* **2010**, *132*, 2821–2831.

211. R. L. Shook, W. A. Gunderson, J. Greaves, J. W. Ziller, M. P. Hendrich, A. S. Borovik, *J. Am. Chem. Soc.* **2008**, *130*, 8888–8889.

212. S. E. Ghachtouli, H. Y. V. Ching, B. Lassalle-Kaiser, R. Guillot, D. F. Leto, S. Chattopadhyay, T. A. Jackson, P. Dorlet, E. Anxolabéhére-Mallart, *Chem. Commun.* **2013**, *49*, 5696–5698.

213. W. Nam, *Acc. Chem. Res.* **2007**, *40*, 522 – 531.

214. M. K. Coggins, J. A. Kovacs, *J. Am. Chem. Soc.* **2011**, *133*, 12470 – 12473.

215. M. K. Coggins, V. Martin-Diaconescu, S. DeBeer, J. A. Kovacs, *J. Am. Chem. Soc.* **2013**, *135*, 4260 – 4272.

216. H. E. Colmer, A. W. Howcroft, T. A. Jackson, *Inorg. Chem.* **2016**, *55*, 2055−2069.

217. J. Cho, R. Sarangi, W. Nam, *Acc. Chem. Res.* **2012**, *45*, 1321− 1330.

218. Q. Zhang, A. Bell-Taylor, F. M. Bronston, J. D. Gorden, C. R. Goldsmith, *Inorg. Chem.* **2017**, *56*, 773−782.

219. J. Annaraj, J. Cho, Y.-M. Lee, S. Y. Kim, R. Latifi, S. P. de Visser, W. Nam, *Angew. Chem. Int. Ed.* **2009**, *48*, 4150-4153.

CHAPTER – II

Synthesis and Characterization, Materials Employed and Methods Adapted

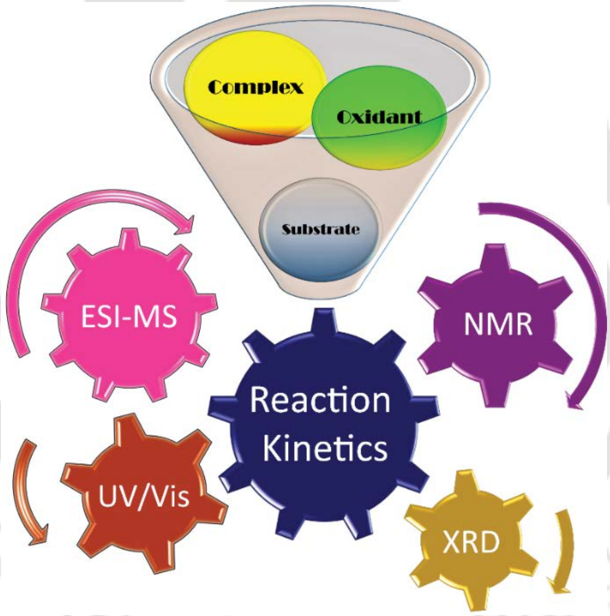

2.1. Introduction

The work presented herewith is an outcome of some meticulously designed experimental procedures and careful observations. A thorough analysis would categorically segregate each work into a set of tasks, *viz.* synthesis of the ligand frameworks, synthesis of the oxidants and substrates (if not commercially available), synthesis of the metal complexes, generation and stabilization of the metal intermediates, optimization of the reaction conditions, kinetic study, product analysis and finally interpretation and evaluation of the obtained results.

Proper safety measures were adopted before every experiment. Also, for flawless experimental results, careful scrutiny of the purity of the chemicals is a must. Procedures followed for the purification, synthesis, characterization and instrumentation is discussed in detail below.

2.2. Experimental Section

2.2.1. Solvents

Solvents were dried following published procedures[1] and distilled under argon before use. Acetonitrile (CH_3CN) was dried over Calcium hydride in a solvent still-head distillation apparatus fitted with a condenser on a heating mantle. A similar setup was followed for other solvents like THF and diethyl ether, although they were dried over sodium using benzophenone as an indicator. Solvents were collected from the solvent still-head distillation apparatus into dry glassware through a cannula using vacuum pumps. Glassware were extensively dried using either flame or kept inside hot oven for prolonged period of time before use.

2.2.2. Oxidants

Generation of the different types of reaction intermediates requires different types of oxidants (such as iodosylbenzene, peracetic acid, oxone, CAN, hydrogen peroxide, (Diacetoxyiodo)benzene, sodium chlorite, *tert*-butyl hydroperoxide, potassium superoxide, etc.) that react with the metal complexes. Some of the oxidants used herewith were purchased commercially while some of them were synthesized using previously reported procedures. The oxidants that were commercially available were (i) (Diacetoxyiodo)benzene ($PhI(OAc)_2$), (Aldrich Chemical Company) (ii) hydrogen peroxide (H_2O_2) (Merck) and (iii) *tert*-butyl hydroperoxide (*t*BuOOH) (Aldrich Chemical Company). Oxidant that was synthesized was PhIO.

Synthesis of Iodosylbenzene (PhIO): Iodosylbenzene was prepared by following a literature method.[2] 32.2 g (100 mM) of finely grounded (iodosobenzene)diacetate was placed in 250 mL beaker, then slowly 150 mL of NaOH solution (3 N) was added over a 5 minutes period with vigorous stirring. Then the lumps formed in the reaction mixture were ground for 15 minutes with glass rod and spatula and the reaction mixture was stirred for another 45 minutes to complete the reaction. Then 100 mL water was added to the reaction mixture, stirred vigorously and filtered through a Büchner funnel. The crude solid iodosylbenzene collected was returned to the beaker and triturated in 200 mL water. The solid was again collected by Büchner funnel, washed with 200 mL of water and dried over vacuum. Finally, it was triturated in 75 mL chloroform in a beaker, filtered, dried and stored in a cold and dark place. Experimental yield: 19 g; m.p. 210 °C (caution: potential explosive).

2.2.3. Substrates

Almost all the chemicals were procured from Sigma-Aldrich Chemical company, were in the best available purity and used without further purification unless otherwise stated. Thioanisole (THA) and its *para*-X-derivatives (X = -OMe, -Me, -Cl), dibenzothiophene (DBT), benzyl alcohol, fluorene, toluene, 1,4-cyclohexadiene (CHD), 2-phenylpropionaldehyde (2-PPA) and cyclohexanecarboxaldehye (CCA) were purchased from Aldrich Chemical company. Triphenylmethane and ethyl chloroformate (95%) were purchased from Avra Synthesis Pvt. Ltd. 9,10-Dihydroanthracene (DHA), ethylbenzene and cumene were obtained from TCI Chemicals Pvt. Ltd. $H_2{}^{18}O$ (99.9% pure, enrichment 97.1 atom %) was procured from Berry and Associates (Icon Isotopes). α-[D1]-2-phenylpropionaldehyde (~ 90 %, D enriched) was purchased from RVL Scientific & Engineering Pvt. Ltd. (Lucknow, India). Benzyl alcohol-D7, ethylbenzene-D10 and toluene-D8 were purchased from Cambridge Isotope Laboratories, Inc. Other deuterated solvents like $CDCl_3$, CD_3CN, D_2O, DMSO-D6 and CD_3OD were bought from Aldrich Chemical Company.

- *Synthesis of α-D-cyclohexanecarboxaldehyde (α-D-CCA)* :

The synthesis of α-D-cyclohexanecarboxaldehyde was accomplished by a slight modification to a reported procedure.[3,4] To a solution of cyclohexanecarboxaldehyde (17 mM) in D_2O (6 mL), DMAP (1.7 mM) was added and heated to refluxing conditions for 4 h. After cooling to room temperature the mixture was diluted with CH_2Cl_2 (20 mL). The organic layer was washed with 1M HCl (10 mL), saturated $NaHCO_3$ (10 mL) and brine (10 mL) successively. The reaction mixture was dried over anhydrous Na_2SO_4 and solvent evaporation under vacuum gave the resultant D-labelled crude product that was distilled by vacuum distillation using Kugelrohr Distillation apparatus to give the desired compound as a colourless liquid. (yield 65%). The purity was verified using ^{1}H-NMR spectroscopy to ensure 95% D-incorporation at the α-position. A comparative ^{1}H-NMR spectra of CCA and α-D-CCA is shown below. (Fig. 2.1, 2.2).

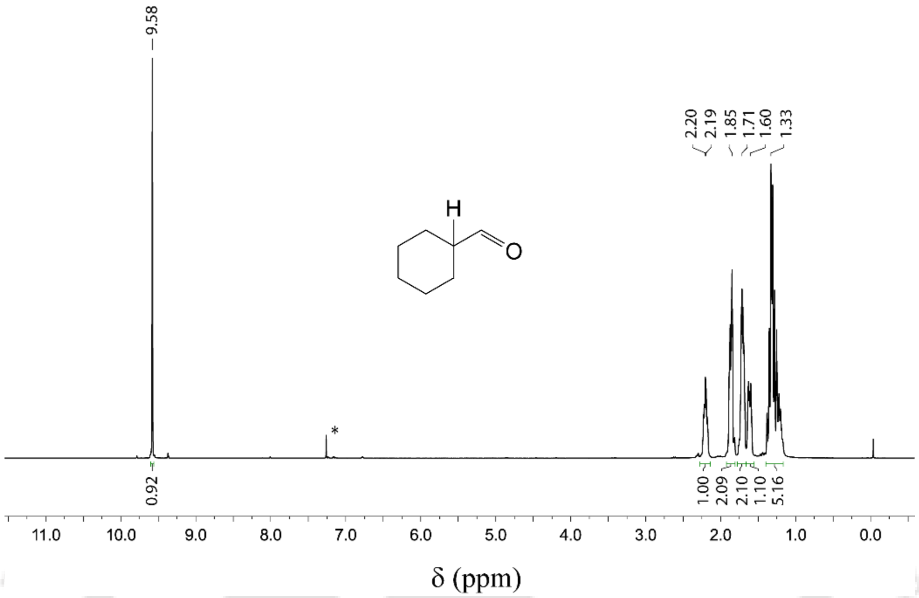

Fig. 2.1. ^{1}H NMR (400 MHz) spectrum of cyclohexanecarboxaldehyde in $CDCl_3$ at 298 K. Solvent peak is denoted by *.

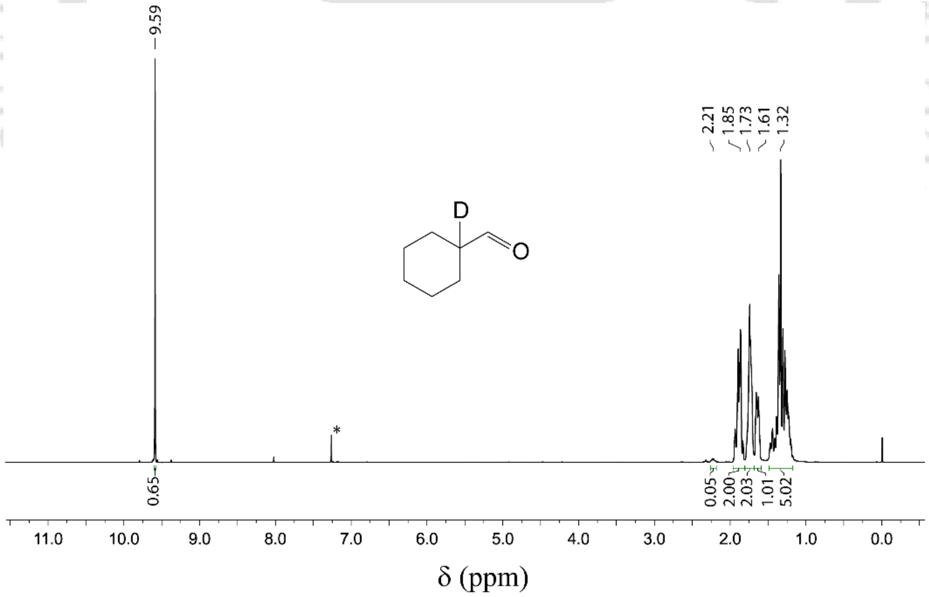

Fig. 2.2. ^{1}H NMR (400 MHz) spectrum of α-D-cyclohexanecarboxaldehyde in $CDCl_3$ at 298 K. Solvent peak is denoted by *.

2.2.4. Ligands

Scheme 2.1. Ligand systems used and discussed throughout.

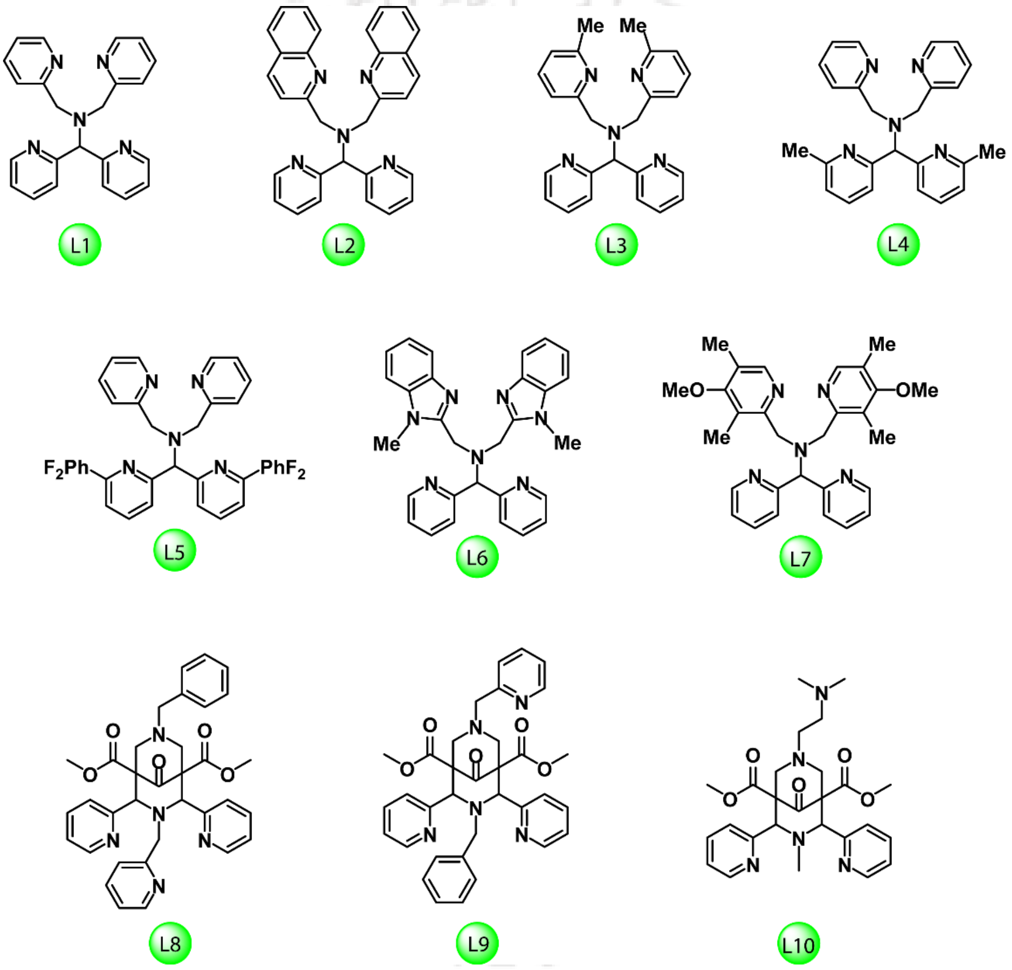

- *Synthesis of the ligand N4Py / L1* :

N,N-bis(2-pyridylmethyl)-N-bis(2-pyridyl)methylamine (L1) was synthesized following a reported procedure.[5]

Synthesis of $^{P}L1^{b}$: Di(2-pyridyl) ketone ($^{P}L1^{a}$) (27 mM, 5 g), hydroxylamine hydrochloride (60 mM, 4.17 g) and ethanol (10 mL) were taken in a 100 mL round-bottomed flask which contained NaOH (4 g) and 20 mL of water. The mixture was refluxed for 3 - 4 hours. The excess ethanol was evaporated *in vacuo* and the solution was diluted to 1 L; next the solution was neutralized (pH = 7) with dilute HCl properly. A pinkish-white precipitate of Di-2-pyridyl ketone oxime appeared, and then the precipitate was filtered off and dried for a day.

Synthesis of $^{P}L1^{c}$: The Di-2-pyridyl ketone oxime thus formed was taken in a three-necked round-bottomed flask with ethanol (90 mL) and fitted with a reflux condenser, 60 mL of Hydrazine hydrate and Zn powder were added in conjugative steps over six hours. Then the solution was kept refluxing overnight. The reduced product thus obtained was dissolved in 5N NaOH solution (40 mL). The alkaline solution was extracted from ethyl acetate (3 x 200 mL) to obtain di(pyridin-2-yl)methanamine as sticky solid.

Synthesis of L1 : Di(pyridin-2-yl)methanamine thus obtained was taken in an alkaline NaOH solution (5N, 50 mL) and 2-(Chloromethyl)pyridine hydrochloride (2.2 equivalents) was added to the solution and kept in reflux condition for two days. A brown solution appeared which was neutralized by $HClO_4$ to get the desired solid compound (yield: 3 g). (see Scheme 2.2).

Scheme 2.2. Synthesis of ligand L1.

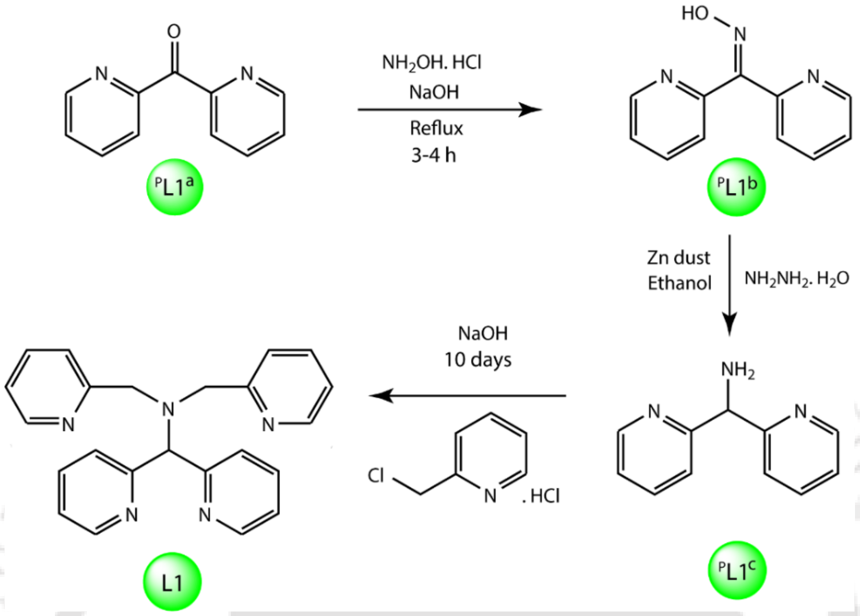

- *Synthesis of the ligand 2PyN2Q / L2* :

Synthesis of 1,1-di(pyridin-2-yl)-*N*,*N*-bis(quinolin-2-ylmethyl)methanamine (L2) was done by slight modifications from the reported procedure.[6]

^{P}L2^{b}and ^{P}L2^{c} are the same compounds as ^{P}L1^{b}and ^{P}L1^{c}.

Synthesis of L2 : 2.2 equivalents of 2-(Chloromethyl)quinoline hydrochloride was added to *^{P}L2^{c}* taken in 50 mL alkaline solution. The reaction mixture was stirred for 10 days at room temperature. Upon continuous stirring a brown solid appeared that was extracted with ethyl acetate (3 x 200 mL), washed with brine and evaporated under vacuum to get the desired ligand in considerable yield. (yield 6.8 g) (see Scheme 2.3) ^{1}H NMR (600 MHz, $CDCl_3$): δ 4.20 (s, 4H, CH_2), 5.43 (s, 1H, CH), 7.14-8.04 (m, 18H), 8.58 (dd, 2H). ^{13}C NMR (150 MHz, $CDCl_3$): δ 58.25, 72.37, 121.30, 122.20, 124.33, 126.01, 127.22, 127.39, 128.99, 129.25, 136.14, 136.36, 147.51, 149.32, 159.88, 160.47. (Fig. 2.3, 2.4; solvent peaks are denoted by *).

NMR Characterization of L2.

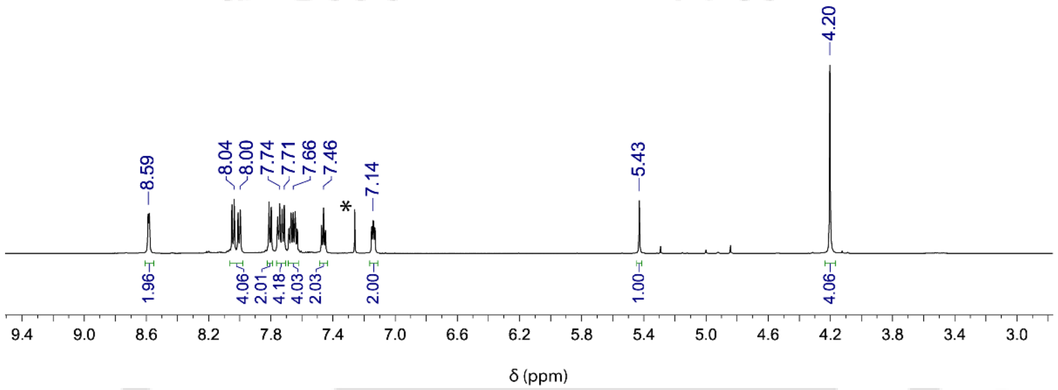

Fig. 2.3. ^{1}H NMR (600 MHz) spectrum of ligand L2 in $CDCl_3$.

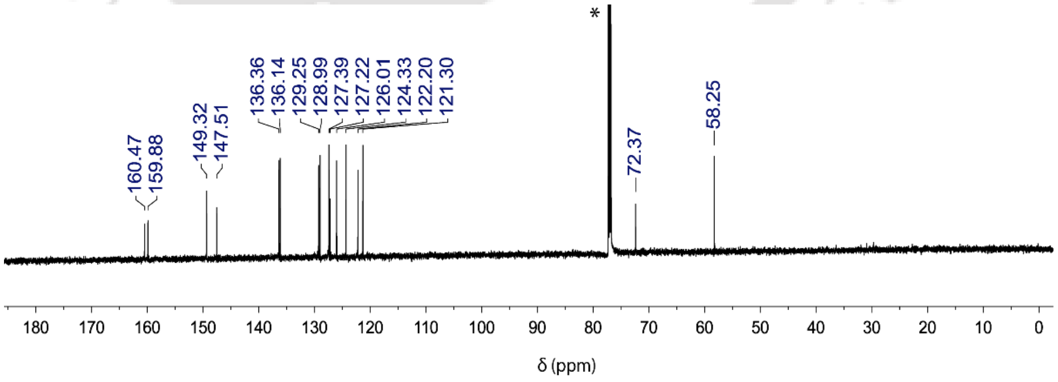

Fig. 2.4. ^{13}C NMR (150 MHz) spectrum of ligand L2 in $CDCl_3$.

Scheme 2.3. Synthesis of ligand L2.

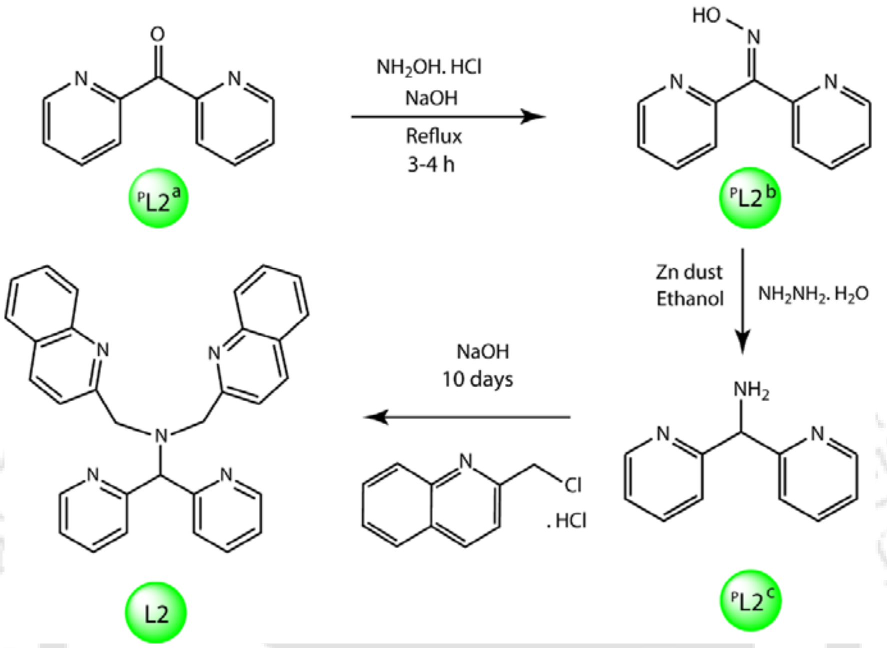

- *Synthesis of the ligand N4Py^{Me} / L3* :

^{P}L3^{b}and ^{P}L3^{c} are the same compounds as ^{P}L1^{b}and ^{P}L1^{c}.

Synthesis of 2-(chloromethyl)-6-methylpyridine hydrochloride[7] : A solution of 6-methyl-2-(hydroxymethyl)pyridine hydrochloride (5.00 g, 40.6 mmol) in DCM (10 mL) was cooled to 0 °C under an inert atmosphere. Thionyl chloride (~25 g, 244.1 mM) was slowly added to the solution over a period of 1 h. The process is an exothermic one along with evolution of HCl gas. The resulting mixture was then allowed to slowly warm to room temperature overnight. The resulting volatiles were sucked under vacuum using a glass trap containing liquid nitrogen to result in a pink-white solid. It then re-dissolved in warm ethanol (30 mL) and slowly layered with cold diethyl ether (100 mL) to cause the rapid precipitation of the desired compound as a white solid. The product was filtered and dried under vacuum overnight (yield: 99%) ^{1}H NMR (400 MHz, $CDCl_3$): δ 8.26 (t, 1H), 7.88 (d, 1H), 7.60 (d, 1H), 3.49 (s, 2H), 3.04 (s, 3H).

Synthesis of L3 : Similar procedure as the final step in L2 was followed in the synthesis of L3. However, 2.2 equivalents of 2-(chloromethyl)-6-methylpyridine hydrochloride was used instead of 2-(Chloromethyl)quinoline hydrochloride. Similar procedure and purification gave ligand L3 as light brown solid (5.6 g). (see Scheme 2.4) ^{1}H NMR (600 MHz, $CDCl_3$): δ 2.49 (s, 6H, CH_3), 3.93 (s, 4H, CH_2), 5.34 (s, 1H, CH), 6.95-7.69 (m, 12H), 8.54 (d, 2H, 6-pyH). ^{13}C NMR (150 MHz, $CDCl_3$): δ 24.33, 57.26, 72.26, 119.72, 121.30, 122.09, 124.03, 136.34, 136.56, 149.19, 157.54, 159.06, 160.07. (Fig. 2.5, 2.6; solvent peaks are denoted by *)

NMR Characterization of L3.

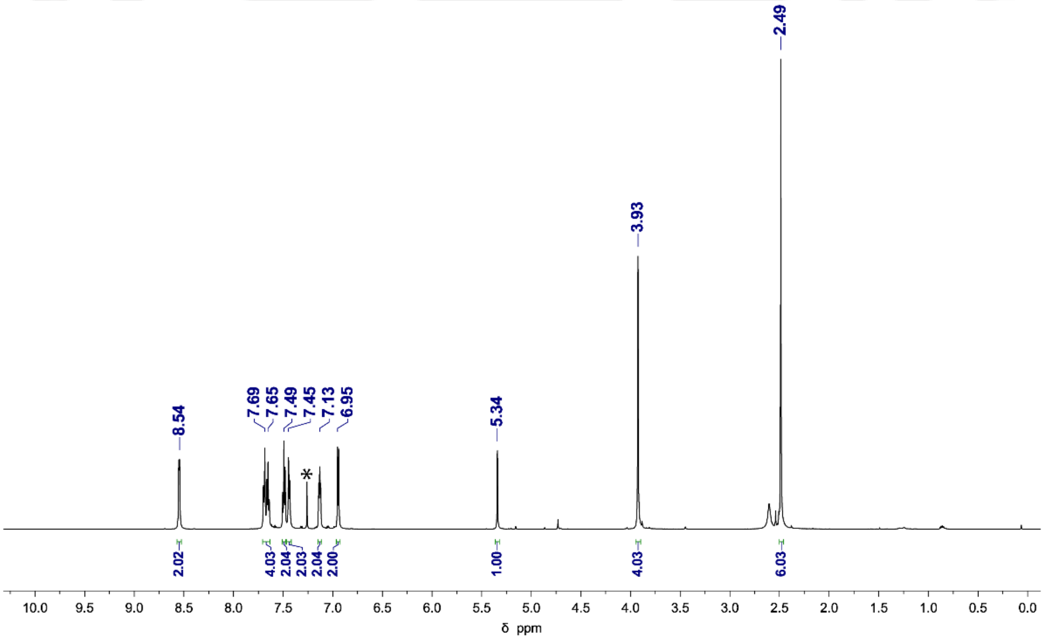

Fig. 2.5. ^{1}H NMR (600 MHz) spectrum of ligand L3 in $CDCl_3$.

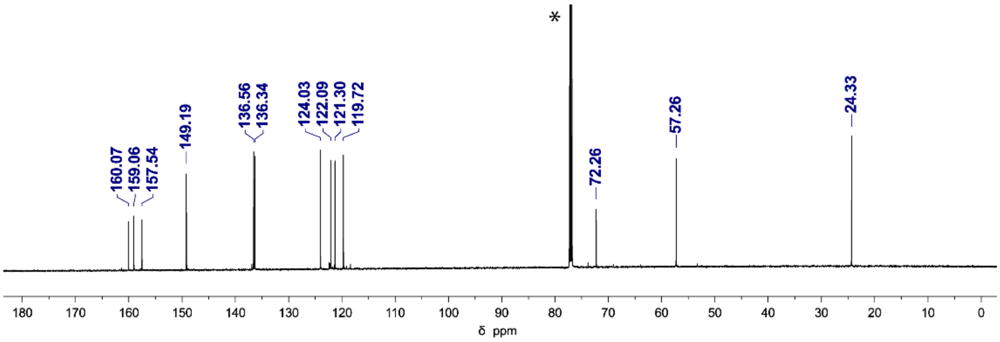

Fig. 2.6. ^{13}C NMR (150 MHz) spectrum of ligand L3 in $CDCl_3$.

Scheme 2.4. Synthesis of ligand L3.

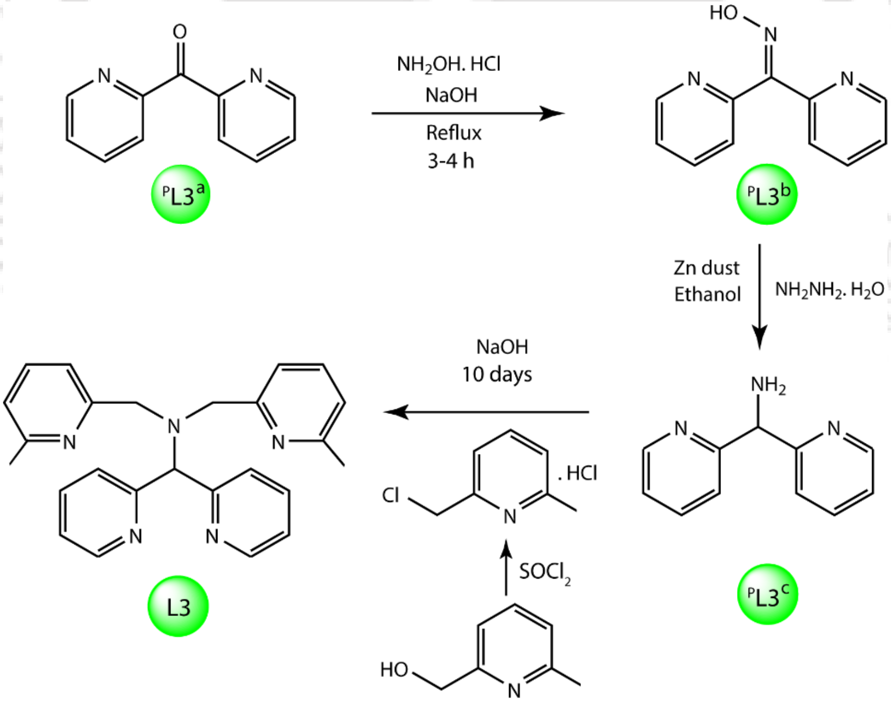

- *Synthesis of the ligand ^{Me}N4Py / L4* :

Synthesis of ^{P}L4^{a} : The synthesis of di(6-methylpyridin-2-yl)methanone (^{P}L4^{a}) was adapted from the procedure reported by Newkome et al.[8] n-Butyl lithium, 2.5 M in hexane (100 mM) was added dropwise to a solution of pre-distilled 2-bromo-6-methylpyridine (110 mM, 19 g) in dry THF (150 mL) at -90 ˚C (using ethanol bath and liquid nitrogen). After stirring it at -90 ˚C for an hour, a solution of ethylchloroformate [¥] (50 mM, 5.5 g) in dry THF (15 mL) was added rapidly to the reaction mixture. After stirring for 1.5 h at -80 ˚C, the reaction was left to stir overnight as the temperature gradually rises to ambience. The reaction mixture was quenched with 5 mL methanol as the colour darkens to deep brown. The solvent was removed in vacuo and the resulting sticky liquid was extracted with dichloromethane (100 mL x 3) and 15 % $NaHCO_3$ solutions several times and washed with brine solution (100 mL). The combined organic extracts were dried over Na_2SO_4, and concentrated to get a deep brown liquid. Column chromatography (silica) with hexane-ethyl acetate (30% and 50%) gave the desired product, di(6-methylpyridin-2-yl)methanone, in 50% yield (5.9 g) as colourless needles which freezes at 6 ˚C. ^{1}H NMR (400 MHz, CD_3OD): δ 2.57 (s, 6H, CH_3), 7.88 (dd, 2H, 5-pyH), 7.84 (dd, 2H, 3-pyH), 7.50 (t, 2H, 4-pyH).

[¥] *Purification of ethyl chloroformate* : Ethyl chloroformate has a very toxic odour and irritating for eyes. It is normally synthesized from commercial Phosgene which contains traces of iron as ferric chloride, and also contains HCl dissolved. During distillation, the presence of iron, along with the application of heat, causes the ethyl chloroformate to severely decompose either to olefenic compounds or to alkyl chlorides. A substantial amount of product is lost, and/or in many cases, the alkyl chloroformates are completely decomposed. The pH of the ethyl chloroformate was checked to be almost 1, *i.e.* highly acidic. So it was treated with

20% NaOH solution in cold resulting in the formation of a salt, NaCl. This reduced the acidity of the compound and also helped in the reduction of the Fe(III) that catalyzes the decomposition of the alkyl chloroformate. Further, it was washed with brine several times to get a clear organic phase, which was distilled thereafter using a fractionating column and short path condenser to get a colorless liquid. Without removal of the iron contamination, alkyl chloroformates, typically ethyl chloroformate, may decompose severely, where only 10-20 % of the chloroformate remains after distillation. Thus obtained colorless ethyl chloroformate was stored in cold for future use.

Synthesis of $^{P}L4^{b}$: Di(6-methylpyridin-2-yl)methanone (26 mM, 5.5 g) was taken into 10 N NaOH solution (20 mL) and hydroxylamine hydrochloride (4.6 g in 10 mL water) was added to it and refluxed for 3-4 h. After removing the solvent *in vacuo* the resulting solution was poured into large excess of ice-cold water (~800 mL) and stirred vigorously, as the pH was adjusted to 7. It was then filtered and the resulting filtrate was extracted using dichloromethane (300 mL x 3), dried over Na_2SO_4 and concentrated under vacuum to get the corresponding oxime, di(6-methylpyridin-2-yl)methanone oxime, in 99% yield (5.5 g) as white solid. ^{1}H NMR (400 MHz, CD_3OD): δ 2.50 (s, 6H, CH_3), 7.08 (dd, 2H, 5-pyH), 7.54 (dd, 2H, 3-pyH), 7.91 (t, 2H, 4-pyH).

Synthesis of $^{P}L4^{c}$: The oxime (24 mM, 5.4 g) was taken in a double-necked round bottomed flask and ethanol (100 mL) was added to it. One spoon full of zinc dust and hydrazine hydrate (10 mL) was added to it under refluxing condition. 3 mL of hydrazine hydrate (every half hour) and one spoon full of Zn dust (every hour) was added to it for 4 h and then left to reflux overnight. The residue was filtered under hot condition and washed several times with hot ethanol. The filtrate was evaporated under reduced pressure the resulting solution was taken into 500 mL water where the pH was adjusted to 7 using conc. HCl and stirred for 20 min. The precipitate was then filtered (if any) and the filtrate was made alkaline using NaOH beads up to pH 12. Extraction of the alkaline solution from ethyl acetate (3 x 200 mL) and dichloromethane (3 x 100 mL) gave di(6-methylpyridin-2-yl)methanamine (4.1 g) as yellow oil. ^{1}H NMR (400 MHz, CD_3OD): δ 2.50 (s, 6H, CH_3), 5.18 (s, 1H, CH), 7.11 (dd, 2H, 5-pyH), 7.21 (dd, 2H, 3-pyH), 7.61 (t, 2H, 4-pyH).

Synthesis of L4 : 2.5 equivalents of 2-(chloromethyl)pyridine hydrochloride was added to 6M NaOH solution (30 mL) in ice-cold condition and stirred for 30 min, and was later added to a heterogeneous mixture of di(6-methylpyridin-2-yl)methanamine (19 mM, 4 g) in 6M NaOH solution (20 mL) and stirred at room temperature for 10 days. It was then neutralized with perchloric acid and the reaction mixture was left to stir overnight and filtered through a G4 crucible and dried to get a powder-like compound. The perchlorate salt was then taken into 5M NaOH solution and extracted from ethyl acetate (3 x 100 mL), washed with brine solution (100 mL) and evaporated under vacuum to get the desired ligand L2 (0.9 g) as brown solid. (see, Scheme 2.5) ^{1}H NMR (600 MHz, $CDCl_3$): δ 2.50 (s, 6H, CH_3), 3.97 (s, 4H, CH_2), 5.26 (s, 1H, CH), 6.96-7.51 (m, 12H), 8.42 (d, 2H, 6-pyH). ^{13}C NMR (150 MHz, $CDCl_3$): δ 24.47, 57.78, 73.66, 120.96, 121.58, 121.65, 123.32, 136.07, 136.43, 148.74, 157.74, 159.63, 159.95. (Fig. 2.7, 2.8; solvent peaks are denoted by *).

NMR Characterization of L4.

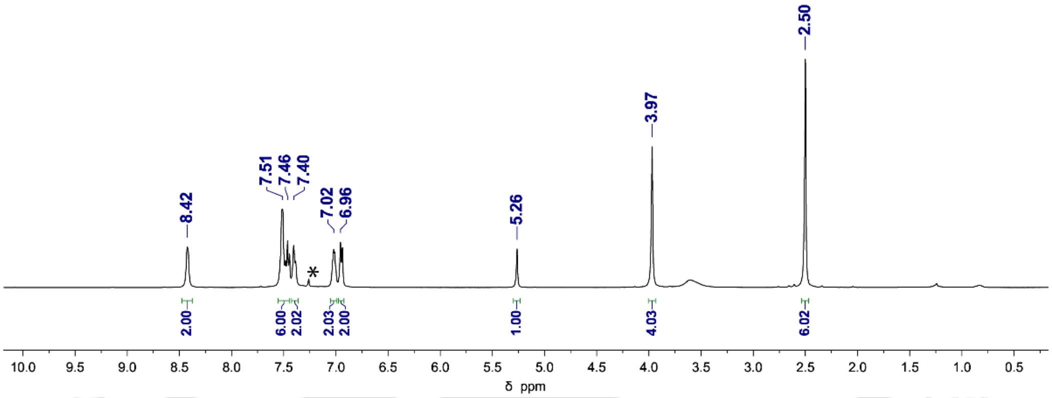

Fig. 2.7. ^{1}H NMR (600 MHz) spectrum of ligand L4 in $CDCl_3$.

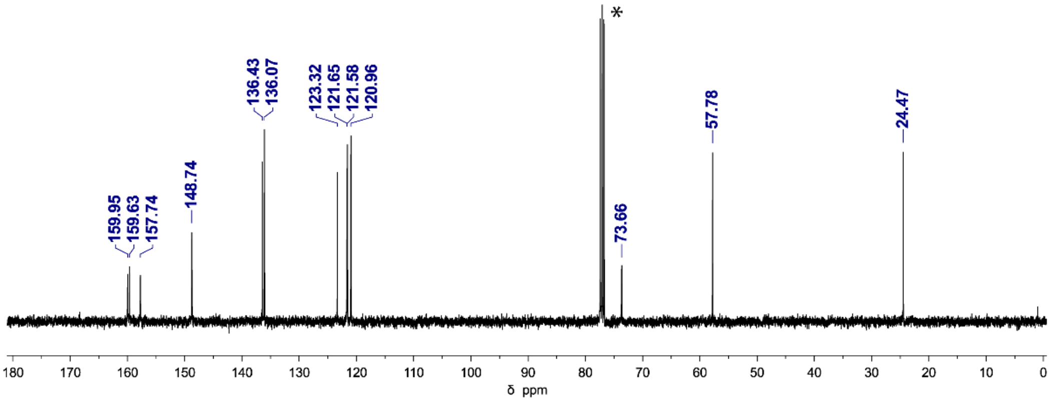

Fig. 2.8. ^{13}C NMR (150 MHz) spectrum of ligand L4 in $CDCl_3$.

Scheme 2.5. Synthesis of ligand L4.

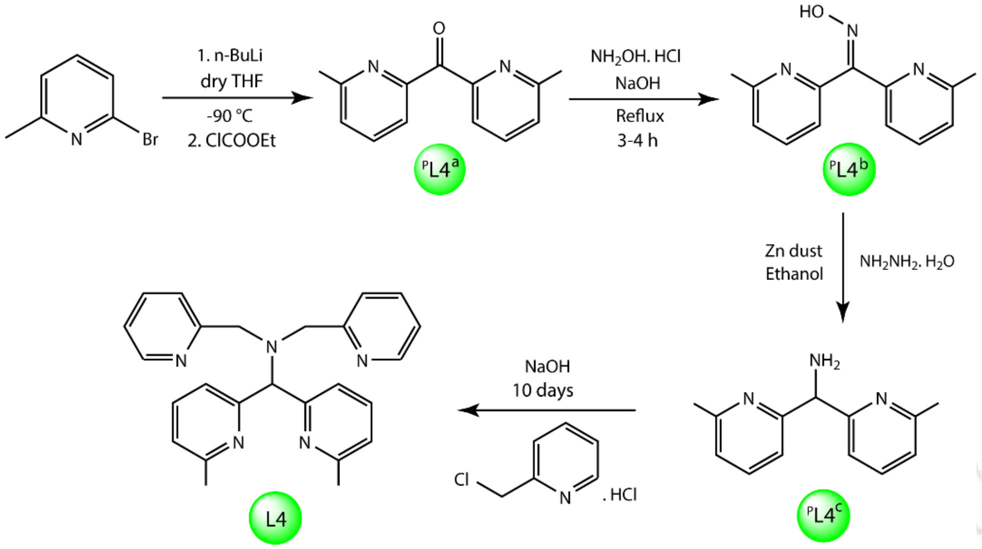

- *Synthesis of the ligand L8, L9 and L10* :

The bispidine ligand L8 and L9 were synthesized by following reported procedures.[9-12] L10 was synthesized with slight modification from the reported procedure.[13]

General Procedure for the Synthesis of ^{P}*L8*, ^{P}*L9 and* ^{P}*L10* : Dimethylacetone dicarboxylate (7.35 mL, 50 mM) was taken in a round-bottomed flask containing 20 mL methanol (for ^{P}L8 and ^{P}L9) or 20 mL ethanol (for ^{P}L10) and was cooled to 0 °C in an ice bath. Subsequently pyridine-2-carboxaldehyde (9.51 mL, 100 mM) and 50 mM of picolyl amine (for ^{P}L8) / benzyl amine (for ^{P}L9) / methyl amine (for ^{P}L10) were slowly added to the cold solution. After complete addition of the amine, the resulting solution was allowed to come to room temperature slowly and stirred overnight. An off-white thick precipitate was formed which was filtered and washed using cold ethanol several times and dried in vacuum. The product was recrystallized from warm ethanol to get colourless crystals in stoichiometric yields (84% for ^{P}L8, 80% for ^{P}L9 and 78% for ^{P}L10).

General Procedure for the Synthesis of L8, L9 and L10 : To the suspension of the piperidone (^{P}L8, ^{P}L9 or ^{P}L10) (36 mM) in 200 mL ethanol were added formaldehyde (37%, 7.3 mL, 90 mM) and 40 mM of benzyl amine (for L8) / picolyl amine (for L9) / N,N-dimethylethylenediamine (for L10) in a dropwise manner. The reaction mixture was refluxed for 4 h. The resulting brown/yellow solution was concentrated under vacuum and layered with diethyl ether and kept at -40 °C for slow diffusion. White crystalline products were obtained after a few days. (Yield: ~40% for L10, m. p. 143 °C) (see Scheme 2.6) ^{1}H NMR for L10 (600 MHz, $CDCl_3$): δ 2.05 (s, 3H, CH_3), 2.28 (s, 6H, CH_3), 2.38 (2H, CH_2), 2.46 (2H, CH_2), 2.60 (d, 2H, CH_2), 3.06 (d, 2H, CH_2), 3.85 (s, 6H, CH_3), 4.75 (s, 2H, CH), 7.24 (2H), 7.79 (2H), 8.17 (2H), 8.53 (2H). (Fig. 2.9, 2.10; solvent peaks are denoted by *).

NMR Characterization of L10.

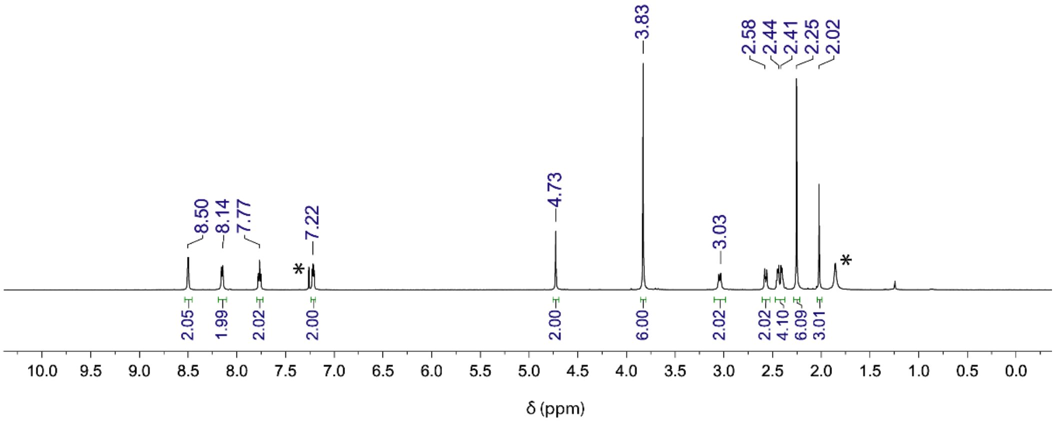

Fig. 2.9. ^{1}H NMR (600 MHz) spectrum of ligand L10 in $CDCl_3$.

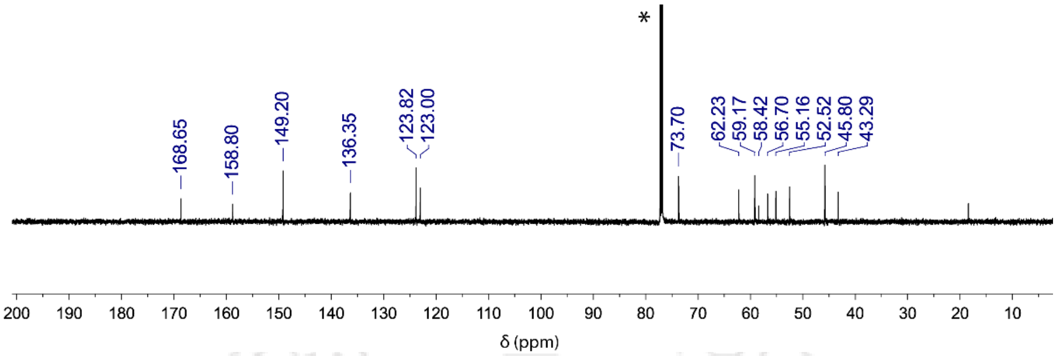

Fig. 2.10. ^{13}C NMR (150 MHz) spectrum of ligand L10 in $CDCl_3$.

Scheme 2.6. Synthesis of ligand L8, L9 and L10.

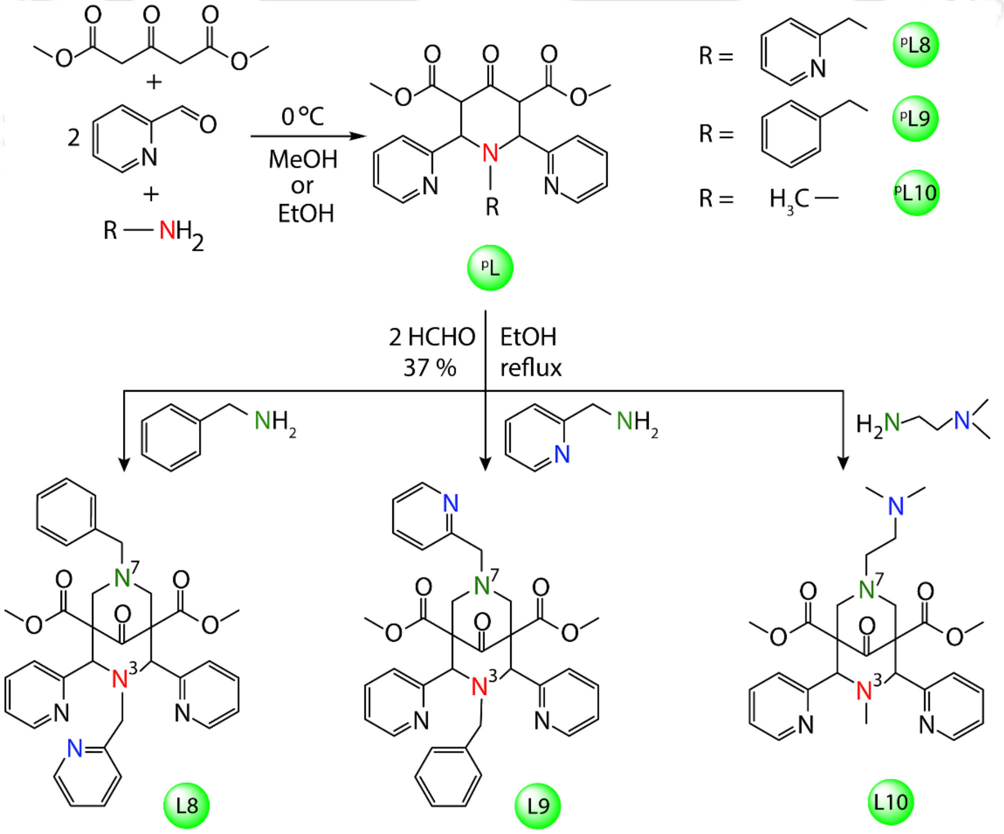

2.2.5. Metal Complexes

- *General Procedure for the synthesis of the Fe(II)-complexes.*

The ferrous complexes were synthesized using the following general procedure. 100 mg ligand was taken in a glass vial and dissolved in CH_3CN / CH_2Cl_2 (3 mL) inside a glove box filled with Argon. To this solution was added 1.2 equivalents of Fe(II)-salts (triflates, perchlorates or tetrafluoroborates) in CH_3CN / CH_2Cl_2 (2 mL) and stirred overnight to ensure complete metalation. The resulting solution was filtered using 0.2 μm PTFE syringe filters and crystallized by slow vapour diffusion of diethyl ether into a CH_3CN solution and stored at -40 ˚C. The complexes obtained were washed with diethyl ether and dried under vacuum to obtain the desired metal complexes. (See Table 2.1).

- *General Procedure for the synthesis of the Mn(II)-complexes.*

Bispidine ligands L8 and L9 (100 mg) were dissolved in CH_3CN and $Mn^{II}(ClO_4)_2$ salt (1.2 equivalents) in CH_3CN was added dropwise under inert conditions. The pale yellow solution was refluxed overnight. After the end of the reaction, the solution was syringe filtered and layered with diethyl ether to obtain colourless crystalline products.

Table 2.1. Synthetic parameters and characteristics of metal complexes.

Complex	Ligand	Metal Salt	Solvent	Colour	Texture	Yield
1a	L1	$Fe^{II}(CH_3CN)_2(OTf)_2$	CH_3CN	Dark red	Crystalline	92%
2a	L2	$Fe^{II}(CH_3CN)_2(OTf)_2$	CH_3CN	Dark yellow	Powder	95%
3a	L3	$Fe^{II}(CH_3CN)_2(ClO_4)_2$	CH_3CN	Yellow	Crystalline	92%
4a	L4	$Fe^{II}(CH_3CN)_2(ClO_4)_2$	CH_3CN	Dark yellow	Powder	85%
		$Fe^{II}(BF_4)_2 . 6H_2O$		Dark red	Crystalline	90%
8a	L8	$Mn^{II}(CH_3CN)_2(ClO_4)_2$	CH_3CN	Colour-less	Crystalline	91%
9a	L9	$Mn^{II}(CH_3CN)_2(ClO_4)_2$	CH_3CN	Colour-less	Crystalline	90%
10a	L10	$Fe^{II}(CH_3CN)_2(OTf)_2$	CH_3CN	Light Yellow	Powder	91%

Caution! Although no accident while dealing with the perchlorate salts was experienced, but they are potential explosives upon heating and should be handled with care.

2.3. Characterization of the Fe(II) Complexes

2.3.1. ESI-MS

The electrospray ionization mass spectra of all the Fe(II)-complexes were recorded in acetonitrile solvent, at room temperature. The concentration of the metal complexes for ESI-MS was generally kept consistent at 1 mM. The samples were thoroughly filtered through syringe filters before injecting into the mass spectrometer.

- *ESI-MS spectrum of $[Fe^{II}(L1)(OTf)]^+$:*

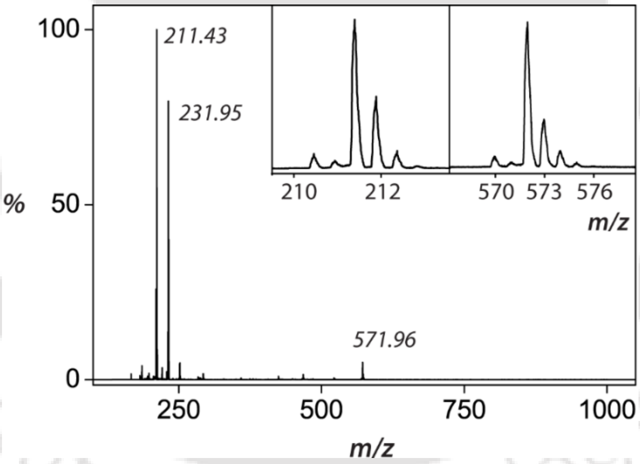

Fig. 2.11. ESI-MS spectrum of $[Fe^{II}(L1)(OTf)]^+$; *m/z* 211.43, 231.95 and 571.96 corresponds to $[Fe^{II}(L1)]^{2+}$, $[Fe^{II}(L1)(CH_3CN)]^{2+}$ and $[Fe^{II}(L1)(OTf)]^+$ respectively. Inset shows the isotopic distribution pattern for the *m/z* values of 211.43 and 571.96.

- *ESI-MS spectrum of [Fe^{II}(L2)(OTf)]$^{+}$:*

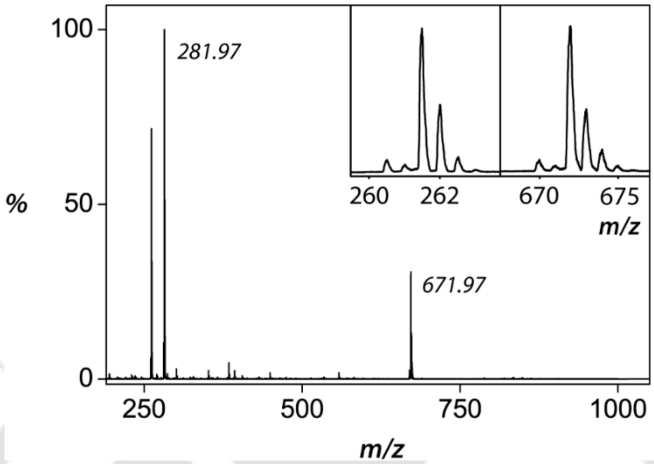

Fig. 2.12. ESI-MS spectrum of [Fe^{II}(L2)(OTf)]$^{+}$; *m/z* 261.49, 281.97 and 671.97 corresponds to [Fe^{II}(L2)]$^{2+}$, [Fe^{II}(L2)(CH$_3$CN)]$^{2+}$ and [Fe^{II}(L2)(OTf)]$^{+}$ respectively. Inset shows the isotopic distribution pattern for the *m/z* values of 261.49 and 671.97.

- *ESI-MS spectrum of [Fe^{II}(L3)(ClO$_4$)]$^{+}$:*

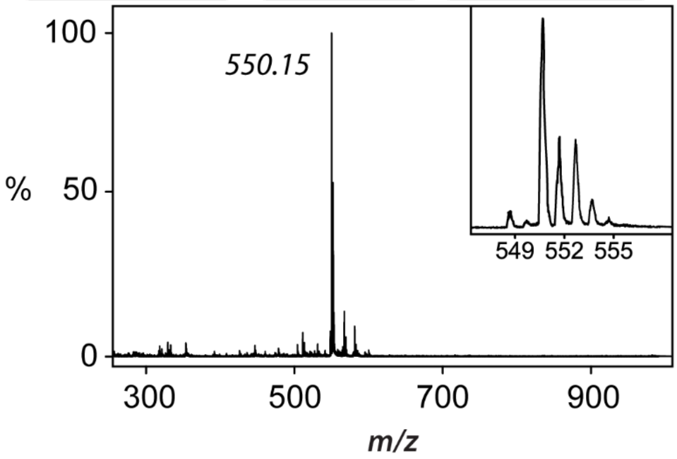

Fig. 2.13. ESI-MS spectrum of [Fe^{II}(L3)(ClO$_4$)]$^{+}$; *m/z* 550.15 corresponds to [Fe^{II}(L3)(ClO$_4$)]$^{+}$. Inset shows the isotopic distribution pattern for the *m/z* 550.15.

- *ESI-MS spectrum of [Fe^{II}(L4)(ClO$_4$)]$^+$:*

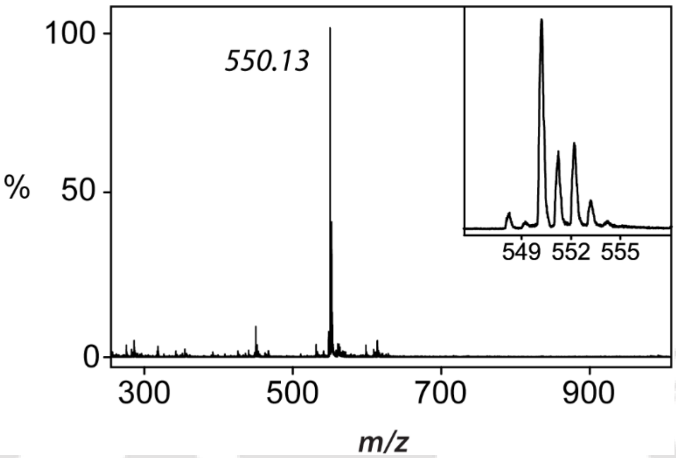

Fig. 2.14. ESI-MS spectrum of [Fe^{II}(L4)(ClO$_4$)]$^+$; *m/z* 550.13 corresponds to [Fe^{II}(L4)(ClO$_4$)]$^+$. Inset shows the isotopic distribution pattern for the *m/z* 550.13.

- *ESI-MS spectrum of [Mn^{II}(L8)(ClO$_4$)]$^+$*

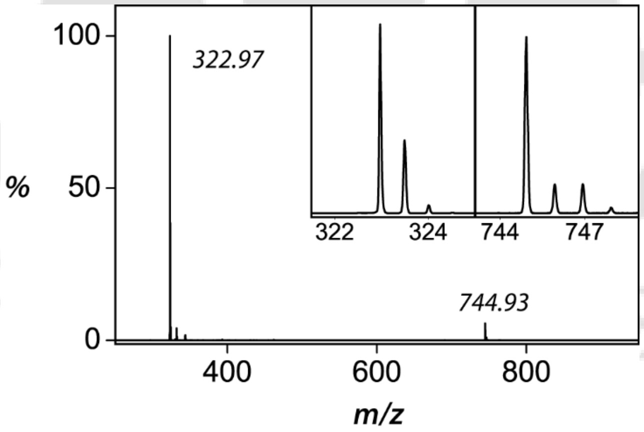

Fig. 2.15. ESI-MS spectrum of [Mn^{II}(L8)(ClO$_4$)]$^+$; *m/z* 322.97 and 744.93 correspond to [Mn^{II}(L8)]$^{2+}$ and [Mn^{II}(L8)(ClO$_4$)]$^+$. Inset shows their isotopic distribution pattern.

- *ESI-MS spectrum of* $[Mn^{II}(L9)(ClO_4)]^+$

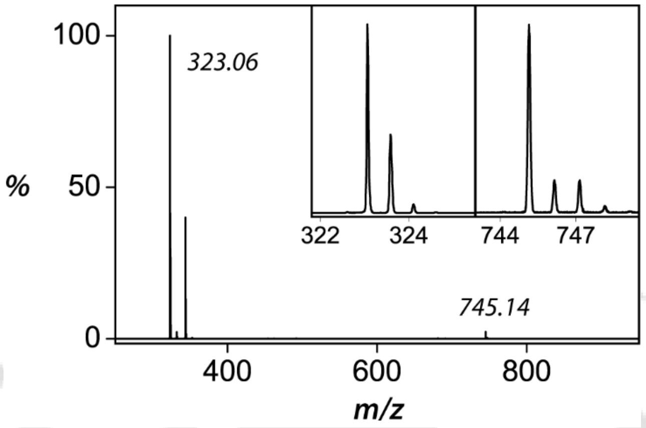

Fig. 2.16. ESI-MS spectrum of $[Mn^{II}(L9)(ClO_4)]^+$; *m/z* 323.06 and 745.14 correspond to $[Mn^{II}(L9)]^{2+}$ and $[Mn^{II}(L9)(ClO_4)]^+$. Inset shows their isotopic distribution pattern.

- *ESI-MS spectrum of* $[Fe^{II}(L10)(OTf)]^+$:

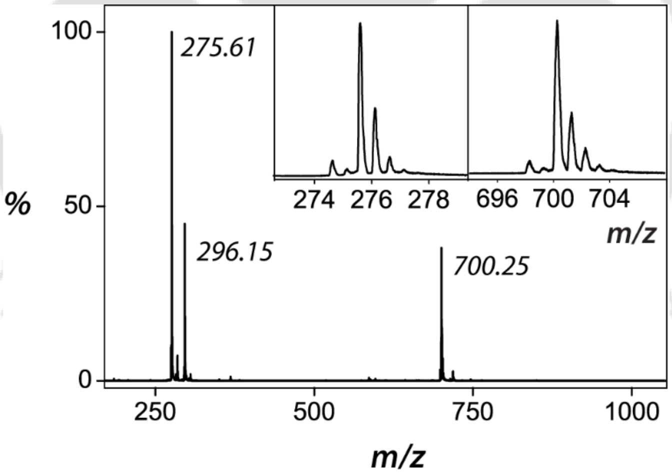

Fig. 2.17. ESI-MS spectrum of $[Fe^{II}(L10)(OTf)]^+$; *m/z* 275.61, 296.15 and 700.25 corresponds to $[Fe^{II}(L10)]^{2+}$, $[Fe^{II}(L10)(CH_3CN)]^{2+}$ and $[Fe^{II}(L10)(OTf)]^+$ respectively. Inset shows the isotopic distribution pattern for the *m/z* values of 275.61 and 700.25.

2.3.2. ^{1}H-NMR

In general, NMR spectroscopy is conducted on diamagnetic molecules, but paramagnetic molecules are also compliant to NMR analysis, which, however, are associated with some unusual effects like broad spectral patterns and huge chemical shifts. But ^{1}H-NMR of the metal complexes indeed provide important structural information and significant insight into bonding patterns, although due to low resolution, the coupling factors are seldom resolvable. Unlike normal organic diamagnetic molecules, the proton NMR spectra of metal complexes are informative of its overall spin state, thereby producing paramagnetically shifted peaks over a wide spectral width of around 200 ppm. These shifted peaks are designated as the *isotropic shift*, which is the difference between the chemical shifts of a compound in the presence and absence of a metal ion. Due to the presence of unpaired electrons in metal complexes, a coupled larger magnetic field is generated which thereby produces huge isotropic shift values that can range from -100 to +200 ppm. These abnormal shifts make peak assignments even more complicated. The α-protons, that are closest to the metal centre, are shifted the furthest (even sometimes not recognizable); in case of substituted α-position, the β-protons are also highly affected by the metal ion. The coordination number, geometry and spatial arrangement of the protons around the metal centre are highly responsible for the different shift patterns in different systems. The σ-mechanism for the delocalization of unpaired spin density commensurate the downfield shift of the pyridine protons in the α-H > β-H > γ-H order.[11-15] Involvement of π-delocalization, however, generates a shift pattern of downfield β-H and upfield α-H and γ-H.[16]

Scheme 2.7. Numbering scheme for metal complexes containing substituted pyridine donors.

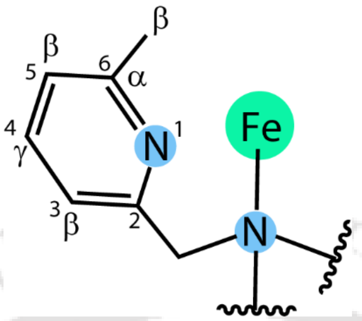

- *^{1}H-NMR spectrum of [Fe^{II}(L2)(OTf)]$^+$:*

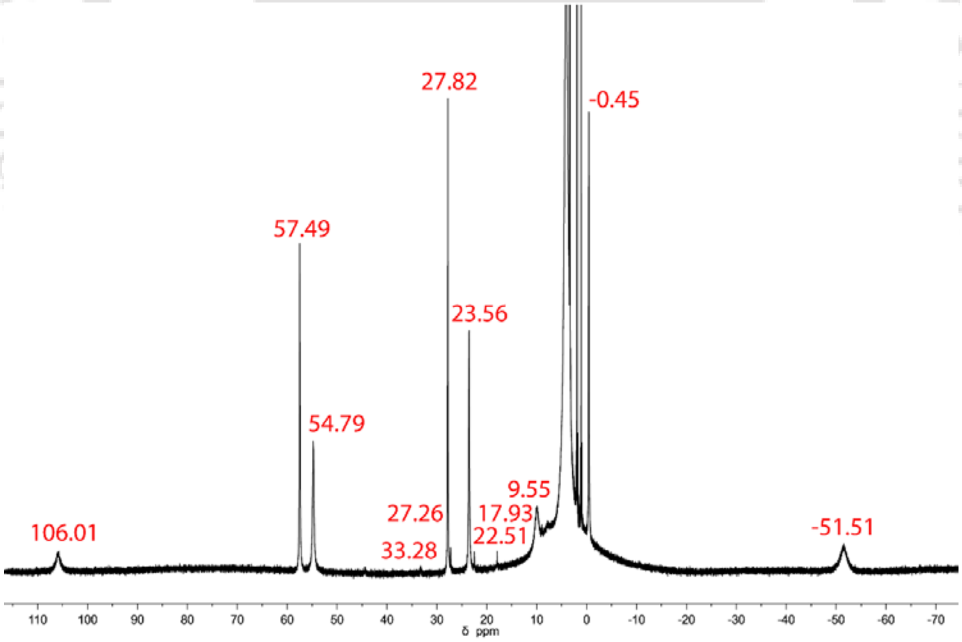

Fig. 2.18. ^{1}H-NMR spectrum (400 MHz) of complex 2a in CD_3CN at 298 K with a spectral width of ~200 ppm (no. of scans = 82).

- ^{1}H-NMR spectrum of [Fe^{II}(L3)(ClO$_4$)]$^+$ and [Fe^{II}(L4)(ClO$_4$)]$^+$:

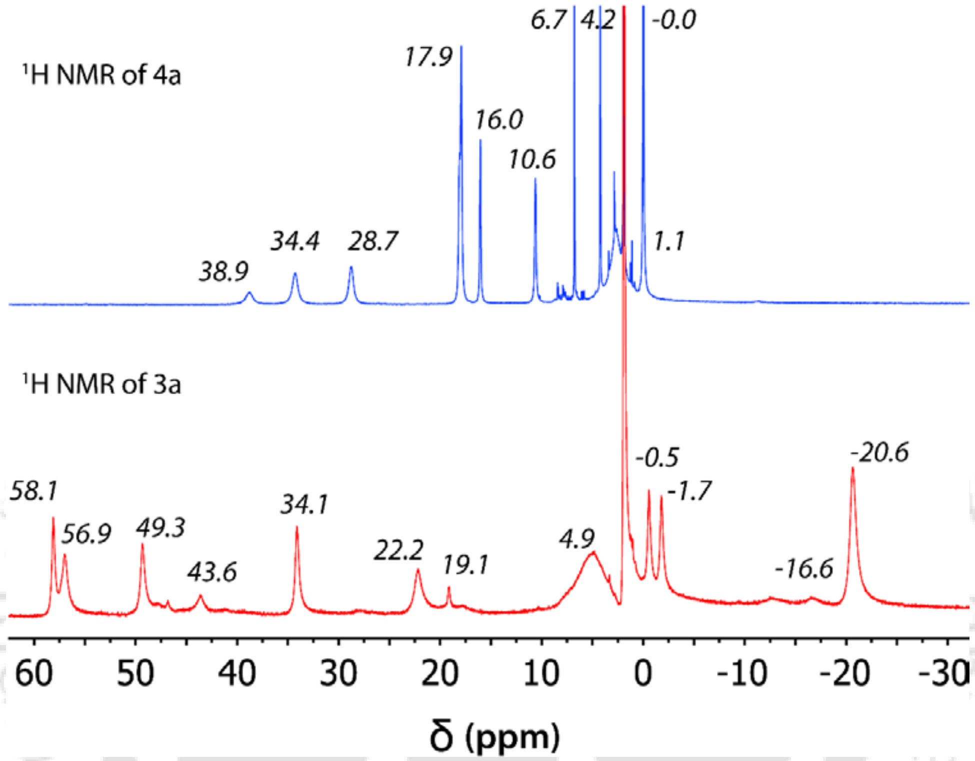

Fig. 2.19. ^{1}H-NMR spectrum (400 MHz) of complex 4a (*top*) and 3a (*bottom*) in CD$_3$CN at 298 K with a spectral width of ~200 ppm (no. of scans = 82).

2.3.3. X-ray crystallography

- *Crystallographic data for complex [Fe^{II}(L4)(CH$_3$CN)](BF$_4$)$_2$ and its structure refinement parameters* :

The crystal structure was recorded at 20 °C on an Agilent Single Crystal X-Ray Diffractometer (XRD) equipped with Mo X-ray source (Mova), CCD detector (Eos), Oxford cryo system and crystal AlisPRO and Autochem software. CCDC 1876766 contains the supplementary crystallographic data for this complex. These data are provided free of charge by The Cambridge Crystallographic Data Centre. Dark red crystals were grown by slow vapour diffusion of diethyl ether into the acetonitrile solution of the Fe(II) complex. The refined structure shows binding of a solvent (CH$_3$CN) molecule to the Fe(II) and two non-bound BF$_4$ counter-anions and aqua molecules.

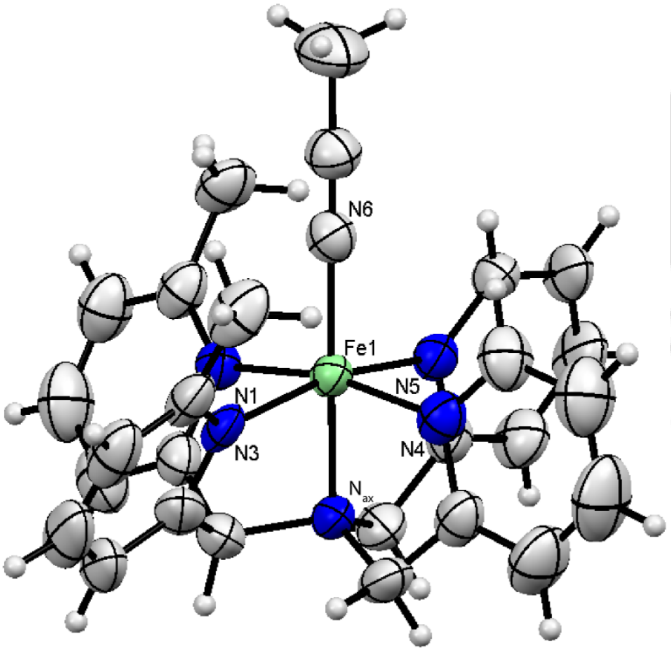

Fig. 2.20. ORTEP plot of [Fe^{II}(^{Me}N4Py)(CH$_3$CN)] (BF$_4$)$_2$ with thermal ellipsoid drawn at 30 % probability level. Counter-ions have been omitted for clarity.

Table 2.2. Structure refinement parameters.

Crystal identification	Fe-L16-BF4	
Empirical formula (Calculated)	$C_{27}\ H_{32}\ B_2\ F_8\ Fe\ N_6\ O_2$	
Formula Weight (Calculated)	702.06 g/mol	
Color, morphology	Deep red, block	
Temperature	293 K	
Wavelength	0.71073 Å	
Space group (Calculated)	P 21/c	
Hall group	-P 2ybc	
Volume (Calculated)	3322.2 (2) $Å^3$	
Bond precision	C-C = 0.0116 Å	
Unit cell parameters	*a* = 11.7022 (4) Å	α = 90 °
	b = 17.7265 (8) Å	β = 109.189 (4) °
	c = 16.9574 (7) Å	γ = 90°
Z (calculated)	4	
Density (calculated) (g cm^{-3})	1.404	
Mu (mm^{-1})	0.533	
F000 (F000')	1440.0 (1442.24)	
h, k, l $_{max}$	13, 21, 20	
N $_{ref}$ (calculated)	5834	
N $_{ref}$ (Reported)	5821	
Minimum transmission (T) (calculated) [reported limit]	0.836 [0.402]	
Maximum transmission (calculated) [reported limit]	0.894 [1.000]	
Absorption correction	Multi-scan	
Data completeness	0.998	
Theta (max)	24.990	
R (Reflections)	0.0858 (3652)	
wR2 (Reflections)	0.2175 (5821)	
R	0.09	
S	0.881	
Npar	418	
Prob (%)	50	

Table 2.3. Selected bond lengths [Å] and bond angles [°] for [Fe^{II}(L4)(CH_3CN)](BF_4)$_2$.

Bonds	Bond-lengths
Fe1-N1	2.049(5)
Fe1-N3	2.043(6)
Fe1-N4	1.974(5)
Fe1-N5	1.981(5)
Fe1-N_{ax}	1.968(5)
Fe1-N6	1.930(5)
Avg Fe-N	1.991
Angles	**Values**
N_{eq}-Fe-N_{ax} [a]	83.3
N_{eq}-Fe-N6 [a]	96.6
N_{ax}-Fe-N6	179.3

***cis*-equatorial bond angles (°)**		***cis*-bond angle of equatorial Fe1-N with N_{ax} (°)**	
∠ N1-Fe1-N5	91.1(2)	∠ N1-Fe1-N_{ax}	82.2(2)
∠ N1-Fe1-N3	86.4(2)	∠ N3-Fe1-N_{ax}	82.5(2)
∠ N3-Fe1-N4	92.4(2)	∠ N4-Fe1-N_{ax}	84.5(2)
∠ N4-Fe1-N5	87.0(2)	∠ N5-Fe1-N_{ax}	84.2(2)
***trans*-equatorial bond angles (°)**		***cis*-bond angle of equatorial Fe1-N with N6 (°)**	
∠ N1-Fe1-N4	166.7(2)	∠ N1-Fe1-N6	98.4(2)
∠ N3-Fe1-N5	166.7(2)	∠ N3-Fe1-N6	97.7(2)
-	-	∠ N4-Fe1-N6	94.9(2)
-	-	∠ N5-Fe1-N6	95.5(2)

[a] Average *cis*-bond angle of equatorial Fe1-N bonds with N_{ax} and N6. Avg = average.

The crystal structure (Fig. 2.20 and Table 2.3) shows clear penta-coordination of the metal to the ^{Me}N4Py ligand in a structural orientation analogous to the reported complexes $[Fe^{II}(N4Py)]^{2+}$ and $[Fe^{II}(N4Py^{Me})(CH_3CN)]^{2+}\cdot 2ClO_4$.[17,18] The Fe-N bond distances, as shown in Table 2.3, are typical for low-spin Fe(II) complexes reported previously.[17-24]

2.4. Generation of the Reactive Metal Intermediates

The formation of the Fe(IV)-O intermediate (1b) was achieved by vigorous stirring of the Fe(II) complex, (1a) with excess solid PhIO in acetonitrile and filtering off the unreacted excess oxidant using 0.2 µm PTFE syringe filters. The resulting clean filtrate was stored in cold and used for further studies. The Fe(IV)-oxo complexes 2b, 3b and 4b were synthesized *in situ* from their respective Fe(II) precursor complexes at room temperature by the addition of 1.5 equivalents of $PhI(OAc)_2$ in acetonitrile. Side on manganese-peroxo complexes $[Mn^{III}(L8)(O_2)]^+$ (8b) and $[Mn^{III}(L9)(O_2)]^+$ (9b) were prepared by reacting their corresponding Mn^{II} complexes with 10 equivalents of H_2O_2 and 2.5 equivalents of triethylamine (TEA) in CH_3CN at 15 ºC. Complex 10b was formed upon addition of little excess (~30 equivalents) of *tert*-butyl hydroperoxide solution (70% in water) in acetonitrile at room temperature. However, the rate of formation, stability and rate of self-decay was highly influenced by the temperature parameter. Also, the formation of the same was tested using other solvents like acetone and DCM, but the stability of the –OOR adduct in both the solvents was not up to the mark as acetonitrile. The stability of these intermediates are crucial considerations in order to successfully characterize them using various spectroscopic techniques like ESI-MS, UV/Vis, NMR, etc. The formation techniques, stability, characterizations and reactivity of these reactive high valent intermediates are discussed latter in their respective chapters.

2.5. Physical Methods

UV/Vis spectra were recorded on a Hewlett Packard 8453 spectrophotometer equipped with either constant temperature circulating water bath or a liquid nitrogen cryostat (Unisoku) with a temperature controller. High-resolution electrospray ionization-mass spectra (ESI-MS) were recorded on a Waters (Micromass MS Technologies) Q-TOF Premier mass spectrometer by infusing analyte samples directly into the source at 15 μL min^{-1} using a syringe pump. The spray voltage was set at 2 kV and the capillary temperature at 80 °C unless otherwise mentioned. Also, few mass spectra were recorded with the help of Agilent-Q-TOF 6520 instrument in positive mode equipped with a Mass hunter workstation; the spray voltage was set at 3 kV and the drying gas flow and temperature were maintained as 5.0 L min^{-1} and 200 °C respectively. NMR spectra were recorded on Bruker Avance III HD 600 MHz and 400 MHz spectrometers and a Jeol Advanced Solution State 400 MHz spectrometer (JNMECZ400S) using TMS as internal standard under ambient conditions unless otherwise mentioned. The reported chemical shifts (in ppm) are in reference to the residual solvent peaks. The crystal structure was recorded on an Agilent Single Crystal X-Ray Diffractometer (XRD) equipped with Mo X-ray source (Mova), CCD detector (Eos), Oxford cryo system and crystal AlisPRO and Autochem software.

2.6. Reaction Kinetics

All the reactions were run in a 10 mm path length UV/Vis cuvette by monitoring UV/Vis spectral changes of reaction solutions. The kinetics studies were performed under pseudo first-order conditions with excess substrate concentration. The reactions were monitored by following the decrease of the absorbance of the characteristic peaks as a function of time. The rate constants were determined by fitting the changes in absorbance of the intermediates under study. Reactions were run at least in triplicate and the data reported represent the average of those. Standard deviation was less than 10 % of the given values.

Kinetic experiments were performed by using the following procedures: 1 mM Fe(IV)-oxo complexes including $[Fe^{IV}(O)(L2)]^{2+}$, (2b), $[Fe^{IV}(O)(L3)]^{2+}$, (3b) and $[Fe^{IV}(O)(L4)]^{2+}$, (4b), were prepared from 1 mM solutions of their ferrous precursor complexes 2a, 3a and 4a respectively by reacting with $PhI(OAc)_2$ in acetonitrile at room temperature. Each time 2.5 mL portion of the Fe(II) solutions were taken in a 4 mL glass vial and 2 mL was transferred into the quartz cuvette and deoxygenated with argon gas sealed with rubber septum and kept in UV/Vis spectrophotometer cuvette holder. For fast reactions, low temperature setup was employed using the low temperature cryostat when the oxidants were added through a 250 μL Hamiltonian syringe, immediately mixed with another 1 ml syringe until the characteristic peaks of intermediates were monitored in the UV/Vis spectrophotometer. Upon the maximum formation of Fe(IV)-oxo chromophore, few minutes were given to equilibrate the solution temperature. The substrates were then slowly added through a 250 μL Hamiltonian syringe into the quartz cuvette and mixed with another 1 mL syringe. The time course of the decay of the Fe(IV)-oxo chromophore was monitored. Concentrations of the substrates used in each case varied and were adjusted to achieve convenient reaction time and control.

2 mM solutions of $[Mn^{III}(L8)(O_2)]^+$ (8b) and/or $[Mn^{III}(L9)(O_2)]^+$ (9b) were prepared from 2 mM solutions of $[Mn^{II}(L8)(ClO_4)_2]$ (8a) and/or $[Mn^{II}(L9)(ClO_4)_2]$ (9a) by reacting with H_2O_2 (20 mM) in the presence of triethylamine (TEA, 5 mM) in CH_3CN at 15 ºC. Each time 2.5 mL of Mn(II) complex solution was taken in a 4 mL glass vial, and 2 mL was of it was transferred into a cuvette and deoxygenated with argon gas sealed with rubber septum and kept in UV/Vis spectrophotometer cuvette holder which was attached to a low temperature cryostat and waited till equilibrated at 1 ºC, then slowly 50 μL of 10 equivalents of H_2O_2 was added in the presence of 2.5 equivalents triethylamine through a 250 μL hamiltonian syringe, immediately mixed with another 1 ml syringe until characteristic peaks of the intermediates were obtained in the visible region. After it reaches the maximum formation of Mn(III)-peroxo intermediate a few minutes were given to equilibrate the solution temperature. Then substrates were slowly added through a 250 μL Hamiltonian syringe to the solutions, mixed with another 1 mL syringe and the time course of the decay of the Mn(III)-peroxo chromophore was monitored.

The formation of the alkylperoxo adduct was identified at normal conditions when 10a was treated with *tert*-butyl hydroperoxide solution (70% in water, 30 eq.). A new blue species (10b) was formed gradually. 1 mM solutions of 10a in CH_3CN was reacted with excess *tert*-butyl hydroperoxide and the formation spectra were optimized with the help of UV/Vis spectrophotometer. The oxidant solution and substrates were prepared in CH_3CN and substrates were added to the intermediates solution formed *in situ* at different temperature depending upon the rates of decay.

Iron(IV)-oxo complex, 1b, was prepared at 25 ºC, from 1 mM solution of its ferrous complexes in CH_3CN. Each time, a 2.5 mL portion of the iron(II) solution in a 4 mL glass vial was taken and excess solid PhIO was added and thoroughly mixed by vortex for a couple of minutes affording the corresponding oxo complex. The solution was filtered through 0.2 μM syringe filters into another clean and dry 4 mL glass vial and deoxygenated with argon gas. 2 mL of it was transferred into a cuvette and sealed with rubber septum and kept in UV/Vis spectrophotometer cuvette holder. The substrates were then slowly added using a 250 μL Hamiltonian syringe to the reaction mixture and mixed with another 1 mL syringe. The time course of the decay of the iron(IV)-oxo chromophore was monitored. Concentrations of the substrates were used ranging from 0.005 M to 0.5 M and were adjusted to achieve convenient reaction times.

In general, reactions were monitored through a minimum of 5 half-lives and the pseudo first-order rate constants (k_{obs}) were determined by fitting the decay profile of the UV/Vis bands for the respective intermediates to the equation:

$$[A] = [A_0] + b*(e^{-kt})$$

Plots of the k_{obs} against substrate concentrations gave the second-order rate constants for each system. The reaction mixtures were removed from the cuvette, oxidation products and metal salts were separated and passed through the silica gel and washed subsequently with CH_3CN. Product yields were determined by peak area ratios relative to the standard samples by different (like GC, NMR and ESI-MS) spectroscopic techniques.

2.7. Product Analysis

Product analyses of the reaction mixtures were done by ESI-MS, NMR (^{1}H and ^{13}C) with a Varian 400/100 MHz spectrometer and LCMS with WATERS ACQUITY UPLC equipped with a variable wavelength UV-200 detector. The products were separated on Waters Symmetry C18 reverse phase column (4.6 x 250 mm), and detection was made at 215 and 254 nm and product yields were determined by comparison with standard curves of known authentic samples.

2.8. References

1. W. L. F. Armarego in *Purification of Laboratory Chemicals*, (Ed: D. D. Perrin), Pergamon Press, Oxford, **1997**.
2. H. Saltzman, in *Organic Syntheses*, Vol. V (Ed: J. G. Sharefkin), Wiley, New York, **1973**, pp. 658.
3. S. A. Moteki, A. Usui, S. Selvakumar, T. Zhang, K. Maruoka, *Angew. Chem. Int. Ed.* **2014**, *53*, 11060–11064.
4. X. Su, Y. Sun, J. Yao, H. Chen, C. Chen, *Chem. Commun*. **2016**, *52*, 4537-4540.
5. M. Lubben, A. Meetsma, E. C. Wilkinson, B. Feringa, L. Que, Jr., *Angew. Chem. Int. Ed.* **1995**, *34*, 1512-1514.
6. W. K. C. Lo, C. J. McAdam, A. G. Blackman, J. D. Crowley, D. A. McMorran, *Inorg. Chim. Acta*, **2015**, *426*, 183-194.
7. M. K. Coggins, S. Toledo, E. Shaffer, W. Kaminsky, J. Shearer, J. A. Kovacs, *Inorg. Chem*. **2012**, *51*, 6633-6644.
8. G. R. Newkome, G. E. Kiefer, Y. A. Frere, M. Onishi, V. K. Gupta, F. R. Fronczek, *Organometallics*, **1986**, *5*, 348-355.
9. H. Börzel, P. Comba, K. S. Hagen, Y. D. Lampeka, A. Lienke, G. Linti, M. Merz, H. Pritzkow, L. V. Tsymbal, *Inorg. Chim. Acta*, **2002**, *337*, 407−419.
10. P. Comba, S. Kuwata, G. Linti, H. Pritzkow, M. Tarnai, H. Wadepohl, *Chem. Commun.* **2006**, 2074− 2076.
11. P. Comba, B. Kanellakopulos, C. Katsichtis, A. Lienke, H. Pritzkow, F. J. Rominger, *Chem. Soc., Dalton Trans.* **1998**, 3997− 4001.
12. P. Barman, A. K. Vardhaman, B. Martin, S. J. Wörner, C. V. Sastri, P. Comba, *Angew. Chem., Int. Ed.* **2015**, *54*, 2095−2099.

13. N. A. Barnes, A. T. Brooker, S. M. Godfrey, P. R. Mallender, R. G. Pritchard, M. Sadler, *Eur. J. Org. Chem*. **2008**, *6*, 1019-1030.
14. L. Duelund, R. Hazell, C. J. McKenzie, L. P. Nielsen, H. Toftlund, *J. Chem. Soc., Dalton Trans.* **2001**, 152–156.
15. R. H. Holm, G. W. Everett Jr., W. D. Horrocks Jr., *J. Am. Chem. Soc*. **1966**, *88*, 1071-1073.
16. J. A. Happe, R. L. Ward, *J. Chem. Phys*. **1963**, *39*, 1211-1218.
17. R. W. Kluiber, W. D. Horrocks Jr., *Inorg. Chem.* **1967**, *6*, 166-168.
18. S. Ménage, Y. Zang, P. Hendrich, L. Que, Jr., *J. Am. Chem. Soc*. **1992**, *114*, 7786-7792.
19. Y. Zang, H. G. Jang, Y.-M. Chiou, P. Hendrich, L. Que, Jr., *Inorg. Chim. Acta*, **1993**, *213*, 41-48.
20. G. N. La Mar, In *NMR of Paramagnetic Molecules*, G. N. La Mar, W. D. Horrocks Jr., R. H. Holm, Eds. Academic Press: New York, **1973**, pp 85-126.
21. G. Roelfes, M. Lubben, K. Chen, R. Y. N. Ho, A. Meetsma, S. Genseberger, R. M. Hermant, R. Hage, S. K. Mandal, V. G. Young, Jr., Y. Zang, H. Kooijman, A. L. Spek, L. Que, Jr., B. L. Feringa, *Inorg. Chem.* **1999**, *38*, 1929–1936.
22. A. L. Spek, M. F. J. Schoondergang, B. L. Feringa, CCDC 232796, *CSD Communication*, **2004**.
23. A. C. McQuilken, Y. Jiang, M. A. Siegler, D. P. Goldberg, *J. Am. Chem. Soc*. **2012**, *134*, 8758–8761.
24. L. R. Widger, C. G. Davies, T. Yang, M. A. Siegler, O. Troeppner, G. N. L. Jameson, I. Ivanović-Burmazović, D. P. Goldberg, *J. Am. Chem. Soc*. **2014**, *136*, 2699–2702.

25. S. Sahu, B. Zhang, C. J. Pollock, M. Dürr, C. G. Davies, A. M. Confer, I. Ivanović-Burmazović, M. A. Siegler, G. N. L. Jameson, C. Krebs, D. P. Goldberg, *J. Am. Chem. Soc*. **2016**, *138*, 12791–12802.
26. M. Mitra, H. Nimir, S. Demeshko, S. S. Bhat, S. O. Malinkin, M. Haukka, J. LloretFillol, G. C. Lisensky, F. Meyer, A. A. Shteinman, W. R. Browne, D. A. Hrovat, M. G. Richmond, M. Costas, E. Nordlander, *Inorg. Chem.* **2015**, *54*, 7152–7164.
27. S. Rana, A. Dey, D. Maiti, *Chem. Commun*. **2015**, *51*, 14469–14472.
28. S. Rana, J. P. Biswas, A. Sen, M. Cl8mancey, G. Blondin, J.-M. Latour, G. Rajaraman, D. Maiti, *Chem. Sci*. **2018**, *9*, 7843–7858.

CHAPTER – III

Dramatic Rate-Enhancement of Oxygen Atom Transfer by an Iron(IV)-Oxo Species by Equatorial Ligand Field Perturbations

● Adapted from *Dalton Trans.* **2018**, *47*, 14945−14957 with permission from the Royal Society of Chemistry ●

3.1. Introduction

Iron-containing metalloenzymes are well-known oxidants that carry out metabolically vital oxidative transformations in the human body.[1-6] High valent iron(IV)-oxo complexes have often been identified as the key reacting species in such oxidative transformations,[7-14] and indeed have been characterized for several non-heme iron dioxygenases.[15-16] Most non-heme iron dioxygenases display typical facial iron coordination *via* two histidines and one carboxylate based residue; usually from Asp or Glu. Many details on the catalytic reaction mechanisms of heme and non-heme metalloenzymes remain unknown. Moreover, many non-heme iron dioxygenases react with substrates in a stereoselective or regiospecific manner. For instance, prolyl-4-hydroxylase activates a proline residue in a peptide chain to give solely the R-4-hydroxyproline product as part of its natural biosynthesis pathway.[17-18] Recent QM/MM studies showed that even though 5-hydroxyproline would be a thermodynamically more stable product, the enzyme manages to avoid this product through substrate binding and orientation.[19-20] In particular, the substrate is held in a tight binding pocket and can only approach the active site through a narrow funnel lined up by a Trp and Tyr residue. Moreover, key hydrogen bonding interactions hold the substrate in a tight conformation and site-selective mutations of one of the residues in the substrate-binding pocket leads to either loss of specificity or complete loss of activity. Other enzymes with tight substrate binding pockets that catalyse a regioselective reaction include the camphor hydroxylating heme enzyme cytochrome P450cam,[21] and the non-heme iron dioxygenase AlkB, which is involved in DNA base repair mechanisms through the demethylation of methylated DNA bases.[22-23] Clearly, the substrate-binding position and orientation in enzymes is important and can determine and affect the product distributions.

To understand the mechanistic aspects of metalloenzymes biomimetic models have been developed that contain the coordination features of the metal but lack the protein environment.[24-28] Artificial/synthetic mimics of these biological systems provide necessary information about their catalytic cycle and their mode of operation. There are several reports in the literature regarding the tuning of the primary coordination sphere of these high valent intermediates and the various factors that affect their reactivity, such as ligand topology, axial ligation, spin state of the metal atom, etc.[29-35] As changes in the primary coordination sphere can be quite dramatic, research has also focused on the influence of secondary coordination sphere modifications, where changes are more subtle.[36-44] Noncovalent interactions in the vicinity of the active site, such as charge induction or stereochemical perturbations influence reaction mechanisms and can change bifurcation pathways.[45-47]

A biomimetic iron(IV)-oxo species that has received quite a lot of attention over the years is the $[Fe^{IV}(O)(N4Py)]^{2+}$ complex with N4Py = N,N-bis(2-pyridylmethyl)-N-bis(2-pyridyl) methylamine: structure 1b in Fig. 3.1. The complex was originally synthesized by Feringa and Que and their co-workers[48] and was one of the first biomimetic iron(IV)-oxo species that was characterized by electron paramagnetic resonance, resonance Raman, Mössbauer, UV/Vis absorption and nuclear magnetic resonance (NMR) spectroscopic methods as well as by X-ray crystallography.[49-50] In addition, many reactivity studies with substrates have been reported, which showed it efficiently reacts through oxygen atom transfer.[51-61] Very recently Que and co-workers showed that substitution of the three pyridine rings of the tetradentate TPA, tris-(2-pyridylmethyl)amine, ligand by quinoline moieties enabled the synthesis of a high-spin ($S = 2$) iron(IV)-oxo species.[62] However, replacement of the pyridine rings by N-methylbenzimidazole moieties, instead generated an $S = 1$ iron(IV)-oxo ground state.[63] Nevertheless, in both of these systems enhanced reactivity towards substrates was observed. Interestingly, such ligand modifications are much less explored in pentadentate iron(IV)-oxo intermediates. Nordlander and co-workers have shown that a systematic replacement of the pyridine groups with N-methylbenzimidazole in the N4Py ligand framework leads to enhanced reaction rates.[64]

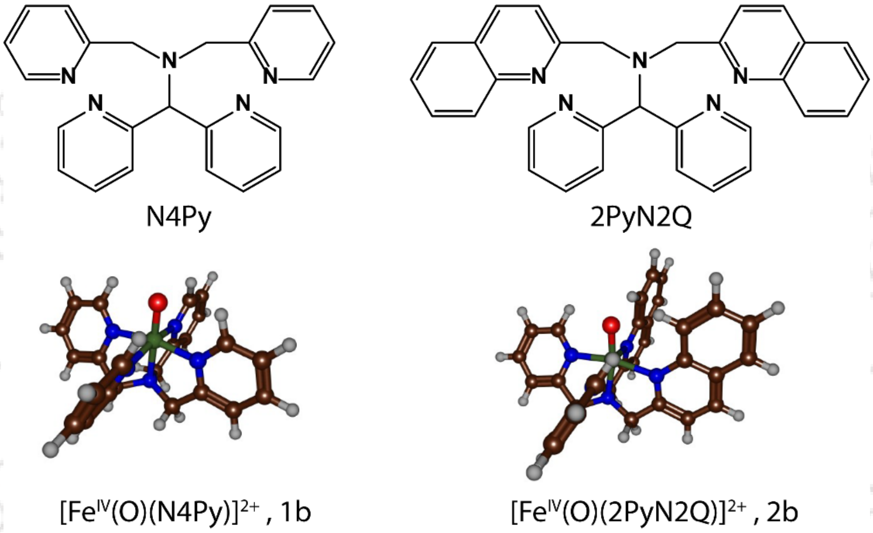

Fig. 3.1. Ligand frameworks (*top*) studied and DFT-optimised structures of the corresponding iron(IV)-oxo complexes.

In particular, the introduction of *ortho*-substituents to a pyridine ring is a well-established design strategy to significantly affect the iron(IV)-oxo core by weakening the Fe–N$_{eq}$ bonds. To gain insight into the influence of the equatorial ligand perturbations in biomimetic complexes, we engineered the N4Py ligand system to 2PyN2Q (1,1-di(pyridin-2-yl)-N,N-bis(quinolin-2-ylmethyl)methanamine). The introduction of bulky quinoline moieties is expected to influence the electronic orbitals and spectroscopic features of the iron(IV)-oxo oxidant and hence its reactivity with substrates. Specifically, we compare the spectroscopy and reactivity of the two non-heme iron(IV)-oxo complexes 1b and 2b (Fig. 3.1), namely $[Fe^{IV}(O)(N4Py)]^{2+}$ and $[Fe^{IV}(O)(2PyN2Q)]^{2+}$. In these complexes, the equatorial ligand perturbations on the oxo group are different, whereby in 2b the oxo group experiences two weak C–H···O hydrogen bonding interactions that are absent in complex 1b. We predicted that the changes in ligand coordination may give different spectroscopic and reactivity patterns.

3.2. Results and Discussion

3.2.1. Synthesis and Characterization

We started with a pentadentate non-heme iron complex $[Fe^{II}(2PyN2Q)(OTf)_2]$, 2a, supported by the 2PyN2Q ligand bearing quinoline moieties.[65-67] Dropwise addition of an acetonitrile solution containing $Fe^{II}(OTf)_2{\cdot}2CH_3CN$ to the ligand resulted in the formation of a dark yellow compound (2a) in 95% yield that could be characterized with UV/Vis, ESI-MS and NMR spectroscopy, (see Fig. 2.12 and 2.18, Chapter-II). Treatment of 2a with 1.5 equivalents of $PhI(OAc)_2$ in CH_3CN under ambient conditions generated the corresponding iron(IV)-oxo complex $[Fe^{IV}(O)(2PyN2Q)]^{2+}$, 2b ($\lambda_{max}$ = 770 nm, ε = 340 L M^{-1} cm^{-1}, $t_{1/2}$ = 50 min at RT), Fig. 3.2. The UV/Vis absorption spectrum of 1b when generated under the same experimental conditions gave an absorption band at λ_{max} = 695 nm with a half-life of over 60 hours typical of $[Fe^{IV}(O)(N4Py)]^{2+}$. Thus, the substitution of the pyridine rings in N4Py with quinoline groups to form 2PyN2Q resulted in a bathochromic shift of the d–d transition band by 75 nm and a significant loss of the thermal stability of the complex.

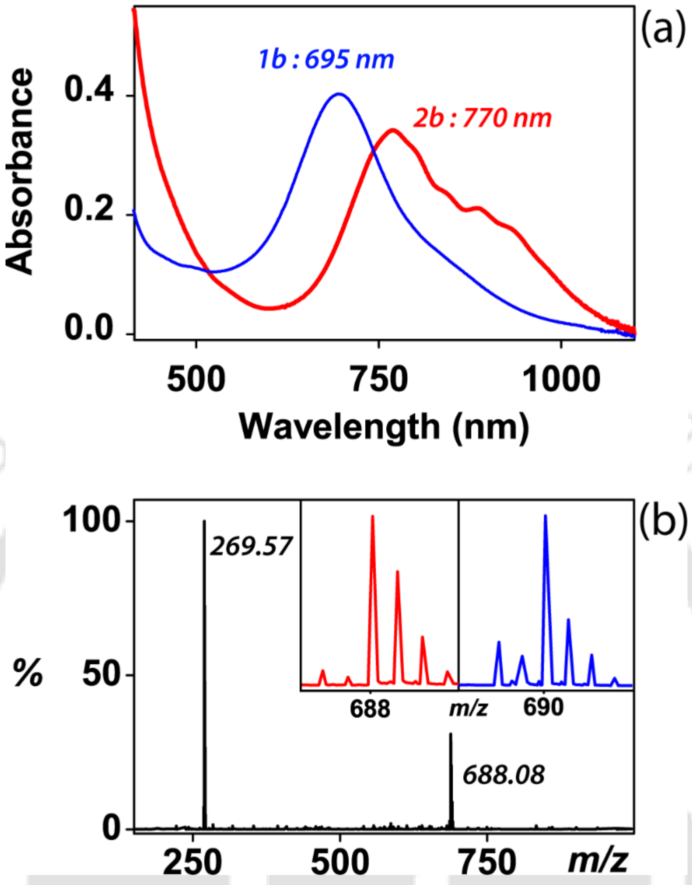

Fig. 3.2. (a) UV/Vis spectra of 1b (blue) and 2b (red) in CH_3CN at 298 K; (b) ESI-MS of 2b in CH_3CN at 298 K. Inset shows the isotopic distribution pattern for $[Fe^{IV}(O^{16})(2PyN2Q)(OTf)]^{+}$ (red) and $[Fe^{IV}(O^{18})(2PyN2Q)(OTf)]^{+}$ (blue).

The new iron(IV)-oxo complex was also characterized successfully with the help of ESI-MS (Fig. 3.2). The ESI-MS gives a major peak at *m/z* 269.57 corresponding to $[Fe^{IV}(O)(2PyN2Q)]^{2+}$ and a minor peak at *m/z* 688.08 representing the $[Fe^{IV}(O)(2PyN2Q)(OTf)]^{+}$ ion. The isotopic patterns for the two species confirm the assignments of the two ions. The formation of $[Fe^{IV}(O)(2PyN2Q)]^{2+}$ was further established by an isotopic labelling experiment using $H_2{}^{18}O$, which leads to oxygen atom exchange with the oxo group. The experiment with $H_2{}^{18}O$ moves the peak in the ESI-MS for $[Fe^{IV}(O)(2PyN2Q)(OTf)]^+$ from *m/z* 688.08 to *m/z* 690.08, while the peak representing the $[Fe^{IV}(O)(2PyN2Q)]^{2+}$ ion shifts by one unit. Hence the isotopic labelling experiment with a positive peak shift of two units shows that one oxygen atom is incorporated into the metal complex in the form of an iron(IV)-oxo species.

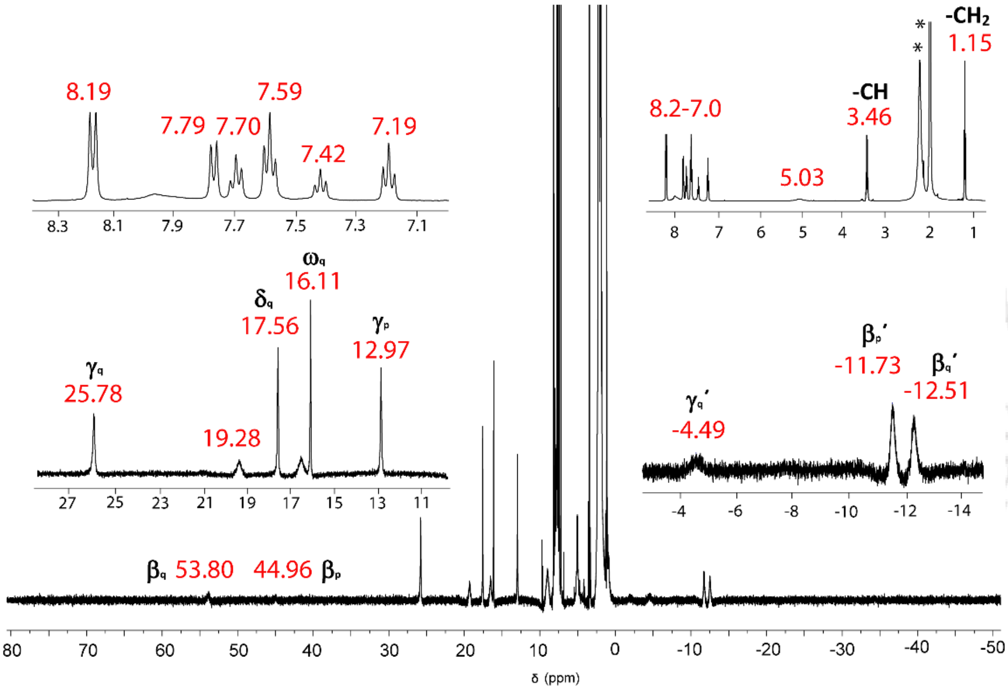

Fig. 3.3. ^1H-NMR spectrum of complex 2b in CD_3CN at 298 K with a spectral width of ~200 ppm (no. of scans = 64). Inset shows the individual expanded portions of the spectrum. Solvent peaks are denoted by (*). The peaks have been assigned based on previously reported literature.

Further employment of ^1H-NMR helped us see the differences between the two iron(IV)-oxo complexes (see Fig. 3.3). The ^1H-NMR spectra for complex 1b as reported by Klinker et al. reveals the presence of mirror symmetry.[50] However, for complex 2b, as expected, a more complicated spectrum with a larger number of signals was obtained compared to 1b, due to the presence of quinoline groups instead of pyridine rings. The observed range of paramagnetic shift in the ^{1}H-NMR spectrum of 2b decreased with respect to its Fe(II) precursor and gave a typical $S = 1$ shift.[36,50] To gain more insight into the electronic structure of 2b, we performed a variable temperature NMR experiment over a temperature range from 233–298 K. With a lowering of the temperature, no upfield shift of peaks was observed in the Curie plot, thereby confirming an $S = 1$ ferryl species as the ground state, see Fig. 3.4 and 3.5. This observation was further supported by Rasheed et al. using Mössbauer spectroscopy.[68]

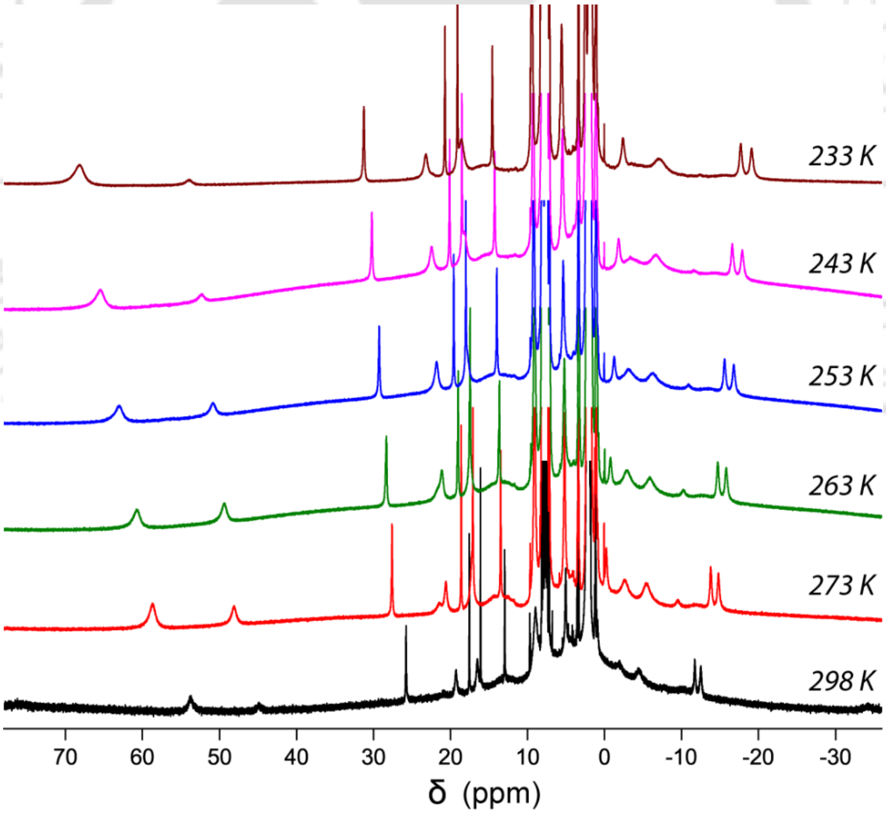

Fig. 3.4. VT-NMR spectrum of complex 2b in CD_3CN recorded within the temperature range of 298 K and 233 K.

The Fourier transform infrared spectral data of 2b showed a Fe=O stretch vibration at 834 cm^{-1} which was at a lower frequency in comparison with 1b.[68] Nevertheless, the lifetime of 2b is sufficiently long to enable us to do a detailed kinetics and spectroscopy study at room temperature alongside those for the analogous complex 1b, *i.e.* $[Fe^{IV}(O)(N4Py)]^{2+}$.

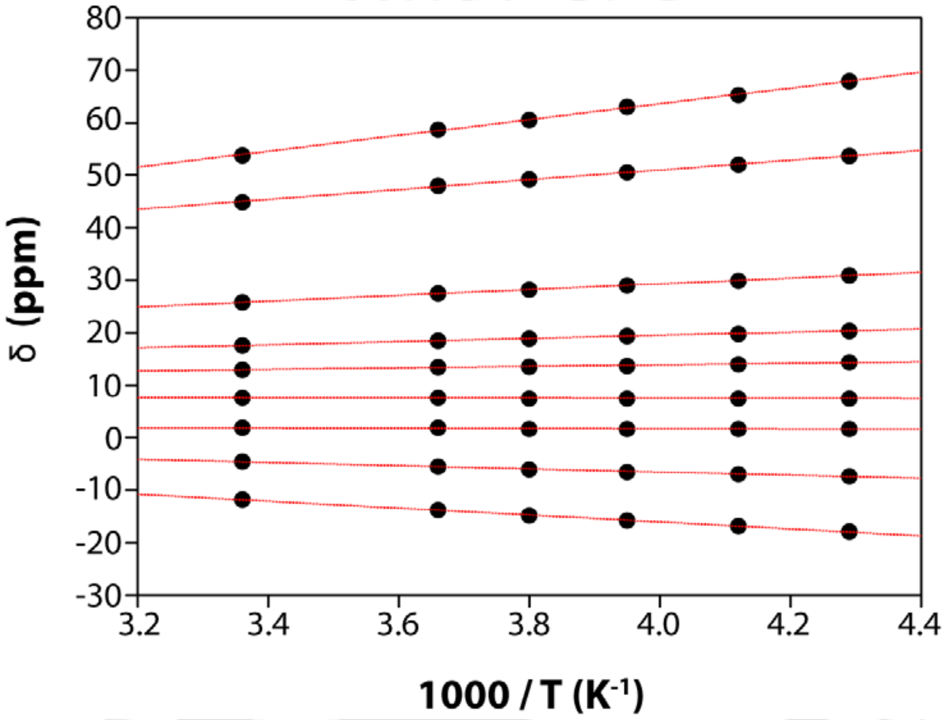

Fig. 3.5. Curie plot showing the linear dependence of chemical shift of the ^{1}H-NMR signals of 2b as a function of temperature.

3.2.2. Reaction Kinetics

In order to find out whether the change in spectroscopic properties of the oxidant (2b versus 1b) has an effect on the oxidation properties, we did a thorough kinetics study using a range of different substrates. Thus, we employed thioanisole and benzyl alcohol as model substrates for heteroatom oxidation and alcohol oxidation reactions, respectively. Addition of thioanisole to 2b at 233 K led to the decay of the iron(IV)-oxo characteristic band at 770 nm in the UV/Vis spectrum concomitant with the appearance of its iron(II) precursor (λ_{max} = 475 nm) with an isosbestic point at 605 nm, thereby generating methyl phenyl sulfoxide as the major product (Fig. 3.6). We measured the change in absorbance from the UV/Vis spectra at 770 nm and plotted it as a function of time, which enabled us to determine the pseudo first-order rate constant (k_{obs}) for the reaction. Subsequently, these observed rate constants were converted into second-order rate constants by plotting k_{obs} as a function of substrate concentration.

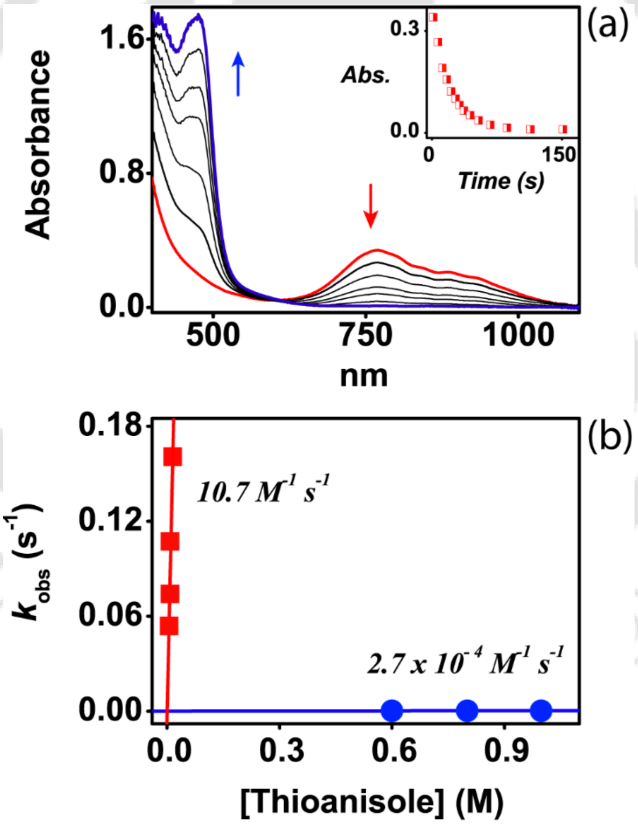

Fig. 3.6. (a) UV/Vis spectral changes of 2b upon addition of 7 equiv. thioanisole in CH_3CN at 233 K. Inset shows the decay profile of the 770 nm band; (b) second order rate constant determined for the reaction of 1b (1 mM) (●) and 2b (1 mM) (■) with thioanisole at 233 K.

The second-order rate constant (k_2) for the reaction of thioanisole with 2b was evaluated to be 10.7(4) M^{-1} s^{-1} at 233 K (Fig. 3.6.b). Previous work on the reaction of thioanisole with 1b under the same reaction conditions,[63] provided a second-order rate constant of 2.7×10^{-4} M^{-1} s^{-1}.

Consequently, under the same experimental conditions, the reactivity of 2b with thioanisole is faster than that of 1b by a factor of almost 4×10^4 fold. This rate increment is much higher than those observed for an analogous ligand system with N-methylbenzimidazole substituents by at least 30 times.[64] The enhanced reaction rate probably originates from the introduction of the *ortho*-substituent on the pyridine ring and consequent weakening of the Fe–N_{eq} bonds relative to that in 1b. To gain insight into the mechanistic details of the reaction, we studied the reaction of 2b with various *para*-X-substituted thioanisole substrates (X = OCH_3, CH_3, H, Cl) and measured their reaction rates (Table 3.1 and Fig. 3.7).[74-75]

Table 3.1. Pseudo first-order rate constants (k_{obs}) determined for the reaction of 2b (1 mM solution in CH_3CN) with 5 equivalents of *para*-X-substituted thioanisole at −40 °C in CH_3CN[a]

x^b	$\sigma_p{}^c$	$\sigma_p{}^{+c}$	$E^0{}_{ox}{}^d$	$k_{obs}{}^e$	$k_X / k_H{}^f$	$\log (k_X/k_H)$
-OCH_3	-0.27	-0.78	1.13	0.177(4)	3.29	0.52
-CH_3	-0.17	-0.31	1.24	0.088(2)	1.64	0.22
-H	0.00	0.00	1.34	0.054(2)	1.00	0.00
-Cl	0.23	0.11	1.37	0.015(3)	0.28	-0.55

[a] All the reactions were followed by monitoring the UV/Vis spectral changes of the reaction solution. [b] *para*-substituents in *para*-X-thioanisole. [c] Data taken from ref. 74. [d] Data taken from ref. 75. [e] In s^{-1}. [f] Relative rate constant obtained by dividing the k_{obs} of *p*-X-thioanisole by k_{obs} of *p*-H-thioanisole.

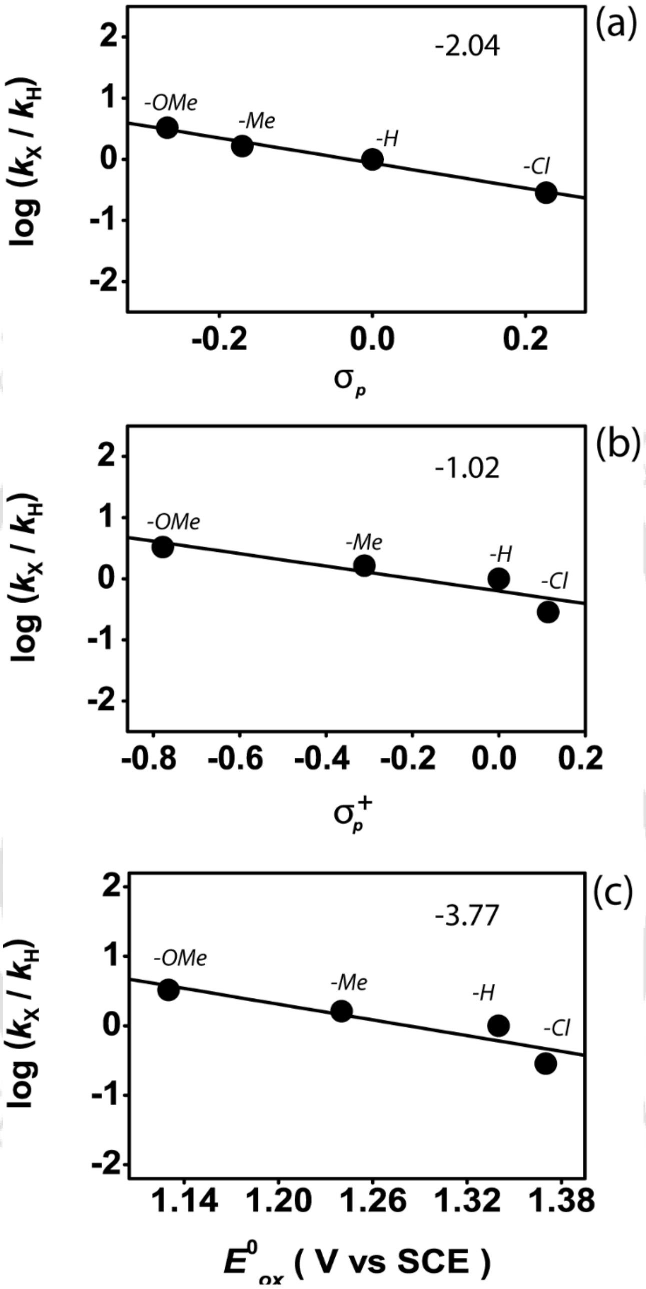

Fig. 3.7. Hammett plot obtained against (a) σ_p (b) σ_p^+ and (c) E^0_{ox} in the reaction of 2b with *p*-X-thioanisole at 233 K, where $\underline{k}_X$ and k_H are the pseudo first-order rate constants of *p*-X-thioanisole and thioanisole respectively.

A plot of the logarithm of the rate constant ratio (k_X/k_H) as a function of the one-electron oxidation potentials (E^0_{ox}) of various *para*-X-substituted thioanisole substrates gives a linear correlation with a slope of $\rho = -3.77$ (Fig. 3.7). The negative ρ value and slope implicates that the reaction proceeds *via* atom transfer through an electrophilic reaction mechanism.[75]

To compare the reactivity difference of 2b over 1b in C–H activation reactions, we subsequently monitored the hydrogen atom abstraction ability of both complexes toward benzyl alcohols. Upon addition of different concentrations of benzyl alcohol to 2b in acetonitrile, the 770 nm band decayed in a pseudo first-order manner as a function of time. Product analysis reveals the formation of benzaldehyde in almost stoichiometric yields (>80% with respect to intermediate formed). The second-order rate constant (k_2) for the reaction of 2b with benzyl alcohol is found to be $51.04(1) \times 10^{-2}$ M^{-1} s^{-1} at 298 K (Fig. 3.8), whereas previous work for 1b found a value of 8.27×10^{-2} M^{-1} s^{-1} under the same reaction conditions.[76] As such, $[Fe^{IV}(O)(2PyN2Q)]^{2+}$ reacts with benzyl alcohol with rates that are more than six times faster than $[Fe^{IV}(O)(N4Py)]^{2+}$. Therefore, the equatorial ligand environment has significant effect on the reaction rates of alcohol oxidation reactions. Its rate-enhancement, however, is not as strong as in oxygen atom transfer (compare Fig. 3.6.b and 3.8.a), but clearly, both reaction processes are favoured with 2b as an oxidant.

To ascertain that hydrogen atom abstraction is indeed the rate-determining step in the reaction mechanism, we repeated the experiment with benzyl alcohol-D7 or $C_6D_5CD_2OH$ as the substrate. A comparison of the rate constants depicted in Fig. 3.8.b (Table 3.2) clearly shows that the substitution of the active hydrogen atom by deuterium reduces the reaction rate by a factor of about 8. Hence, we determine a kinetic isotope effect (KIE) value of 8 for the reaction of 2b with benzyl alcohol at 298 K. This KIE value is indicative of a rate-determining hydrogen atom abstraction step in the reaction mechanism. Our mechanism, therefore, is in excellent agreement with that derived for 1b with benzyl alcohol although an even larger KIE value is obtained upon replacement of hydrogen by deuterium.[76-77]

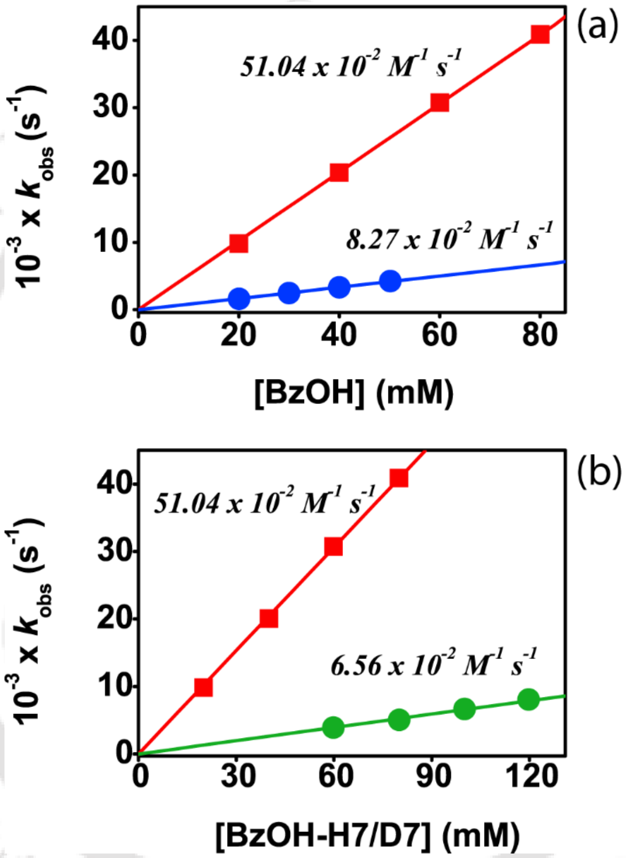

Fig. 3.8. Second-order rate constant determined for the reaction of : (a) 1 mM 1b (●) and 1 mM 2b (■) with benzyl alcohol in CH_3CN at 298 K; (b) 1 mM 2b with benzyl alcohol (■) and benzyl alcohol-D7 (●) in CH_3CN at 298 K.

Further evidence of the mechanism was obtained through studies of *para*-X-substituted benzyl alcohols in a reaction with $[Fe^{IV}(O)(2PyN2Q)]^{2+}$, 2b. In particular, we monitored the influence of electron-withdrawing or electron-donating *para*-X-substituents on the reaction rate of 2b with benzyl alcohols at 298 K. When we plot the log (k_X/k_H) values as a function of the Hammett parameters, σ_p, a linear trend was found with a slope of $\rho = -0.27$, Fig. 3.9 and Table 3.3. This small Hammett ρ value implicates little electronic effects as a result of the addition of *para*-substituents to benzyl alcohol. Mechanistically, therefore, 2b shows a reactivity pattern close to that previously reported on 1b, where a ρ value of −0.10 was found under similar reaction conditions.[76]

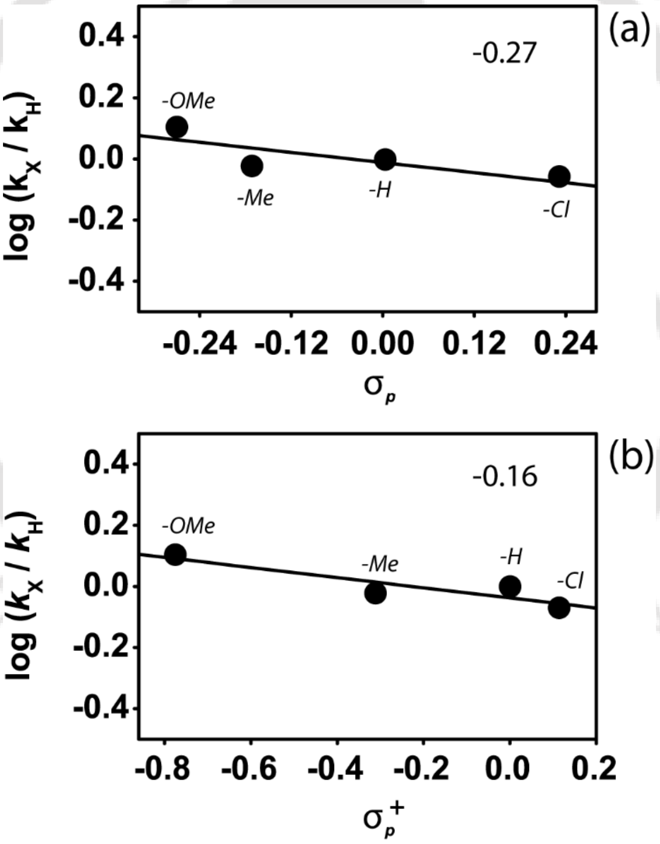

Fig. 3.9. Plot of log (k_X/k_H) against (a) σ_p values and (b) σ_p^+ values in the reaction of 2b with *p*-X-benzyl alcohol at 298 K, where k_X and k_H are the second-order rate constants of *p*-X-benzyl alcohol and benzyl alcohol respectively.

Table 3.2. Pseudo first-order rate constant (k_{obs}) determined in the reaction of 2b (1 mM solution in CH_3CN) with benzyl alcohol and benzyl alcohol-D7 at 25 °C in CH_3CN.

[Benzyl alcohol – H7] (mM)	*10^{-3} x k_{obs} (s^{-1})*	*[Benzyl alcohol - D7] (mM)*	*10^{-3} x k_{obs} (s^{-1})*
20	9.83(2)	60	3.90(2)
40	20.29(1)	80	5.08(3)
60	30.76(2)	100	6.63(2)
80	40.89(2)	120	9.97(3)

Table 3.3. Second-order rate constants (k_2) determined for the reaction of 2b (1 mM solution in CH_3CN) with various *para*-X-benzyl alcohols at 25 °C in CH_3CN[a]

x^b	$\sigma_p{}^c$	$\sigma_p{}^{+\,c}$	$k_2{}^d$	$k_x / k_H{}^e$	log (k_x/k_H)
-OCH_3	-0.27	-0.78	0.648(3)	1.270	0.104
-CH_3	-0.17	-0.31	0.484(2)	0.948	-0.023
-H	0.00	0.00	0.510(1)	1.000	0.000
-Cl	0.23	0.11	0.434(2)	0.851	-0.069

[a] All the reactions were followed by monitoring the UV/vis spectral changes of the reaction solution. [b] *para*-substituents in *para*-X-benzyl alcohol. [c] Data taken from ref. 74. [d] In M^{-1} s^{-1}. [e] Relative rate constant obtained by dividing the k_{obs} of *p*-X-benzyl alcohol by k_{obs} of *p*-H- benzyl alcohol.

We then studied the hydrogen atom abstraction ability of 2b and 1b with a selection of substrates with known C–H bond strengths. Previously, it was shown that reactions proceeding with a rate-determining hydrogen atom abstraction have the natural logarithm of the rate constant linearly related to the C–H bond dissociation energy ($BDE_{C–H}$).[78-81] We investigated the hydrogen atom abstraction reactions of 2b with substrates including triphenylmethane, cumene, ethylbenzene and toluene (Fig. 3.10 and Table 3.4). These substrates span a range of C–H bond dissociation energies ($BDE_{C–H}$) typical for hydrogen atom abstraction reaction rates.[49,82-91] As can be seen from Fig. 3.10, a linear correlation between the natural logarithm of the rate constant versus $BDE_{C–H}$ is found for the reactions of 2b/1b with substrates. The linearity of the Bell–Evans–Polanyi plot (log k_2' versus $BDE_{C–H}$) provides evidence of a rate-determining hydrogen atom abstraction.

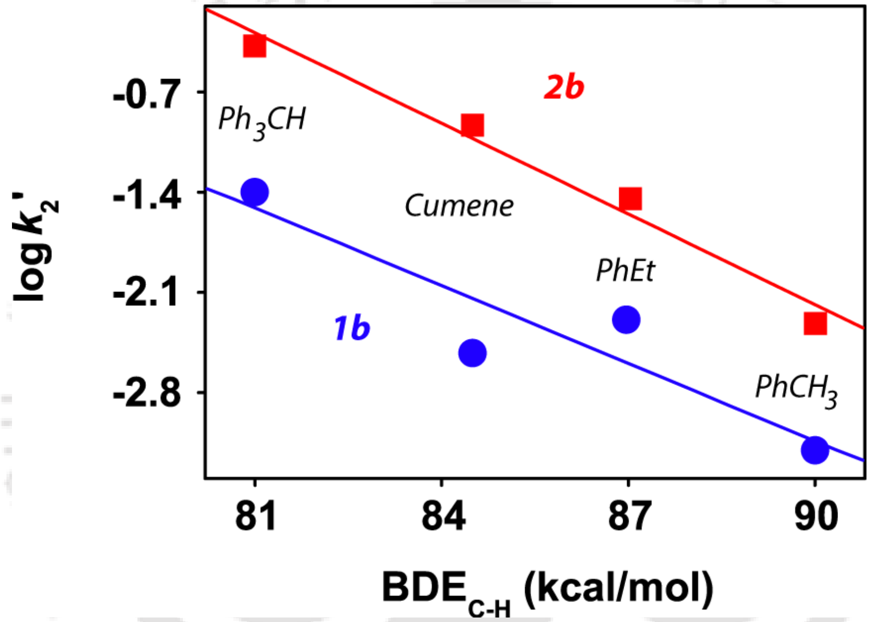

Fig. 3.10. Correlation between C–H bond dissociation energies of different hydrocarbons and log k_2' for their reactions with 1b (●) and 2b (🟥) at 298 K; k_2' is the second-order rate constant divided by the number of equivalent C–H bonds on the substrate that would react with the iron(IV)-oxo.

Product analysis of the dead reaction mixture after the decay of the characteristic band in UV/Vis spectrum indicated the production of the corresponding alcohols (and aldehydes) in variable yields (e.g. $Ph_3C–OH$, 88%; $PhC(OH)(CH_3)_2$, 60%; $PhCH(OH)CH_3$, 32% and PhCHO, 55%). It is not surprising to see that the rate-enhancement for sulfoxidation is different from hydrogen atom abstraction as sulfoxidation generally is a concerted two-electron reaction mechanism, whereas substrate hydroxylation is stepwise reaction via a radical intermediate.[92] Clearly, the change of the ligand and the introduction of equatorial ligand perturbations do not affect the reaction mechanism of 2b/1b with substrates. However, the change in ligand does affect their absolute reactivity.

Table 3.4. C–H Bond dissociation energies and second-order rate constant values for the reaction of 1b (1 mM) and 2b (1 mM) with various substrates in CH_3CN at 25 °C.

Substrate [a]	***BDE***$_{C\text{-}H}$ [b]	***Complex***	***k***$_2$ [c]	***k***$_2$' [c,d]	***log k***$_2$'
Ph_3CH (1)	81	1b	0.043(2)	0.043	-1.37
		2b	0.376(4)	0.376	-0.42
$PhCH(CH_3)_2$ (1)	84.5	1b	0.003(3)	0.003	-2.55
		2b	0.125(3)	0.125	-0.90
$PhCH_2CH_3$ (2)	87	1b	0.011(1)	0.005	-2.26
		2b	0.082(2)	0.041	-1.38
$PhCH_3$ (3)	90	1b	0.0006(2)	0.0002	-3.68
		2b	0.015(4)	0.005	-2.29

[a] The number in parenthesis indicates the number of equivalent H-atoms on the substrate that would react with the iron(IV)-oxo species. [b] From ref. 49-50; in kcal mol^{-1}. [c] In M^{-1} s^{-1}. [d] The k_2' values are obtained by dividing k_2 values by the number of equivalent hydrogen atoms in the substrate that would react with the iron(IV)-oxo species.

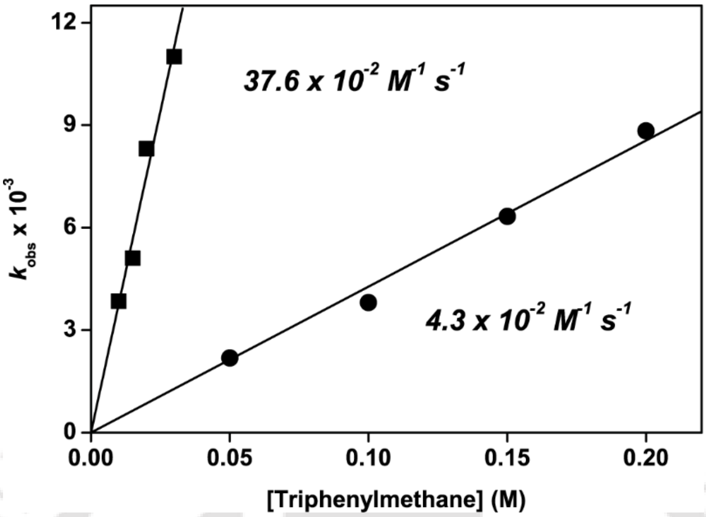

Fig. 3.11. Second-order rate constant determined for the reaction of 1b (●) and 2b (■) with triphenylmethane in CH_3CN at 298 K.

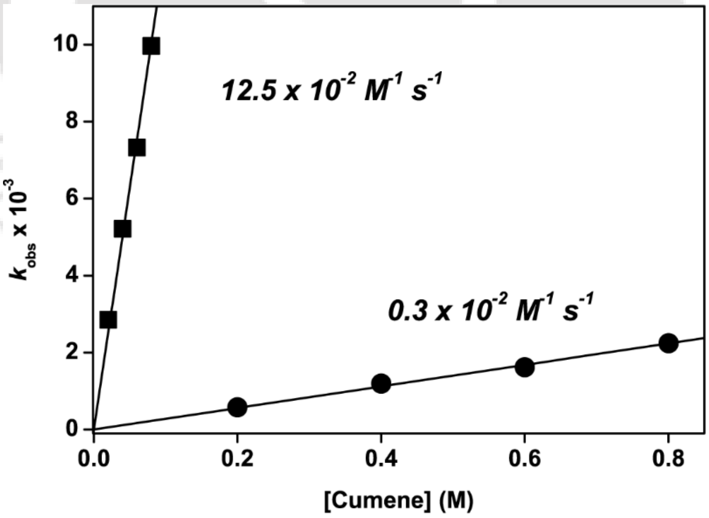

Fig. 3.12. Second-order rate constant determined for the reaction of 1b (●) and 2b (■) with cumene in CH_3CN at 298 K.

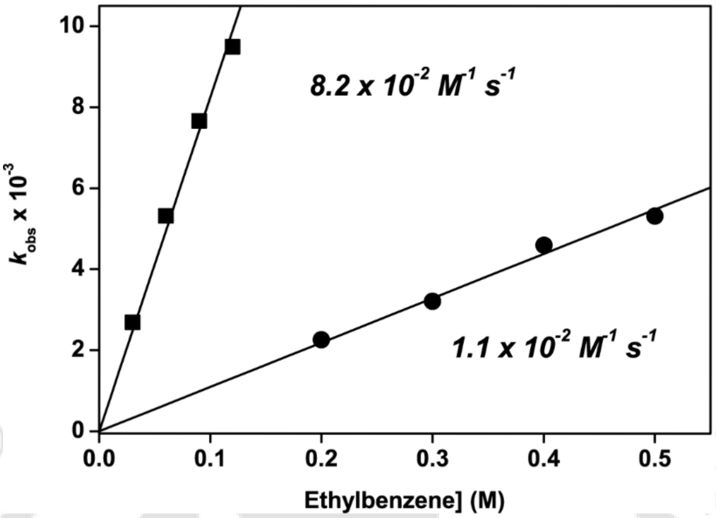

Fig. 3.13. Second-order rate constant determined for the reaction of 1b (●) and 2b (■) with ethylbenzene in CH_3CN at 298 K.

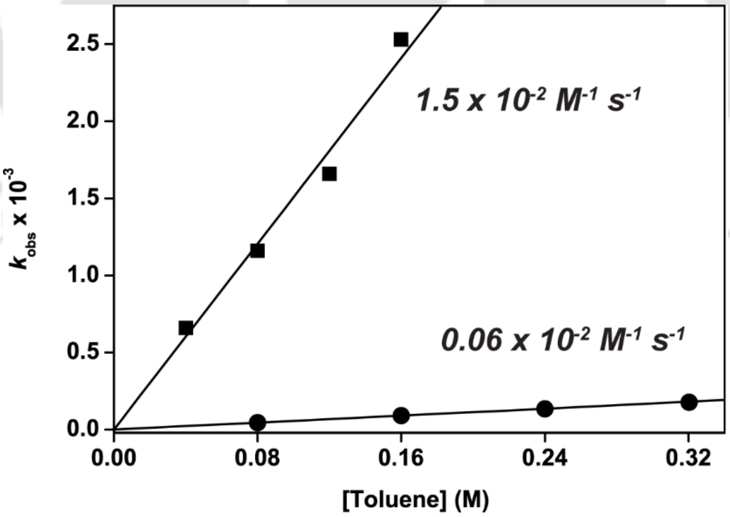

Fig. 3.14. Second-order rate constant determined for the reaction of 1b (●) and 2b (■) with toluene in CH_3CN at 298 K.

Finally, a reactivity study of 2b with cyclobutanol was performed, which is often used as a mechanistic probe.[76-77] In particular, the formation of cyclobutanone as a product indicates a single step two-electron process, whereas two sequential one-electron steps involve ring-opening of the substrate and the subsequent formation of 4-hydroxybutyraldehyde. We find that 2b reacts with cyclobutanol to give cyclobutanone as the major product, thereby, confirming that alcohol oxidation by complex 2b proceeds by a direct two-electron transfer pathway.

Scheme 3.1. Oxidation of cyclobutanol used as a mechanistic probe by product analysis.

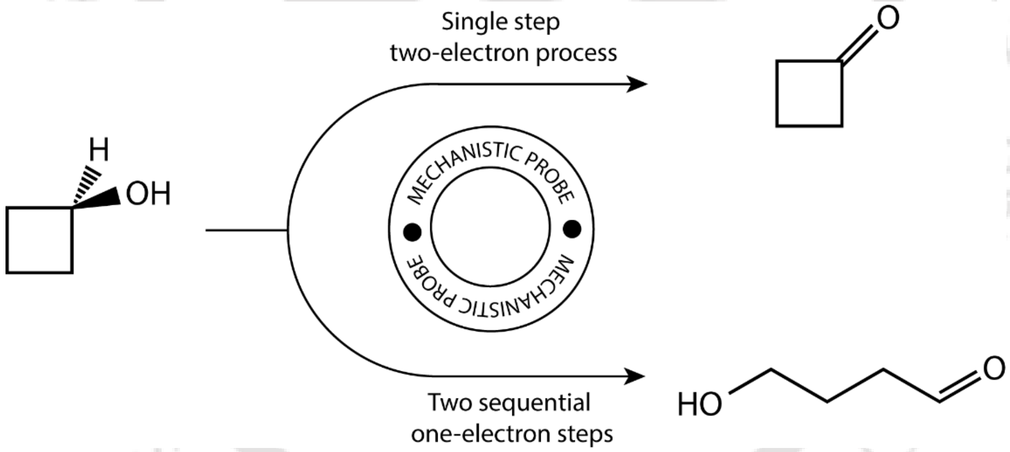

3.2.3. Computational Backup

In order to understand the rate-enhancement of 2b over 1b in oxygen atom transfer reactions, we initiated a density functional theory (DFT) study[93] using methods and procedures calibrated against experimental rate constants for $[Fe^{IV}(O)(N4Py)]^{2+}$ reactivities previously.[76,94,95] It was observed that the equatorial ligand perturbation has a major effect on the molecular orbital shapes and energies that deviate dramatically from those typically found for pentadentate non-heme iron(IV)-oxo complexes without these effects.[96-101] As a result the triplet–quintet spin state gap is narrowed from 7.5 kcal mol^{-1} for $[Fe(O)(N4Py)]^{2+}$ to 2.8 kcal mol^{-1} for $[Fe(O)(2PyN2Q)]^{2+}$. This result is in line with Nordlander et al who also observed similar effect for hydrogen atom abstraction through equatorial ligand field perturbations.[66] In our particular system, the ^{3,5}2b complex has a small triplet–quintet energy gap due to equatorial ligand perturbations that affect the structure and molecular orbitals along the Fe–O axis. Particularly, the change in O–Fe–N_{axial} angle will affect the $\sigma_{z2}/\sigma^*_{z2}$ orbital interactions of the oxo with iron atoms and specifically their energy levels and energy splitting. Since, the reduction of the iron(IV)-oxo complexes leads to filling of the σ^*_{z2} orbital with one electron this bending also should lower the energy of the complex to pick up an electron, *i.e.* its electron affinity (EA). Indeed, we find a considerably lower electron affinity for 2b than for 1b as predicted: EA_{2b} = 123 kcal mol^{-1} and EA_{1b} = 134 kcal mol^{-1}. Therefore, the change in electron affinity should affect the reactivity differences with substrates as well in agreement with the experimental data reported above. To further test the reactivity changes of 1b versus 2b with substrates for either hydrogen atom abstraction or oxygen atom transfer, we calculated the reaction mechanisms of 1b/2b with several model substrates, namely 1,3-cyclohexadiene (CHD), toluene (Tol) and dimethylsulfide (DMS).

The dehydrogenation of 1,3-cyclohexadiene to benzene by ^{3,5}2b and ^{3,5}1b were investigated and the results are given in Fig. 3.15. The reaction is stepwise with an initial hydrogen atom abstraction *via* transition state TS_{HA} leading to a radical intermediate I_{HA}. In the next step, a second hydrogen atom abstraction occurs *via* transition state TS_{desat} to form benzene products (P_{HA}). During the HAT a spin state crossing occurs from the triplet to the quintet spin state to give the quintet spin products. With ^{3,5}2b this spin state crossing is early and probably happens before the hydrogen atom abstraction transition state, so that $^{5}TS_{HA,2b}$ will be rate-determining. Optimized geometries of the hydrogen atom abstraction transition states are given in Fig. 3.15. The triplet spin structures are very similar with C–H and H–O distances of 1.239/1.421 Å for $^{3}TS_{HA,1b}$ versus 1.260/1.381 Å for $^{3}TS_{HA,2b}$.

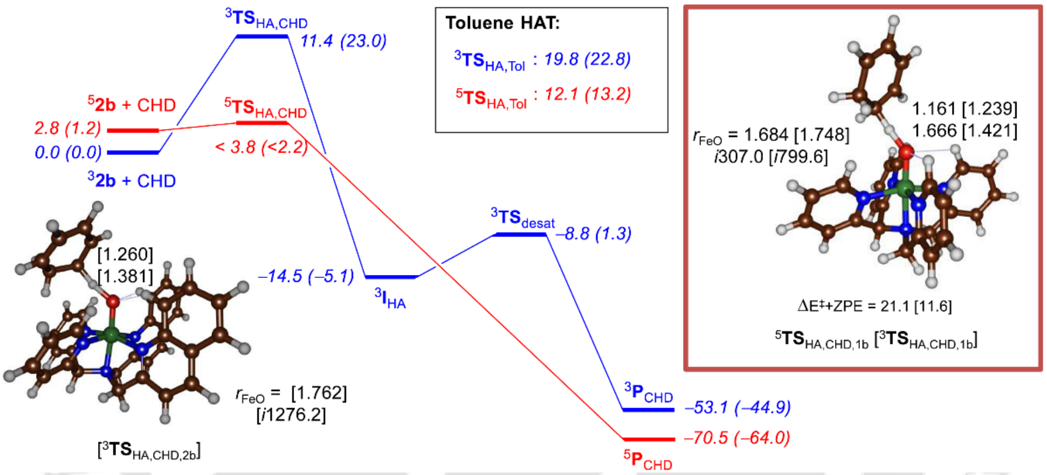

Fig. 3.15. Potential energy profile, ΔE + ZPE + E_{solv} and ΔG + E_{solv} (in parenthesis) with values in kcal mol^{-1} for CHD dehydrogenation and toluene hydrogen atom abstraction by ^{3,5}2b as calculated at UB3LYP/BS2//UB3LYP/BS1 level of theory. Also shown are optimized geometries of $^{3,5}TS_{HA,CHD,2b}$ with bond lengths in angstroms, angles in degrees and the imaginary frequency in wave numbers. The value for $^{5}TS_{HA,CHD}$ was estimated from the geometry scan.

Also given in Fig. 3.15 are the hydrogen atom abstraction barriers from toluene by 2b. In general, the barriers are considerably higher than those seen for 1,3-cyclohexadiene as a significantly stronger C–H bond is broken in the process. Indeed, triplet and quintet spin free energies of activation of 22.8 and 13.2 kcal mol^{-1}, respectively for hydrogen atom abstraction from toluene are found. These values are in reasonable agreement with the rate constants reported in Table 3.4 above. Moreover, in comparison with the toluene hydrogen atom abstraction barriers by [Fe^{IV}(O)(N4Py)]$^{2+}$ reported previously,[102] it implies a substantial rate-enhancement can be expected.

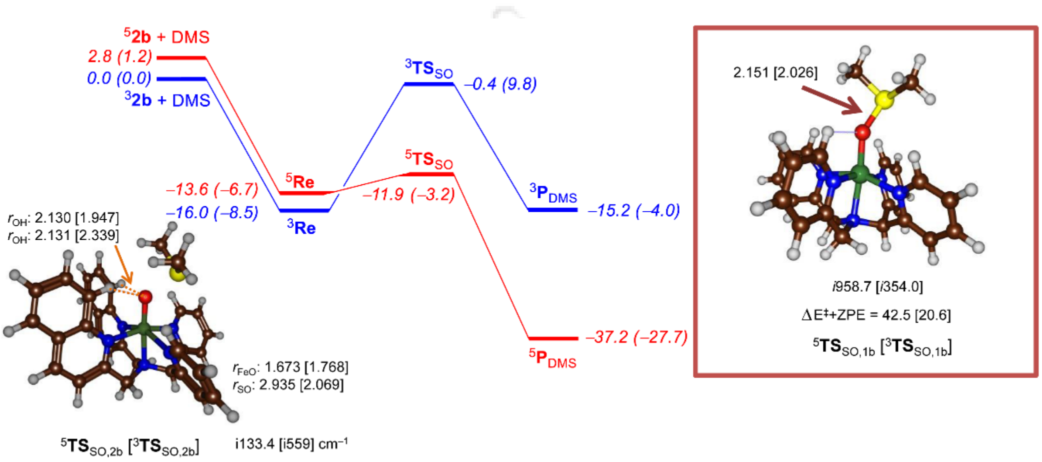

Fig. 3.16. Potential energy profile ($\Delta E + ZPE + E_{solv}$) with values in kcal mol^{-1} for sulfoxidation of DMS by ^{3,5}2b as calculated at UB3LYP/BS2//UB3LYP/BS1 level of theory. Also shown are optimized geometries of ^{3,5}TS$_{SO,2b}$ with bond lengths in angstroms, angles in degrees and the imaginary frequency in wave numbers. The inset gives the ^{3,5}TS$_{SO,1b}$ optimized geometries from ref. 74,75.

To further understand the reactivity differences of 1b and 2b in oxygen atom transfer (OAT), dimethylsulfide was used as a typical substrate. Fig. 3.16 shows the potential energy landscape of OAT by ^{3,5}2b from DMS. As can be seen, the reaction proceeds by forming a reactant complex (^{3,5}Re) of oxidant and substrate in a highly exothermic reaction step of −16.0 kcal mol^{-1}, which retains the spin state ordering between triplet and quintet. Upon approach of the substrate on the oxo group, an OAT transition state (TS$_{SO}$) is encountered prior to the formation of the sulfoxide product complexes (P_{DMS}). The quintet spin state barrier is very small (1.7 kcal mol^{-1} above ^{5}Re), whereas the triplet spin barrier is considerably higher in energy. Therefore, the reaction will proceed through a spin state crossing from triplet to quintet during the OAT reaction. Moreover, these calculations imply much faster oxygen atom transfer than the bare N4Py complex, whereas the reactivity differences between 1b and 2b are much less for hydrogen atom abstraction in line with the experimental observations. Consequently, 2b is a more efficient oxidant than 1b because of a lower-lying quintet spin state that enables a fast spin state crossing from triplet to quintet.

3.3. Conclusion

In conclusion, we have synthesized a room temperature stable iron(IV)-oxo intermediate (2b) that acts as an efficient oxidant of substrates. Instead of contributing to the steric fencing around the iron(IV)-oxo core and prohibiting molecular approach, the introduction of two bulky quinoline groups in the N4Py ligand framework has notably enhanced the HAT and OAT reactivity of the iron(IV)-oxo complex. We did a comparative study of thioanisole oxidation and hydrogen atom abstraction reactions with various substrates. We show that 2b reacts with substrates with increased rate constants with respect to those obtained with oxidant 1b which is attributed to subtle changes in the ligand skeleton. These engineered structures show that small perturbations on the equatorial ligand may have major influences in substrate positioning and reactivity in line with what is found for enzymatic reaction mechanisms. The work highlights how tweaking the ligand architecture of a catalyst can affect its performance, which will help in designing novel synthetic scaffolds for enzymatic mimics.

3.4. References

1. E. I. Solomon, T. C. Brunold, M. I. Davis, J. N. Kemsley, S. K. Lee, N. Lehnert, F. Neese, A. J. Skulan, Y. S. Yang, J. Zhou, *Chem. Rev.*, **2000**, *100*, 235-349.
2. M. Costas, M. P. Mehn, M. P. Jensen, L. Que, Jr., *Chem. Rev.*, **2004**, *104*, 939-986.
3. M. M. Abu-Omar, A. Loaiza, N. Hontzeas, *Chem. Rev.*, **2005**, *105*, 2227-2252.
4. P. C. A. Bruijnincx, G. van Koten, R. J. M. Klein Gebbink, *Chem. Soc. Rev.*, **2008**, *37*, 2716-2744.
5. A. R. McDonald, L. Que, Jr., *Coord. Chem. Rev.*, **2013**, *257*, 414-428.
6. W. Nam, Y.-M. Lee, S. Fukuzumi, *Acc. Chem. Res.*, **2014**, *47*, 1146-1154.
7. M. Sono, M. P. Roach, E. D. Coulter, J. H. Dawson, *Chem. Rev.*, **1996**, *96*, 2841-2888.
8. J. T. Groves, *Proc. Natl. Acad. Sci. U. S. A.*, **2003**, *100*, 3569-3574.
9. B. Meunier, S. P. de Visser, S. Shaik, *Chem. Rev.*, **2004**, *104*, 3947-3980.
10. I. G. Denisov, T. M. Makris, S. G. Sligar and I. Schlichting, *Chem. Rev.*, **2005**, *105*, 2253-2278.
11. S. V. Kryatov, E. V. Rybak-Akimova, S. Schindler, *Chem. Rev.*, **2005**, *105*, 2175-2226.
12. R. van Eldik, *Coord. Chem. Rev.*, **2007**, *251*, 1649-1662.
13. P. R. Ortiz de Montellano, *Chem. Rev.*, **2010**, *110*, 932-948.
14. *Iron-containing enzymes: Versatile catalysts of hydroxylation reactions in nature*, ed. S. P. de Visser and D. Kumar, RSC Publishing, Cambridge, **2011**.

15. D. A. Proshlyakov, T. F. Henshaw, G. R. Monterosso, M. J. Ryle, R. P. Hausinger, *J. Am. Chem. Soc.*, **2004**, *126*, 1022-1023.

16. J. M. Bollinger Jr., J. C. Price, L. M. Hoffart, E. W. Barr, C. Krebs, *Eur. J. Inorg. Chem.*, **2005**, 4245-4254.

17. K. Gorres, R. T. Raines, *Crit. Rev. Biochem. Mol. Biol.*, **2010**, *45*, 106-124.

18. M. A. McDonough, V. Li, E. Flashman, R. Chowdhury, C. Mohr, B. M. Lienard, J. Zondlo, N. J. Oldham, I. J. Clifton, J. Lewis, L. A. McNeill, R. J. Kurzeja, K. S. Hewitson, E. Yang, S. Jordan, R. S. Syed, C. J. Schofield, *Proc. Natl. Acad. Sci. U. S. A.*, **2006**, *103*, 9814-9819.

19. A. Timmins, M. Saint-André, S. P. de Visser, *J. Am. Chem. Soc.*, **2017**, *139*, 9855-9866.

20. A. Timmins, S. P. de Visser, *Front. Chem.*, **2017**, *5*, 94.

21. R. Davydov, T. M. Makris, V. Kofman, D. E. Werst, S. G. Sligar, B. M. Hoffman, *J. Am. Chem. Soc.*, **2001**, *123*, 1403-1415.

22. P. J. O'Brien, *Chem. Rev.*, **2006**, *106*, 720-752.

23. C. Yi, C. G. Yang, C. He, *Acc. Chem. Res.*, **2009**, *42*, 519-529.

24. M. Atanasov, P. Comba, S. Hausberg, B. Martin, *Coord. Chem. Rev.*, **2009**, *253*, 2306-2314.

25. M. Costas, *Coord. Chem. Rev.*, **2011**, *255*, 2912-2932.

26. C. V. Sastri, J. Lee, K. Oh, Y. J. Lee, J. Lee, T. A. Jackson, K. Ray, H. Hirao, W. Shin, J. A. Halfen, J. Kim, L. Que, Jr., S. Shaik, W. Nam, *Proc. Natl. Acad. Sci. U. S. A.*, **2007**, *104*, 19181-19186.

27. C. Buron, K. Sénéchal-David, R. Ricoux, J.-P. Le Caër, V. Guérineau, P. Méjanelle, R. Guillot, C. Herrero, J.-P. Mahy, F. Banse, *Chem. – Eur. J.*, **2015**, *21*, 12188-12193.

28. X. Engelmann, I. Monte-Pérez, K. Ray, *Angew. Chem., Int. Ed.*, **2016**, *55*, 7632-7649.

29. I. Prat, L. Gómez, M. Canta, X. Ribas, M. Costas, *Chem. – Eur. J.*, **2013**, *19*, 1908-1913.
30. M. G. Quesne, D. Senthilnathan, D. Singh, D. Kumar, P. Maldivi, A. B. Sorokin and S. P. de Visser, *ACS Catal.*, **2016**, *6*, 2230-2243.
31. P. Barman, A. S. Faponle, A. K. Vardhaman, D. Angelone, A.-M. Löhr, W. R. Browne, P. Comba, C. V. Sastri, S. P. de Visser, *Inorg. Chem.*, **2016**, *55*, 10170-10181.
32. S. P. de Visser, L. Tahsini, W. Nam, *Chem. – Eur. J.*, **2009**, *15*, 5577-5587.
33. J. Annaraj, J. Cho, Y.-M. Lee, S. Y. Kim, R. Latifi, S. P. de Visser, W. Nam, *Angew. Chem., Int. Ed.*, **2009**, *48*, 4150-4153.
34. A. Takahashi, D. Yamaki, K. Ikemura, T. Kurahashi, T. Ogura, M. Hada, H. Fujii, *Inorg. Chem.*, **2012**, *51*, 7296-7305.
35. T. A. Jackson, J.-U. Rohde, M. S. Seo, C. V. Sastri, R. DeHont, A. Stubna, T. Ohta, T. Kitagawa, E. Münck, W. Nam, L. Que, Jr., *J. Am. Chem. Soc.*, **2008**, *130*, 12394-12407.
36. S. Sahu, L. R. Widger, M. G. Quesne, S. P. de Visser, H. Matsumura, P. Moënne-Loccoz, M. A. Siegler, D. P. Goldberg, *J. Am. Chem. Soc.*, **2013**, *135*, 10590-10593.
37. D. C. Lacy, R. Gupta, K. L. Stone, J. Greaves, J. W. Ziller, M. P. Hendrich, A. S. Borovik, *J. Am. Chem. Soc.*, **2010**, *132*, 12188-12190.
38. Ü. İşci, A. S. Faponle, P. Afanasiev, F. Albrieux, V. Briois, V. Ahsen, F. Dumoulin, A. B. Sorokin, S. P. de Visser, *Chem. Sci.*, **2015**, *6*, 5063-5075.
39. J.-G. Liu, T. Ohta, S. Yamaguchi, T. Ogura, S. Sakamoto, Y. Maeda, Y. Naruta, *Angew. Chem., Int. Ed.*, **2009**, *48*, 9262-9267.
40. T. Taguchi, R. Gupta, B. Lassalle-Kaiser, D. W. Boyce, V. K. Yachandra, W. B. Tolman, J. Yano, M. P. Hendrich, A. S. Borovik, *J. Am. Chem. Soc.*, **2012**, *134*, 1996-1999.

41. Z. Gordon, M. J. Drummond, E. M. Matson, J. A. Bogart, E. J. Schelter, R. L. Lord, A. R. Fout, *Inorg. Chem.*, **2017**, *56*, 4852-4863.
42. M. Sørensen Vad, A. Lennartson, A. Nielsen, J. Harmer, J. E. McGrady, C. Frandsen, S. Mørup, C. J. McKenzie, *Chem. Commun.*, **2012**, *48*, 10880-10882.
43. F. Wang, W. Sun, C. Xia, Y. Wang, *J. Biol. Inorg. Chem.*, **2017**, *22*, 987-998.
44. F. Burg, M. Gicquel, S. Breitenlechner, A. Pöthig, T. Bach, *Angew. Chem., Int. Ed.*, **2018**, *57*, 2953-2957.
45. C. E. MacBeth, R. Gupta, K. R. Mitchell-Koch, V. G. Young Jr., G. H. Lushington, W. H. Thompson, M. P. Hendrich, A. S. Borovik, *J. Am. Chem. Soc.*, **2004**, *126*, 2556-2567.
46. T. Ishizuka, S. Ohzu, H. Kotani, Y. Shiota, K. Yoshizawa, T. Kojima, *Chem. Sci.*, **2014**, *5*, 1429-1436.
47. M. Mitra, J. Lloret-Fillol, M. Haukka, M. Costas, E. Nordlander, *Chem. Commun.*, **2014**, *50*, 1408-1410.
48. M. Lubben, A. Meetsma, E. C. Wilkinson, B. Feringa, L. Que, Jr., *Angew. Chem., Int. Ed. Engl.*, **1995**, *34*, 1512-1515.
49. J. Kaizer, E. J. Klinker, N. Y. Oh, J.-U. Rohde, W. J. Song, A. Stubna, J. Kim, E. Münck, W. Nam, L. Que, Jr., *J. Am. Chem. Soc.*, **2004**, *126*, 472-473.
50. E. J. Klinker, J. Kaizer, W. W. Brennessel, N. L. Woodrum, C. J. Cramer, L. Que, Jr., *Angew. Chem., Int. Ed.*, **2005**, *44*, 3690-3694.
51. D. Lakk-Bogáth, R. Csonka, G. Speier, M. Réglier, A. J. Simaan, J.-V. Naubron, M. Giorgi, K. Lázár, J. Kaizer, *Inorg. Chem.*, **2016**, *55*, 10090-10093.

52. S. K. Padamati, A. Draksharapu, D. Unjaroen, W. R. Browne, *Inorg. Chem.*, **2016**, *55*, 4211-4222.
53. S. Kim, K.-B. Cho, Y.-M. Lee, J. Chen, S. Fukuzumi, W. Nam, *J. Am. Chem. Soc.*, **2016**, *138*, 10654-10663.
54. D. Wang, K. Ray, M. J. Collins, E. R. Farquhar, J. R. Frisch, L. Gómez, T. A. Jackson, M. Kerscher, A. Waleska, P. Comba, M. Costas, L. Que, Jr., *Chem. Sci.*, **2013**, *4*, 282-291.
55. A. Draksharapu, D. Angelone, M. G. Quesne, S. K. Padamati, L. Gómez, R. Hage, M. Costas, W. R. Browne, S. P. de Visser, *Angew. Chem., Int. Ed.*, **2015**, *54*, 4357-4361.
56. A. K. Vardhaman, P. Barman, S. Kumar, C. V. Sastri, D. Kumar, S. P. de Visser, *Chem. Commun.*, **2013**, *49*, 10926-10928.
57. C. V. Sastri, K. Oh, Y. J. Lee, M. S. Seo, W. Shin, W. Nam, *Angew. Chem., Int. Ed.*, **2006**, *45*, 3992-3995.
58. S. P. de Visser, Y.-M. Lee, W. Nam, *Eur. J. Inorg. Chem.*, **2008**, 1027-xxx.
59. J. Park, Y. Morimoto, Y.-M. Lee, W. Nam, S. Fukuzumi, *J. Am. Chem. Soc.*, **2011**, *133*, 5236-5239.
60. K. Benzing, P. Comba, B. Martin, B. Pokrandt, F. Keppler, *Chem. – Eur. J.*, **2017**, *23*, 10465-10472.
61. R. Turcas, D. Lakk-Bogáth, G. Speier, J. Kaizer, *Dalton Trans.*, **2018**, *47*, 3248-3252.
62. A. N. Biswas, M. Puri, K. K. Meier, W. N. Oloo, G. T. Rohde, E. L. Bominaar, E. Münck. L. Que, Jr., *J. Am. Chem. Soc.*, **2015**, *137*, 2428-2431.
63. M. S. Seo, N. H. Kim, K. B. Cho, J. E. So, S. K. Park, M. Clémancey, R. G. Serres, J. M. Latour, S. Shaik, W. Nam, *Chem. Sci.*, **2011**, *2*, 1039-1045.
64. M. Mitra, H. Nimir, S. Demeshko, S. S. Bhat, S. O. Malinkin, M. Haukka, J. Lloret-Fillol, G. C. Lisensky, F. Meyer, A. A. Shteinman, W. R. Browne,

D. A. Hrovat, M. G. Richmond, M. Costas, E. Nordlander, *Inorg. Chem.*, **2015**, *54*, 7152-7164.

65. W. K. C. Lo, C. J. McAdam, A. G. Blackman, J. D. Crowley, D. A. McMorran, *Inorg. Chim. Acta*, **2015**, *426*, 183-194.
66. A. A. Massie, M. C. Denler, L. T. Cardoso, A. N. Walker, M. K. Hossain, V. W. Day, E. Nordlander, T. A. Jackson, *Angew. Chem., Int. Ed.*, **2017**, *56*, 4178-4182.
67. A. A. Massie, A. Sinha, J. D. Parham, E. Nordlander, T. A. Jackson, *Inorg. Chem.*, **2018**, *57*, 8253-8263.
68. W. Rasheed, A. Draksharapu, S. Banerjee, V. G. Young Jr., R. Fan, Y. Guo, M. Ozerov, J. Nehrkorn, J. Krzystek, J. Telser, L. Que, Jr., *Angew. Chem., Int. Ed.*, **2018**, *57*, 9387-9391.
69. K. Ray, J. England, A. T. Fiedler, M. Martinho, E. Münck, L. Que, Jr., *Angew. Chem., Int. Ed.*, **2008**, *47*, 8068-8071.
70. A. Company, G. Sabenya, M. González-Béjar, L. Gómez, M. Clémancey, G. Blondin, A. J. Jasniewski, M. Puri, W. S. Browne, J. M. Latour, L. Que, Jr., M. Costas, J. PérezPrieto, J. Lloret-Fillol, *J. Am. Chem. Soc.*, **2014**, *136*, 4624-4633.
71. S. Sahu, M. G. Quesne, C. G. Davies, M. Dürr, I. Ivanović-Burmazović, M. A. Siegler, G. N. L. Jameson, S. P. de Visser, D. P. Goldberg, *J. Am. Chem. Soc.*, **2014**, *136*, 13542-13545.
72. L. R. Widger, C. G. Davies, T. Yang, M. A. Siegler, O. Troeppner, G. N. L. Jameson, I. Ivanović-Burmazović, D. P. Goldberg, *J. Am. Chem. Soc.*, **2014**, *136*, 2699-2702.
73. S. Sahu, B. Zhang, C. J. Pollock, M. Dürr, C. G. Davies, A. M. Confer, I. Ivanović-Burmazović, M. A. Siegler, G. N. L. Jameson, C. Krebs, D. P. Goldberg, *J. Am. Chem. Soc.*, **2016**, *138*, 12791-12802.

74. H. C. Brown, Y. Okamoto, *J. Am. Chem. Soc.*, **1958**, *80*, 4979-4987.
75. Y. Goto, T. Matsui, S. I. Ozaki, Y. Watanabe, S. Fukuzumi, *J. Am. Chem. Soc.*, **1999**, *121*, 9497-9502.
76. S. Kumar, A. S. Faponle, P. Barman, A. K. Vardhaman, C. V. Sastri, D. Kumar, S. P. de Visser, *J. Am. Chem. Soc.*, **2014**, *136*, 17102-17115.
77. N. Y. Oh, Y. Suh, M. J. Park, M. S. Seo, J. Kim, W. Nam, *Angew. Chem., Int. Ed.*, **2005**, *44*, 4235-4239.
78. L. E. Friedrich, *J. Org. Chem.*, **1983**, *48*, 3851-3852.
79. F. G. Bordwell, J.-P. Cheng, *J. Am. Chem. Soc.*, **1991**, *113*, 1736-1743.
80. J. M. Mayer, *Acc. Chem. Res.*, **1998**, *31*, 441-450.
81. J. M. Mayer, *Annu. Rev. Phys. Chem.*, **2004**, *55*, 363-390.
82. J. Yoon, S. A. Wilson, Y. K. Jang, M. S. Seo, K. Nehru, B. Hedman, K. O. Hodgson, E. Bill, E. I. Solomon, W. Nam, *Angew. Chem., Int. Ed.*, **2009**, *48*, 1257-1260.
83. D. E. Lansky, D. P. Goldberg, *Inorg. Chem.*, **2006**, *45*, 5119-5125.
84. A. J. McGown, W. D. Kerber, H. Fujii, D. P. Goldberg, *J. Am. Chem. Soc.*, **2009**, *131*, 8040-8048.
85. S. R. Bell, J. T. Groves, *J. Am. Chem. Soc.*, **2009**, *131*, 9640-9641.
86. Y. Kang, H. Chen, Y. J. Jeong, W. Lai, E. H. Bae, S. Shaik, W. Nam, *Chem. – Eur. J.*, **2009**, *15*, 10039-10046.
87. J. J. Warren, T. A. Tronic, J. M. Mayer, *Chem. Rev.*, **2010**, *110*, 6961-7001.
88. K. A. Prokop, S. P. de Visser, D. P. Goldberg, *Angew. Chem., Int. Ed.*, **2010**, *49*, 5091-5095.
89. J. M. Mayer, E. A. Mader, J. P. Roth, J. R. Bryant, T. Matsuo, A. Dehestani, B. C. Bales, E. J. Watson, T. Osako, K. Valliant-Saunders, W. H. Lam, D. A. Hrovat, W. T. Borden, E. R. Davidson, *J. Mol. Catal. A: Chem.*, **2006**, *251*, 24-33.

90. C. Arunkumar, Y. M. Lee, J. Y. Lee, S. Fukuzumi, W. Nam, *Chem. – Eur. J.*, **2009**, *15*, 11482-11489.
91. A. K. Vardhaman, P. Barman, S. Kumar, C. V. Sastri, D. Kumar, S. P. de Visser, *Angew. Chem., Int. Ed.*, **2013**, *52*, 12288-12292.
92. T. Yang, M. G. Quesne, H. M. Neu, F. G. Cantú Reinhard, D. P. Goldberg, S. P. de Visser, *J. Am. Chem. Soc.*, **2016**, *138*, 12375-12386.
93. The DFT calculations were done in collaboration with Dr. Samuel P. de Visser and his research group. This theoretical study was vital for understanding the factors affecting the drastic rate-enhancements observed experimentally; see DOI: 10.1039/c8dt02142b.
94. A. K. Vardhaman, C. V. Sastri, D. Kumar, S. P. de Visser, *Chem. Commun.* **2011**, *47*, 11044-11046.
95. F. G. Cantú Reinhard, A. S. Faponle, S. P. de Visser, *J. Phys. Chem. A*, **2016**, *120*, 9805-9814.
96. L. Bernasconi, E.-J. Baerends, *J. Am. Chem. Soc.* **2013**, *135*, 8857-8867.
97. Y. Liu, X. Guan, E. L.-M. Wong, P. Liu, J.-S. Huang, C.-M. Che, *J. Am. Chem. Soc.* **2013**, *135*, 7194-7204.
98. A. Dey, *J. Am. Chem. Soc.* **2010**, *132*, 13892-13901.
99. H. Hirao, F. Li, L. Que, Jr., K. Morokuma, *Inorg. Chem.* **2011**, *50*, 6637-6648.
100. D. Usharani, D. C. Lacy, A. S. Borovik, S. Shaik, *J. Am. Chem. Soc.* **2013**, *135*, 17090-17104.
101. S. P. de Visser, *J. Am. Chem. Soc.* **2006**, *128*, 9813-9824.
102. D. Kumar, H. Hirao, L. Que, Jr., S. Shaik, *J. Am. Chem. Soc.* **2005**, *127*, 8026-8027.

CHAPTER – IV

Interplay Between Steric and Electronic Effects: A Joint Spectroscopy and Computational Study of Non-Heme Iron(IV)-Oxo Complexes

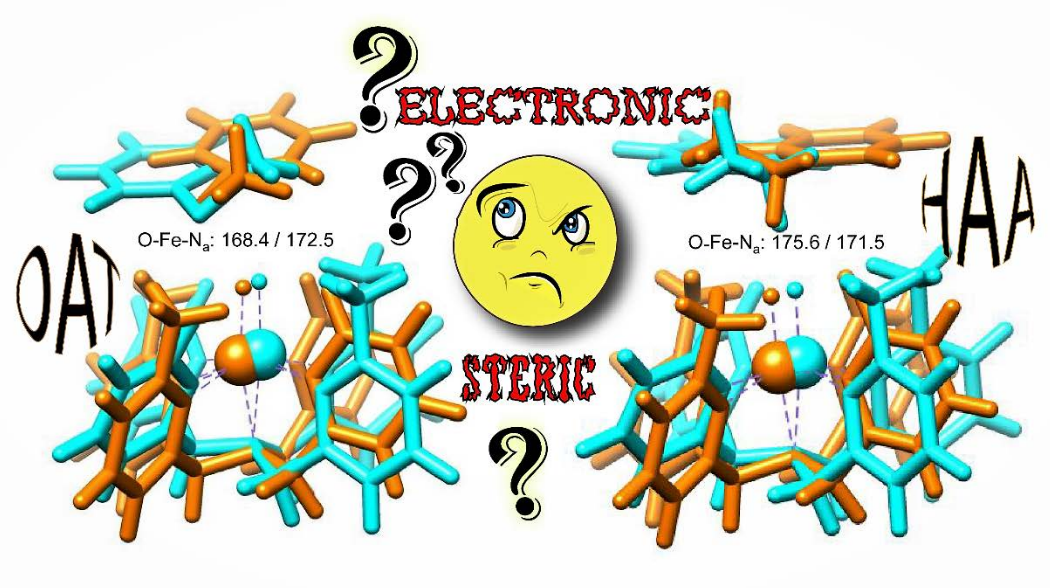

● Adapted from *Chemistry – A European Journal*, **2019**, 25, 5086-5098 with permission from John Wiley & Sons, Inc. ●

4.1. Introduction

Metalloenzymes play vital functions for human health and are involved in the biosynthesis of essential compounds in the body as well as the biodegradation of xenobiotics and damaging products.[1-13] Due to the large natural abundance of iron, metalloenzymes with either mononuclear or binuclear iron are relatively common in biology. Studies on the details of enzymatic reaction mechanisms are challenging due to the short lifetime of catalytic cycle intermediates and hence, it is not always clear what the active species is that performs the transformations or what features of the active site affect the rate-determining reaction step. To understand the functional properties of these metal-containing active sites, biomimetic models have been developed that comprise the metal with a similar coordination environment but dissolved in an organic solvent.[14-18] Biomimetic models give insight into the effect of the ligands on the chemical properties and reactivity of the oxidant as well as the first and second coordination sphere on the reaction mechanism and rate constants.

Often biomimetic models contain mononuclear iron embedded in a ligand scaffold and pentadentate ligands have proven to be very popular because they generally give few isomeric structures. One particular N5-based pentadentate ligand that has been extensively studied is N,N-bis(2-pyridylmethyl)-N-bis(2-pyridyl)methylamine (N4Py, Fig. 4.1).[19-22] In the iron(IV)-oxo form, the $[Fe^{IV}(O)(N4Py)]^{2+}$ complex (1b) bears four equatorially bound nitrogen donor atoms (N_{eq}) perpendicular to the iron(IV)-oxo axis and an axial amine nitrogen atom (N_{ax}) *trans* to the oxo group. Structurally, this ligand framework offers a perfect bowl-like cavity for the iron(IV)-oxo for reactions with substrates. In terms of bond-atom distances, all the equatorial $Fe-N_{eq}$ distances appear to be equivalent and give the iron an octahedral symmetry. Over the years, the Fe(IV)-oxo complex

(1b) has been thoroughly characterized and extensively studied, which makes it an ideal candidate to engineer with substituents and ligands and study the interplay between the steric and electronic effects on its properties and reactivity.

There have been quite a few reports on the derivatization of pyridine rings that are bound to the iron(IV)-oxo core in 1b,[23-32] particularly at the pyridine 6-position, which is closest to the oxo group. However, most studies on modified N4Py structures have focused on the two pyridine rings that are tethered to the axial nitrogen atom (N_{ax} atom) through methylene carbon atoms. Therefore, we were wondering what the effect would be of *ortho*-substitution of the two pyridine rings that bind through a methine carbon to the axial N-atom. Our study reveals the in-equivalence of the four bound pyridine rings, which otherwise appear similar in terms of equatorial ligand field perturbation when the pyridine C6 positions are substituted and this results in dramatic changes in reactivity.

It has been shown that substitution of the sixth position of a pyridine ring leads to the weakening of the equatorial field resulting in elongation of the Fe-N_{eq} bonds due to enhanced electrophilicity of the iron(IV)-oxo species.[30-32] Thus, using the tetradentate TPA ligand system [TPA=tris-(2-pyridylmethyl)- amine], Que and co-workers showed that introduction of at least one methyl group in the ligand framework (in the form of 6-MeTPA, 6-Me_2TPA and 6-Me_3TPA) led to changes in the electronic ground state of the ferrous and ferric species from low to high-spin.[33]

Introduction of bulkier quinoline groups instead of pyridine led to the formation of a highly reactive high-spin ferryl-oxo intermediate with spectroscopic features analogous to the active species of the enzyme taurine/α-ketoglutarate dioxygenase (TauD).[34] Furthermore, drastic improvement in catalytic reactivity has been successfully achieved by replacement of pyridine groups in TPA by bulkier heterocycles such as N-methylbenzimidazole.[35] There are also reports of other (S=2) iron(IV)-oxo intermediates, in which the metal centre is positioned in a sterically encumbered cavity with forceful occupation of a trigonal bipyramidal geometry.[36-38]

On account of steric bulk and better σ-donor ability, these engineered ligand frameworks can offer enhanced perturbations in the equatorial ligand field that can make the iron(IV)-oxo core more susceptible to approaching substrates. Steric and electronic effects are two vital tuning probes that manifest the reactivity profiles for these systems and a delicate borderline exists between the two factors.[39-46] It is understood that along with the stretched Fe-N_{eq} bonds, the distortion in the ferryl axis, specifically the N_{ax}-Fe-O bond angle, plays a pivotal role in their stabilities, spectroscopic properties and various oxidative reactivities.[30-32] These examples from the literature implicate that substitution of the sixth position of a metal-bound pyridine ring leads to better hydrogen-atom abstraction (HAA) and oxygen-atom transfer (OAT) reactivity. However, what most of these metal complexes have in common is that the manipulations have been done in the sixth position of two specific methylene bound pyridine rings in N4Py, whereas any sort of engineering on the other two methine-carbon-bound pyridine rings in the primary coordination sphere has rarely been reported. Hence, an effort has been made by our groups to dig deeper into this issue. Both experimental and theoretical studies reveal the intrinsic parity between the two sets of pyridine rings, contributing to the overall reactivity profiles of the two catalysts. Considering the frameworks shown in Fig. 4.1, the ligands are named 2PyN_{ax}2(6-MePy) or N4Py^{Me} and 2(6-MePy)N_{ax}2Py or ^{Me}N4Py in short and their iron(II) complexes are designated 3a and 4a, respectively.

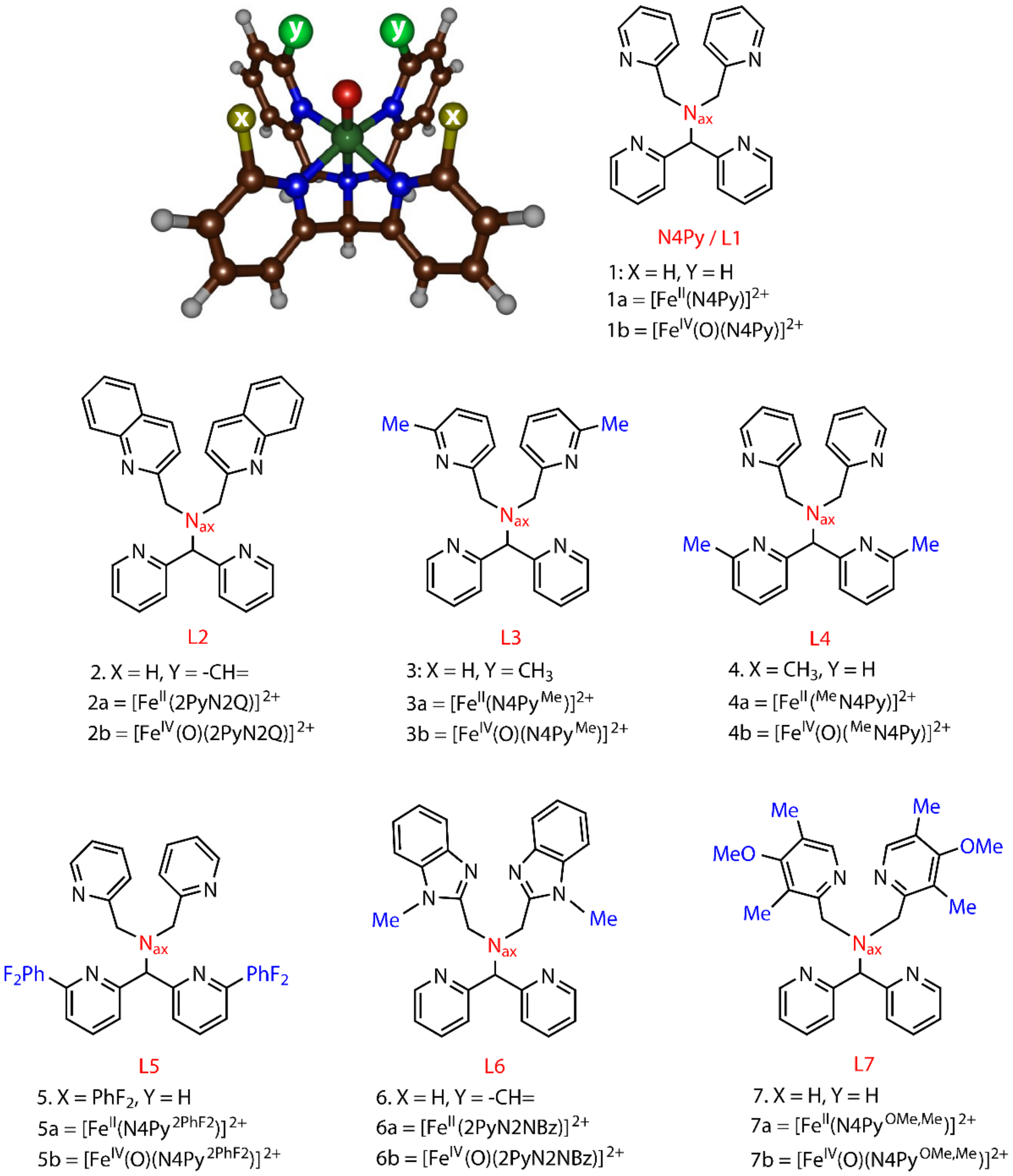

Fig. 4.1. Basic ligand framework and structures of oxidants discussed in this work.

The distinct spectroscopic properties and stability of the two complexes $[Fe^{IV}(O)(N4Py^{Me})]^{2+}$ (3b) and $[Fe^{IV}(O)(^{Me}N4Py)]^{2+}$ (4b) allowed us to pursue a detailed kinetic analysis and probe the very definitive factors that govern the reactivity and stability of these high valent metal-oxo species. Our studies concern the fine line between steric and electronic factors that orchestrate the reaction rates and selectivity, and also reveal the intricate details of second coordination sphere effects related to substrate approach to a metal-oxo species.

4.2. Results and Discussion

4.2.1. Synthesis and Characterization

Ligands $N4Py^{Me}$ and $^{Me}N4Py$ were synthesized starting from di(pyridine-2-yl)methanone or di(6-methyl-pyridin-2-yl)methanone and, in a reaction with hydroxylamine, converted into an oxime, and subsequently over Zn, were reduced further to their amine form. Upon addition of either 2-(chloromethyl)-6-methyl-pyridine or 2-(chloromethyl)-pyridine in NaOH, we reacted the amines to form the $N4Py^{Me}$ and $^{Me}N4Py$ structures, respectively, in good yield (detailed synthetic procedures for ligand syntheses are discussed in Chapter-II). Subsequently, the $N4Py^{Me}$ and $^{Me}N4Py$ ligands were reacted with $[Fe^{II}(CH_3CN)_2{\cdot}2ClO_4]$ in acetonitrile to form the metal complexes $[Fe^{II}(N4Py^{Me})](ClO_4)_2$ (3a) and $[Fe^{II}(^{Me}N4Py)](ClO_4)_2$ (4a), which were characterized with UV/Vis, ESI-MS and crystallographic methods. High resolution ESI-MS spectrum of complex 3a and 4a in CH_3CN at 298 K, showed prominent peaks at *m/z* 550 that were assigned to $[Fe^{II}(L)(ClO_4)]^+$ (L=$N4Py^{Me}$ and $^{Me}N4Py$). The isotopic distribution pattern corresponds to the formation of the ferrous complexes (See Chapter-II, section 2.3.1.).

Single crystals of 4a were obtained by vapour diffusion of diethyl ether into an acetonitrile solution of $[Fe^{II}(^{Me}N4Py)(CH_3CN)]^{2+}\cdot 2BF_4$. The crystal structure (Fig. 4.2 and Table 4.1) shows clear penta-coordination of the metal to the ^{Me}N4Py ligand in a structural orientation analogous to the reported complexes $[Fe^{II}(N4Py)]^{2+}$ and $[Fe^{II}(N4Py^{Me})(CH_3CN)]^{2+}\cdot 2ClO_4$.[47-48] The Fe-N bond distances for 4a, as shown in Table 4.1, are typical for low-spin Fe^{II} complexes reported previously.[23-32,39-48] In comparison to the crystal structure of Feringa and co-workers,[48] (Fig. 4.2.b, Table 4.1) the two metal complexes 3a and 4a indicate minor differences.

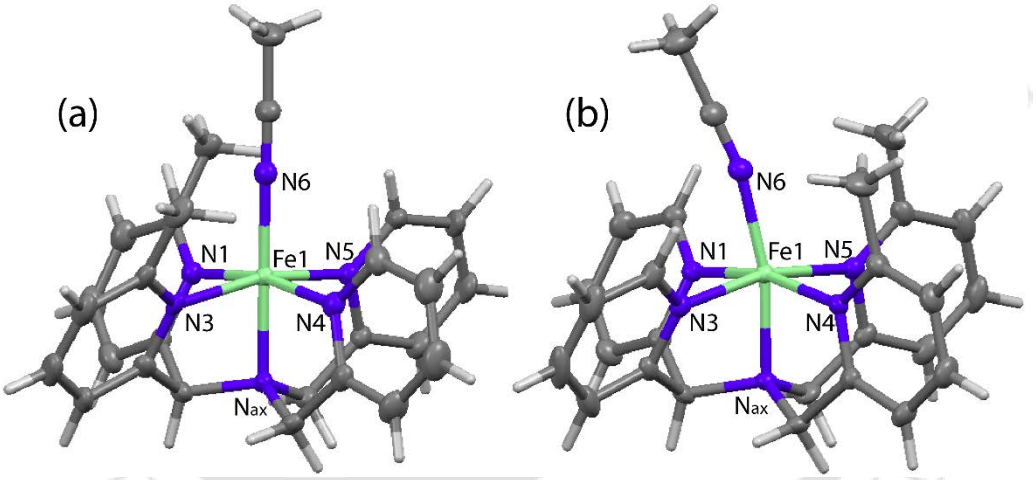

Fig. 4.2. ORTEP diagram (30% ellipsoid probability) of complex (a) $Fe^{II}(^{Me}N4Py)(CH_3CN)](BF_4)_2$ and (b) $Fe^{II}(N4Py^{Me})(CH_3CN)](ClO_4)_2$.[48] Colour coding: Hydrogen (off-white), carbon (gray), iron (green), nitrogen (violet). Counter-ions have been omitted for clarity.

In particular, the sixth coordination position, *trans* to the N_{ax}, is occupied by the solvent CH_3CN in both the complexes, but there is a substantial bending in the N_{ax}-Fe-solvent axis for 3a (167.58), as compared to 4a (179.38). This is the largest bend observed among the fellow structures (Table 4.1) and is close to that in 2a, in which a triflate counter-anion occupies the apical position instead of a solvent molecule.[32] The huge tilt accounts for an induced steric effect imparted by the methyl groups in the structure of 3a.

Table 4.1. Selected bond lengths [Å] and bond angles [°] for $\mathrm{Fe^{II}}$ complexes 1a–7a.

Complex	***1a*** [47]	***2a*** [32]	***3a*** [48]	***4a*** [a]	***5a*** [26]	***6a*** [28]	***7a*** [29]
Bonds	***Bond Lengths***						
Fe1-N1	1.976(3)	2.199(6)	2.004(4)	2.049(5)	2.057(1)	1.964(3)	1.963(8)
Fe1-N3	1.967(3)	2.233(8)	1.981(4)	2.043(6)	2.031(1)	1.983(3)	1.971(8)
Fe1-N4	1.975(3)	2.223(6)	2.083(4)	1.974(5)	1.979(1)	1.983(3)	1.965(7)
Fe1-N5	1.968(3)	2.226(6)	2.078(3)	1.981(5)	1.966(1)	1.979(2)	1.984(8)
Fe1-N_{ax}	1.961(3)	2.192(6)	1.990(2)	1.968(5)	1.967(1)	1.983(3)	1.959(7)
Fe1-N6	1.915(3)	2.045(6)	1.959(3)	1.930(5)	1.931(1)	1.901(3)	1.918(7)
Avg Fe-N	1.960	2.186	2.016	1.991	1.988	1.965	1.960
Angles	***Bond Angles***						
N_{eq}-Fe-N_{ax} [b]	84.0	77.2	82.7	83.3	83.5	83.6	84.0
N_{eq}-Fe-N6 [b]	96.0	102.6	97.1	96.6	96.6	96.4	96.0
N_{ax}-Fe-N6	177.3	168.3	167.5	179.3	175.5	175.7	176.9

[a] This work; [b] Average *cis*-bond angle of equatorial Fe-N bonds with N_{ax} and N6. Avg = average.

Another interesting observation is that in 4a, the N_{ax}-Fe-solvent axis is close to 180° in agreement with 1a (177.3°). Thus, in the absence of any substituent the bond angle deviates from 180° to an acute value (177.3° in 1a), and substituents in the methylene bound pyridine rings (168.3° in 2a, 167.5° in 3a, 175.7° in 6a and 176.9° in 7a) as well as methine bound pyridine rings (as in 5a) display the same tilt. By contrast, in 4a, the steric effect acts from the opposite direction thereby making the axis almost as straight as 180°. The $<N_{eq}$-Fe-N_{ax} and $<N_{eq}$-Fe-N6 angles (compiled in Table 4.1) give a measure of the position of Fe in the equatorial plane inside the ligand framework and signifies the depth to which the metal centre is located inside the cavity. Again, complex 3a and 4a both have the lowest $<N_{eq}$-Fe-N_{ax} and highest $<N_{eq}$-Fe-N6 values compared to the rest, indicative of the strain inside the cavity (although there are intrinsic differences in ligation ability for the sixth donor, which is N for 3a and O for 2a).

Furthermore, the average Fe-N bond distance is higher in 3a (2.016 Å) than that in 1a (1.960 Å), 4a (1.991 Å), 5a (1.988 Å), 6a (1.965 Å) and 7a (1.96 Å). This is suggestive of a weakened equatorial ligand field in complex 3a. Considering the cavity provided by the N5 donor centre in all the ligand systems, the sixth coordination site is occupied by the solvent molecule that is susceptible to be replaced by the oxygen atom during the formation of the oxo species. Indeed, the fragility of the Fe-solvent bond is indicated by the Fe1-N6 bond length, which is also longer in 3a (1.959(3) Å) compared to 1a (1.915(3) Å), 4a (1.930(5) Å), 5a (1.931(1) Å), 6a (1.901(3) Å) and 7a (1.918(7) Å). The Fe-O_{OTf} bond length in 2a (2.045(6) Å) is even longer than the Fe-N6 bond in 3a. The higher bond length values in 2a are most probably due to the high-spin nature of the complex, as a result of anion binding (triflate) to the sixth coordination site instead of CH_3CN, which generally results in low-spin complexes. Thus, notwithstanding the intrinsic differences between the Fe-N and Fe-O bonds, the quinoline groups impart a strong influence on the vertical N_{ax}-Fe-O axis, which is obvious from the huge OAT rates.[31] Clearly, the positioning of the methyl groups is responsible for similar steric effects in 3a that can be anticipated for the corresponding oxo complex (3b) as well.

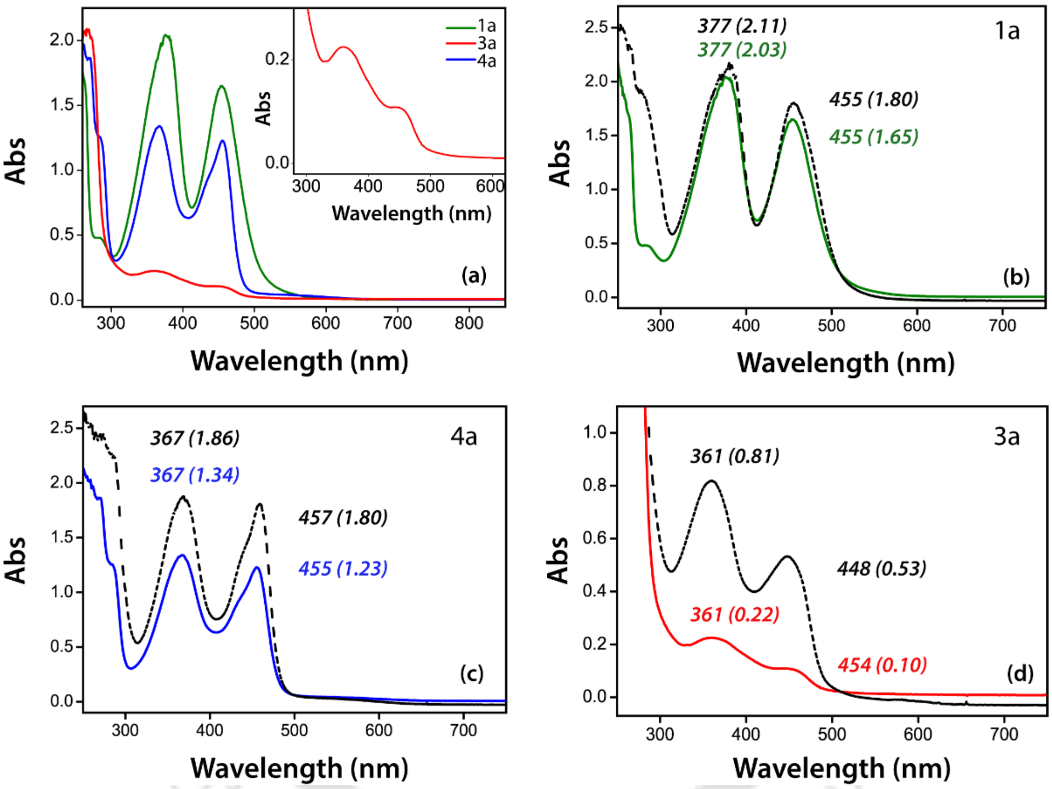

Fig. 4.3. (a) UV/Vis spectra of 1a (green line), 3a (red line) and 4a (blue line) (0.25 mM each) in CH_3CN at 298 K; inset shows the expanded region for 3a. (b, c, d) UV/Vis spectra of 1a (b, green line), 4a (c, blue line) and 3a (d, red line) respectively at 298 K. Black dotted lines in (b, c and d) represents corresponding spectra at 233 K.

Unlike in the solid state, structural tuning of the ligand skeleton of such Fe^{II} complexes often leads to spin equilibrium in the solution phase. The absorption spectra of all Fe^{II} complexes 1a, 3a and 4a, show two MLCT bands with notable differences in their epsilon values (1a, $\varepsilon = 8120, 6600$ L M^{-1} cm^{-1}; 3a, $\varepsilon = 880, 400$ L M^{-1} cm^{-1}; and 4a, $\varepsilon = 5360, 4920$ L M^{-1} cm^{-1}; see Fig. 4.3.a. The low ε values are speculative of substantial spin crossover in 3a and 4a, which is absent in 1a. Steric hindrance of the methyl groups increases the bond lengths in the solid state; however, in the solution state, the spin equilibrium is mostly shifted towards the high-spin form that also rationalizes the low ε values of the new complexes. As the temperature is lowered to 233 K, the population of the low-spin state increases effectively in 3a and 4a thereby increasing their absorbance values, see Fig. 4.3.

The ^{1}H-NMR spectra of 3a and 4a further support these findings and expectedly, paramagnetic shifting of the peaks was observed in both the cases (see Fig. 2.19, Chapter-II). However, the extent of peak-shifting and broadening is more in the case of 3a than in 4a, thereby confirming larger contribution of the high-spin form in 3a in equilibrium with the low-spin species. Similar paramagnetic shifting of proton resonances for ferrous complexes was also observed for 2a and 6a.[31,28]

Complexes 3b and 4b were generated *in situ*, as 1b, by treating the iron(II) precursor complexes with 1.5 equivalents of $PhI(OAc)_2$ in an acetonitrile solution at room temperature. These ferryl-oxo complexes were characterized by UV/Vis, ESI-MS and ^{1}H-NMR spectroscopy. Upon addition of oxidant to the Fe^{II} species, the $Fe^{IV}=O$ chromophores were formed almost instantaneously for both 3b and 4b, as observed from the UV/Vis spectrum. Subtle differences in the absorption spectrum were seen for the iron(IV)-oxo complexes 1b, 4b and 3b (Fig. 4.4). Cumulative bathochromic and hypochromic shifts range from 695 nm ($\varepsilon = 400$ L M^{-1} cm^{-1}) for 1b to 750 nm ($\varepsilon = 340$ L M^{-1} cm^{-1}) for 4b to 775 nm ($\varepsilon = 200$ L M^{-1}

cm^{-1}) for 3b. These changes in the d–d transition bands are indicative of the sequential increment of the equatorial ligand field perturbation along the series and weakening of the same. Furthermore, this also leads to distortions in the bell-shaped absorption curve of 4b and 3b due to the appearance of shoulder humps in the NIR region as compared to that of 1b. The stability of these complexes also follows the same trend with half-lives of 3600, 130 and 30 minutes for 1b, 4b and 3b respectively.

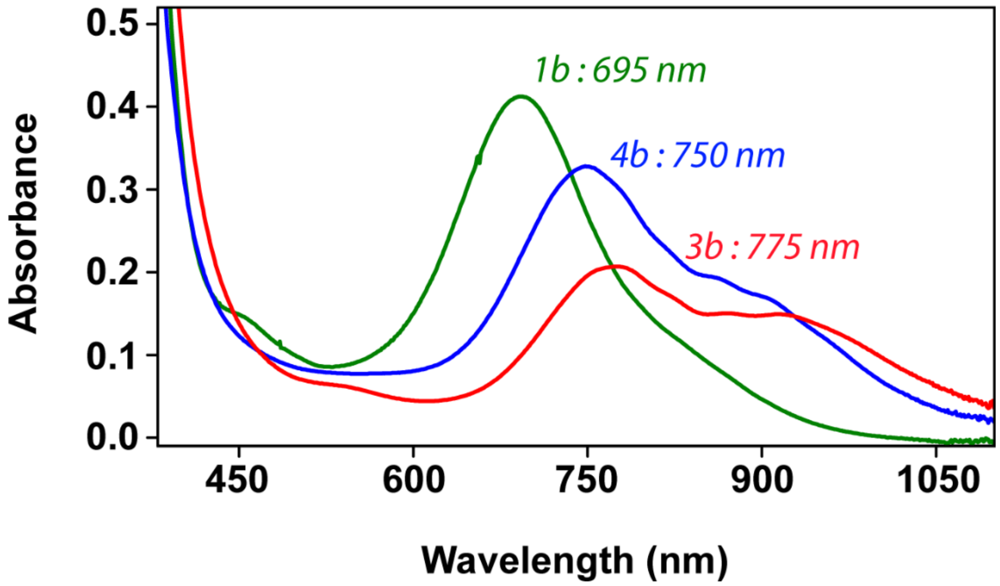

Fig. 4.4. UV/Vis absorption spectrum of 1b (green), 4b (blue) and 3b (red) in CH_3CN at 298 K.

The relatively less stable nature of the new oxo complexes (as evident from their half-lives) made it difficult to record their ESI-MS spectra at room temperature. Therefore, the ESI-MS spectra for 2b and 3b were recorded at lower temperatures by infusing cold samples directly into the source. Both complexes gave a major peak at *m/z* 233.6 corresponding to $[Fe^{IV}(O)(L)]^{2+}$ (Fig. 4.5).

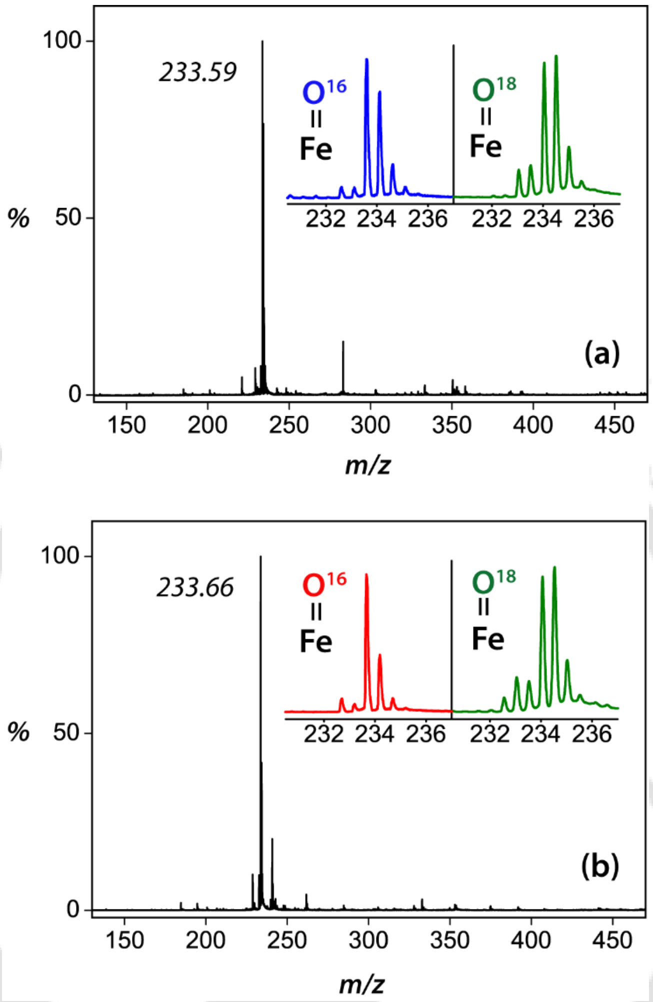

Fig. 4.5. Positive ESI-MS spectrum of complex (a) 4b and (b) 3b in CH_3CN recorded by infusing pre-cooled samples directly into the source. The signal at ~233.6 corresponds to $[Fe^{IV}(O)(L)]^{2+}$. Inset shows the isotopic distribution pattern for the $Fe=O^{16}$ and $Fe=O^{18}$. The latter was obtained by exchanging the terminal oxygen by $H_2{}^{18}O$ after an incubation period of 10-15 min.

To further confirm the existence of iron(IV)-oxo, we did an isotope-labelling experiment. The iron-oxo complexes are known to exchange oxygen from water.[49] Thus upon addition of $H_2{}^{18}O$ to the new iron-oxo complexes, a positive peak shift of one unit for the M/2 ion-cluster was observed in the mass spectrum after an incubation spell of 10 – 15 minutes thereby confirming the existence of iron(IV)-oxo complexes.

We also carried out ^{1}H-NMR spectroscopy experiments to discriminate between the two new iron(IV)-oxo species, 4b and 3b, (Fig. 4.6) and compare the spectra with the existing ^{1}H-NMR spectrum of complex 1b.[50]

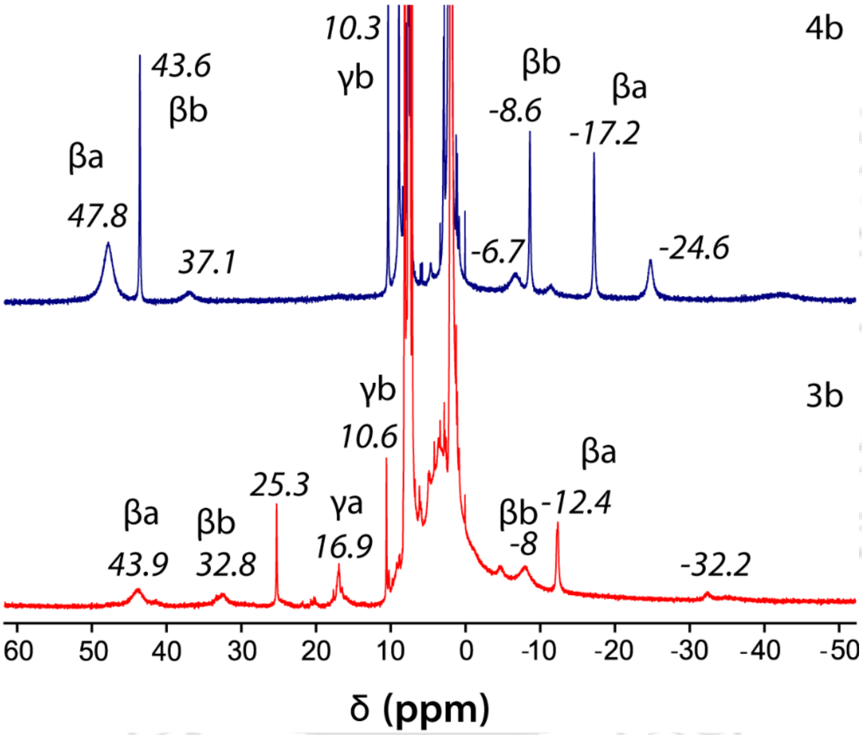

Fig. 4.6. ^{1}H-NMR spectra of 4b (top) and 3b (bottom) in CD_3CN at 298 K.

Clearly, there are shifting of peaks resulting from the typical $S = 1$ ferryl species that unequivocally exists in the octahedral environment.[50-52] The low-spin Fe^{IV} centre in 4b exhibits more relaxation properties compared to 3b, thereby producing sharper signals although both the complexes give rise to paramagnetically shifted proton resonances. As compared to the ^{1}H-NMR spectra of 2b, the same for 4b and 3b appears less complex due to the absence of the quinoline ring protons.[31-32] The ^{1}H-NMR spectra for 4b and 3b were recorded over a spectral width of 200 ppm at 298 K temperature. Both complexes show a unique shift pattern for the pyridine protons of low-spin Fe^{IV} centres, with one β-proton shifted upfield (-17.2, -8.6 ppm for 4b and -12.4, -8 ppm for 3b) and one β-proton shifted downfield (43.6, 47.8 ppm for 4b and 32.8, 43.9 ppm for 3b), as observed previously for analogous complexes.[24-27,50-52] However, in the case of Fe^{III}-pyridine complexes, both the β-protons shift downfield with comparable paramagnetic shift.[33] The difference in the extent of paramagnetic shifting and peak integrations in the NMR spectra of 4b and 3b justify the unequal interaction of the two different sets of pyridine rings with the Fe d-orbitals that have an uneven load of unpaired spin density.

4.2.2. Reaction Kinetics

The reactivity of these complexes was investigated for the oxygen-atom transfer (OAT) and hydrogen-atom abstraction (HAA) reactions from substrates. Thioanisole was employed initially for OAT reactivity, whereas HAA properties were tested using a range of substrates having varied C-H bond dissociation energies and active hydrogen availability. Addition of substrates to a solution containing 3b or 4b in acetonitrile led to the first-order decay of the characteristic d–d transition band in the respective UV/Vis spectrum. The second-order rate constants (k_2) were determined by plotting the pseudo first-order rate constants (k_{obs}) as a function of the proportional increment of substrate concentration. In the case of OAT, the sulphur atom of the organic substrate acts as the active recipient of the oxygen atom and eventually forms the oxidized product in the form of sulfoxides or sulfones.[53-61] $[Fe^{IV}(O)(N4Py)]^{2+}$ (1b) reacts with thioanisole with a k_2 of 50 x 10^{-3} M^{-1} s^{-1} at 273 K.[59-60] Under identical conditions, complex 4b shows around 25 times enhanced reaction rates with a second-order rate constant of 1.24 M^{-1} s^{-1}, see Fig. 4.7.a.

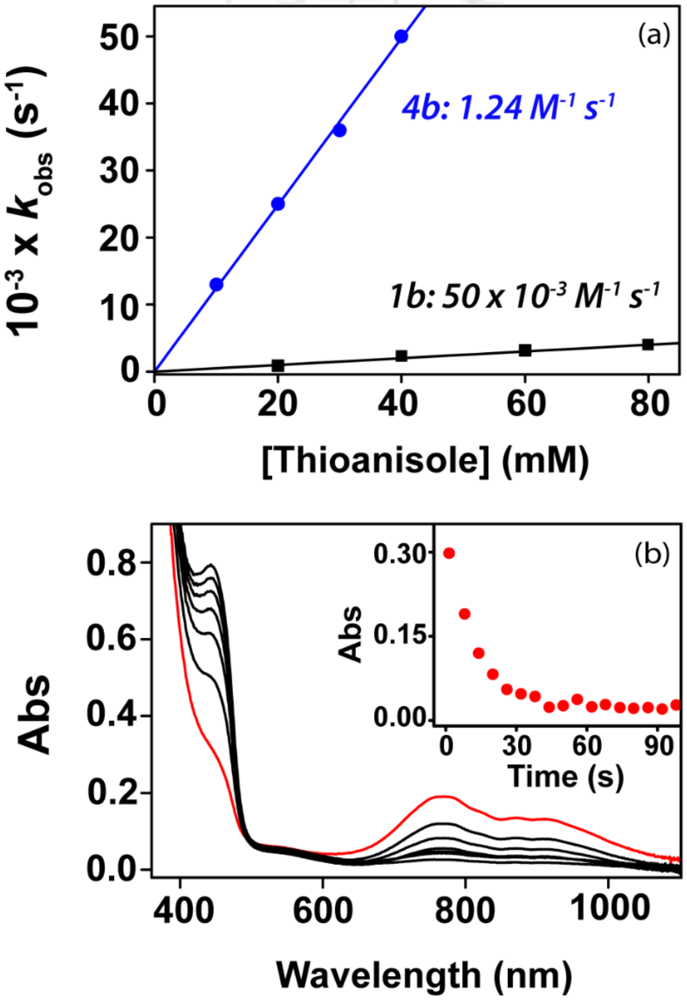

Fig. 4.7. (a) Second-order rate constants determined for the reaction of 1b (1 mm, ■) and 4b (1 mm, ●) with thioanisole at 273 K. (b) Decay profile for the reaction of 3b with THA (5 equivalents) at 233 K; inset shows the time trace for the decay of the 775 nm band.

However, upon addition of 10 equivalents of thioanisole to 1 mm solution of 3b, the 775 nm band vanished in less than 20 seconds at even lower temperatures (233 K), see Fig. 4.7.b. As such, complex 3b reacts with thioanisole at even faster rates than the $[Fe^{IV}(O)(2PyN2Q)]^{2+}$ complex (2b) under identical conditions: for 5 equivalents THA at 233 K, the k_{obs} values for 2b and 3b are 5.4(2) x 10^{-2} s^{-1} and 8.9(4) x 10^{-2} s^{-1} respectively.[31] Therefore, to procure a comparative analysis for S-oxidation under identical conditions, we employed dibenzothiophene (DBT) as the model substrate for OAT reactions for all three oxidants. DBT has two benzene rings fused to thiophene, in conjugation with the heteroatom, and delocalizes the electron density through a number of canonical structures thereby making the reaction slower compared to thioanisole.[61] Thus, it is a more suitable substrate for a comparative study of all three complexes than thioanisole.

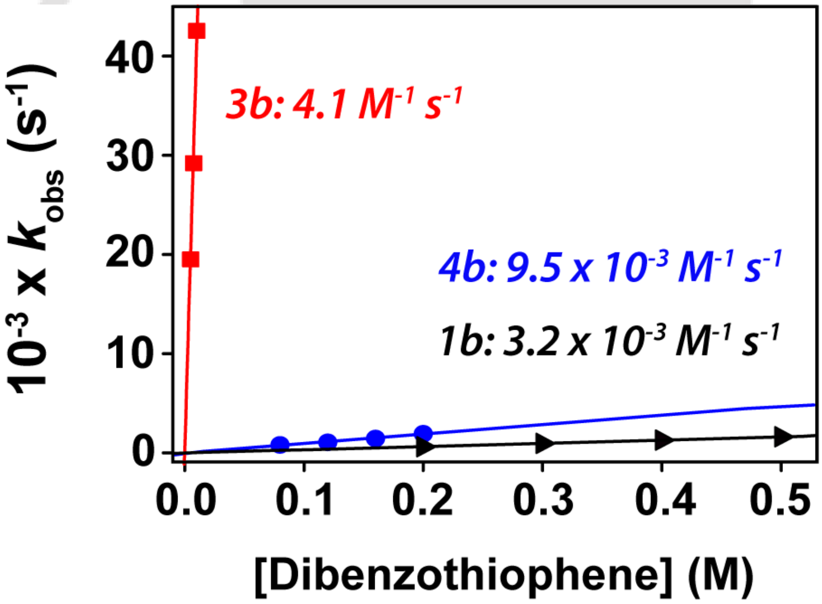

Fig. 4.8. Second-order rate constants determined for the reaction of 1b (1 mm, ▶), 4b (1 mm, ●) and 3b (1 mm, ■) with DBT in CH_3CN at 298 K.

Table 4.2. Pseudo first-order rate constants for the reaction of 1b, 3b and 4b with Thioanisole in CH_3CN.

1b [a]		**3b** [b]		**4b** [a]	
Thioanisole (mM)	***$10^{-3} \times k_{obs}$ (s^{-1})***	***Thioanisole (mM)***	***$10^{-2} \times k_{obs}$ (s^{-1})***	***Thioanisole (mM)***	***$10^{-3} \times k_{obs}$ (s^{-1})***
20	0.95	5	8.94	10	13.12
40	1.80			20	25.01
60	3.22			30	35.98
80	4.00	Recorded at 233 K		40	50.60
$k_2 = 1.24\ M^{-1}\ s^{-1}$				$k_2 = 50 \times 10^{-3}\ M^{-1}\ s^{-1}$	

[a] Kinetics at 273 K; [b] kinetics at 233 K.

Table 4.3. Pseudo first-order rate constants for the reaction of 1b, 3b and 4b with Dibenzothiophene in CH_3CN at 298 K.

1b		**3b**		**4b**	
[DBT] (mM)	***$10^{-3} \times k_{obs}$ (s^{-1})***	***[DBT] (mM)***	***$10^{-3} \times k_{obs}$ (s^{-1})***	***[DBT] (mM)***	***$10^{-3} \times k_{obs}$ (s^{-1})***
200	0.62	5	19.52	80	0.79
300	0.96	7.5	29.22	120	1.06
400	1.28	10	42.55	160	1.45
500	1.61	-	-	200	1.93
$k_2 = 3.2 \times 10^{-3}\ M^{-1}\ s^{-1}$		$k_2 = 4.1\ M^{-1}\ s^{-1}$		$k_2 = 9.5 \times 10^{-3}\ M^{-1}\ s^{-1}$	

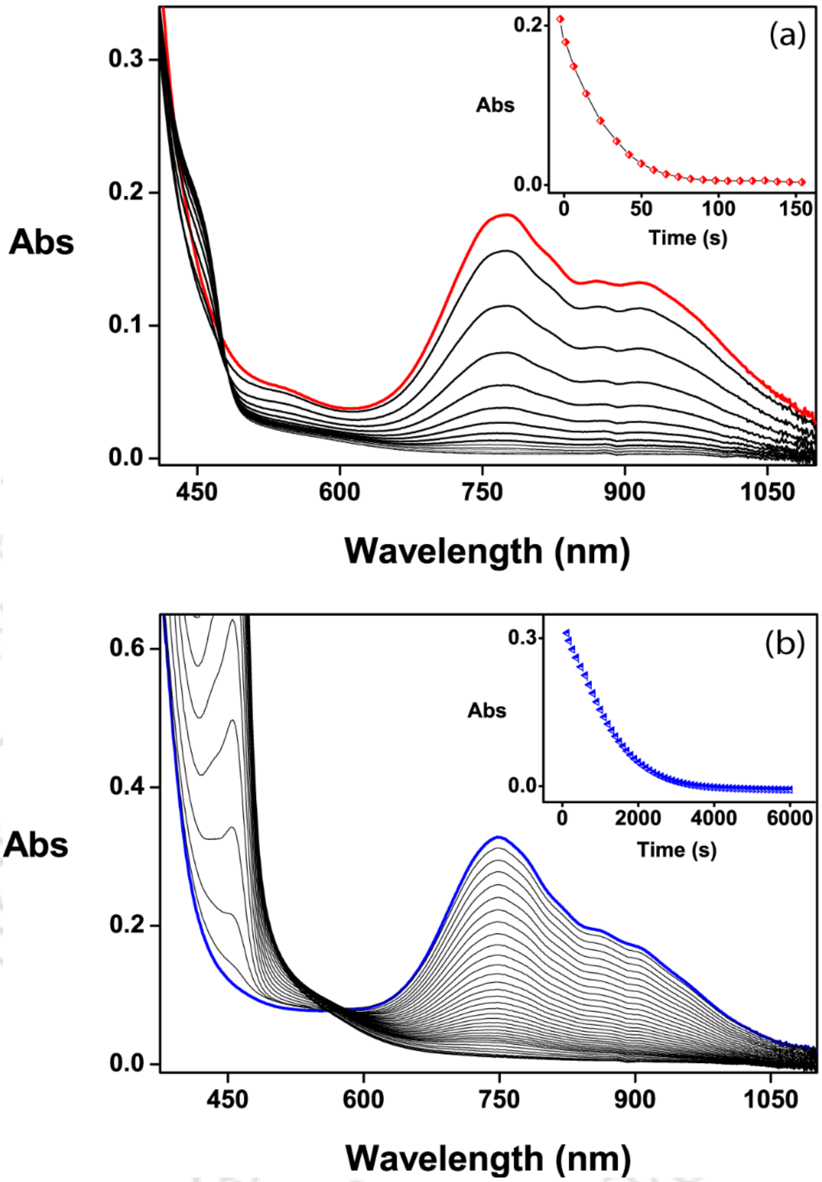

Fig. 4.9. UV/Vis spectral changes of (a) 3b (1 mM) and (b) 4b (1 mM) upon addition of DBT [(a) 10 and (b) 80 equivalents] in CH_3CN at 298 K. Insets shows the decay of the 775 nm and 750 nm band respectively as a function of time.

Complex 3b transfers an oxygen atom to DBT about a thousand times faster (k_2 = 4.1 M^{-1} s^{-1}) than 1b (k_2 = 3.2 x 10^{-3} M^{-1} s^{-1}),[61] whereas 4b (k_2 = 9.5 x 10^{-3} M^{-1} s^{-1}) could only triple the rate of 1b (see Fig. 4.8) at 298 K. These rates agree with the fact that complex 3b, compared to 4b, has an underlying weaker equatorial Fe-N bonding and more ferryl-oxo distortions thereby making the catalyst more susceptible towards heteroatom oxidation reactions. Hence, the introduction of methyl groups at the two methylene bound pyridine rings exerts a prolific effect on the iron-oxo core compared to the one containing methyl groups on the pyridine rings connected by the methine carbon in the case of OAT reactions.

To verify the sustainability of this reactivity trend for HAA, we evaluated the C-H activation abilities of the complexes under study. The conversion of ethylbenzene to 1-phenylethanol was tested with 1b, 3b and 4b. Reaction rates with 3b (k_2 = 155.3 x 10^{-3} M^{-1} s^{-1}) was around twenty times faster than 1b (k_2 = 7.9 x 10^{-3} M^{-1} s^{-1}), whereas 4b (k_2 = 9.7 x 10^{-3} M^{-1} s^{-1}) almost mirrors 1b in terms of C-H activation rates at 298 K (see Fig. 4.10).

Table 4.4. Pseudo first-order rate constants for the reaction of 1b, 3b and 4b with Ethylbenzene in CH_3CN at 298 K.

1b		**3b**		**4b**	
Ethylbenzene (M)	***$10^{-3} \times k_{obs}$ (s^{-1})***	***Ethylbenzene (M)***	***$10^{-3} \times k_{obs}$ (s^{-1})***	***Ethylbenzene (M)***	***$10^{-3} \times k_{obs}$ (s^{-1})***
0.1	0.79	0.03	3.69	0.12	1.08
0.2	1.62	0.06	8.19	0.18	1.70
0.3	2.36	0.09	13.84	0.24	2.44
0.4	3.21	0.12	19.55	0.30	3.10
k_2 = 7.9 × 10^{-3} M^{-1} s^{-1}		k_2 = 155.3 × 10^{-3} M^{-1} s^{-1}		k_2 = 9.7 x 10^{-3} M^{-1} s^{-1}	

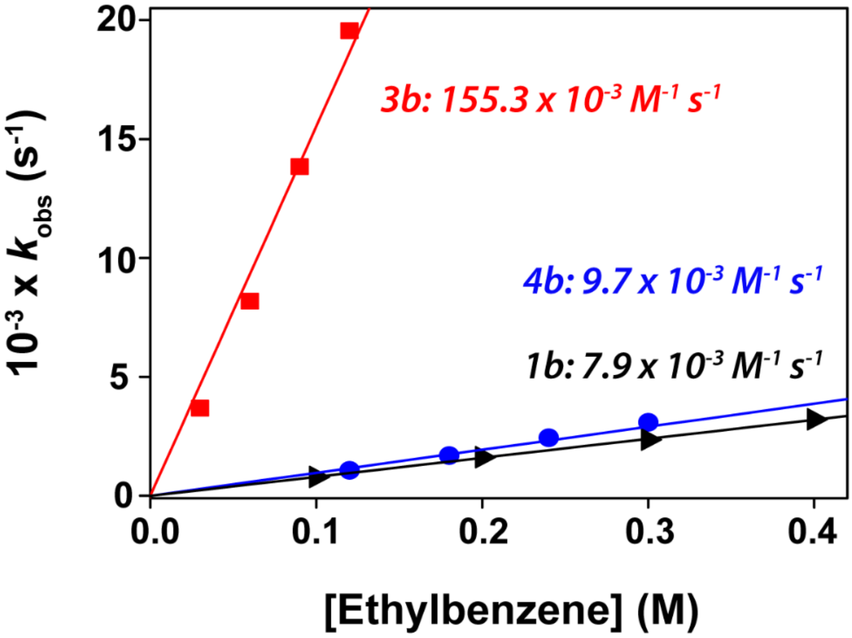

Fig. 4.10. Second-order rate constants determined for the reaction of 1b (1 mm, ▶), 4b (1 mm, ●) and 3b (1 mm, ■) with ethylbenzene in CH_3CN at 298 K.

As evident, complex 3b reacts much faster as compared to 1b and/or 4b. This trend was again verified with cumene as a substrate (Fig. 4.11). Second-order rate constants thereby obtained (Table 4.5) established that 3b is much more susceptible to react with C-H bonds of hydrocarbons than 1b or 4b. Therefore, the trend observed for OAT was also applicable to HAA reactions.

Table 4.5. Pseudo first-order rate constants for the reaction of 1b, 3b and 4b with Cumene in CH_3CN at 298 K.

1b		3b		4b	
Cumene (M)	*$10^{-3} \times k_{obs}$ (s^{-1})*	*Cumene (M)*	*$10^{-3} \times k_{obs}$ (s^{-1})*	*Cumene (M)*	*$10^{-3} \times k_{obs}$ (s^{-1})*
0.2	0.66	0.05	8.47	0.2	0.79
0.4	1.19	0.10	15.89	0.4	1.62
0.6	1.62	0.15	22.18	0.6	2.34
0.8	2.24	0.20	30.39	0.8	2.91
$k_2 = 2.8 \times 10^{-3}$ M^{-1} s^{-1}		$k_2 = 152.2 \times 10^{-3}$ M^{-1} s^{-1}		$k_2 = 3.8 \times 10^{-3}$ M^{-1} s^{-1}	

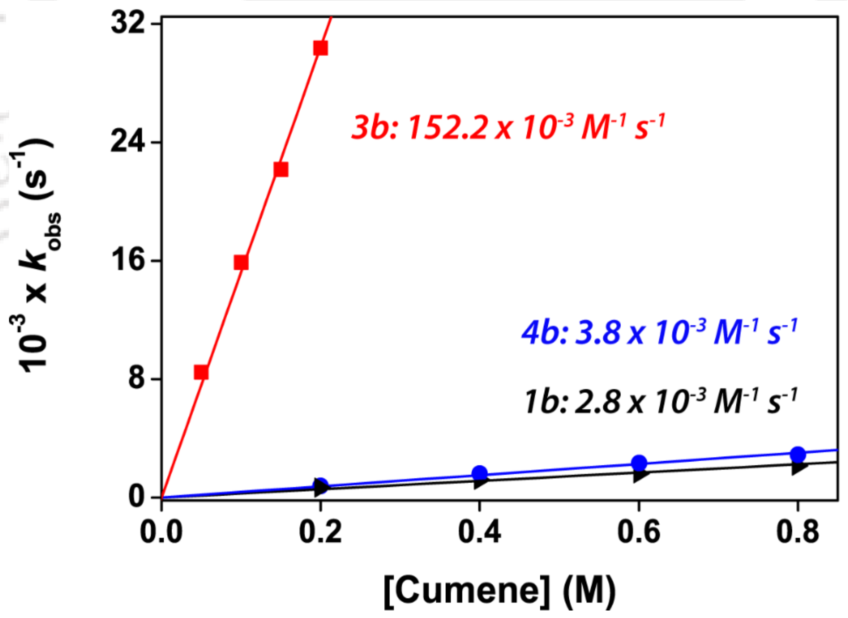

Fig. 4.11. Second-order rate constants determined for the reaction of 1b (1 mm, ▶), 4b (1 mm, ●) and 3b (1 mm, ■) with cumene in CH_3CN at 298 K.

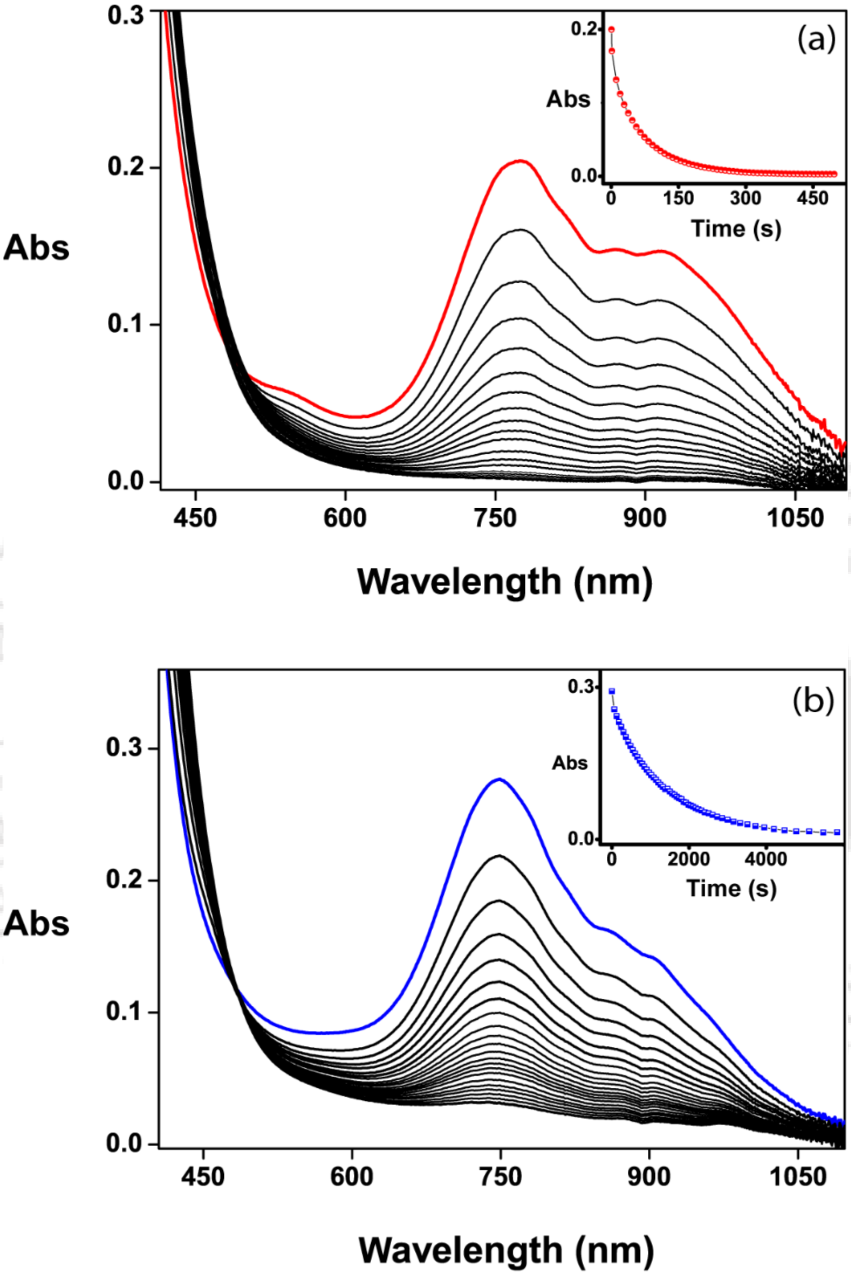

Fig. 4.12. UV/Vis spectral changes of (a) 3b (1 mM) and (b) 4b (1 mM) upon addition of ethylbenzene [120 equivalents] in CH_3CN at 298 K. Insets shows the decay of the 775 nm and 750 nm band respectively as a function of time.

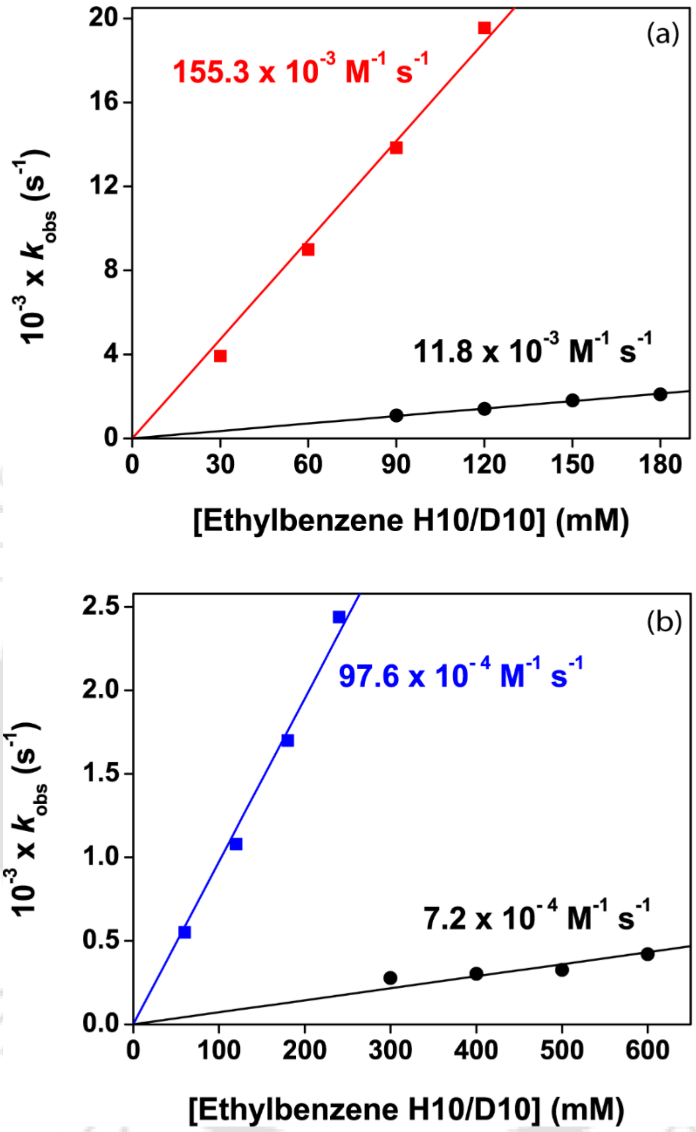

Fig. 4.13. Comparison of second-order rate constants determined in the reaction of (a) 3b (🟥) and (b) 4b (🟦) with ethylbenzene and ethylbenzene-D10 (●) at 298 K in CH_3CN.

To ensure that HAA is the rate-determining step, we repeated the experiments with ethylbenzene-D10 (see Table 4.6).[20] The isotopomers react differently due to vibrational differences in the C-H and C-D bond frequencies, and kinetic isotope effect (KIE) values of 13 and 14 were obtained for 3b and 4b, respectively. Hence, C-H bond cleavage was confirmed to be the rate-determining step in the HAA reactions.

Table 4.6. Pseudo first-order rate constants for the reaction of 3b and 4b with ethylbenzene and ethylbenzene-D10 in CH_3CN at 298 K.

<table>
<tr><th colspan="4">For 3b</th></tr>
<tr><th><i>[Ethylbenzene-H_{10}] (mM)</i></th><th><i>$10^{-3} \times k_{obs}$ (s^{-1})</i></th><th><i>[Ethylbenzene-D_{10}] (mM)</i></th><th><i>$10^{-3} \times k_{obs}$ (s^{-1})</i></th></tr>
<tr><td>30</td><td>3.93</td><td>90</td><td>1.11</td></tr>
<tr><td>60</td><td>8.99</td><td>120</td><td>1.41</td></tr>
<tr><td>90</td><td>13.84</td><td>150</td><td>1.81</td></tr>
<tr><td>120</td><td>19.55</td><td>180</td><td>2.12</td></tr>
<tr><td colspan="2">$k_2 = 155.3 \times 10^{-3}\ M^{-1}\ s^{-1}$</td><td colspan="2">$k_2 = 11.8 \times 10^{-3}\ M^{-1}\ s^{-1}$</td></tr>
<tr><th colspan="4">For 4b</th></tr>
<tr><th><i>[Ethylbenzene-H_{10}] (mM)</i></th><th><i>$10^{-3} \times k_{obs}$ (s^{-1})</i></th><th><i>[Ethylbenzene-D_{10}] (mM)</i></th><th><i>$10^{-3} \times k_{obs}$ (s^{-1})</i></th></tr>
<tr><td>60</td><td>0.55</td><td>300</td><td>0.28</td></tr>
<tr><td>120</td><td>1.08</td><td>400</td><td>0.30</td></tr>
<tr><td>180</td><td>1.70</td><td>500</td><td>0.32</td></tr>
<tr><td>240</td><td>2.44</td><td>600</td><td>0.42</td></tr>
<tr><td colspan="2">$k_2 = 97.6 \times 10^{-4}\ M^{-1}\ s^{-1}$</td><td colspan="2">$k_2 = 7.2 \times 10^{-4}\ M^{-1}\ s^{-1}$</td></tr>
</table>

A more pragmatic approach was taken to study the effect of the methyl groups towards substrate approach and reactivity using the conventionally available substrates with varying C-H bond dissociation energies (BDE).[20,59] In the Bell–Evans–Polanyi plot, the log k_2' values for five different complexes (1b, 2b, 3b, 4b and 6b) are portrayed against the C-H BDE of the sacrificial C-H bond(s) ranging from 77–90 kcal mol^{-1} (see Table 4.7). As is evident from Fig. 4.14, 1b and 4b display comparable reaction rates for all the substrates. The only exceptions being 9,10-dihydroanthracene (DHA), fluorene and triphenylmethane, in which 4b happens to react very sluggishly compared to 1b. Clearly, the steric effect imparted by the methyl groups in 4b during the approach of these three bulky substrates can be perceived.

Other complexes, such as 3b, 2b and 6b, have substantially higher reaction rates than 1b/4b for all the substrates irrespective of the C-H bond strength, one specific case, again, being the reactivity of 3b with triphenylmethane, in which a significant drop in reaction rate was observed. All the points in the plot shown here have been recorded under similar reaction conditions. Therefore, the sudden drop in reactivity for 3b and 4b with triphenylmethane can only be attributed to the steric factor between the oxo complex and the approaching substrate. The only active hydrogen atom in Ph_3CH is deeply embedded inside its "propeller-shaped" structure, the abstraction of which by 3b and/or 4b is highly hindered by the steric fencing provided by the methyl groups in both the complexes. This observation portrays the steric effect of Fe(IV)-oxo complexes with bulky substrates like Ph_3CH (also 9,10-DHA and fluorene), whereas all other complexes (like 1b, 2b and 6b) follow the thermodynamic trend of bond strength versus reactivity and the corresponding points for BDE 81 kcal mol^{-1} falls close to the best-fitted line. For substrates other than Ph_3CH, the active hydrogen(s) is/are easily accessible to all the complexes depending on the geometry and approach pathway.

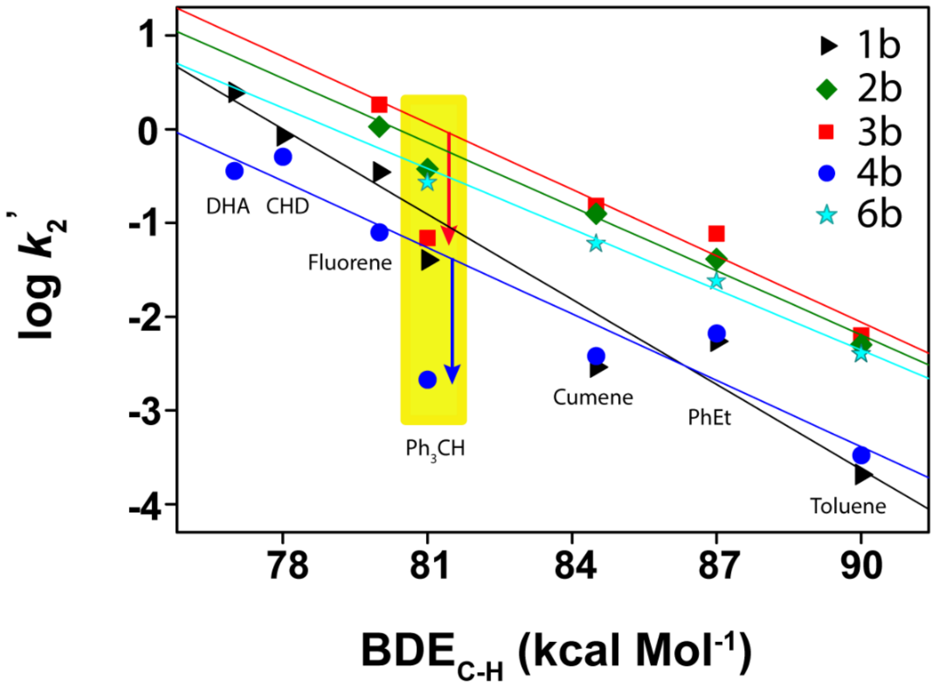

Fig. 4.14. Bell–Evans–Polanyi plot for their reaction of 1b (▶), 2b (◆) 3b (■), 4b (●) and 6b (★) with different substrates at 298 K in CH_3CN; k_2' is k_2 divided by the number of equivalent C-H bonds on the substrate that would react with the iron(IV)-oxo species. Best-fit lines exclude points for Ph_3CH to show the deviation.

Complexes 2b and 6b have almost similar reactivity profile to 3b but no reluctance towards Ph_3CH was observed; as such, the influence of the added substituents in the pyridine-6 position is primarily electronic, thereby enhancing their reactivity compared to 1b.[28,31] The longer Fe-N bond length in Fe(IV)-oxo, in general, gives rise to a more reactive complex. The average Fe-N bond lengths in 2b and 6b are 2.053 Å and 1.999 Å, respectively, whereas the same for 1b is 1.972 Å.[30] Again in complex 3b and 4b, the introduction of the methyl groups in the *ortho*-position of the pyridine rings leads to a flagpole-like interaction with the oxo moiety, and the sp^3-hybridization of the methyl carbon thus adds up to the flexibility in terms of C-C bond rotation and bending. In 2b and 6b, however, the added bulk is tethered to the *ortho*- and *meta*-positions of the pyridine ring and that to the immediate vicinity of the binding N is an sp^2-carbon, thereby restricting its free movement and rotation (see Fig. 4.1). Thus, in 3b and 4b, the steric factor precedes the electronic factor to determine the fate and rate of a reaction, and triphenylmethane (in spite of having a lower BDE_{C-H}) is an ideal substrate to make such an inference.

Scheme 4.1. Substrates used in this work.

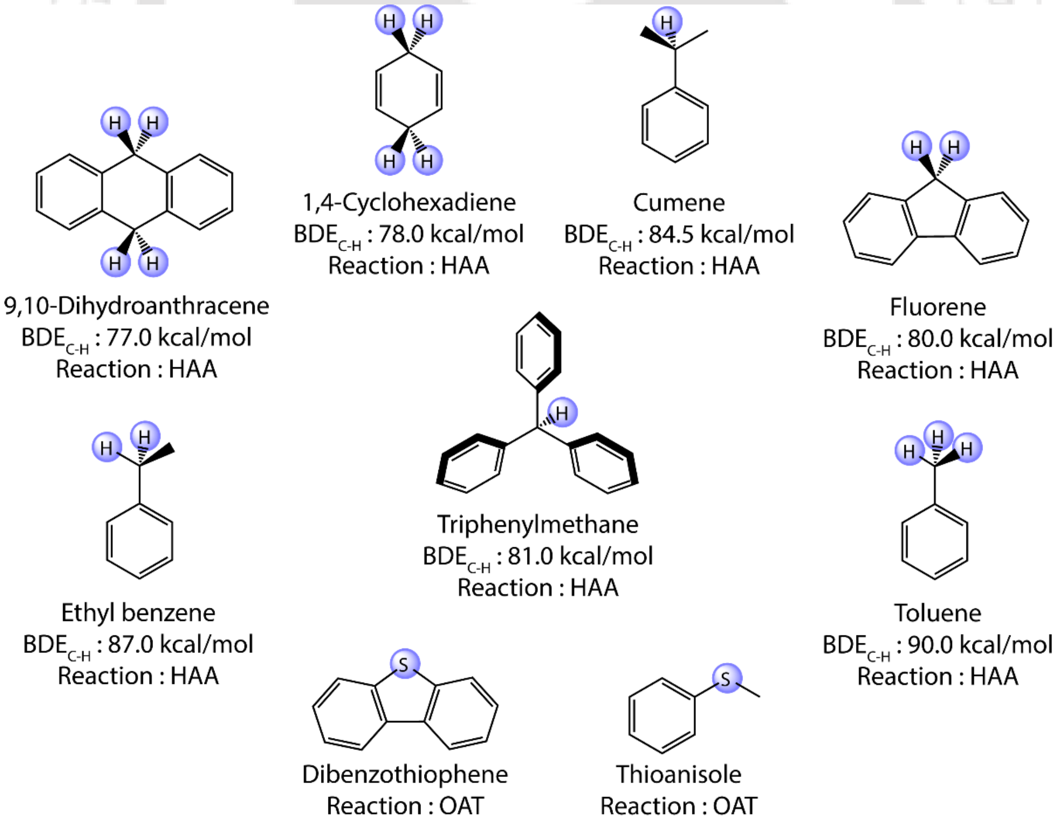

Table 4.7. Bond dissociation energies and second-order rate constants for the reaction of 1b, 2b, 3b, 4b and 6b with different substrates at 298 K in CH_3CN.

Substrate *$BDE_{C\text{-}H}$ in kcal/mol* [a] *no. of active H atoms*	*Complex*	*k_2 $(M^{-1}\ s^{-1})$*	*k_2' $(M^{-1}\ s^{-1})$* [b]	*log k_2'*
9,10-DHA 77.0 4	1b	9.853(3)	2.463	0.392
	2b	NR [c]	-	-
	3b	NR	-	-
	4b	1.429(6)	0.357	-0.447
	6b	NR	-	-
1,4-CHD 78.0 4	1b	3.385(3)	0.846	-0.072
	2b	NR	-	-
	3b	NR	-	-
	4b	2.034(4)	0.509	-0.294
	6b	NR	-	-
Fluorene 80.0 2	1b [d]	0.697(5)	0.348	-0.458
	2b	2.131(5)	1.065	0.027
	3b	3.653(3)	1.825	0.261
	4b	0.159(4)	0.079	-1.098
	6b	NR	-	-
Triphenylmethane 81.0 1	1b [a]	0.037(2)	0.037	-1.432
	2b [e]	0.376(3)	0.376	-0.424
	3b	0.069(5)	0.069	-1.161
	4b	0.002(2)	0.002	-2.699
	6b [f]	0.270(10)	0.270	-0.569

• ***Substrate*** • ***BDE$_{C-H}$ in kcal/mol*** [a] • ***no. of active H atoms***	***Complex***	***k_2 ($M^{-1}\ s^{-1}$)***	***k_2' ($M^{-1}\ s^{-1}$)*** [b]	***log k_2'***
• Cumene • 84.5 • 1	1b [e]	0.003(2)	0.003	-2.538
	2b [e]	0.125(3)	0.125	-0.902
	3b	0.152(4)	0.152	-0.818
	4b	0.004(2)	0.004	-2.420
	6b [f]	0.060(1)	0.060	-1.222
• Ethylbenzene • 87.0 • 2	1b [a]	0.008(1)	0.004	-2.403
	2b [e]	0.083(5)	0.041	-1.384
	3b	0.155(3)	0.077	-1.114
	4b	0.009(7)	0.004	-2.319
	6b [f]	0.048(1)	0.024	-1.620
• Toluene • 90.0 • 3	1b [e]	0.0006(2)	0.0002	-3.685
	2b [e]	0.015(4)	0.005	-2.299
	3b	0.019(4)	0.006	-2.201
	4b	0.001(3)	0.0003	-3.478
	6b [f]	0.012(5)	0.004	-2.398

[a] Ref 20, 59; [b] k_2' is the k_2 divided by the number of active H atoms on the substrate that would react with the oxo species, [c] "NR" stands for "Not Recorded", [d] Ref 60, [e] Ref 31, [f] Ref 28.

4.2.3. Computational Backup

To understand the anomaly in reactivity among 1b, 3b and 4b, a theoretical investigation was conducted.[62] From a comparative geometry optimization of the complexes under study, it was observed that in all the cases, the triplet spin state was the ground state and well-separated from the nearest quintet spin state. Also, the methyl substituents have a small effect on the spin state energies of 1b, 3b and 4b but do not change the spin state ordering (Fig. 4.15).

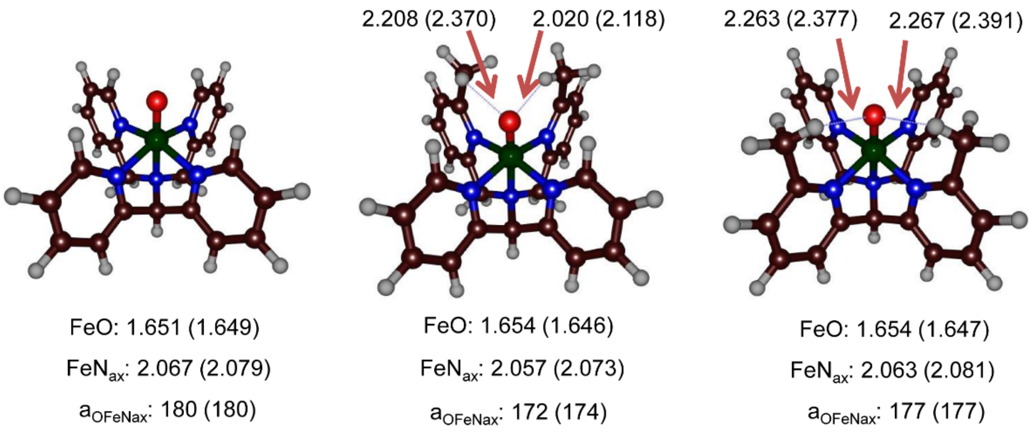

^{3}**1b** (^{5}**1b**) ^{3}**3b** (^{5}**3b**) ^{3}**4b** (^{5}**4b**)

Fig. 4.15. Optimized UB3LYP/BS1 geometries of ^{3,5}1b, ^{3,5}3b and ^{3,5}4b with bond lengths in angstroms and the O-Fe-N$_{ax}$ angle in degrees with N$_{ax}$ the axial amine nitrogen atom.

Upon addition of the methyl substituents to the pyridine scaffold, no dramatic changes in iron(IV)-oxo distances were observed. Similarly, the distances of the iron atom to the axial amine nitrogen atom (N$_{ax}$) did not vary a lot between the individual complexes. The only structural change that was seen was a modestly bent O-Fe-N$_{ax}$ angle in ^{3,5}3b to 172° (triplet) and 174° (quintet), respectively, that was envisaged from the crystal structures for the ferrous complexes (Fig. 4.2).

Again it was computed that the addition of methyl substituents to the N4Py scaffold nearby the oxo group in the iron(IV)-oxo species has little effect on the electronic configuration of the oxidant and the orbital energies and shapes. Thus, any change in reactivity must, therefore, come from differences in the substrate approach through electrostatic interactions. Moreover, the thermochemical parameters of the three iron(IV)-oxo complexes, 1b, 3b and 4b were calculated and as portrayed in Fig. 4.16, similar physical-chemical properties were obtained for all the three complexes.

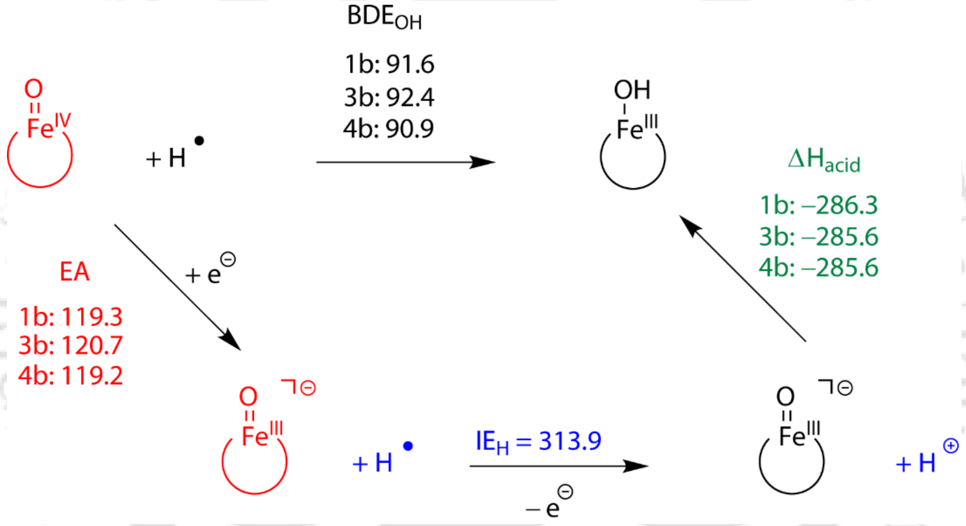

Fig. 4.16. Thermochemical analysis of the differences of structure 1b, 3b and 4b in electron affinity (EA), gas-phase acidity (ΔH_{acid}) and O-H bond strength (BDE_{OH}) with values in kcal mol^{-1}.

Therefore, external perturbations must be at play that influences the reactivity of these oxidants with substrates. Most likely the reaction rates are affected due to differences in the approach of the substrate to the oxidant, which must show structural and electronic differences. The structural differences between the rate-determining transition states is evident from an overlay of $^{5}TS_{SO,3b}$ and $^{5}TS_{SO,4b}$ as

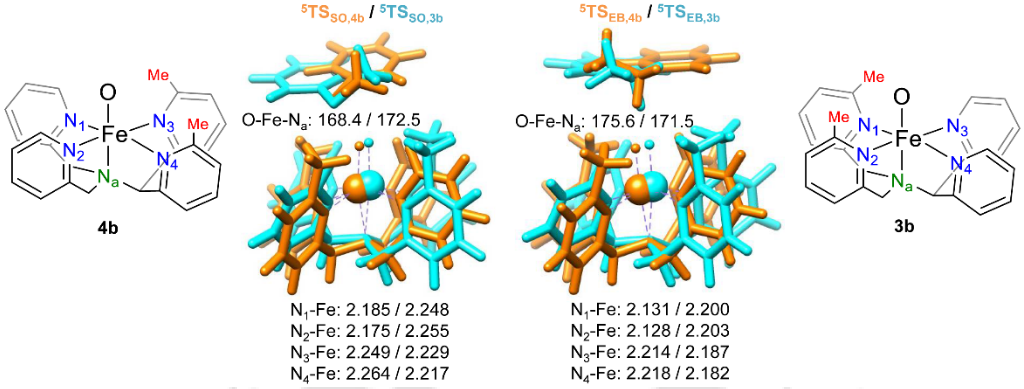

Fig. 4.17. Overlay of optimized geometries of the quintet spin transition states for OAT and HAA by ^{5}3b and ^{5}4b. Bond lengths are given in angstroms (Å) and the O-Fe-N_{ax} angle is in degrees.

can be seen from Fig. 4.17, where the substrate is located in roughly the same position with respect to the oxidant. However, the metal centre has shifted slightly within the ligand scaffold. Thus, in $^5TS_{SO,3b}$ and $^5TS_{EB,3b}$ the metal is located nearby the centre of the four pyridine nitrogen atoms that give Fe-N distances within a range of 0.038 and 0.021 Å, respectively. By contrast, for the structures originating from 4b the Fe-N distances are much wider apart (0.089 and 0.090 Å), so that the metal is not located in the centre of the ligand scaffold. Overall, the calculations showed that the methyl substituents affect the positioning of the metal in the ligand framework such that it is pulled back into the centre of the four pyridine rings during the rate-determining transition state. This has a dramatic effect on lowering the activation barrier height and consequently affect the reaction rate. As such, the methyl substituents masquerade the oxidant and effectively position the substrate and oxidant for ideal HAA or OAT reactions.

4.3. Conclusion

With the benchmarking of existing and new iron(IV)-oxo complexes in oxidation reactions, an experimental overview of the various reactivity trends has been provided. Understanding the fine interplay between electronic and steric effects generated by substituents is crucial that can be utilized as guidelines for a more rational synthetic approach for developing more efficient and selective systems. Overall, the intricate details of subtle modifications to the primary- and secondary-coordination sphere of mononuclear non-heme iron(IV)-oxo model systems in an octahedral environment have been projected that brings forth the competitiveness of electronic and steric factors that influence their reactivity. With the synthesis and characterization of two new pentadentate ligand frameworks that are isomeric in mass and geometry, we have evidenced that the corresponding iron(IV)-oxo complexes possess differences in reactivity profiles towards HAA and OAT reactions. In fact, this study is unique in that regioselective substitution by methyl moieties in the same ligand skeleton thereby provoking substantially different reactivity of the oxo species. In addition, the methyl groups shield the bulkier substrate *viz*. triphenylmethane, to make the catalysts reluctant towards these substrates. Computational modelling rules out the electronic features of the complexes under study and establishes that a steric factor is the driving force behind this eccentric reactivity. Indeed, the methyl groups employed at the specified positions act as shafts to position the substrate and oxidant in a definite orientation in space. These substituents direct the corridors of substrate approach to the active site thereby tuning the efficiency of HAA or OAT reactions.

4.4. References

1. M. Costas, M. P. Mehn, M. P. Jensen, L. Que, Jr., *Chem. Rev.*, **2004**, *104*, 939–986.
2. M. M. Abu-Omar, A. Loaiza, N. Hontzeas, *Chem. Rev.*, **2005**, *105*, 2227–2252.
3. C. Krebs, D. G. Fujimori, C. T. Walsh, J. M. Bollinger, Jr., *Acc. Chem. Res.*, **2007**, *40*, 484–492.
4. P. C. A. Bruijnincx, G. van Koten, R. J. M. Klein Gebbink, *Chem. Soc. Rev.*, **2008**, *37*, 2716–2744.
5. E. I. Solomon, K. M. Light, L. V. Liu, M. Srnec, S. D. Wong, *Acc. Chem. Res.*, **2013**, *46*, 2725–2739.
6. K. Ray, F. F. Pfaff, B. Wang, W. Nam, *J. Am. Chem. Soc.*, **2014**, *136*, 13942–13958.
7. X. Engelmann, I. Monte-Pérez, K. Ray, *Angew. Chem. Int. Ed.*, **2016**, *55*, 7632–7649.
8. B. Meunier, S. P. de Visser, S. Shaik, *Chem. Rev.*, **2004**, *104*, 3947–3980.
9. I. G. Denisov, T. M. Makris, S. G. Sligar, I. Schlichting, *Chem. Rev.*, **2005**, *105*, 2253–2278.
10. P. R. Ortiz de Montellano, *Chem. Rev.*, **2010**, *110*, 932–948.
11. D. Li, Y. Wang, K. Han, *Coord. Chem. Rev.*, **2012**, *256*, 1137– 1150.
12. M. R. A. Blomberg, T. Borowski, F. Himo, R.-Z. Liao, P. E. M. Siegbahn, *Chem. Rev.*, **2014**, *114*, 3601–3658.
13. *Iron-containing enzymes: Versatile catalysts of hydroxylation reaction in nature* (Eds.: S. P. de Visser, D. Kumar), RSC, Cambridge, **2011**.

14. E. I. Solomon, T. C. Brunold, M. I. Davis, J. N. Kemsley, S. K. Lee, N. Lehnert, F. Neese, A. J. Skulan, Y. S. Yang, J. Zhou, *Chem. Rev.*, **2000**, *100*, 235–349.

15. J. U. Rohde, J. H. In, M. H. Lim, W. W. Brennessel, M. R. Bukowski, A. Stubna, E. Münck, W. Nam, L. Que, Jr., *Science*, **2003**, *299*, 1037–1039.

16. C. V. Sastri, J. Lee, K. Oh, Y. J. Lee, T. A. Jackson, K. Ray, H. Hirao, W. Shin, J. A. Halfen, J. Kim, L. Que, Jr., S. Shaik, W. Nam, *Proc. Natl. Acad. Sci. USA*, **2007**, *104*, 19181–19186.

17. P. Comba, S. Wunderlich, *Chem. Eur. J.*, **2010**, *16*, 7293–7299.

18. S. V. Kryatov, E. V. Rybak-Akimova, S. Schindler, *Chem. Rev.*, **2005**, *105*, 2175–2226.

19. M. Lubben, A. Meetsma, E. C. Wilkinson, B. Feringa, L. Que, Jr., *Angew. Chem. Int. Ed.*, **1995**, *34*, 1512–1515.

20. J. Kaizer, E. J. Klinker, N. Y. Oh, J.-U. Rohde, W. J. Song, A. Stubna, J. Kim, E. Münck, W. Nam, L. Que, Jr., *J. Am. Chem. Soc.*, **2004**, *126*, 472–473.

21. E. J. Klinker, T. A. Jackson, M. P. Jensen, A. Stubna, G. Juhász, E. L. Bominaar, E. Münck, L. Que, Jr., *Angew. Chem. Int. Ed.*, **2006**, *45*, 7394–7397.

22. D. Wang, K. Ray, M. J. Collins, E. R. Farquhar, J. R. Frisch, L. Gómez, T. A. Jackson, M. Kerscher, A. Waleska, P. Comba, M. Costas, L. Que, Jr., *Chem. Sci.*, **2013**, *4*, 282–292.

23. A. C. McQuilken, Y. Jiang, M. A. Siegler, D. P. Goldberg, *J. Am. Chem. Soc.*, **2012**, *134*, 8758–8761.

24. S. Sahu, L. R. Widger, M. G. Quesne, S. P. de Visser, H. Matsumura, P. Moënne-Loccoz, M. A. Siegler, D. P. Goldberg, L. R. Widger, C. G. Davies, T. Yang, M. A. Siegler, O. Troeppner, G. N. L. Jameson, I.

Ivanović-Burmazović, D. P. Goldberg, *J. Am. Chem. Soc.*, **2013**, *135*, 10590–10593.

25. L. R. Widger, C. G. Davies, T. Yang, M. A. Siegler, O. Troeppner, G. N. L. Jameson, I. Ivanović-Burmazović, D. P. Goldberg, *J. Am. Chem. Soc.*, **2014**, *136*, 2699–2702.
26. S. Sahu, M. G. Quesne, C. G. Davies, M. Dürr, I. Ivanović-Burmazović, M. A. Siegler, G. N. L. Jameson, S. P. de Visser, D. P. Goldberg, *J. Am. Chem. Soc.*, **2014**, *136*, 13542–13545.
27. S. Sahu, B. Zhang, C. J. Pollock, M. Dürr, C. G. Davies, A. M. Confer, I. Ivanović-Burmazović, M. A. Siegler, G. N. L. Jameson, C. Krebs, D. P. Goldberg, *J. Am. Chem. Soc.*, **2016**, *138*, 12791–12802.
28. M. Mitra, H. Nimir, S. Demeshko, S. S. Bhat, S. O. Malinkin, M. Haukka, J. Lloret-Fillol, G. C. Lisensky, F. Meyer, A. A. Shteinman, W. R. Browne, D. A. Hrovat, M. G. Richmond, M. Costas, E. Nordlander, *Inorg. Chem.*, **2015**, *54*, 7152–7164.
29. S. Rana, A. Dey, D. Maiti, *Chem. Commun.*, **2015**, *51*, 14469–14472.
30. W. Rasheed, A. Draksharapu, S. Banerjee, V. G. Young Jr., R. Fan, Y. Guo, M. Ozerov, J. Nehrkorn, J. Krzystek, J. Telser, L. Que, Jr., *Angew. Chem. Int. Ed.*, **2018**, 57, 9387–9391.
31. G. Mukherjee, C. W. Z. Lee, S. S. Nag, A. Alili, F. G. Cantú Reinhard, D. Kumar, C. V. Sastri, S. P. de Visser, *Dalton Trans.*, **2018**, *47*, 14945–14957.
32. S. Rana, J. P. Biswas, A. Sen, M. Clémancey, G. Blondin, J.-M. Latour, G. Rajaraman, D. Maiti, *Chem. Sci.*, **2018**, *9*, 7843–7858.
33. Y. Zang, J. Kim, Y. Dong, E. C. Wilkinson, E. H. Appelman, L. Que, Jr., *J. Am. Chem. Soc.*, **1997**, *119*, 4197–4205.

34. A. N. Biswas, M. Puri, K. K. Meier, W. N. Oloo, G. T. Rohde, E. L. Bominaar, E. Münck, L. Que, Jr., *J. Am. Chem. Soc.*, **2015**, *137*, 2428–2431.
35. M. S. Seo, N. H. Kim, K.-B. Cho, J. E. So, S. K. Park, M. Clémancey, R. G. Serres, J.-M. Latour, S. Shaik, W. Nam, *Chem. Sci.*, **2011**, *2*, 1039–1045.
36. C. E. Macbeth, A. P. Golombek, V. G. Young Jr., C. Yang, K. Kuczera, M. P. Hendrich, A. S. Borovik, *Science*, **2000**, *289*, 938–941.
37. J. England, M. Martinho, E. R. Farquhar, J. R. Frisch, E. L. Bominaar, E. Münck, L. Que, Jr., *Angew. Chem. Int. Ed.*, **2009**, *48*, 3622–3626.
38. J. P. Bigi, W. H. Harman, B. Lassalle-Kaiser, D. M. Robles, T. A. Stich, J. Yano, R. D. Britt, C. J. Chang, *J. Am. Chem. Soc.*, **2012**, *134*, 1536–1542.
39. A. K. Patra, M. M. Olmstead, P. K. Mascharak, *Inorg. Chem.*, **2002**, *41*, 5403–5409.
40. S. Kundu, J. V. K. Thompson, A. D. Ryabov, T. J. Collins, *J. Am. Chem. Soc.*, **2011**, *133*, 18546–18549.
41. S. A. Wilson, J. Chen, S. Hong, Y.-M. Lee, M. Clémancey, R. Garcia-Serres, T. Nomura, T. Ogura, J.-M. Latour, B. Hedman, K. O. Hodgson, W. Nam, E. I. Solomon, *J. Am. Chem. Soc.*, **2012**, *134*, 11791–11806.
42. I. Prat, A. Company, T. Corona, T. Parella, X. Ribas, M. Costas, *Inorg. Chem.*, **2013**, *52*, 9229–9244.
43. E. Wong, J. Jeck, M. Grau, A. J. P. White, G. J. P. Britovsek, *Catal. Sci. Technol.*, **2013**, *3*, 1116–1122.
44. M. Mitra, J. Lloret-Fillol, M. Haukka, M. Costas, E. Nordlander, *Chem. Commun.*, **2014**, *50*, 1408–1410.
45. X. Sun, C. Geng, R. Huo, U. Ryde, Y. Bu, J. Li, *J. Phys. Chem. B*, **2014**, *118*, 1493–1500.

46. R. Turcas, D. Lakk-Bogath, G. Speier, J. Kaizer, *Dalton Trans.*, **2018**, *47*, 3248–3252.
47. G. Roelfes, M. Lubben, K. Chen, R. Y. N. Ho, A. Meetsma, S. Genseberger, R. M. Hermant, R. Hage, S. K. Mandal, V. G. Young, Jr., Y. Zang, H. Kooijman, A. L. Spek, L. Que, Jr., B. L. Feringa, *Inorg. Chem.*, **1999**, *38*, 1929–1936.
48. A. L. Spek, M. F. J. Schoondergang, B. L. Feringa, CCDC 232796, *CSD Communication*, **2004**.
49. M. S. Seo, J.-H. In, S. O. Kim, N. Y. Oh, J. Hong, J. Kim, L. Que, Jr., W. Nam, *Angew. Chem. Int. Ed.*, **2004**, *43*, 2417–2420.
50. E. J. Klinker, J. Kaizer, W. W. Brennessel, N. L. Woodrum, C. J. Cramer, L. Que, Jr., *Angew. Chem. Int. Ed.*, **2005**, *44*, 3690–3694.
51. K. Ray, J. England, A. T. Fiedler, M. Martinho, E. Münck, L. Que, Jr., *Angew. Chem. Int. Ed.*, **2008**, *47*, 8068–8071.
52. A. Company, G. Sabenya, M. González-Béjar, L. Gómez, M. Clémancey, G. Blondin, A. J. Jasniewski, M. Puri, W. S. Browne, J. M. Latour, L. Que, Jr., M. Costas, J. PérezPrieto, J. Lloret-Fillol, *J. Am. Chem. Soc.*, **2014**, *136*, 4624–4633.
53. M. H. Lim, J.-U. Rohde, A. Stubna, M. R. Bukowski, M. Costas, R. Y. N. Ho, E. Münck, W. Nam, L. Que, Jr., *Proc. Natl. Acad. Sci. U. S. A.*, **2003**, *100*, 3665–3670.
54. M. S. Seo, H. G. Jang, J. Kim, W. Nam, *Bull. Korean Chem. Soc.*, **2005**, *26*, 971–974.
55. M. You, M. S. Seo, K. M. Kim, W. Nam, J. Kim, *Bull. Korean Chem. Soc.*, **2006**, *27*, 1140–1144.
56. W. Nam, *Acc. Chem. Res.*, **2007**, *40*, 522–531.
57. S. Paria, S. Chatterjee, T. K. Paine, *Inorg. Chem.*, **2014**, *53*, 2810–2821.

58. D. Sheet, T. K. Paine, *Chem. Sci.*, **2016**, *7*, 5322–5331.

59. A. K. Vardhaman, P. Barman, S. Kumar, C. V. Sastri, D. Kumar, S. P. de Visser, *Angew. Chem. Int. Ed.*, **2013**, *52*, 12288–12292.

60. S. Kumar, A. S. Faponle, P. Barman, A. K. Vardhaman, C. V. Sastri, D. Kumar, S. P. de Visser, *J. Am. Chem. Soc.*, **2014**, *136*, 17102–17115.

61. A. K. Vardhaman, S. Sikdar, C. V. Sastri, *Ind. J. Chem.*, **2011**, *50A*, 427–431.

62. The computational modelling was done in collaboration with Dr. Samuel P. de Visser and his research group. This theoretical study was pivotal in this work to understand the intrinsic factors dictating the reaction trends and mechanism; see DOI: 10.1002/chem.201806430.

CHAPTER – V

Keto−Enol Tautomerization Triggers an Electrophilic Aldehyde Deformylation Reaction by a Non-Heme Manganese(III)-Peroxo Complex

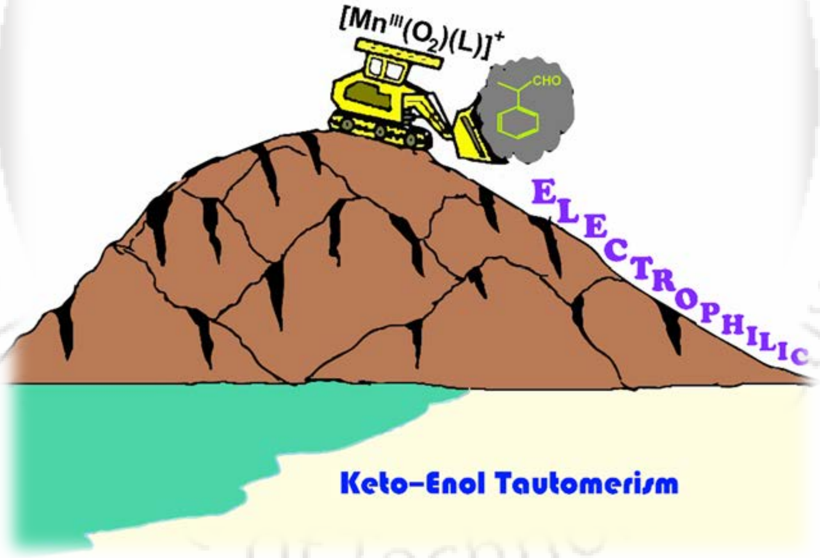

● Adapted from *J. Am. Chem. Soc.* **2017**, *139*, 18328−18338 with permission from the ACS Publications Support; further permissions related to the material excerpted should be directed to the ACS. ●

5.1. Introduction

Metalloenzymes are powerful oxidants in nature that catalyse important reactions for Biosystems.[1-9] Most of these metalloenzymes utilize iron as their central cofactor, due to its high natural abundance. Another transition metal in relatively large abundance in the earth crust is manganese and, as such, nature has found key uses of it in various biological transformations.[10-11] Thus, manganese complexes are strong oxidizers, and consequently, the active site of superoxide dismutase (SOD) contains a central Mn atom.[12-18] SOD is involved in the biodegradation of superoxide radicals and converts them on a manganese centre to hydrogen peroxide. Often SOD enzymes are anchored to a catalase enzyme that reacts and detoxifies hydrogen peroxide. Another biological system with manganese coordination is the Photosystem II (PSII) active cluster, which contains four manganese atoms held together with bridging oxygen atoms and a dangling Ca^{2+} ion in a cubane-type Mn_4O_5Ca cluster.[19-22] This cluster binds water molecules and reacts them to one molecule of molecular oxygen with the release of four protons.

In biomimetic chemistry, synthetic manganese-containing models of SOD and PSII have been created and studied for their chemical properties and reactivity.[23-26] In several of these studies, a manganese-peroxo was investigated and the spectroscopic features of the complexes were established with UV/Vis, resonance Raman, infrared absorption and electron paramagnetic resonance (EPR) spectroscopy.[27-37] Furthermore, the reactivity of manganese-peroxo with respect to substrates was investigated and efficient conversion to aldehyde products *via* deformylation was obtained.[38-42] However, the exact details of the mechanism remain a mystery. Therefore, manganese(III)-peroxo shows interesting reactivity patterns with substrates that are still poorly understood.

Recently, an interesting result was reported that shows a bispidine ligated manganese(III)-peroxo reacts with aldehydes through a rate-determining hydrogen atom abstraction reaction as evidenced from a large kinetic isotope effect (KIE) for the replacement of the α-hydrogen atom by deuterium.[43] Radical trapping experiments and density functional theory calculations further confirmed the rate-determining hydrogen atom abstraction and rationalized that this is originating from a more feasible electron transfer from peroxo to Mn as compared to substrate carbonyl. The question, therefore, is how the ligand system of the metal influences the bifurcation pathways between hydrogen atom abstraction (*i.e.*, the electrophilic pathway) versus a nucleophilic pathway.

To test the effect of the ligand architecture on the bifurcation pathways, we followed up a detailed study on two functionally isomeric pentadentate manganese(III)-peroxo complexes, resulting in different orientations of two pyridine groups with respect to N3 nitrogen of the bispidine backbone. In particular, we synthesized manganese(III)-peroxo complexes with bispidine ligand systems (see Fig. 5.1), namely $[Mn^{III}(O_2)(L8)]^+$ (8b) and $[Mn^{III}(O_2)(L9)]^+$ (9b) with L8 = dimethyl-2,4-di(2-pyridyl)3-(pyridin-2-ylmethyl)-7-benzyl-3,7-diaza-bicyclo[3.3.1] nonan-9-one-1,5-dicarboxylate) and L9 = dimethyl 2,4-di(2-pyridyl)-3-benzyl-7-(pyridin-2-ylmethyl)-3,7-diazabicyclo[3.3.1] nonan-9-one-1,5-dicarboxylate). Thus, ligand L8 has three pyridine groups pointing upward (*i.e.*, along the molecular z-axis with the *ortho* C−H groups in hydrogen bonding distance to the sixth ligand), whereas in ligand L9 only one of those points upward and the other two are aligned with the xy-plane. Our combined experimental and computational study gives evidence of a novel reaction mechanism starting with a rate-determining hydrogen atom abstraction reaction and followed by a reshuttle of the hydrogen atom through a keto-enol tautomerization to set up a low-energy nucleophilic attack of peroxo on an olefin bond of the substrate. Our observations are confirmed with computational modelling that rationalizes the reaction mechanism.

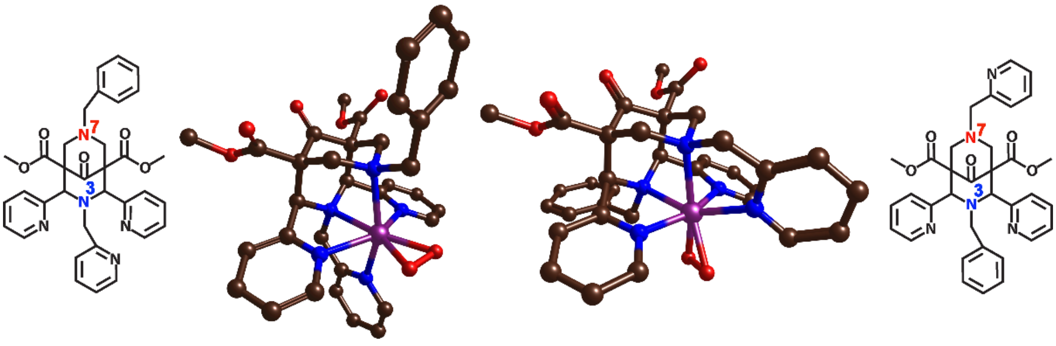

$[Mn^{III}(O_2)(L8)]^+$, 8b

$[Mn^{III}(O_2)(L9)]^+$, 9b

Fig. 5.1. Ligand frameworks and Manganese(III)-peroxo complexes investigated in this work.

5.2. Results and Discussion

5.2.1. Synthesis and Characterization

In this work, we describe the synthesis, characterization and reactivity patterns of two novel side-on manganese(III)-peroxo complexes with pentadentate bispidine ligands, *i.e.*, $[Mn^{III}(O_2)(L8)]^+$ (8b) and $[Mn^{III}(O_2)(L9)]^+$ (9b), Fig. 5.1. These two ligand systems have their equatorial pyridine groups either axial or equatorial to the manganese(III)-peroxo group and, hence, interact differently with an approaching substrate. The weak intermolecular interactions separating the two complexes may incur in functional differences due to the way substrate can approach to the catalytic centre and/or the stability of the reactant complex. Therefore, these models may give insight into the properties and functions of enzymatic catalysts where substrate approach is often tightly controlled.[44-45]

The piperidone backbone of the ligands L8 and L9 were prepared according to a literature protocol[46-49] and used to generate the $[Mn^{II}(L8)](ClO_4)_2$ and $[Mn^{II}(L9)](ClO_4)_2$ complexes. These Mn(II) complexes were synthesized using previously reported procedures and characterized accordingly.[49]

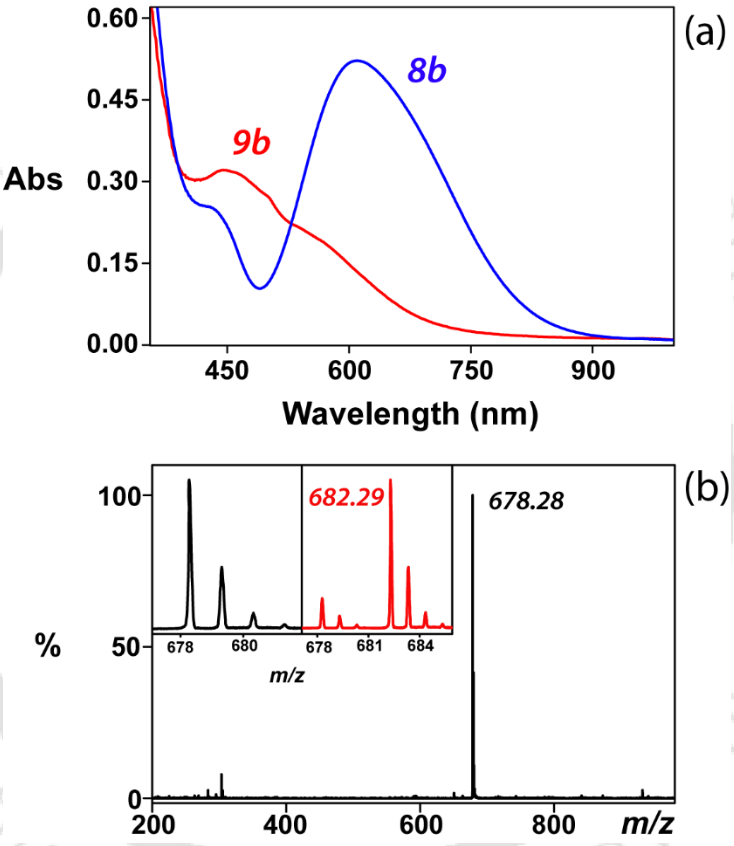

Fig. 5.2. (a) UV/Vis spectra of the formation of $[Mn^{III}(O_2)(L8)]^+$ (8b) and $[Mn^{III}(O_2)(L9)]^+$ (9b) (2 mM) upon addition of $[Mn(L9)]^{2+}$ in the presence of TEA (5 mM) and H_2O_2 (20 mM) in CH_3CN at 15 °C. (b) ESI-MS spectrum of $[Mn^{III}(O_2)(L9)]^+$ in CH_3CN at 15 °C. Mass peak at m/z = 678.28 is assigned for $[Mn(L9)(^{16}O_2)]^+$. Inset shows observed isotopic distribution patterns of $[Mn(L9)(^{16}O_2)]^+$ (left panel) and $[Mn(L9)(^{18}O_2)]^+$ (right panel).

Upon addition of 10 equivalents of H_2O_2 to the Mn(II) complexes (8a and 9a, *i.e.* $[Mn^{II}(L8)(ClO_4)_2]^{2+}$ and $[Mn^{II}(L9)(ClO_4)_2]^{2+}$ respectively) in the presence of 2.5 equivalents of triethylamine (TEA) at 15 °C in acetonitrile, blue[43] and brown intermediates were formed respectively with distinctive absorption features, Fig. 5.2a. Such considerable absorption features are indicative of the fact that subtle changes in the ligand skeleton could impart notable changes in the spectral features. The ESI mass spectra of 8b and 9b were recorded by infusing pre-cooled samples directly into the source at 15 μL min^{-1} using a syringe pump.[43] The spray voltage was set at 2 kV and the capillary temperature at 80 °C. Prominent peak at *m/z* 678.28 was obtained and an isotope distribution pattern indicates the formation of $[Mn^{III}(O_2)(L9)]^+$. When $H_2{}^{18}O_2$ was added instead of $H_2{}^{16}O_2$ to the reaction mixture, the mass of the parent ion shifted by four-unit to the right (*m/z* 682.29) indicating the formation of a dioxygen-bound complex (Fig. 5.2.b).

5.2.2. Reaction Kinetics

We investigated the deformylation behaviour of compounds 8b and 9b in their reaction with 2-phenylpropionaldehyde (2-PPA). This was done by monitoring the changes in the UV/Vis absorption spectra as a function of time after the addition of substrate. In particular, the aldehyde deformylation reaction and the mechanism of substrate activation by side-on manganese(III)-peroxo was investigated experimentally from the reactivity of $[Mn^{III}(O_2)(L8)]^+$ and $[Mn^{III}(O_2)(L9)]^+$ with 2-PPA under the same reaction conditions (Fig. 5.3). Addition of 2-PPA to 9b in acetonitrile at 15 °C led to the immediate decay of the intermediate and the formation of acetophenone as identified by NMR. The pseudo first-order rate constant (k_{obs}) for the decay of 9b increased linearly with increasing concentration of 2-PPA.

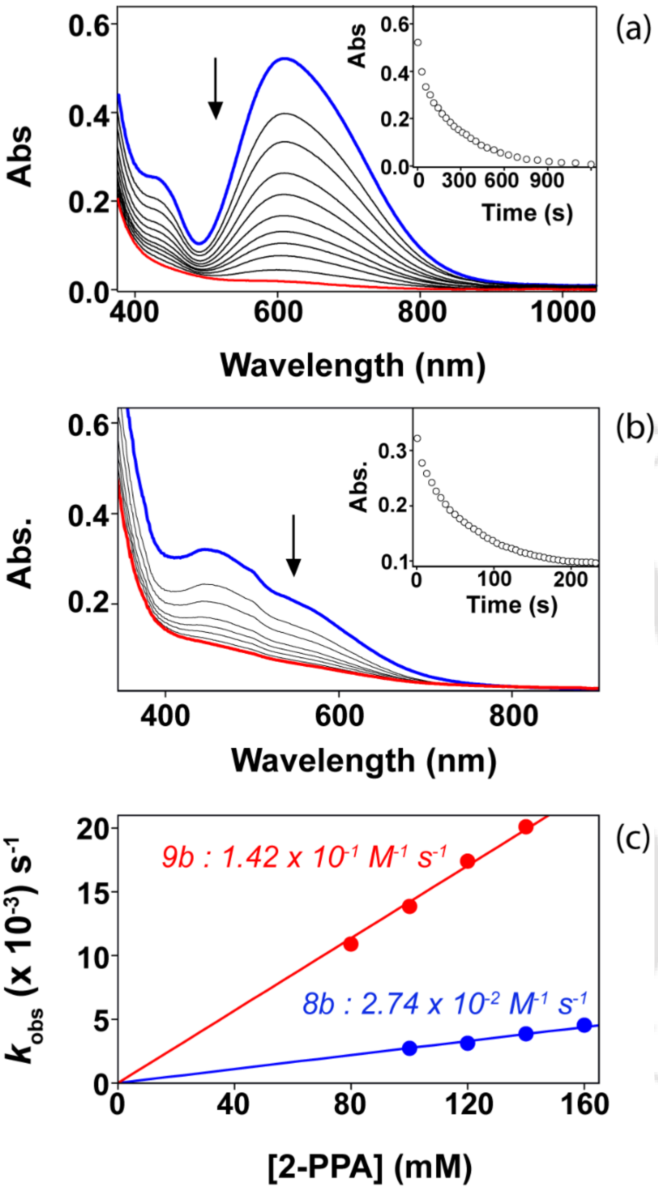

Fig. 5.3. UV/Vis spectral changes of (a) 8b (2mM) and (b) 9b (2 mM) upon addition of 2-PPA (160 mM and 120 mM for 8b and 9b respectively) in the presence of TEA (5 mM) and hydrogen peroxide (20 mM) in CH_3CN at 15 °C. The insets show the time course for the decay of the respective absorption bands. (c) Plot of k_{obs} against the concentration of 2-PPA and the derived second-order rate constants for the reaction of 8b (●) and 9b (●) with 2-PPA in CH_3CN at 15 °C.

This enabled us to measure the second-order rate constants for the reaction of 9b with 2-PPA: $k_2 = 1.42 \times 10^{-1}$ M^{-1} s^{-1}. For comparison, the second-order rate constant for the reaction of $[Mn^{III}(O_2)(L8)]^+$ with 2-PPA was 2.74×10^{-2} M^{-1} s^{-1}.[43] Therefore, it appears that small tweak in the ligand skeleton has induced subtle changes in the reactivity and consequently $[Mn^{III}(O_2)(L9)]^+$ reacts with 2-PPA about five times faster than the isomeric oxidant with ligand L8. These results were, in fact, opposite in trend to those obtained in the reactivity of the corresponding manganese(IV)-oxo complexes $[Mn^{IV}(O)(L8)]^{2+}$ and $[Mn^{IV}(O)(L9)]^{2+}$.[49] A possible reason for the change in rate constant ordering is the shape of the ligand system, whereby the L8 ligand (see Fig. 5.1) has protons pointing upward toward the peroxo group, whereas in the L9 ligand the pyridine moieties are in the xy-plane and will not interact with the approaching substrate.

To understand the details of the rate-determining step for the reaction of $[Mn^{III}(O_2)(L8)]^+$ and $[Mn^{III}(O_2)(L9)]^+$ with 2-PPA, we decided to investigate the kinetic isotope effect (KIE) for replacing the α-hydrogen atom with deuterium (Fig. 5.4). Thus, upon addition of α-[D1]-PPA (~90%, D-enriched) to 9b in acetonitrile at 15 °C, the absorption spectrum for the intermediates started decaying by which we determined a second-order rate constant of $k_2 = 2.67 \times 10^{-2}$ M^{-1} s^{-1}. Hence, the reaction between 9b and 2-PPA proceeds with a KIE = 5.3, and it can be concluded that the reaction has a rate-determining hydrogen atom abstraction step. A comparable KIE value of 5.4 was determined for the reactivity difference of 8b with 2-PPA/α-[D1]-PPA.[43] Consequently, both $[Mn^{III}(O_2)(L8)]^+$ and $[Mn^{III}(O_2)(L9)]^+$ react with 2-PPA through a rate-determining hydrogen atom abstraction as evident from their KIE values and most likely their reaction mechanisms will be similar.

Table 5.1. Second-order rate constants for the reaction of 8b and 9b with 2-PPA and α-D1-2-PPA at 15 °C.

Catalyst	k_2 (2-PPA)	k_2 (α-D1-2-PPA)
$[Mn^{III}(O_2)(L8)]^+$ (8b)	0.0274 M^{-1} s^{-1}	0.005 M^{-1} s^{-1}
$[Mn^{III}(O_2)(L9)]^+$ (9b)	0.142 M^{-1} s^{-1}	0.0267 M^{-1} s^{-1}

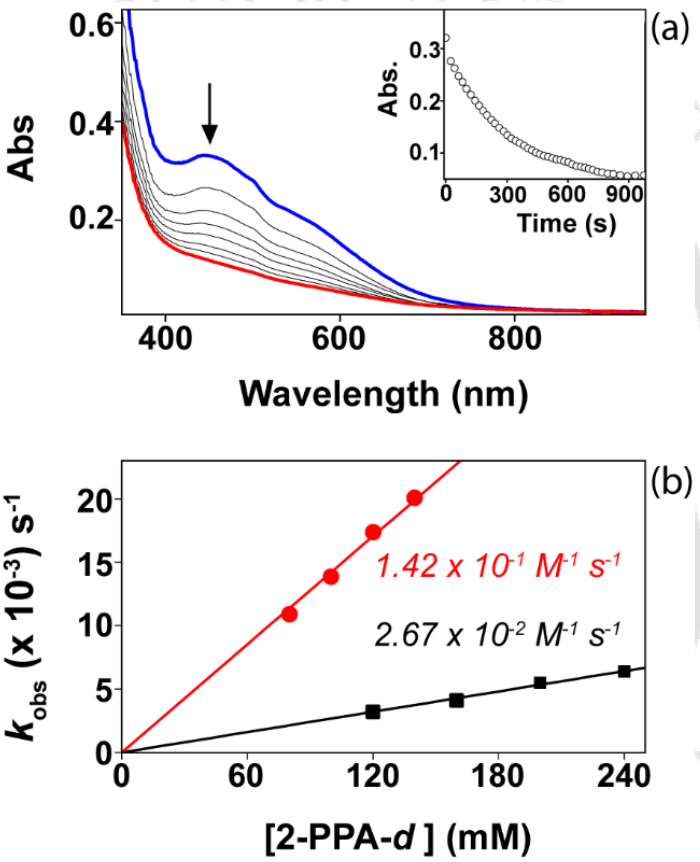

Fig. 5.4. (a) UV/Vis spectral changes of $[Mn^{III}(O_2)(L9)]^+$ (2 mM) upon addition of α-D1-2-phenylpropionaldehyde (120 mM) in the presence of TEA (5 mM) and hydrogen peroxide (20 mM) in CH_3CN at 15 °C. Inset shows the time trace during the course of the reaction. (b) Plot of k_{obs} against various concentrations of 2-PPA (●) and α-[D1]-PPA (~90%, D enriched, ■) in their reaction with 9b in CH_3CN at 15 °C.

To test whether the manganese(III)-peroxo can react efficiently through hydrogen atom abstraction, we decided to test alternative substrates with weak C−H bonds. Spectroscopic features after addition of 1,4-cyclohexadiene to either 8b or 9b showed no decay in the absorption bands of the manganese(III)-peroxo complexes, hence $[Mn^{III}(O_2)(L8)]^+$ and $[Mn^{III}(O_2)(L9)]^+$ are unable to react *via* desaturation pathways. This is surprising as the deformylation reaction described above appears to have a rate-determining hydrogen atom abstraction step from 2-PPA to $[Mn^{III}(O_2)(L9)]^+$. Moreover, the mechanistic probes ruled out the more commonly seen nucleophilic attack on the carbonyl group. Computational modelling established the reasons behind the lack of reactivity toward 1,4-cyclohexadiene as resulting from an energetically high second hydrogen atom abstraction.

Finally, we employed another mechanistic probe to establish the proposed reaction mechanism with conviction. A radical trapping experiment with bromotrichloromethane was performed to establish that the reaction mechanism of manganese(III)-peroxo with aldehydes proceeds through a radical intermediate species.[43,50-51]

Scheme 5.1. Reaction of $[Mn^{III}(O_2)(L9)]^+$ with radical trapping substrate.

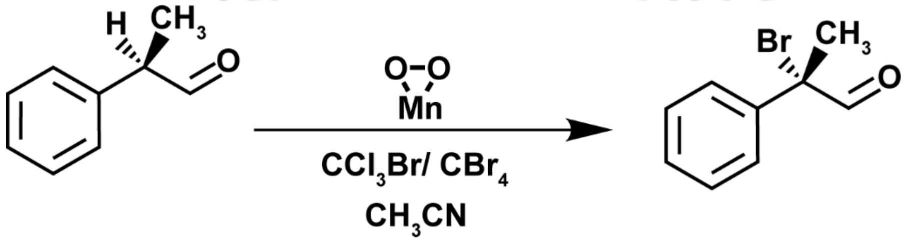

Addition of 2-PPA to intermediate 9b in the presence of excess $CBrCl_3$ or CBr_4 in acetonitrile at 15 °C leads to the formation of α-brominated product of the 2-PPA exclusively, Scheme 5.1, which was confirmed by NMR analysis (Fig. 5.5). Consequently, our radical trapping experiment confirms a radical mechanism that most likely starts with hydrogen atom abstraction from the α-position of 2-PPA.

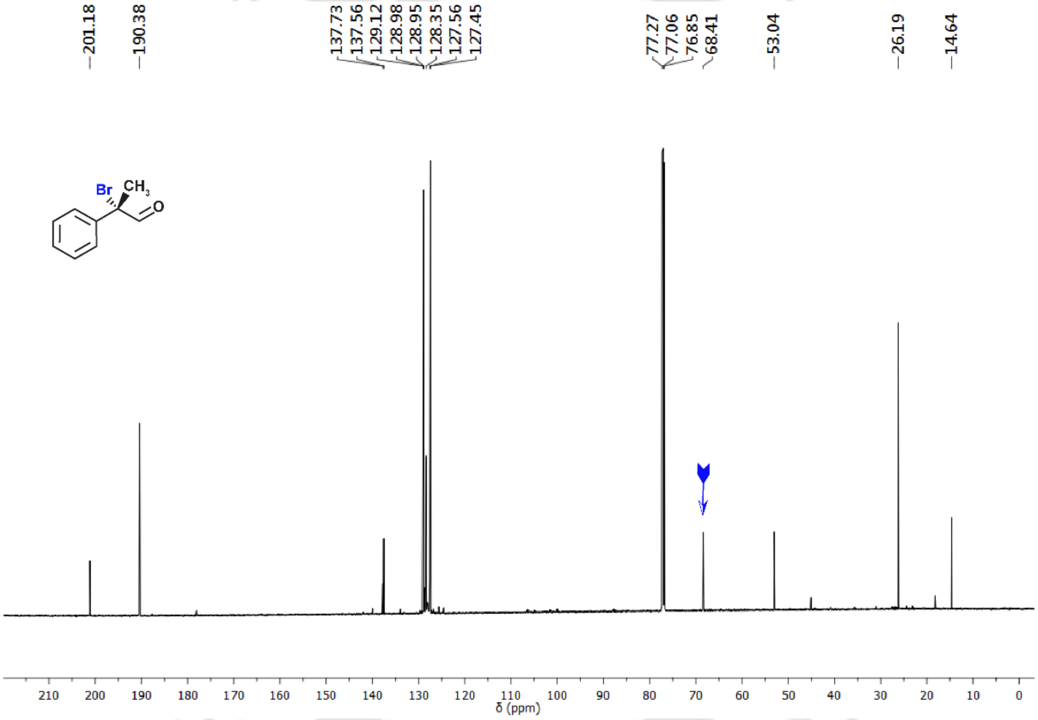

Fig. 5.5. ^{13}C-NMR spectrum of 2-bromo-2-phenylpropionaldehyde. The product was formed by the addition of 2-phenylpropionaldehyde to the intermediate $[Mn^{III}(O_2)(L9)]^+$ in the presence of excess CCl_3Br (or CBr_4) in CH_3CN at 15 °C.

5.2.3. Reaction Mechanism

To explain the experimentally obtained results on the reactivity of side-on manganese(III)-peroxo with aldehydes, we embarked on a density functional theory study on the possible reaction mechanisms leading to aldehyde deformylation by these complexes.[56] Although many possible mechanisms (including the common nucleophilic attack at the carbonyl position by the side-on peroxo moiety) and spin states were tested, the lowest-energy pathway leading to the first oxygen atom transfer was found on a quintet spin state (see Scheme 5.2). The reaction starts with a hydrogen atom abstraction *via* a transition state and forms a manganese(II)-hydroperoxo with a radical intermediate I_1. In the quintet spin state, a barrier of 19.2 kcal mol^{-1} was obtained and the reaction was endothermic by 7.0 kcal mol^{-1}.

Rather than a radical rebound, however, as is common in typical hydrogen atom abstraction reactions,[52-55] actually the hydrogen atom is bounced back to the substrate to give the enol form of the substrate and manganese(III)-peroxo *via* a subsequent barrier of 4.5 kcal mol^{-1}. The enol form of the reactant is slightly less stable than the keto form (by 5.4 kcal mol^{-1}). Once the reactant is in the enol-form, the manganese(III)-peroxo part of the reactant complex attacks the substrate olefin bond *via* a nucleophilic transition state to form the radical intermediate I_2. Energetically, I_2 is close in energy to I_1 and enol, and reacts *via* an O−O cleavage barrier to form a manganese(III)-oxo complex and an epoxide (I_3) in a highly exothermic process. As such, the computational studies implicated that probably the first steps in the reaction mechanism could be reversible, but the step from I_2 to I_3 should be irreversible. In order to give the final deformylation products from the epoxide, the manganese(III)-oxo group abstracts a hydrogen atom in I_3 from the alcohol position of the substrate, which breaks the epoxide ring to form a complex between manganese(II)-hydroxo and a radical (I_4). The subsequent OH rebound leads to the simultaneous epoxide ring-opening, C−C bond cleavage and the formation of formic acid and acetophenone products. The overall reaction mechanism has two highly exothermic reaction steps, namely the formation of the manganese(III)-oxo species (I_3) and the final reaction step leading to methylphenylketone and formic acid products. These two steps will be irreversible, although other reactions steps may be reversible.

Scheme 5.2. Reaction mechanism as computed by DFT analysis and energy levels of the respective possible intermediates and products in kcal mol^{-1} (calculated against the keto form of the reactant complex taken as 0.0 kcal mol^{-1}).

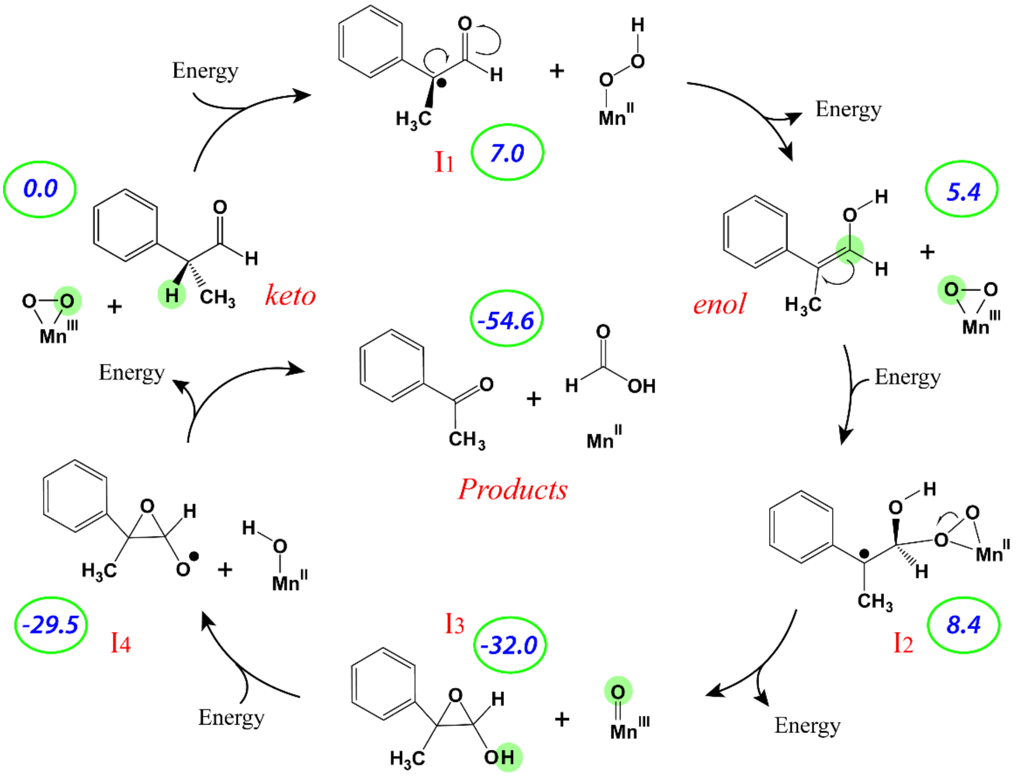

In summary, the lowest-energy pathway for aldehyde deformylation by side-on manganese(III)-peroxide of 2-PPA is α-hydrogen atom abstraction followed by reshuttle and tautomerization to form the enol form and nucleophilic attack on the olefin bond. Oxygen atom transfer then gives epoxide that through a low-barrier hydrogen atom transfer gives formic acid and methylphenylketone products.

5.3. Conclusion

Herein, we report a study on aldehyde deformylation reaction by side-on manganese-(III)-peroxo complexes. We identify a novel reaction mechanism that starts with a hydrogen atom abstraction and reshuttle to give a keto-enol tautomerization in the substrate as the rate-determining step. Subsequently, a nucleophilic attack on the olefin bond in the enol form leads to a low-energy mechanism to products. Alternative pathways were tested and ruled out. Thus, in the enol form, the olefin π-bond is easy to break, whereas breaking the carbonyl π-bond is more energetically demanding. As the reaction starts with a hydrogen atom abstraction from aldehyde, we also considered the manganese(III)-peroxo species as a general oxidant for substrate hydroxylation and desaturation reactions. Unfortunately, high reaction barriers for radical rebound are encountered and substrate hydroxylation and desaturation are unfeasible pathways at room temperature. Various mechanistic probes were employed to experimentally establish the mechanism. A positive KIE value of ~5 is indicative of the α-C-H bond cleavage. Also, a radical trapping experiment was conducted and the product identified again supports the newly proposed mechanism.

5.4. References

1. E. I. Solomon, T. C. Brunold, M. I. Davis, J. N. Kemsley, S.-K. Lee, N. Lehnert, F. Neese, A. J. Skulan, Y.-S. Yang, J. Zhou, *Chem. Rev.* **2000**, *100*, 235−349.
2. T. D. H. Bugg, *Curr. Opin. Chem. Biol.* **2001**, *5*, 550−555.
3. M. J. Ryle, R. P. Hausinger, *Curr. Opin. Chem. Biol.* **2002**, *6*, 193−201.
4. M. Costas, M. P. Mehn, M. P. Jensen, L. Que, Jr., *Chem. Rev.* **2004**, *104*, 939−986.
5. M. M. Abu-Omar, A. Loaiza, N. Hontzeas, *Chem. Rev.* **2005**, *105*, 2227−2252.
6. C. Krebs, D. Galonić Fujimori, C. T. Walsh, J. M. Bollinger Jr., *Acc. Chem. Res.* **2007**, *40*, 484−492.
7. P. C. A. Bruijnincx, G. van Koten, R. J. M. Klein Gebbink, *Chem. Soc. Rev.* **2008**, *37*, 2716−2744.
8. E. I. Solomon, K. M. Light, L. V. Liu, M. Srnec, S. D. Wong, *Acc. Chem. Res.* **2013**, *46*, 2725−2739.
9. A. R. McDonald, L. Que, Jr., *Coord. Chem. Rev.* **2013**, *257*, 414−428.
10. W. Zhu, N. G. J. Richards, *Essays Biochem.* **2017**, *61*, 259−270.
11. J. D. Aguirre, V. C. Culotta, *J. Biol. Chem.* **2012**, *287*, 13541−13548.
12. T. A. Jackson, T. C. Brunold, *Acc. Chem. Res.* **2004**, *37*, 461−470.
13. B. R. Streit, B. Blanc, G. S. Lukat-Rodgers, K. Rodgers, J. L. Dubois, *J. Am. Chem. Soc.* **2010**, *132*, 5711−5724.
14. S. Hofbauer, C. Gruber, K. F. Pirker, A. Sündermann, I. Schaffner, C. Jakopitsch, C. Oostenbrink, P. G. Furtmüller, C. Obinger, *Biochemistry*, **2014**, *53*, 3145−3157.

15. L. E. Grove, J. Xie, E. Yikilmaz, A.-F. Miller, T. C. Brunold, *Inorg. Chem.* **2008**, *47*, 3978−3992.
16. I. Kenkel, A. Franke, M. Dürr, A. Zahl, C. Dücker-Benfer, J. Langer, M. R. Filipović, M. Yu, R. Puchta, S. R. Fiedler, M. P. Shores, C. R. Goldsmith, I. Ivanović-Burmazović, *J. Am. Chem. Soc.* **2017**, *139*, 1472−1484.
17. A.-F. Miller, *FEBS Lett.* **2012**, *586*, 585−595.
18. A. Q. Lee, B. R. Streit, M. J. Zdilla, M. M. Abu-Omar, J. L. DuBois, *Proc. Natl. Acad. Sci. U. S. A.* **2008**, *105*, 15654−15659.
19. D. J. Vinyard, G. M. Ananyev, G. C. Dismukes, *Annu. Rev. Biochem.* **2013**, *82*, 577−606.
20. G. Renger, T. Renger, *Photosynth. Res.* **2008**, *98*, 53−80.
21. J. Q. Barber, *Rev. Biophys.* **2003**, *36*, 71−89.
22. P. E. M. Siegbahn, *Chem. - Eur. J.* **2008**, *14*, 8290−8302.
23. S. V. Kryatov, E. V. Rybak-Akimova, S. Schindler, *Chem. Rev.* **2005**, *105*, 2175−2226.
24. W. Nam, *Acc. Chem. Res.* **2007**, *40*, 522−531.
25. S. Sahu, D. P. Goldberg, *J. Am. Chem. Soc.* **2016**, *138*, 11410−11428.
26. P. Saisaha, J. W. de Boer, W. R. Browne, *Chem. Soc. Rev.* **2013**, *42*, 2059−2074.
27. G. Roelfes, V. Vrajmasu, K. Chen, R. Y. N. Ho, J.-U. Rohde, C. Zondervan, R. M. la Crois, E. P. Schudde, M. Lutz, A. L. Spek, R. Hage, B. L. Feringa, E. Münck, L. Que, Jr., *Inorg. Chem.* **2003**, *42*, 2639−2653.
28. J. Annaraj, Y. Suh, M. S. Seo, S. O. Kim, W. Nam, *Chem. Commun.* **2005**, 4529−4531.
29. A. Thibon, J.-F. Bartoli, S. Bourcier, F. Banse, *Dalton Trans.* **2009**, 9587−9584.

30. A. Mukherjee, M. A. Cranswick, M. Chakrabarti, T. K. Paine, K. Fujisawa, E. Münck, L. Que, Jr., *Inorg. Chem.* **2010**, *49*, 3618−3628.
31. J. Cho, S. Jeon, S. A. Wilson, L. V. Liu, E. A. Kang, J. J. Braymer, M. H. Lim, B. Hedman, K. O. Hodgson, J. S. Valentine, E. I. Solomon, W. Nam, *Nature*, **2011**, *478*, 502−505.
32. J. Annaraj, J. Cho, Y.-M. Lee, S. Y. Kim, R. Latifi, S. P. de Visser, W, Nam, *Angew. Chem., Int. Ed.* **2009**, *48*, 4150−4153.
33. D. F. Leto, S. Chattopadhyay, V. W. Day, T. A. Jackson, *Dalton Trans.* **2013**, *42*, 13014−13025.
34. M. Zlatar, M. Gruden, O. Y. Vassilyeva, E. A. Buvaylo, A. N. Ponomarev, S. A. Zvyagin, J. Wosnitza, J. Krzystek, P. Garcia-Fernandez, C. Duboc, *Inorg. Chem.* **2016**, *55*, 1192−1201.
35. C.-M. Lee, C.-H. Chuo, C.-H. Chen, C.-C. Hu, M.-H. Chiang, Y.-J. Tseng, C.-H. Hu, G.-H. Lee, *Angew. Chem., Int. Ed.* **2012**, *51*, 5427−5430.
36. M. Gennari, D. Brazzolotto, J. Pécaut, M. V. Cherrier, C. J. Pollock, S. DeBeer, M. Retegan, D. A. Pantazis, F. Neese, C. Duboc, *J. Am. Chem. Soc.* **2015**, *137*, 8644−8653.
37. D. Brazzolotto, F. G. Cantú Reinhard, J. Smith-Jones, M. Retegan, L. Amidani, A. S. Faponle, K. Ray, C. Philouze, S. P. de Visser, M. Gennari, C. Duboc, *Angew. Chem., Int. Ed.* **2017**, *56*, 8211−8215.
38. M. K. Coggins, J. A. Kovacs, *J. Am. Chem. Soc.* **2011**, *133*, 12470−12473.
39. M. K. Coggins, V. Martin-Diaconescu, S. DeBeer, J. A. Kovacs, *J. Am. Chem. Soc.* **2013**, *135*, 4260−4272.
40. H. E. Colmer, A. W. Howcroft, T. A. Jackson, *Inorg. Chem.* **2016**, *55*, 2055−2069.
41. J. Cho, R. Sarangi, W. Nam, *Acc. Chem. Res.* **2012**, *45*, 1321−1330.

42. Q. Zhang, A. Bell-Taylor, F. M. Bronston, J. D. Gorden, C. R. Goldsmith, *Inorg. Chem.* **2017**, *56*, 773−782.

43. P. Barman, P. Upadhyay, A. S. Faponle, J. Kumar, S. S. Nag, D. Kumar, C. V. Sastri, S. P. de Visser, *Angew. Chem., Int. Ed.* **2016**, *55*, 11091−11095.

44. M. G. Quesne, R. Latifi, L. E. Gonzalez-Ovalle, D. Kumar, S. P. de Visser, *Chem. - Eur. J.* **2014**, *20*, 435−446.

45. A. Timmins, M. Saint-Andre, S. P. de Visser, *J. Am. Chem. Soc.* **2017**, *139*, 9855−9866.

46. H. Börzel, P. Comba, K. S. Hagen, Y. D. Lampeka, A. Lienke, G. Linti, M. Merz, H. Pritzkow, L. V. Tsymbal, *Inorg. Chim. Acta*, **2002**, *337*, 407−419.

47. P. Comba, S. Kuwata, G. Linti, H. Pritzkow, M. Tarnai, H. Wadepohl, *Chem. Commun.* **2006**, 2074− 2076.

48. P. Comba, B. Kanellakopulos, C. Katsichtis, A. Lienke, H. Pritzkow, F. J. Rominger, *Chem. Soc., Dalton Trans.* **1998**, 3997− 4001.

49. P. Barman, A. K. Vardhaman, B. Martin, S. J. Wörner, C. V. Sastri, P. Comba, *Angew. Chem., Int. Ed.* **2015**, *54*, 2095−2099.

50. J. T. Groves, T. E. Nemo, *J. Am. Chem. Soc.* **1983**, *105*, 6243−6248.

51. S. Rana, A. Dey, D. Maiti, *Chem. Commun.* **2015**, *51*, 14469−14472.

52. K. Yoshizawa, T. Kamachi, Y. Shiota, *J. Am. Chem. Soc.* **2001**, *123*, 9806−9816.

53. S. Shaik, D. Kumar, S. P. de Visser, A. Altun, W. Thiel, *Chem. Rev.* **2005**, *105*, 2279−2328.

54. S. Shaik, D. Kumar, S. P. de Visser, *J. Am. Chem. Soc.* **2008**, *130*, 10128−10140.

55. D. Li, Y. Wang, K. Han, *Coord. Chem. Rev.* **2012**, *256*, 1137− 1150.

56. The computational modelling was done in collaboration with Dr. Samuel P. de Visser and his research group. This theoretical study was pivotal in this work to understand the reaction mechanism in detail. Also detailed thermochemical and valence bond analysis of the structures of intermediates and reactants explains the need of the keto−enol tautomerization; see, DOI: 10.1021/jacs.7b10033.

CHAPTER – VI

Amphoteric Reactivity of an Iron(III)-Alkylperoxo Complex

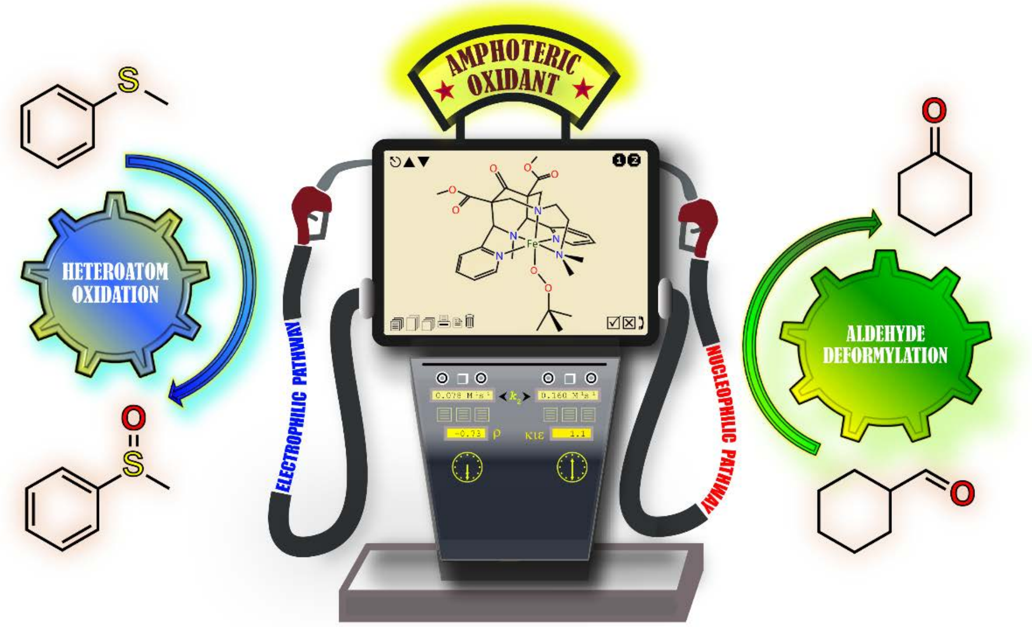

6.1. Introduction

Over the past decades, extensive research has been carried out on metal dioxygen adducts, that are known to be key species in many biological transformations and catalytic oxidation reactions.[1-3] Synthetic complexes for Cu^{II}-alkylperoxo sites served as models for lipid peroxidation reactions.[4-7] These Cu^{II}-OOR species are in general electrophilic in nature. Recently, however, few cases have been reported where the Cu^{II}-OOR species act as active oxidant towards nucleophilic aldehyde deformylation reactions.[8-10] These alkylperoxido complexes of copper mainly reacts via a concerted homolytic cleavage of the O-O bond.[11] As an example of amphoteric reactivity, a Ni^{II}-alkylperoxo has been reported that can oxidize a heteroatom (P in PPh_3) by an electrophilic pathway, while the same oxidant attacks the carbonyl carbon of benzaldehyde in a nucleophilic fashion.[12] Again like few other reported metastable Mn^{III}-alkylperoxo complexes, a thiolate-ligated Mn^{III}-OOR has also been isolated but it is reportedly irresponsive towards excess of organic substrates.[13] Another Mn^{III}-dioxygen adduct have been recently observed by Nam and co-workers to exhibit amphoteric reactivity as well.[14] In biological reactions, iron-dioxygen adducts are known to be pivotal in the catalytic cycles of dioxygen activation by various heme and non-heme enzymes.[15-20] For example in 'activated bleomycin', the oxygen ligated Fe(III) complex is reportedly competent to initiate DNA cleavage.[21-23] There is also evidence for the influence of a Fe^{III}-alkylperoxo complex in Purple Lipoxygenase and homo-protocatechuate-2,3-dioxygenase.[24-26]

Several synthetic analogues of iron-containing enzymes have been prepared and characterized. However, unlike other metal-alkylperoxo complexes, Fe^{III}-alkylperoxo moieties have been reported to be only sluggish oxidants towards a variety of organic substrates.[27-28] The reluctance towards reactivity with organic substrates stems from the competitive cleavage of the O-O bond, resulting in the in-situ formation of $Fe^{IV}=O$ complexes that reportedly are reactive in electrophilic reactions. In fact, the presence of an exogenous Lewis base like pyridine N-oxide or thiocyanate are known to accelerate the conversion of Fe^{III}-OOR to $Fe^{IV}=O$ by a ‘push effect’ on the homolytic O-O cleavage for heme and non-heme enzymatic models.[29-32] However, these additives act as the sixth proximal ligand in the Fe^{III}-OOR adducts with tetradentate ligands that typically promote the scission of the O-O bond.[31-32] There is a handful of literature reports of synthetic models of Fe^{III}-alkylperoxo systems.[2,31-59] Studies of these adducts have led to their successful spectroscopic characterization. However, the nature of these short-lived species still remains elusive. The oxidative reactivity of these species has always been a debatable topic due to their competitive nature towards bifurcated reaction pathways. Over the past few decades, reports have emerged of either homolytic or heterolytic O-O bond cleavage.[45-50] The spin state of the metal centre is known to play a pivotal role in determining the reaction pathway by modulating the bond strength of Fe-O and O-O bonds.[51-52] Quantum-chemical calculations (generally density functional theory, DFT) have led to the conclusion that the high-spin Fe^{III}-alkylperoxo complexes preferentially cleave the Fe-O bond, while the low-spin Fe^{III}-OOR contains an activated O-O bond and eventually undergoes homolytic O-O bond scission.[41-44,53-54]

6.2. Results and Discussion

6.2.1. Synthesis and Characterization

Here, we report the synthesis, characterization and reaction kinetics of a novel Fe^{III}-alkylperoxo moiety as the first example of amphoteric reactivity by a ferric alkylperoxo complex towards electrophilic and nucleophilic reactions.

Although a handful of reports on the successful characterization of Fe^{III}-alkylperoxo complexes is available in the literature, detailed kinetic studies are lacking, owing to the poor thermal stability of these complexes and their sluggish nature.[33-44,53-59] Unlike previously reported tetradentate ligand systems like TPA and TMC, where short-lived intermediates could only be stabilized at low temperature, the bispidine derivative used here offers secondary interactions that stabilizes the dioxygen adduct.[60] The bispidine L10 employed here (Scheme 6.1) shows an optimum balance of rigidity and flexibility, as the pendant N,N-dimethyl substituent is part of a flexible chelate ring, tethered to N^7 that, together with N^3 and the equatorial pyridine rings are part of the rigid bispidine backbone.[61] Overall, L10 enforces a square pyramidal geometry with N^7 occupying the apical position, *trans* to which is the accessible coordination site for a labile solvent molecule or oxygen adducts (see Chapter-II for detailed synthetic procedures of L10).

Scheme 6.1. Synthetic procedures for the formation of the ligand L10, the metal complex 10a and the intermediate 10b.

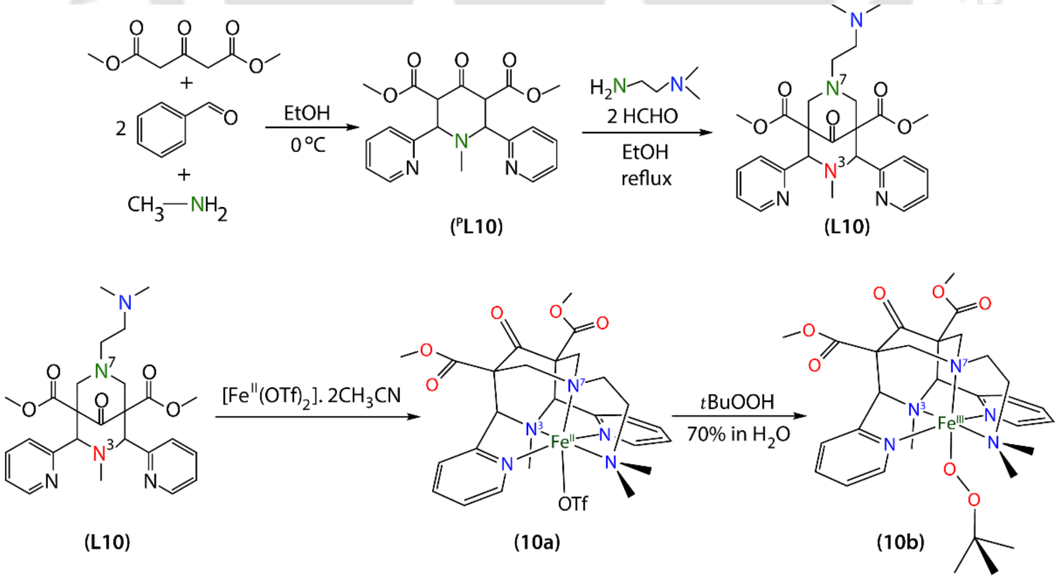

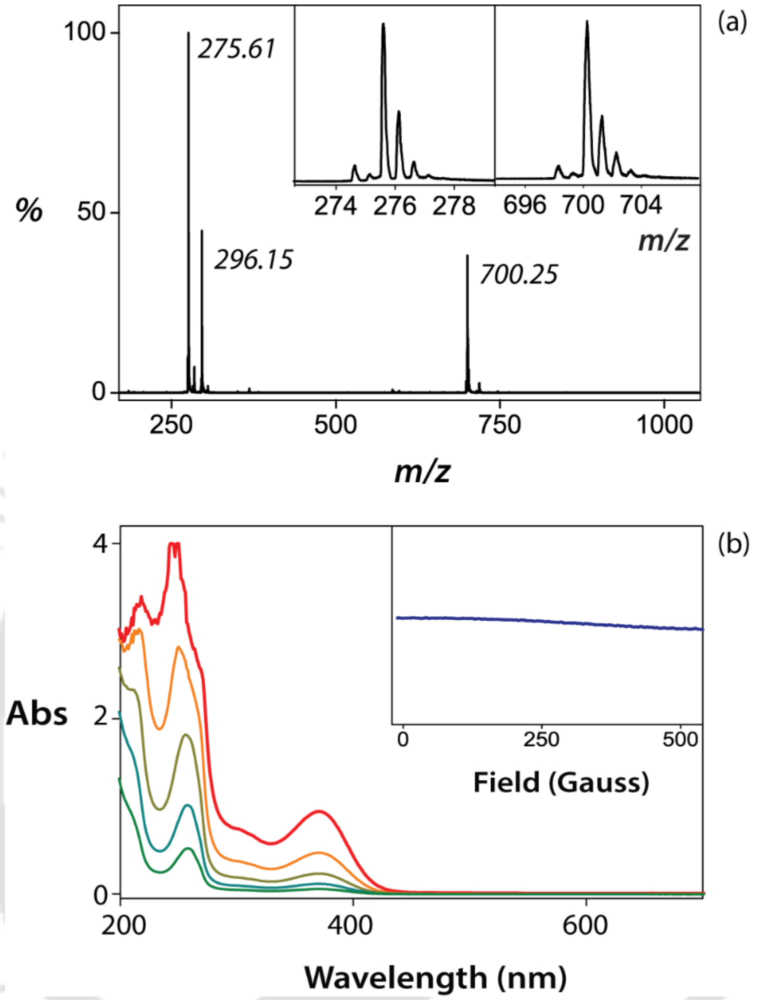

Fig. 6.1. (a) ESI-MS spectrum of complex 10a in CH_3CN at 298 K. Inset shows the isotopic distribution pattern corresponding to ion clusters $[Fe^{II}(L)]^{2+}$ (left, *m/z* 275.61) and $[Fe^{II}(L)(OTf)]^{+}$ (right, *m/z* 700.25). (b) UV/Vis spectrum of 10a (concentration increases as 0.0625, 0.125, 0.25, 0.5 and 1 mM) in CH_3CN at room temperature; inset shows the silent nature of Fe(II) in the X-band EPR spectrum of 10a in CH_3CN at 77 K.

The iron(II) complex $[Fe^{II}(L10)(OTf)](OTf)$ (10a) was synthesized under inert conditions by addition of 1.2 equivalents of $[Fe^{II}(CH_3CN)_2](OTf)_2$ in acetonitrile solution. The complex obtained was washed with diethyl ether and dried under vacuum to obtain pure 10a as a light-yellow powder. It was further characterized spectroscopically by ESI-MS, UV/Vis and X-band EPR spectroscopy (Fig. 6.1). When 10a was treated with *tert*-butyl hydroperoxide (70% in water, 30 eq., CH_3CN, room temperature), it forms a new blue species 10b. Complex 10b exhibits an intense absorption band at 598 nm (Ɛ = 1000 L M^{-1} cm^{-1}, 0 ˚C, see Fig. 6.2).

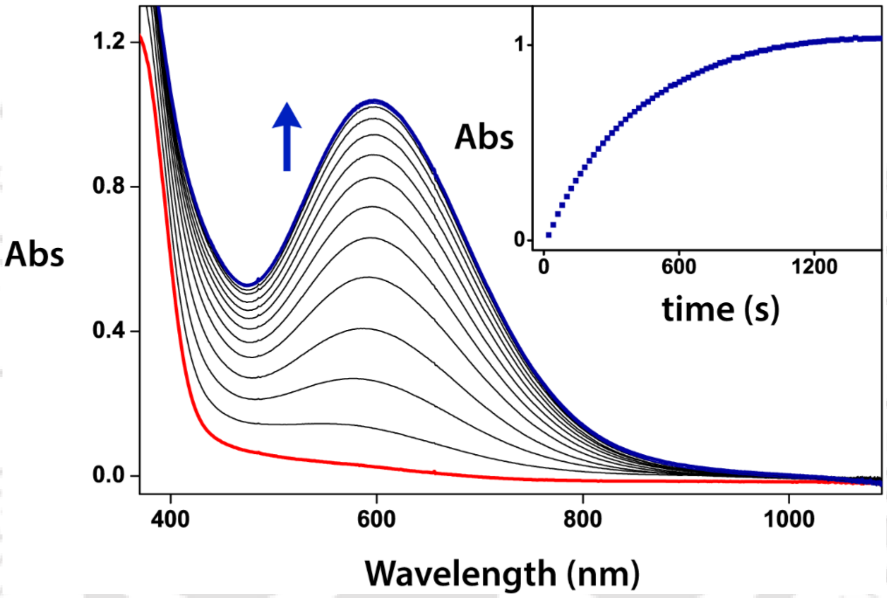

Fig. 6.2. UV/Vis spectrum for the formation of 10b from 10a at 0 °C in CH_3CN (inset shows the time trace for the absorbance at 598 nm).

The peak maximum and molar absorptivity are affirmative of the formation of $[Fe^{III}(L10)(tBuOO)]^{2+}$ and characteristic of the alkylperoxo to Fe^{III} LMCT.[62-63] Under identical conditions, such spectral features were absent when the pendant aliphatic chain tethered to N^7 was replaced by a picolyl group, that further reinforces the importance of the aliphatic side-chain fastened to N^7. In fact, complex 10b exhibits sufficient stability with half-lives of 40 and 100 min at 15°C and 5°C, respectively.

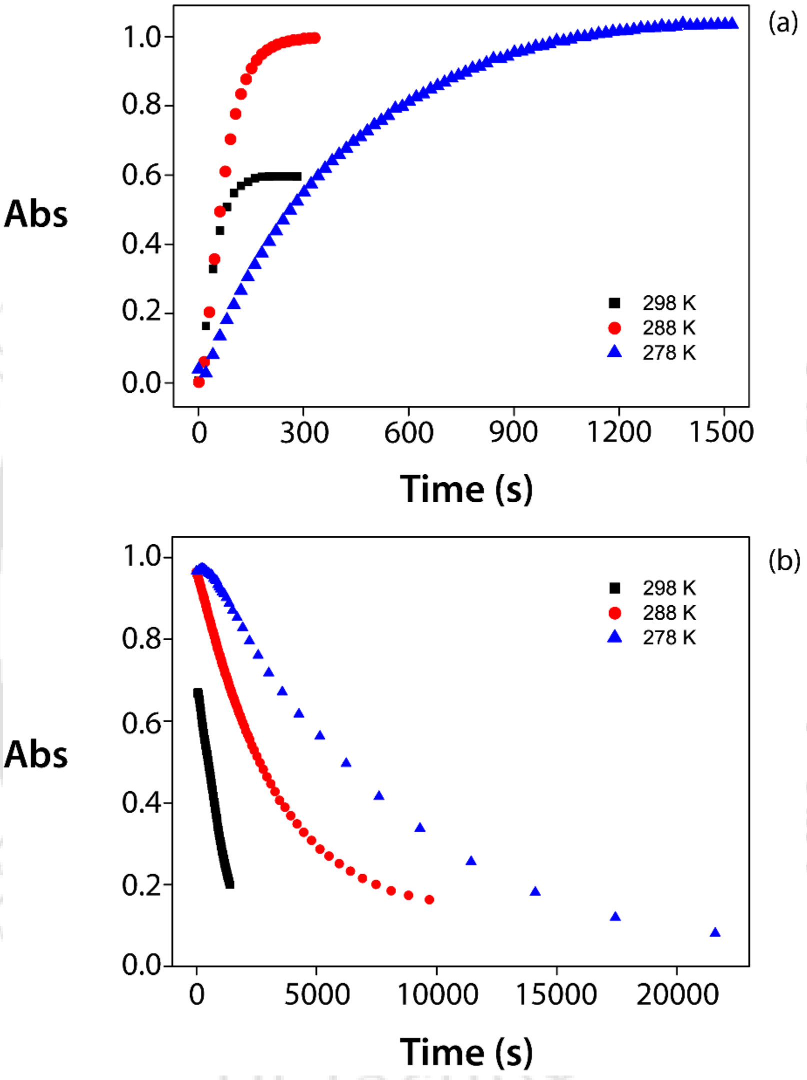

Fig. 6.3. Temperature dependent (a) formation and (b) self-decay of 10b using 30 equivalents of oxidant and a 1 mM solution of 10a in CH_3CN at different temperatures.

The positive ESI-MS spectrum of 10b showed major peaks at *m/z* 284.12, 320.18 and 717.29, corresponding to the fragments $[Fe^{III}(L10)(OH)]^{2+}$, $[Fe^{III}(L10)(tBuOO)]^{2+}$ and $[Fe^{III}(L10)(OH)(OTf)]^{+}$, respectively, and a minor peak at *m/z* 789.62 corresponding to the ion cluster $[Fe^{III}(L10)(tBuOO)(OTf)]^{+}$ (Fig. 6.4). The isotopic distribution patterns confirmed the existence of the Fe-complexes.

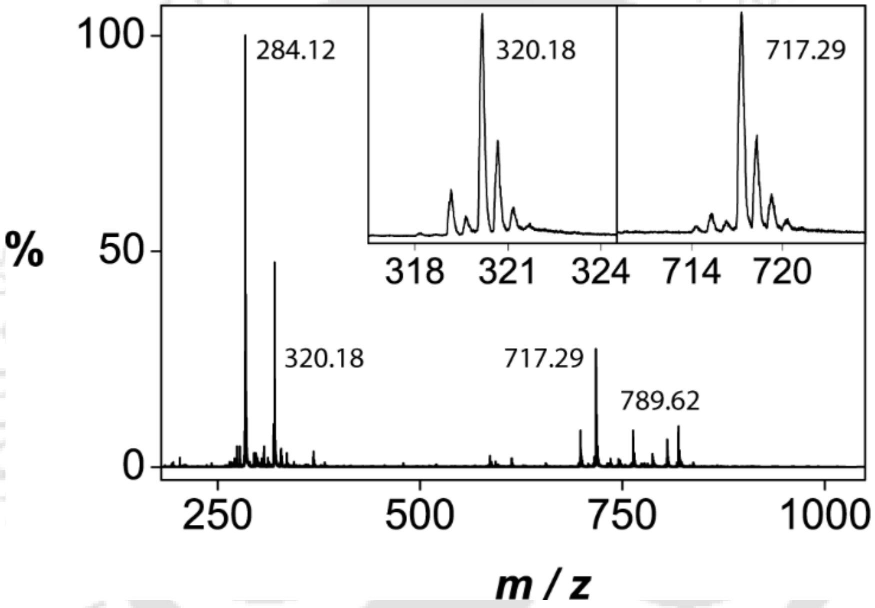

Fig. 6.4. Positive ESI-MS spectrum of 10b recorded from pre-cooled samples, inset shows the observed isotopic distribution pattern corresponding to the $[Fe(L10)(OOtBu)/2]^{+}$ fragment.

The negative ESI mass spectrum of 10b gave prominent peaks at higher mass range of *m/z* values 998.15 and 1015.11, corresponding to the fragments $[Fe^{III}(L10)(tBuOO)(CH_3CN)(OH)(OTf)_2]^{-}$ and $[Fe^{III}(L10)(OH)(OTf)_3]^{-}$, respectively (Fig. 6.5). The source of hydroxyl ions observed in the mass spectra can either be the fragmentation of $tBuOO^{-}$ or of the water molecule from the oxidant solution. The possibility of seven coordination cannot be ruled out and has been observed for similar Fe^{III} complexes.[65-66]

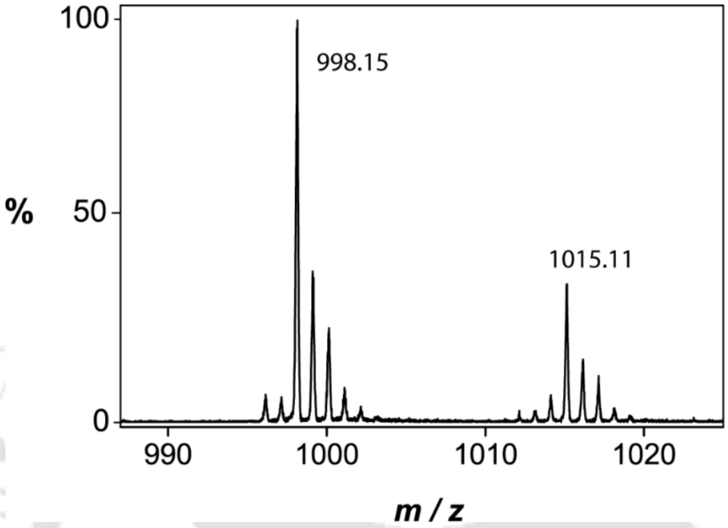

Fig. 6.5. Negative mode ESI-MS spectrum of complex 10b in CH_3CN obtained by infusing pre-cooled samples directly into the source.

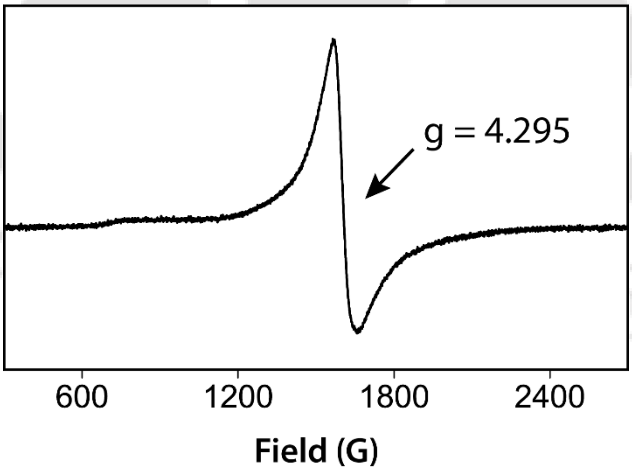

Fig. 6.6. X-band EPR spectrum of 10b at 5.3 K in CH_3CN. EPR parameters: microwave power: 1.994 mW, receiver gain: 60 dB, modulation frequency: 100 kHz, modulation amplitude: 0.1 mT, microwave frequency: 9.636926 MHz.

The X-band EPR spectrum of 10b obtained at 5 K shows a broad spectral feature at g = 4.295, suggestive of the presence of a high-spin Fe^{III}-OOR complex (Fig. 6.6).

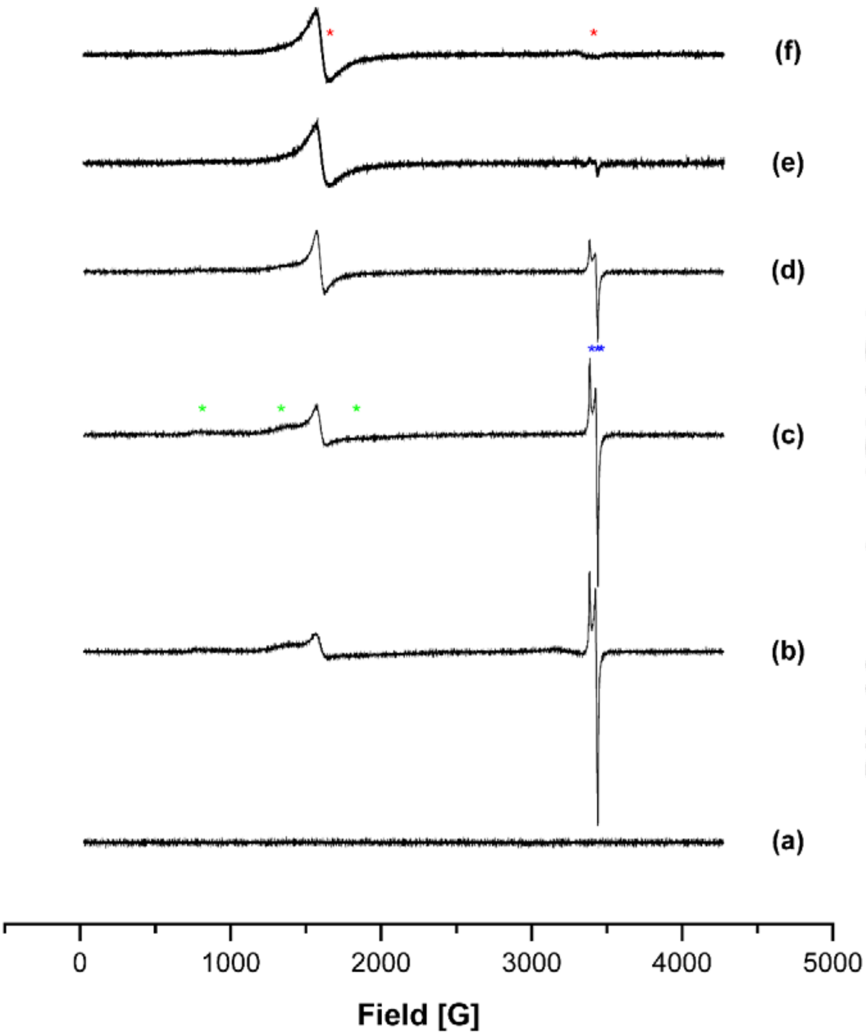

Fig. 6.7. Time dependent X-band EPR spectra at 5.3 K following the reaction of [Fe^{II}(L)(OTf)]OTf (1mM) with 30 equivalents *t*BuOOH in CH$_3$CN at 277K.

Shown is the spectrum of the starting material [Fe^{II}(L)(OTf)]OTf (a) as well as the frozen solution spectra of the reaction mixture frozen after 45 s reaction at 277 K (b);110 s (c); 300 s (d); 2.5 h (e) and 8.5 h (f). Spectra were obtained with a microwave power of 1.994 mW, receiver gain of 60 dB, modulation frequency of 100 kHz, modulation amplitude of 0.1 mT and a microwave frequency of 9.639621 MHz (a); 9.636698 MHz (b); 9.63998 MHz (c); 9.637177 MHz (d); 9.636926 MHz (e); 9.637755 MHz (f).

* ls Fe(III) signal with g = 2.0345; 2.0082; 2.0018.

* hs Fe(III) signal with g ≈ 4.295; 2.021.

* Species with a multiplicity >2 (g ≈ 8.69; 4.99; 3.60).

Samples of the oxidation of $[Fe^{II}(L)(MeCN)]^{2+}$ treated with *t*BuOOH in a similar way were frozen after various time intervals (45s < t < 8.5h) to 5.3K for EPR spectroscopy. These spectra show initial fast formation of a low-spin Fe(III) component was observed that decays at 278 K over a period of time. This can be interpreted as a low-spin meta-stable $[Fe^{III}(L)(MeCN)]^{3+}$ precursor, formed by outer-sphere electron transfer from 10a with 0.5 eq. of *t*BuOOH, and the relatively slow ligand exchange (MeCN / *t*BuOO$^-$), expected with a low-spin Fe(III) complex, then forms the alkylperoxido complex 10b. This is supported by a shift of the electronic transition of initially approx. 550 nm to 598 nm (see Fig. 6.2) and by the observation that the formation of the alkylperoxido complex 10b is much faster in CH_2Cl_2 (Fig. 6.8). However, the complex of interest, $[Fe^{III}(L)(tBuOO)]^{2+}$ (10b), unambiguously is a high-spin alkylperoxido complex with moderate stability.

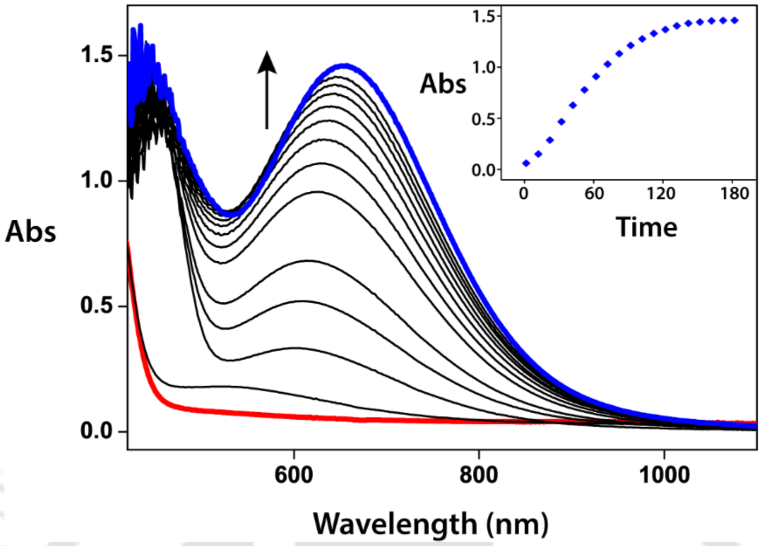

Fig. 6.8. UV/Vis spectrum for the formation of 10b at 278 K in DCM; inset shows the time trace of the formation spectra.

6.2.2. Reaction Kinetics

The unusual stability of this Fe(III)-*t*BuOO complex (10b) prompted further investigation for its reactivity with organic substrates. The self-decay rate of the complex 10b was observed to be 1.76(7) x 10^{-4} s^{-1} at 283 K. However, addition of organic substrates drastically improved the rate of decay of the corresponding LMCT band, thereby approving the reaction of the substrates with complex 10b. Addition of excess substrate leads to the decomposition of 10b under pseudo first-order condition as monitored with the 598 nm band in the UV/Vis spectrum. Oxygen atom transfer reactivity was tested using thioanisole as the model substrate. A linear dependence between k_{obs} and thioanisole concentration was obtained at 15 ˚C in CH_3CN, giving a second-order rate constant k_2 = 7.8 x 10^{-2} M^{-1} s^{-1}. Interestingly, this Fe(III)-OOR species have comparable reaction rates in thioanisole oxidation as reported for similar Fe(IV)-oxo complex.[67] To further understand the intrinsic details of the oxygen atom transfer (OAT) reaction, we decided to study *para*-substituted thioanisole substrates and created a Hammett plot (see Fig. 6.9.b).[68-69]

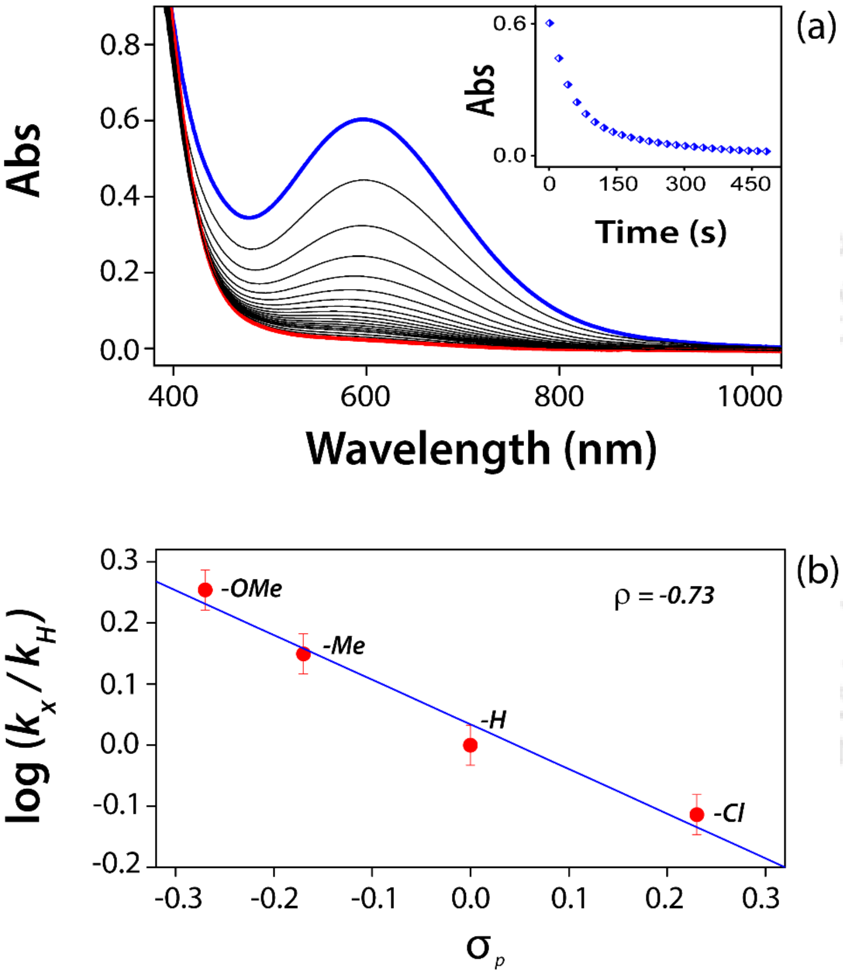

Fig. 6.9. (a) Decay profile of 10b upon addition of 200 equivalents of thioanisole in CH_3CN at 288 K. Inset shows the time trace for the decay of the 598 nm band as a function of time. (b) Hammett plot for the reaction of 10b with *para*-X-thioanisole in CH_3CN at 288 K.

This Hammett plot reveals that the reaction rates are not greatly dependent on the *para*-substituent and both electron-donating and electron-withdrawing groups produced similar reaction rates. When the reactions rates were plotted as a function of σ_p (*para*-substituent Hammett parameter), a linear trend was found with a small Hammett ρ value (-0.73).

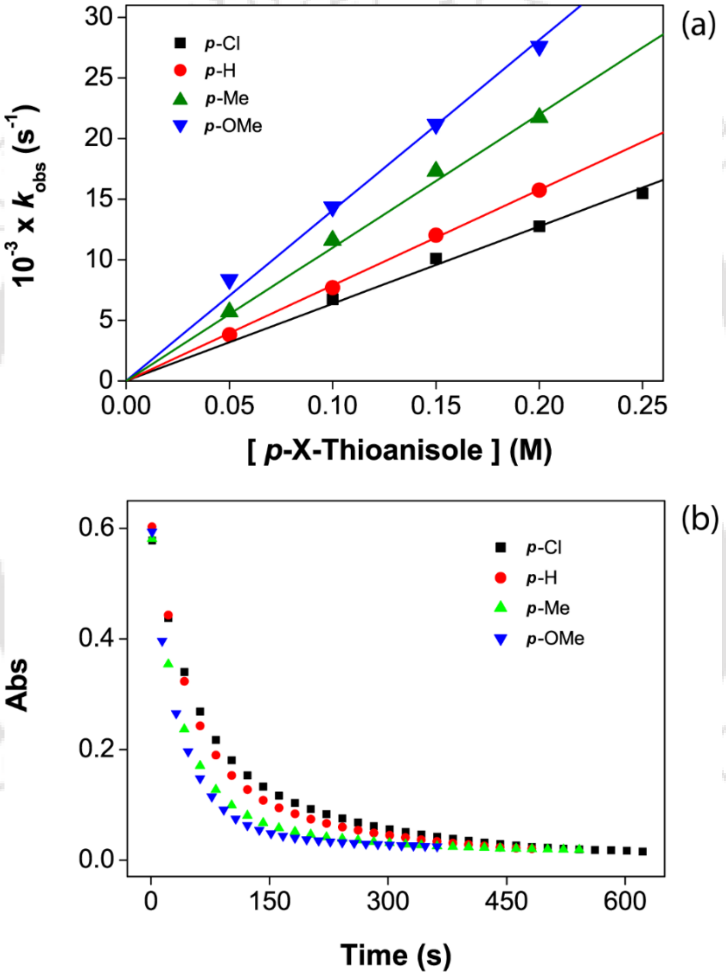

Fig. 6.10. (a) Second-order rate constant determined in the reaction of 1 mM of 10b with *para*-X-thioanisole, X = -OMe, -Me, -H, -Cl in CH_3CN at 288 K. (b) Comparison of time trace for the decay of the 598 nm band during the reaction of 10b with *para*-X-thioanisole, X = -OMe, -Me, -H, -Cl in CH_3CN at 288 K.

Table. 6.1. Pseudo first-order rate constants determined for the reaction of 10b (1 mM) with *para*-X-thioanisole at 288 K in CH_3CN.[a]

Substrate Concentration (mM)	Pseudo first-order rate constants (s^{-1}) x 10^{-3}			
	***para*-OMe**	***para*-Me**	***para*-H**	***para*-Cl**
50	8.37(2)	5.70(1)	3.81(4)	-
100	14.37(2)	11.62(3)	7.77(3)	6.74(4)
150	21.17(4)	17.34(3)	12.03(4)	10.10(2)
200	27.61(3)	21.73(3)	15.75(5)	12.76(4)
250	-	-	-	15.49(4)

[a] All the reactions were followed by monitoring the UV/Vis spectral changes of the reaction solution.

Table. 6.2. Second-order rate constants and Hammett parameters determined for the reaction of 10b (1 mM) with *para*-substituted thioanisole at 288 K in CH_3CN.[a]

***para*-X-thioanisols**	σ_p [b]	**Second-order rate constant (k_2) ($M^{-1}s^{-1}$)**	k_x / k_H [c]	**log (k_x / k_H)**
-OMe	-0.27	0.14	1.795	0.254
-Me	-0.17	0.11	1.410	0.149
-H	0	0.078	1	0
-Cl	0.23	0.06	0.769	-0.114

[a] All the reactions were followed by monitoring the UV/Vis spectral changes of the reaction solution; [b] Ref. 55; [c] Relative rate constant obtained by dividing the k_{obs} of *p*-X-thioanisole by k_{obs} of *p*-H-thioanisole.

This implied little electronic effect due to the addition of *para*-substituents to thioanisole (Table 6.1 and 6.2). The negative ρ value and slope in Fig. 6.9.b. indicates that the reaction proceeds *via* an electrophilic atom transfer pathway[69] as observed in non-heme Fe(IV)-oxo complexes.[67] Thus, against the common cliché, Fe(III)-OOR complex (10b) is reactive enough with thioanisole and the linear dependence in the Hammett plot is indicative of the fact that an oxygen atom transfer takes place during the oxidation. However, 10b was found to be non-reactive with other oxygen atom acceptors like cyclooctene or styrene, thereby precluding the study of olefin epoxidation reactions.

In general, homolytic cleavage of the peroxo (O-O) bond results in the formation of a putative Fe(IV)-oxo moiety. However, such mechanism is usually narrated for low-spin Fe(III)-OOR complexes.[53-54] Also, the Lewis bases (viz. 4-picoline, pyridine-N-oxide, thiocyanate, 2,6-lutidine, etc.) coordinate to the metal ion of such Fe(III)-OOR complexes and promotes the scission of the peroxo bond by a *push effect* thereby accelerating the conversion of Fe(III)-OOR to Fe(IV)-oxo species.[29-32] Such effect is also very well established for heme systems.[70-77] However, upon addition of pyridine-N-oxide (12 equivalents) to 10b, the existing LMCT band was monitored to decay very slowly, (comparable to its self-decay rate) and no formation of any other band (corresponding to an Fe(IV)-oxo formation) was observed in the UV/Vis-NIR region of the spectrum. Previously reported literature suggest that the *push effect* drastically accelerates the decay of the LMCT band and formation of the Fe(IV)-oxo chromophore was visible within seconds. This phenomenon interdicts the possibility of O-O bond cleavage and generation of an Fe(IV)-oxo species. It also serves as a secondary evidence that the OAT reactivity of 10b was not that of an Fe(IV)-oxo species. Another possibility is the heterolytic cleavage of the O-O bond thereby producing an Fe(V)-oxo moiety; however, no spectroscopic evidence was detected to infer such phenomenon (although such species may be extremely transient to be detected under normal conditions). Also, the Fe-oxos are, in general, irresponsive towards nucleophilic reactions. Therefore, we tested the reactivity of 10b towards aldehyde deformylation reactions.

The metal-dioxygen adducts in the form of peroxo, hydroperoxo or alkylperoxo complexes are known as efficient aldehyde deformylating agents. The majority of these deformylation reactions proceed *via* direct attack of the oxidant at the electrophilic carbonyl carbon atom.[78-84] Recently, however, an alternative electrophilic pathway was established in the reaction of manganese-peroxo species with aldehydes having an α-hydrogen atom.[85-86] A similar α-C-H abstraction was also identified in the reaction of a Cu^{II}-alkylperoxo intermediate towards aldehydes.[87] To ascertain the nature of reactivity of the Fe^{III}-alkylperoxo species presented here towards aldehydes, we did a thorough kinetic study with 10b as the catalyst and cyclohexanecarboxaldehyde (CCA) and 2-Phenylpropionaldehyde (2-PPA) as the model substrates.

Upon addition of CCA to 10b in CH_3CN at 15 ˚C, the intermediate decayed, giving cyclohexene as the major product (Fig. 6.11). The rate of decay of the 598 nm band in the UV/Vis spectrum increased linearly as a function of time indicating a bimolecular reaction mechanism. The resulting second-order rate constant (k_2) for the deformylation of CCA by 10b at 288 K is $1.6(4) \times 10^{-1}\ M^{-1}\ s^{-1}$. Thus, 10b is a unique example of a Fe^{III}-alkylperoxo species that exhibits amphoteric character and reacts efficiently towards both electrophiles and nucleophiles.

Irrespective of the mode of reactivity, in aldehyde deformylation reactions, an identical set of products are usually encountered. Hence product analysis is not a decisive tool to confirm the reaction mechanism. Therefore, we used the kinetic isotope effect (KIE) as a mechanistic tool to mitigate the conflict of the reactivity pathway.

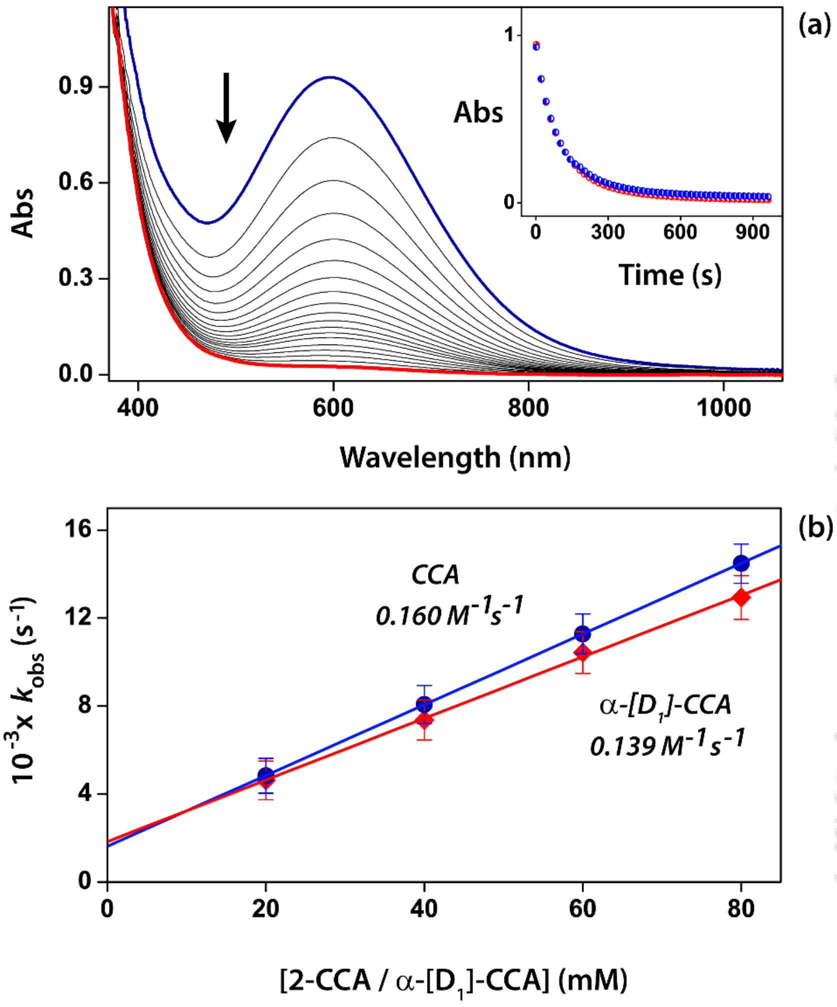

Fig. 6.11. (a) Decay profile of 10b in its reaction with CCA (60 equiv.) at 288 K in CH_3CN; the inset shows the comparative time trace of decay of the 598 nm band upon addition of 60 equivalents of CCA (red circles) and D-CCA (blue circles) to 10b in CH_3CN; (b) Second-order rate constants in the reaction of 10b with CCA (●) and α-[D_1]-CCA (●) in CH_3CN at 288 K.

Replacement of the α-hydrogen atom in CCA by deuterium, therefore, acts as a mechanistic probe to identify the rate-determining step in the deformylation reaction. The reaction profile of 10b was studied under similar conditions with α-[D_1]-CCA and a second-order rate constant of 1.4(2) x 10^{-1} M^{-1} s^{-1} was obtained at 288 K. Thus, no substantial deceleration in the reaction rate was observed upon incorporation of deuterium instead of hydrogen at the α–position of the aldehyde group (Fig. 6.11). A KIE value of 1.1 is indicative of a nucleophilic attack at the carbonyl position of the aldehyde by the oxidant, resulting in the deformylated products. Upon repeating the same with 2-PPA and α-[D_1]-PPA, a similar trend was observed with a KIE value of 1.0 (see Fig. 6.12).

Table. 6.3. Pseudo first-order rate constants determined for the reaction of 10b (1 mM) with CCA and α-[D_1]-CCA in CH_3CN at 15°C.

Concentration (mM)	k_{obs} x 10^{-2} for CCA	k_{obs} x 10^{-2} for α-[D_1]-CCA
20	0.48(3)	0.46(2)
40	0.80(7)	0.73(7)
60	1.12(9)	1.04(3)
80	1.44(8)	1.29(4)

Table. 6.4. Pseudo first-order rate constants determined for the reaction of 10b (1 mM) with 2-PPA and α-[D_1]-PPA in CH_3CN at 10°C.

Concentration (mM)	k_{obs} x 10^{-3} for 2-PPA	k_{obs} x 10^{-3} for α-[D_1]-PPA
50	2.02(4)	2.09(3)
100	3.37(2)	3.18(3)
150	4.26(3)	4.19(4)
200	5.45(3)	5.34(5)

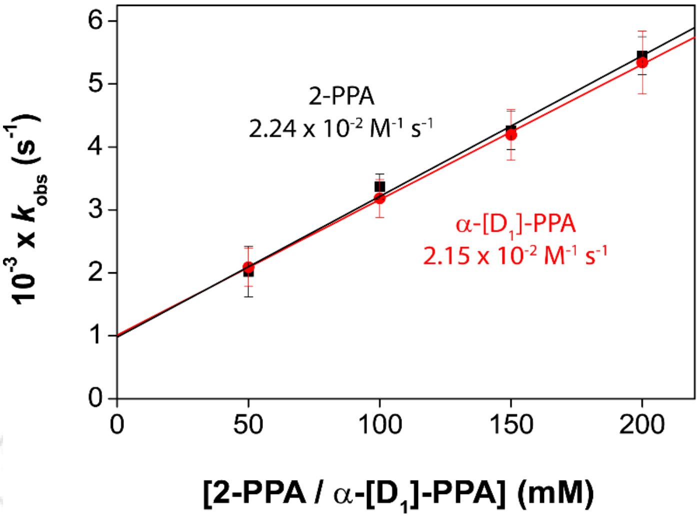

Fig. 6.12. Second-order rate constants in the reaction of 10b with 2-PPA (■) and α-[D_1]-PPA (●) in CH_3CN at 283 K.

Scheme 6.2. Possible reaction sites on CCA and 2-PPA by 10b.

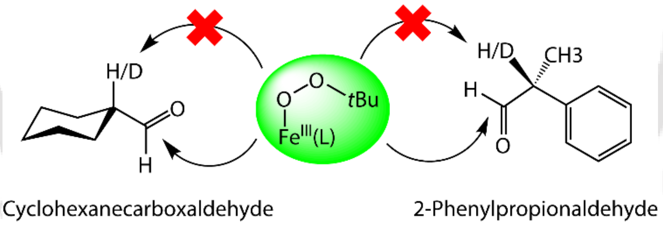

Further evidence of nucleophilic reactivity was obtained from the reactivity study of 10b with aromatic aldehydes. Upon addition of benzaldehyde to 10b the 598 nm band was observed to deplete. This encouraged us to study the effect of substitution at the *para*-position of benzaldehyde with electron donating and withdrawing groups. The reaction rates thus obtained were plotted against their *para*-substituent constants (σ_p), a Hammett plot with a positive slope (ρ= +0.23) was obtained (Fig.

6.13). This is assertive of a nucleophilic attack at the carbonyl center of the substrates by complex 10b.

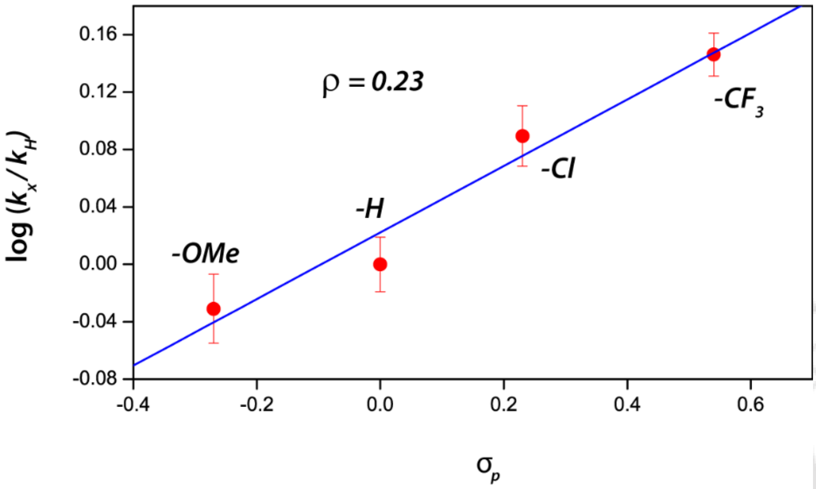

Fig. 6.13. Hammett plot for the reaction of 10b with various *para*-X-benzaldehyde derivatives (X = OMe, H, Cl and CF_3) in CH_3CN at 283 K.

Table. 6.5. Pseudo first order rate constants determined for the reaction of 10b (1 mM) with various *para*-substituted benzaldehydes (100 mM) at 10 °C. [a]

***para*-X**	**σ_p**[b]	**10^{-3} x Pseudo first-order rate constant (k_{obs}) (s^{-1})**	**k_X / k_H**[c]	**log (k_X / k_H)**
-OMe	-0.27	5.56(2)	0.931	-0.031
-H	0	5.97(3)	1	0
-Cl	0.23	7.34(4)	1.228	0.089
$-CF_3$	0.54	8.36(4)	1.400	0.146

[a] All the reactions were followed by monitoring the UV/Vis spectral changes of the reaction solution; [b] data taken from ref. 68; [c] Relative rate constant obtained by dividing the k_{obs} of *p*-X-benzaldehyde by k_{obs} of *p*-H-benzaldehyde.

6.3. Conclusion

In summary, a new iron(III)-alkylperoxo complex was successfully synthesized and characterized. Unlike other Fe(III)-OOR species, this complex was extraordinarily stable due to non-covalent secondary interactions from the ligand skeleton. Variable temperature EPR characterization established the high-spin character of the ferric moiety. Against the notion, this Fe(III)-OOR species was observed to be reactive towards oxidation reactions of organic model substrates. OAT reactions to thioanisole and Hammett analysis confirmed the atom transfer pathway in the reaction mechanism. Aldehyde deformylation reaction was also tested positive and nucleophilic attack at the carbonyl centre was revealed from mechanistic investigations. Thus, this complex appears to be the first iron(III)-alkylperoxo species that exhibits amphoteric reactivity.

6.4. References

1. F. A. Chavez, P. K. Mascharak, *Acc. Chem. Res.* **2000**, *33*, 539-545.
2. M. Costas, M. P. Mehn, M. P. Jensen, L. Que, Jr., *Chem. Rev.* **2004**, *104*, 939-986.
3. S. Hikichi. M. Akita, Y. Moro-oka, *Coord. Chem. Rev.* **2000**, *198*, 61-87.
4. C. Würtele, E. Gaoutchenova, K. Harms, M. C. Holthausen, J. undermeyer, S. Schindler, *Angew. Chem. Int. Ed.* **2006**, *45*, 3867-3869.
5. S. Itoh, *Acc. Chem. Res.* **2015**, *48*, 2066-2074.
6. J. J. Liu, D. E. Diaz, D. A. Quist, K. D. Karlin, *Isr. J. Chem.* **2016**, *56*, 738-755.
7. C. E. Elwell, N. L. Gagnon, B. D. Neisen, D. Dhar, A. D. Spaeth, G. M. Yee, W. B. Tolman, *Chem. Rev.* **2017**, *117*, 2059-2107.
8. B. Kim, D. Jeong, J. Cho, *Chem. Commun.* **2017**, *53*, 9328-9331.
9. B. Kim, D. Jeong, T. Ohta, J. Cho, *Commun Chem.* **2019**, 2:81.
10. H. Oh, W.-Min Ching, J. Kim, W.-Zen Lee, S. Hong, *Inorg. Chem.* **2019**, 58, 12964-12974.
11. T. Tano, M. Z. Ertem, S. Yamaguchi, A. Kunishita, H. Sugimoto, N. Fujieda, T. Ogura, C. J. Cramer, S. Itoh, *Dalton Trans*, **2011**, *40*, 10326-10336
12. S. Hikichi, H. Okuda, O. Yoshiko, M. Akita, *Angew. Chem. Int. Ed.* **2009**, *48*, 188-191.
13. M. K. Coggins, J. A. Kovacs, *J. Am. Chem. Soc.* **2011**, *133*, 12470-12473.
14. M. Sankaralingam, Y.-Min Lee, S. H. Jeon, M. S. Seo, K.-Bin Cho, W. Nam, *Chem. Commun.* **2018**, *54*, 1209-1212.
15. W. Nam, *Acc. Chem. Res.* **2007**, *40*, 465-465.
16. E. G. Kovaleva, J. D. Lipscomb, *Nat. Chem. Biol.* **2008**, *4*, 186-193.

17. E. I. Solomon, S. D. Wong, L. V. Liu, A. Decker, M. S. Chow, *Curr. Opin. Chem. Biol.* **2009**, *13*, 99-113.
18. P. R. Ortiz de Montellano, *Chem. Rev.* **2010**, *110*, 932-948.
19. J. Rittle, M. T. Green, *Science*, **2010**, *330*, 933-937.
20. S. Shaik, S. Cohen, Y. Wang, H. Chen, D. Kumar, W. Thiel, *Chem. Rev.* **2010**, *110*, 949-1017.
21. R. M. Burger, T. A. Kent, S. B. Horwitz, E. Münck, J. Peisach, *J. Biol. Chem.* **1983**, *258*, 1559-1564.
22. J. W. Sam, X.-J. Tang, J. Peisach, *J. Am. Chem. Soc.* **1994**, *116*, 5250-5256.
23. A. Decker, M. S. Chow, J. N. Kemsley, N. Lehnert, E. I. Solomon, *J. Am. Chem. Soc*. **2006**, *128*, 4719-4733.
24. M. J. Nelson, S. Seitz, *Active Oxygen in Biochemistry*, J. S. Valentine, C. S. Foote, A. Greenberg, J. F. Liebman, Eds. Blackie Academic and Professional, Chapman and Hall, Glasgow, UK, **1995**, 276-312;
25. E. Skrzypczak-Jankun, R. A. Bross, R. T. Carroll, W. R. Dunham, M. O. Funk Jr., *J. Am. Chem. Soc.* **2001**, *123*, 10814-10820.
26. E. G. Kovaleva, J. D. Lipscomb, *Science*, **2007**, *316*, 453-457.
27. M. S. Seo, T. Kamachi, T. Kouno, K. Murata, M. J. Park, K. Yoshizawa, W. Nam, *Angew. Chem. Int. Ed.* **2007**, *46*, 2291-2294.
28. M. J. Park, J. Lee, Y. Suh, J. Kim, W. Nam, *J. Am. Chem. Soc.* **2006**, *128*, 2630-2634.
29. K. Yamaguchi, Y. Watanabe, I. Morishima, *J. Am. Chem. Soc.* **1993**, *115*, 4058-4065.
30. S. Hong, L. Yong-Min, C. Kyung-Bin, M. S. Seo, D. Song, J. Yoon, R. Garcia-Serres, M. Clémancey, T. Ogura, W. Shin, J.-M. Latour, W. Nam, *Chem. Sci.* **2014**, *5*, 156-162.

31. M. Sono, M. P. Roach, E. D. Coulter, J. H. Dawson, *Chem. Rev.* **1996**, *96*, 2841-2887.
32. J. Kaizer, M. Costas, L. Que, Jr., *Angew. Chem. Int. Ed.* **2003**, *42*, 3671-3673.
33. T. Ogihara, S. Hikichi, M. Akita, T. Uchida, T. Kitigawa, Y. Moro-oka, *Inorg. Chem. Acta*, **2000**, *297*, 162-170.
34. A. P. Sobolev, D. E. Babushkin, E. P. Talsi, *J. Mol. Catal. A* **2000**, *159*, 233-245.
35. J. Kim, Y. Zang, M. Costas, R. G. Harrison, E. C. Wilkinson, L. Que, Jr., *J. Biol. Inorg. Chem.* **2001**, *6*, 275-284.
36. M. P. Jensen, S. J. Lange, M. P. Mehn, E. L. Que, L. Que, Jr., *J. Am. Chem. Soc.* **2003**, *125*, 2113-2128.
37. N. Lehnert, K. Fujisawa, E. I. Solomon, *Inorg. Chem.* **2003**, *42*, 469-481.
38. J.-U. Rohde, S. Torelli, X. Shan, M. H. Lim, E. J. Klinker, J. Kaizer, K. Chen, W. Nam, L. Que, Jr., *J. Am. Chem. Soc.* **2004**, *126*, 16750-16761.
39. M. P. Jensen, M. Costas, R. Y. N. Ho, J. Kaizer, A. Mariata i Payeras, E. Münck, L. Que, Jr., J.-U. Rohde, A. Stubna, *J. Am. Chem. Soc.* **2005**, *127*, 10512-10525.
40. T. K. Paine, M. Costas, J. Kaizer, L. Que, Jr., *J. Biol. Inorg. Chem.* **2006**, *11*, 272-276.
41. J. Bautz, P. Comba, L. Que, Jr., *Inorg. Chem.* **2006**, *45*, 7077-7082.
42. X. Shan, J.-U. Rohde, K. D. Koehntop, Y. Zhou, M. R. Bukowski, M. Costas, K. Fujisawa, L. Que, Jr., *Inorg. Chem.* **2007**, *46*, 8410-8417.
43. F. Namuswe, G. D. Kasper, A. A. N. Sarjeant, T. Hayashi, C. M. Krest, M. T. Green, P.Moënne-Loccoz, D. P. Goldberg, *J. Am. Chem. Soc.* **2008**, *130*, 14189-14200.

44. F. Namuswe, T. Hayashi, Y. Jiang, G. D. Kasper, A. A. N. Sarjeant, P. Moënne-Loccoz, D. P. Goldberg, *J. Am. Chem. Soc.* **2010**, *132*, 157-167.
45. S. Ménage, E. C. Wilkinson, L. Que, Jr., M. Fontecave, *Angew. Chem. Int. Ed.* **1995**, *34*, 203-205.
46. R. Y. Ho, G. Roelfes, B. L. Feringa, L. Que, Jr. *J. Am. Chem. Soc.* **1999**, *121*, 264-265.
47. A. Bassan, M. R. Blomberg, P. E. Siegbahn, L. Que, Jr. *J. Am. Chem. Soc.* **2002**, *124*, 11056-11063.
48. W. N. Oloo, A. J. Fielding, L. Que, Jr. *J. Am. Chem. Soc.* **2013**, *135*, 6438-6441.
49. S. Bang, S. Park, Y.-M. Lee, S. Hong, K.-B. Cho, W. Nam, *Angew. Chem. Int. Ed.* **2014**, *53*, 7843-7847.
50. I. Ghosh, S. Banerjee, S, Paul, T. Corona, T. K. Paine, *Angew. Chem. Int. Ed.* **2019**, *58*, 12534-12539.
51. J. J. Girerd, F. Banse, A. J. Simaan, *Struct. Bonding (Berlin)*, **2000**, *97*, 145-177.
52. M. P. Jensen, A. Mariata i Payeras, A. T. Fiedler, M. Costas, J. Kaizer, A. Stubna, E. Münck, L. Que, Jr., *Inorg. Chem.* **2007**, *46*, 2398-2408.
53. N. Lehnert, R. Y. N. Ho, L. Que, Jr., E. I. Solomon, *J. Am. Chem. Soc.* **2001**, *123*, 8271-8290.
54. N. Lehnert, R. Y. N. Ho, L. Que, Jr., E. I. Solomon, *J. Am. Chem. Soc.* **2001**, *123*, 12802-12816.
55. L. R. Widger, Y. Jiang, A. C. McQuilken, T. Yang, M. A. Siegler, H. Matsumura, P. Moënne-Loccoz, D. Kumar, S. P. de Visser, D. P. Goldberg, *Dalton Trans.* **2014**, *43*, 7522-7532.
56. Y. Zang, J. Kim, Y. Dong, E. C. Wilkinson, E. H. Appelman, L. Que, Jr., *J. Am. Chem. Soc.* **1997**, *119*, 4197-4205.

57. M. R. Bukowski, H. L. Halfen, T. A. van den Berg, J. A. Halfen, L. Que, Jr., *Angew. Chem. Int. Ed*. **2005**, *44*, 584-587.

58. D. Krishnamurthy, G. D. Kasper, F. Namuswe, W. D. Kerber, A. A. N. Sarjeant, P. Moënne-Loccoz, D. P. Goldberg, *J. Am. Chem. Soc*. **2006**, *128*, 14222-14223.

59. J. Stasser, F. Namuswe, G. D. Kasper, Y. Jiang, C. M. Krest, M. T. Green, J. Penner-Hahn, D. P. Goldberg, *Inorg. Chem*. **2010**, *49*, 9178-9190.

60. N. A. Barnes, A. T. Brooker, S. M. Godfrey, P. R. Mallender, R. G. Pritchard, M. Sadler, *Eur. J. Org. Chem*. **2008**, *6*, 1019-1030.

61. P. Comba, M. Kerscher, K. Rück, M. Starke, *Dalton. Trans*. **2018**, *47*, 9202-9220.

62. J. Kim, E. Larka, E. C. Wilkinson, L. Que, Jr., *Angew. Chem. Int. Ed. Engl*. **1995**, *34*, 2048-2051.

63. A. Wada, S. Ogo, Y. Watanabe, M. Mukai, T. Kitagawa, K. Jitsukawa, H. Masuda, H. Einaga, *Inorg. Chem*. **1999**, *38*, 3592-3593.

64. J. Bautz, P. Comba, L. Que, Jr., *Inorg. Chem*. **2006**, *45*, 7077-7082.

65. M. Bukowski, P. Comba, C. Limberg, M. Merz, L. Que, Jr., T. Wistuba, *Angew. Chem. Int. Ed*. **2004**, *43*, 1283-1287.

66. S. Gosiewska, H. P. Permentier, A. P. Bruins, G. van Koten, R. J. M. K. Gebbink, *Dalton Trans*. **2007**, 3365-3368.

67. D. Wang, K. Ray, M. J. Collins, E. R. Farquhar, J. R. Frisch, L. Gómez, T. A. Jackson, M. Kerscher, A. Waleska, P. Comba, M. Costas, L. Que, Jr., *Chem. Sci*. **2013**, *4*, 282-291.

68. H. C. Brown, Y. Okamoto, *J. Am. Chem. Soc*. **1958**, *80*, 4979-4987.

69. Y. Goto, T. Matsui, S. I. Ozaki, Y. Watanabe, S. Fukuzumi, *J. Am. Chem. Soc*. **1999**, *121*, 9497-9502.

70. F. Minisci, F. Fontana, S. Araneo, F. Recupero, S. Banfi, S. Quici, *J. Am. Chem. Soc.* **1995**, *117*, 226–232.
71. T. L. Poulos, *J. Biol. Inorg. Chem.* **1996**, *1*, 356–359.
72. D. B. Goodin, *J. Biol. Inorg. Chem.* **1996**, *1*, 360–363.
73. T. Matsui, S. Ozaki, Y. Watanabe, *J. Am. Chem. Soc.* **1999**, *121*, 9952–9957.
74. W. Nam, H. J. Choi, H. J. Han, S. H. Cho, H. J. Lee, S.-Y. Han, *Chem. Commun.* **1999**, 387–388.
75. S. Yoshioka, S. Takahashi, K. Ishimori, I. Morishima, *J. Inorg. Biochem.* **2000**, *81*, 141–151.
76. W. Nam, H. J. Han, S.-Y. Oh, Y. J. Lee, M.-H. Choi, S.-Y. Han, C. Kim, S. K. Woo, W. Shin, *J. Am. Chem. Soc.* **2000**, *122*, 8677–8684.
77. N. Hessenauer-Ilicheva, A. Franke, D. Meyer, W.-D. Woggon, R. van eldik, *Chem.–Eur. J.* **2009**, *15*, 2941–2959.
78. A. D. N. Vaz, E. S. Roberts, M. J. Coon, *J. Am. Chem. Soc.* **1991**, *113*, 5887-5889.
79. E. S. Roberts, A. D. N. Vaz, M. J. Coon, *Proc. Natl. Acad. Sci. USA* **1991**, *88*, 8963-8966.
80. A. D. N. Vaz, S. J. Pernecky, G. M. Raner, M. J. Coon, *Proc. Natl. Acad. Sci. USA* **1996**, *93*, 4644-4648.
81. Y. Goto, S. Wada, I. Morishima, Y. Watanabe, *J. Inorg. Biochem.* **1998**, *69*, 241-247.
82. K. Sen, J. C. Hackett, *J. Am. Chem. Soc.* **2010**, *132*, 10293-10305.
83. K. G. Aukema, T. M. Makris, S. A. Stoian, J. E. Richman, E. Münck, J. D. Lipscomb, L. P. Wackett, *ACS Catal.* **2013**, *3*, 2228-2238.
84. A. Shokri, L. Que, Jr. *J. Am. Chem. Soc.* **2015**, *137*, 7686-7691.

85. P. Barman, P. Upadhyay, A. S. Faponle, J. Kumar, S. S. Nag, D. Kumar, C. V. Sastri, S. P. de Visser, *Angew. Chem. Int. Ed.* **2016**, *55*, 11091-11095.

86. F. G. Cantú Reinhard, P. Barman, G. Mukherjee, J. Kumar, D. Kumar, D. Kumar, C. V. Sastri, S. P. de Visser, *J. Am. Chem. Soc.* **2017**, *139*, 18328-18338.

87. S. S. Nag, G. Mukherjee, P. Barman, C. V. Sastri, *Inorg. Chim. Acta*, **2019**, *485*, 80-85.

CHAPTER-VII

- Thesis Overview & Future Prospects

This thesis has aimed to explore the generation, characterization and reactivity of high valent non-heme metal intermediates of iron and manganese. In particular, the chemistry of non-heme iron(IV)-oxo, manganese(III)-peroxo and iron(III)-alkylperoxo systems have been discussed. Here in Chapter-III, it has been shown how subtle modifications in the ligand skeleton induces a substantial effect on the reactivity of the corresponding iron(IV)-oxo species. In Chapter-IV, the factors that lead to such drastic effects have been identified. Thus, intricate detailing is necessary while designing ligand scaffolds for containment of highly reactive systems. In Chapter-V, a new mechanism has been established in detail that leads to aldehyde deformylation reactions by manganese(III)-peroxo moieties. Thus, blind-fold assumption of nucleophilic mechanism in an aldehyde deformylation reactions can be misleading, given, there is active hydrogen residing in the α-position of the carbonyl centre. In Chapter-VI, a new bispidine-based iron complex has been synthesized and successful generation of a comparatively stable iron(III)-alkylperoxo species has been achieved. This iron(III)-OOR species exhibits amphoteric properties towards electrophilic and nucleophilic reactions and hence, is a versatile intermediate.

This field of bio-inorganic chemistry is promising as well as challenging in terms of the uncertainty it inflicts. Very minute modifications can lead to dramatic ramifications and thus, the presumption becomes very difficult. For example, the substitution of the pyridine rings by bulkier quinoline groups in TPA makes the resulting iron(IV)-oxo complex, $[Fe^{IV}(O)(TQA)]^{2+}$, high-spin in nature. While the same modifications in N4Py fail to alter the spin state of the iron(IV)-oxo species, $[\mathrm{Fe}^{\mathrm{IV}}(\mathrm{O})(2\mathrm{PyN2Q})]^{2+}$, that retains its low-spin character. Thus, the enhancement in reactivity cannot be attributed to a change in spin state, which is solely due to enhanced perturbation in the equatorial ligand field. Again, in $\mathrm{Me_3TPA}$, all the three pyridine rings are substituted in the *ortho*-position, results in high-spin nature of the ferrous and ferric species. While the same experiments in BnTPEN ligand framework fail to reproduce similar effects as the three methyl groups block the passage of the incoming oxygen, thereby, blocking the formation of the iron-oxo species. Also, the quest for the formation of high-spin iron(IV)-oxo moieties in non-heme model systems always remains an enigma.

In the case of aldehyde deformylation reactions, a new frontier has been explored. A brand-new pathway of electrophilic α-C-H bond abstraction from 2-PPA has been discovered that goes *via* keto-enol tautomerism (Chapter V). However, the presence of active hydrogen atom in the α-position does not promise the attainment of this pathway, as was seen in the case of iron(III)-alkylperoxo species (Chapter VI), that undergoes nucleophilic mechanism while deformylating CCA. Thus, this effect can be speculated to be metal-ion dependent, as there has been a change in metal ion from Chapter V to VI. Also, the mechanism can be manifested in terms of the stability of the resulting radical that is formed after the α-C-H abstraction. The radical formed in 2-PPA is more stable than that in CCA, and thereby enabling the possibility of keto-enol tautomerism in 2-PPA, unlike in CCA. Thus, the overall reactivity and mechanisms can be reliant on several factors that act in tandem. It would be a nice journey to explore such effects that segregate each species from the other.

List of Publications

1. Colomban, C.; Tombing, A. H.; Mukherjee, G.; Sastri, C. V.; Sorokin, A. B.; de Visser, S. P. Mechanism of Oxidative Activation of Fluorinated Aromatic Compounds by N-Bridged Diiron-Pthalocynanine. What determines the Reactivity? *Chem. Eur. J.* **2019**, *25*, 14320-14331.

2. Mukherjee, G.; Alili, A.; Barman, P.; Kumar, D.; Sastri, C. V.; de Visser, S. P. Interplay Between Steric and Electronic Effects: A Joint Spectroscopic and Computational Study of Nonheme Iron(IV)-Oxo Complexes. *Chem. Eur. J.* **2019**, *25*, 5086-5098. **(HOT Paper)**

3. Nag, S. S.; Mukherjee, G.; Barman, P.; Sastri, C. V. Influence of Induced Steric on the Switchover Reactivity of Mononuclear Cu(II)-Alkylperoxo Complexes. *Inorg. Chim. Acta,* **2019**, *485*, 80-85. **(Invited Article)**

4. Mukherjee, G.; Lee, C. W. Z.; Nag, S. S.; Alili, A.; Cantú Reinhard, F. G.; Kumar, D.; Sastri, C. V.; de Visser, S. P. Dramatic Rate-Enhancement of Oxygen Atom Transfer by an Iron(IV)-oxo Species by Equatorial Ligand Field Perturbations. *Dalton. Trans.* **2018**, *47*, 14945-14957.

5. Cantu Reinhard, F. G.; Barman, P.; Mukherjee, G.; Kumar, J.; Kumar D.; Kumar D.; Sastri, C. V.; de Visser, S. P. Keto-Enol Tautomerism Trigger an Electrophilic Aldehyde Deformylation Reaction by a nonheme Manganese(III) - peroxo Complex. *J. Am. Chem. Soc.* **2017**, *139*, 18328-18338.

List of Presentations

1. Gourab Mukherjee, ***Poster Presenter*** at International Conference: "Modern Trends in Inorganic Chemistry" (MTIC-XVIII) IIT Guwahati, India, on December 11-14, 2019.
2. Gourab Mukherjee, ***Invited talk*** at Indo-French Symposium: CEFIPRA 2019, IACS Kolkata on November 27-29, 2019.
3. Gourab Mukherjee, ***Oral Presenter*** at National Conference: Research Conclave 2019, IIT Guwahati, Guwahati, India, on March 14-17, 2019. (***awarded the Best Oral Presenter Prize***)
4. Gourab Mukherjee, ***Oral Presenter*** at International Conference: "New Frontiers in Chemical Science" (NFCS), IIT Bombay, Bombay, India, on December 13-14, 2018.
5. Gourab Mukherjee, ***Poster Presenter*** at International Conference: "Frontiers in Chemical Science" (FICS), IIT Guwahati, Guwahati, India, on December 06-08, 2018. (***awarded the Best Poster Prize***)
6. Gourab Mukherjee, ***Poster Presenter*** at National Conference: Research Conclave 2018, IIT Guwahati, Guwahati, India, on March 8-11, 2018.
7. Gourab Mukherjee, ***Poster Presenter*** at International Conference: "Modern Trends in Inorganic Chemistry" (MTIC-XVII), CSIR-NCL, IISER-Pune, Pune, India, on December 11-14, 2017.
8. Gourab Mukherjee, ***Poster Presenter*** at National Seminar: "Recent Developments in Synthesis and Catalysis" (RDSC), Dibrugarh University, Assam, India, on March 10-11, 2017.

~: Short Biography :~

Gourab Mukherjee *is a post-graduate researcher at the Department of Chemistry, IIT Guwahati. He was born to Shri. Amar Sankar Mukherjee and Smt. Smita Mukherjee in the city of Durgapur, West Bengal, India. He did his schooling from Modern High School, Durgapur, and graduated in 2012 with Chemistry (Hons.) from Durgapur Government College. He completed his Master's Degree (M.Sc.) in Inorganic Chemistry from the University of Burdwan, West Bengal in 2014. Later that year he joined the research group of Prof. Chivukula Vasudeva Sastri at IIT Guwahati and enjoyed his Ph.D. research work based on the mechanistic elucidations and reaction kinetics of high-valent enzymomimetic model systems. Also as a part of the DST-UKIERI project, he has twice visited the research group of Dr. Samuel P. de Visser at the University of Manchester, UK, where he gained research experience in computational modeling. In the future, he is quite inquisitive about exploring other areas in Chemistry.*